Iron-oxide Nanoparticles Coated on *Helicobacter pylori* for Gastric Cancer Treatment *via* Magnetic Hyperthermia

Thesis submitted in the fulfilment of the requirement of the degree of

Doctor of Philosophy

Submitted by

Komal Attri

(Regn. No. 901909030)

Under the Supervision of

Dr. Diptiman Choudhury

Associate Professor

Department of Chemistry & Biochemistry

Co-leader of Cancer Detection and Treatment

Centre of Excellence in Emerging Materials

Thapar Institute of Engineering & Technology

Patiala, Punjab, India-147004

Dr. Bhupendra Chudasama

Professor

Department of Physics and Material Sciences

Associate Faculty of BioX,

Centre of Excellence in Emerging Materials

Thapar Institute of Engineering & Technology

Patiala, Punjab, India-147004

Dr. Roop L. Mahajan

L.E. Hester Chair Professor

Department of Mechanical Engineering, Department of Materials Science & Engineering, Virginia Tech, Blacksburg, VA 24061, United States

Chair Professor

Centre of Excellence in Emerging Materials

Thapar Institute of Engineering & Technology

Patiala, Punjab, India-147004

DEPARTMENT OF CHEMISTRY AND BIOCHEMISTRY THAPAR INSTITUTE OF ENGINEERING AND TECHNOLOGY

PATIALA-147004, PUNJAB, INDIA

March 2025

Certificate

This is to certify that thesis entitled **"Iron-oxide Nanoparticles Coated on *Helicobacter pylori* for Gastric Cancer Treatment *via* Magnetic Hyperthermia"** being submitted by Komal Attri **in the fulfilment of the requirement for the award of the Degree of Philosophy,** Department of Chemistry and Biochemistry, Thapar Institute of Engineering and Technology, Patiala, is an authentic record of candidate's own work carried out by her under our supervision and guidance. The matter embodied in this thesis has not been submitted in part or full to any other university or institute for the award of any degree in India or Abroad.

(Supervisor)
Dr. Diptiman Choudhury

Associate Professor
Department of Chemistry & Biochemistry
Co-leader of Cancer Detection and Treatment
Centre of Excellence in Emerging Materials
Thapar Institute of Engineering & Technology
Patiala, Punjab, India-147004

(Supervisor)
Dr. Bhupendra Chudasama

Professor
Department of Physics and Material Sciences
Associate Faculty of BioX,
Centre of Excellence in Emerging Materials
Thapar Institute of Engineering & Technology
Patiala, Punjab, India-147004

(Supervisor)
Dr. Roop L. Mahajan

L.E. Hester Chair Professor
Department of Mechanical Engineering,
Department of Materials Science & Engineering, Virginia Tech, Blacksburg, VA 24061, United States
Chair Professor
Centre of Excellence in Emerging Materials
Thapar Institute of Engineering & Technology
Patiala, Punjab, India-147004

(Head)

Dr. Manmohan Chhibber

Professor & Head

Department of Chemistry & Biochemistry

TIET, Patiala - 147004

Candidate's Declaration

I, hereby declare that the work presented in the thesis entitled "**Iron-oxide Nanoparticles Coated on *Helicobacter pylori* for Gastric Cancer Treatment *via* Magnetic Hyperthermia**" in partial **fulfilment of the requirement for the award of the Degree of Philosophy**, Department of Chemistry and Biochemistry, Thapar Institute of Engineering and Technology, Patiala, is an authentic recordof my own work carried out under the supervision of Dr. Diptiman Choudhury (Associate Professor, Department of Chemistry and Biochemistry, TIET, Patiala, India), Dr. Bhupendra Chudasama (Professor, Department of Physics and Material Science and Assistant DoRDC) and Dr. Roop L. Mahajan (Chair Professor, TIET-VT, CEEMS). The matter embodied in this thesis has not been submitted in part or full to any other university or institute for the award of any degree in India or Abroad.

Komal Attri

“ Radha Soami ”

Acknowledgements

I wholeheartedly thank my mighty God and my Guru Mr. Gurinder Singh Dhillon ji for giving me the vision, power, spirit and endurance to complete the interesting research.

Completion of this doctoral dissertation was possible with the support of people. I would like to express my sincere gratitude to all of them.

First and foremost, I would like to express my sincere gratitude to my esteemed research supervisors, **Dr. Diptiman Choudhury**, **Dr. Bhupendra Chudasama**, and **Dr. Roop L. Mahajan**, for introducing me to this exciting field of science. Their valuable guidance, continuous support, motivation, patience, scholarly insights, and consistent encouragement have been instrumental throughout my Ph.D. work. I have learned extensively from them, including how to view established questions from new perspectives and how to approach problems with systematic thinking. Despite their busy schedules, they have always been available to clarify my doubts, for which I am deeply appreciative. It has been a tremendous privilege to undertake my doctoral program under their guidance and to benefit from their research expertise. Their mentorship has provided me with a comprehensive and enriching experience. Their persistent courage and confidence will continue to inspire me, and I look forward to further engaging with their innovative ideas.

I extend my heartfelt gratitude to **Dr. Manmohan Chhibber, Professor and Head, DCBC, TIET, Patiala**. I am sincerely thankful to my doctoral committee members, **Dr. Mily Bhattacharya (Assistant Professor, Department of Chemistry and Biochemistry), Dr. Manmohan Chhibber (Professor and Head, Department of Chemistry and Biochemistry)** and **Dr. Siddhartha Sharma (Professor, Department of Biotechnology)** for their valuable feedback during half yearly progress reports and dedication to ensuring the highest quality of research.

I am also very thankful to **Dr. Padmakumar Nair, Director, TIET and Dr. N. Tejo Prakash, Dean of Research and Development Cell (DoRDC)** for providing an excellent research environment and top-notch facilities for execution of my project work. Also, I would like to acknowledge the laboratories like **SAI Labs**, **TIET, Patiala**, **TIET-SEM Lab**, **Sprint Testing Solutions, Mumbai** and **Institute Instrumentation Centre, IIT**

Roorkee from where I received significant assistance with characterization.

I wish to extend my sincerest thanks to **TIET-VT, the Centre of Excellence in Emerging Materials (CEEMS)**. I am glad to have been granted with the wonderful opportunity to collaborate with CEEMS, allowing me to broaden my horizons. My research progress would not have been as seamless without the financial backing provided by CEEMS.

I am grateful to my seniors and fellow lab mates **Dr. Pawandeep Kaur, Dr. Vanshita Goel, Poulomi Chandra, Parmandeep Kaur, Sunidhi Sharma, Anjali Sharma, Disha Jindal, Isha Tanwar and Priyanshu Gautam** for their generous sharing of knowledge, insights and companionship during this academic journey. I extend my special thanks to **Dr. Deepinder Sharda** for his compassionate support and constant motivation in every aspect. The cooperative atmosphere within the academic community has deeply enhanced my experience and expanded my outlook.

I am profoundly grateful to my friends **Anjali Sharma, Disha Jindal, Isha Tanwar, Dr. Anushka Garg, Apoorva Chauhan and Priyanka Malik** for their unwavering emotional support and their presence in every possible way. Their encouragement, empathy, and companionship have provided a steady source of strength throughout my journey.

I am deeply indebted to **my family**, my father, **Mr. Subhash Chander Attri**, my mother, **Mrs. Sangeeta Attri**, my grandfather, **Mr. Shanker Das**, my grandmother, **Mrs. Maya Devi** and my brother, **Mr. Abhishek Attri** for their resolute support, encouragement and patience throughout my Ph.D journey. They always stood by my side, whether facing challenges or celebrating triumphs. Their beliefs in my abilities fuels my confidence and determination to pursue my dreams.

Throughout this journey, I've encountered both challenges and rewards. I feel incredibly lucky to have received support and encouragement from many exceptional individuals. Thank you all for contributing significantly to my academic and personal development. Thank you for your everlasting love and support.

“DEVOTED TO

MY BELOVED FAMILY”

Table of contents

List of Abbreviations

LF	Lactoferrin
%	Percentage
µl	Microliter
µM	Micro molar
ºC	Degree Celsius
Å	Angstrom
AGS	Gastric Adenocarcinoma
AMF	Alternating Magnetic Field
AO	Acridine orange
ART	Artemisinin
ART-MNPs	Artemisinin-Magnetic Nanoparticles
ATCC	American Type Culture Collection
BHI	Brain Heart Infusion Media
BSA	Bovine Serum Albumin
CI	Combination index
cm	Centimeter
CO_2	Carbon dioxide
DAMPs	Damage Associated Molecular Patterns
DLS	Dynamic Light Scattering
DMSO	Dimethyl sulphoxide
DNA	Deoxyribonucleic Acid
DOX	Doxorubicin
EDC	Ethylene Dichloride
EDS	Energy Dispersive Spectra
FACS	Flow Activated Cell Sorting
FBS	Fetal Bovine Serum
$FeCl_3$	Ferric chloride

FE-SEM	Field Emission Scanning Electron Microscope
$FeSO_4$	$FeSO_4$ Ferrous sulfate
FTIR	Fourier transform infrared
g	Gram
h	Hour
H. pylori	*Helicobacter pylori*
Hc	Coercivity
HCl	Hydrochloric acid
HM	Hyperthermia
HR- TEM	High-resolution transmission electron microscopy
Hz	Hertz
IL	Interleukin
IONPs	Iron Oxide Nanoparticles
KBr	Potassium Bromide
kDa	Kilo Dalton
kHz	Kilo Hertz
LF-IONPs	Lactoferrin- Iron Oxide Nanoparticles
MDC	Monodansylcadaverine
mg	Milligram
MHT	Magnetic Hyperthermia
MIB	Metal Ion binding
min	Minutes
mm	Millimetre
M_r	Remanence Magnetization
mT	Magnetic Field
MTT	3-(4, 5-dimethylthiazol-2-yl)-2, 5-diphenyltetrazolium bromide

NaOH	Sodium hydroxide
NH_4OH	Ammonium hydroxide
NHS	N-hydroxysuccinimide
NK	Natural killer
NLR	Nod Like Receptors
nm	Nanometre
OD	Optical density
PAMPs	Pathogen Associated Molecular Patterns
PBS	Phosphate Buffer Saline
PDB	Protein data bank
PEG	Polyethylene glycol
pH	Potential of hydrogen
PI	Propidium iodide
ROS	Reactive oxygen species
s	Seconds
SAED	Selected Area Electron Diffraction
SERS	Surface Enhanced Raman Spectroscopy
TGF	Transforming growth factor
TLR	Toll like receptor
VSM	Vibrating Sample Magnetometer
WHO	World Health Organisation
XRD	X-ray Diffraction

Abstract

Nearly one million cases of gastric cancer are diagnosed annually, making it the fourth most common cancer worldwide. It is also the second leading cause of cancer-related deaths, with approximately 700,000 fatalities each year. There is lack of early symptoms leading to delays diagnosis of gastric cancer, resulting in a five-year survival rate of just 15%.

Since 1994, *Helicobacter pylori* (*H. pylori*) has been perceived as a type I carcinogen for gastric cancer and is now observed as the most prominent etiologic source for cancer linked with infection, contributing to 5.5% of the cancer burden globally and 25% of all infection-associated cancers. *H. pylori* is responsible for 70-85% of gastric ulcers and 90-95% of duodenal ulcers. Nearly half of the world's population is having *H. pylori* infection, and while most infected individuals develop chronic inflammation, many do not exhibit any symptoms.

This work aimed towards developing a technology using a non-pathogenic strain of *H. pylori* coated with Iron-Oxide Nanoparticles (IONPs) to specifically target gastric cancer. The approach leverages hyperthermia-induced activation of the body's natural immune system. Given that *H. pylori* naturally infect the human stomach and duodenum, it can effectively deliver treatment to these tissues. IONPs serve as MRI sensitizers, allowing for the visualization of infected tissues, and they are responsive to Magnetic hyperthermia. After applying external high-frequency magnetic field, IONPs generate heat on the surface of the bacteria. This ruptures the bacterial membrane and in turn, spillage occurs in the tumor microenvironment, thereby activating the natural immunity. Further, this leads to the infiltration of immune cells like macrophages in the tumor microenvironment. These activated macrophages then cleanse the spillage along with the tumor cells. This proposed cancer treatment does not involve chemotherapeutic drugs, thereby avoiding the unsolicited aftereffects linked with chemotherapy.

The thesis entitled **"Iron-oxide Nanoparticles Coated on *Helicobacter pylori* for Gastric Cancer Treatment *via* Magnetic Hyperthermia"** represents the findings of the study and it is arranged into 5 chapters:

Chapter 1 gives a comprehensive introduction to gastric cancer and explores the existing literature on the subject, with a particular focus on the therapeutic approach of magnetic hyperthermia. This

chapter outlines the background, significance, and current understanding of gastric cancer, followed by a detailed review of studies and advancements linked with the utilization of magnetic hyperthermia for treating cancer.

Chapter 2 deals with the discussion of different kinds of terpenes derived from plants and their potential applications in gastric cancer treatment

Chapter 3 addresses protein-based iron oxide nanoparticles. This formulation aims to achieve targeted delivery of lactoferrin conjugated with iron oxide nanoparticles (LF-IONPs) to gastric tissue. When combined with hyperthermia, it is expected to offer enhanced efficacy in the treatment of gastric cancer.

Chapter 4 delves into the idea of immune activation through hyperthermia-treated *Helicobacter pylori* coated with iron oxide nanoparticles. It examines how this method employs the bacterium as a vehicle to deliver heat-sensitive therapeutic agents to a specific site in the body, with the goal of triggering the immune system to potentially achieve therapeutic effects.

Chapter 5 discusses a terpene-based nanoformulation involving artemisinin-loaded iron oxide nanoparticles. It explores the concept that delivering artemisinin conjugated with magnetic nanoparticles (ART-MNPs) into the gastric tissue, followed by hyperthermia treatment, could increase the effectiveness of gastric cancer therapy by overcoming tumor cell resistance to hyperthermia.

Chapter 6 summarizes the key findings, addressing how the research objectives were met and highlighting the study's contributions and limitations. It also outlines potential future research directions, suggesting areas for further exploration and practical applications of the findings to advance the field.

Chapter 1: Introduction and Literature review

1.1 Introduction

Globally, cancer is the second most deadly disease after heart disease [1]. In cancer, the body cells lose the property of normal division and undergo uncontrolled division, giving rise to abnormal cells that collectively lead to tumor formation [2]. The primary causative agents of cancer are ultraviolet radiation or ionizing radiation, bacterial infections, viral infections, parasitic infections, etc. [3]. Among different forms of cancer, gastric cancer is the 4th deadly after lung, breast, and colon cancer, costing 769,000 lives in 2020, with more than 1.09 million new cases being diagnosed [4], [5]. India's cancer burden will rise to 30 million by 2025. The primary causative agent of gastric cancer is the *Helicobacter pylori (H. pylori)* infection [6], which is a Gram-negative, microaerophilic, motile, flagellated spiral-shaped bacterium associated with 70- 85% of gastric cancer and considered a type I carcinogen for the disease. It is the most prominent etiologic source that is associated with other cancers, such as duodenal cancers (90-95%), and is responsible for 1/4th of all infection-linked cancers [7]. Infection with *H. pylori* typically begin in childhood, with many individuals remaining asymptomatic carriers until symptoms emerge later in life, if at all. Interestingly, most people infected with *H. pylori* do not experience any related symptoms [8]. Epidemiological data indicate that *H. pylori* infection rates are extremely high, affecting 85-95% of the population in developing nations and around 30-50% in developed nations [9] [10] [11]. Nearly 50% of the world's population is having *H. pylori* infection and majority of such colonized individuals develop coexisting chronic inflammation. Apart from *H. pylori*, various other factors, including smoking and consumption of tobacco-related products, a low-fiber diet, long-term stomach inflammation, obesity, family history, and salty and smoked eatables, increase the risk of gastric cancer [12].

The transmission mode of *H. pylori* is associated with the intake of contaminated food and water [13] [14] [15]. Factors such as poor hygiene, inadequate nutrition, and varying geographical conditions leads to the risk of infection. *H. pylori* has developed adaptive mechanisms, including acquiring virulence factors that help it survive in low pH environments. While the bacterium itself doesn't produce acid, it can neutralize stomach acid through the action of the urease enzyme [16]. Afterward, the bacterium utilizes its flagella for movement toward the gastric epithelium. *H. pylori* then uses adhesins to bind to host cell receptors, allowing for successful colonization and a long-lasting infection. Once established, the bacterium releases various effector proteins and toxins that damage host tissues. During the infection process, the release of chemokines activates the innate

immune response, leading to the recruitment of neutrophils and eventual onset of clinical symptoms [17]. Its pathogenicity is basically due to its genes, including *CagA, VacA, BabA, SabA, OipA, DupA, and FlaA* [6]. The role of these mentioned genes are given as follows:

***CagA*:** The *cytotoxin-associated gene A (CagA)* modulates the pathogenesis of *Helicobacter pylori (H. pylori)* infection. It is a virulent factor encoded by the cag pathogenicity island (cagPAI), a segment of the bacterial genome that enhances the bacterium's ability to cause disease. When *H. pylori* infects the gastric epithelium, it injects *CagA* into host cells *via* a secretion system i.e. type IV. After entering the host cell, *CagA* experiences phosphorylation and engages with various intracellular signaling pathways. This interaction disrupts normal cellular functions, leading to several pathological outcomes: Alteration of Cell Morphology, Increased Inflammation, Cellular Proliferation and Survival, and Disruption of Tight Junctions. The occurence of *CagA-positive H. pylori* strains is closely linked with more severe disease outcomes, including a higher risk of peptic ulcers and gastric cancer. Therefore, *CagA* plays a central role in the virulence of *H. pylori* and the pathogenesis of its related diseases [18].

***VacA*:** The vacuolating cytotoxin A (*VacA*) is another significant virulence factor in the pathogenesis of *Helicobacter pylori (H. pylori)*. The *VacA* protein, encoded by the *VacA* gene, contributes to the bacterium's ability to cause disease by inducing vacuole formation in host cells; *VacA* triggers the generation of large vacuoles in gastric epithelial cells, disrupting cellular function and contributing to cell death. It also interferes with immune responses and promotes inflammation [19].

BabA: Its ability to bind specifically to the Lewis B antigen allows *H. pylori* to adhere tightly to the gastric epithelium. This attachment is crucial for colonization and contributes to the bacterium's ability to resist being cleared by the gastric environment. The interaction between *BabA* and host cells triggers inflammatory responses, including the release of cytokines, which contribute to the chronic gastritis associated with *H. pylori* infection [20].

SabA: It facilitates *H. pylori's* binding to sialylated glycan structures on the inflamed gastric epithelium, which enhances bacterial colonization, especially in areas of the stomach where inflammation is present. The expression of *SabA* is upregulated in response to inflammation, which allows *H. pylori* to persist better in the hostile environment of the inflamed gastric mucosa [21].

OipA: *OipA* is a pro-inflammatory protein that stimulates the production of interleukin-8 (IL-8), a potent chemokine that recruits neutrophils to the site of infection. The presence of neutrophils and other immune cells leads to chronic inflammation, which is a hallmark of *H. pylori* infection and contributes to mucosal damage [22].

DupA: Studies have shown that the presence of the *dupA* gene is correlated with a higher incidence of duodenal ulcers. *DupA* is believed to enhance the inflammatory response in the gastric and duodenal mucosa, leading to ulcer formation [23].

FlaA: The *flaA* gene in *Helicobacter pylori* encodes *flagellin A*, a major structural component of the bacterium's flagella. Flagella are essential for the motility of *H. pylori*, enabling the bacterium to navigate through the viscous environment of the stomach mucus and colonize the gastric epithelium. This motility is critical for the bacterium's ability to establish infection and contribute to disease. The motility provided by the flagella also helps *H. pylori* evade the host's immune defenses. By moving through the mucus layer and avoiding areas of intense immune activity, the bacterium can maintain a persistent infection [24].

Unfortunately, in most cases, the diagnosis of gastric cancer is delayed due to the absence of early specific symptoms, and the five-year survival rate is only 15% [25]. This low rate is despite different treatment modalities for gastric cancer, such as chemotherapy, surgical treatments, radiation therapy, and immunotherapy. Therefore, prevention is a more efficient way of gastric cancer management than treating it. The treatment options for gastric cancer vary significantly depending on the stage of the disease. For each stage, different treatments are listed below:

Stage 0:

Endoscopic Mucosal Resection (EMR): This procedure is used when cancer is confined to the innermost layer of the stomach (the mucosa). EMR involves using an endoscope to remove the cancerous tissue without the need for open surgery.

Subtotal Gastrectomy: For larger or more extensive lesions, part of the stomach may be surgically removed. This might include the removal of nearby lymph nodes to check for any spread of the disease.

Stage I:

Partial or Total Gastrectomy: The primary treatment is surgery, which may involve removing part (subtotal gastrectomy) or all of the stomach (total gastrectomy), along with nearby lymph nodes.

Endoscopic Submucosal Dissection (ESD): For very early-stage IA cancers that are small and confined to the mucosa, this minimally invasive procedure might be used instead of major surgery

Adjuvant Chemotherapy: For stage IB, chemotherapy is often recommended after surgery to eliminate any remaining cancer cells and reduce the risk of recurrence. Common chemotherapy regimens include capecitabine (1000 mg/m^2) and oxaliplatin (85 mg/m^2).

Stage II:

Neoadjuvant Chemotherapy: Chemotherapy is administered before surgery to shrink the tumor and

improve the chances of successful surgical removal.

Surgery: The mainstay treatment is still surgery (partial or total gastrectomy) with lymphadenectomy (removal of lymph nodes).

Adjuvant Chemotherapy/Radiation Therapy: After surgery, patients often receive chemotherapy (such as FLOT: 5-FU (2600 mg/m²), leucovorin (200 mg/m²), oxaliplatin (85 mg/m²), and docetaxel (50 mg/m²)) or chemoradiation (combined chemotherapy and radiation therapy) to target any remaining microscopic disease.

Stage III:

Neoadjuvant Chemotherapy: Like stage II, chemotherapy before surgery is standard to reduce the tumor size.

Surgery: Partial or total gastrectomy is performed, along with the removal of lymph nodes and possibly surrounding tissues if the cancer has spread locally.

Adjuvant Chemoradiation: After surgery, a combination of chemotherapy and radiation therapy is often recommended to eliminate remaining cancer cells and reduce the risk of recurrence.

Targeted Therapy: For patients with HER2-positive tumors (metastatic gastric cancer), trastuzumab (Herceptin 8 mg/kg IV infusion) is often added to the chemotherapy regimen.

Stage IV:

Palliative Care: The primary goal at this stage is symptom relief and improvement of the life quality, as the cancer is typically not curable. This includes pain management, nutritional support, and relief from obstruction using stents or other surgical interventions.

Chemotherapy: Systemic chemotherapy is used to control the disease, often with regimens like FOLFOX or CAPOX (Capecitabine-1000 mg/m² + Oxaliplatin-130 mg/m²). The goal is to slow the progression of the cancer and prolong survival.

Targeted Therapy: HER2-positive cancers may be treated with trastuzumab (8 mg/kg IV infusion) in combination with chemotherapy. Additionally, ramucirumab (8 mg/kg IV infusion) (a VEGF inhibitor) may be used either alone or with chemotherapy.

Immunotherapy: For cancers that are PD-L1 positive or have high microsatellite instability (MSI-H), immunotherapy with pembrolizumab (200 mg IV infusion) (Keytruda) or nivolumab (240 mg IV infusion) (Opdivo) may be used.

Clinical Trials: Participation in clinical trials may provide access to new therapies and treatment approaches that are not yet widely available [26].

Further, available treatments involving modern chemotherapeutic agents show many limitations and side effects, including hair and weight loss, diarrhea, anemia, blood clots, and heart, kidney, and

liver damage, compromising the life quality of the patient [27]. Additionally, the effectiveness of surgery and radiation therapy is primarily limited to the early stages of gastric cancer progression [28]. There is an urgent need for alternative strategies to manage the disease more effectively. The high recurrence rate, the development of resistance to standard chemotherapy, and the often late-stage diagnosis of gastric cancer contribute to poor prognosis and limited treatment options.

One potential alternative is the use of the microbiome to invoke an immune response is an emerging and promising approach in treating gastric cancer. The gut microbiome, which consists of trillions of microorganisms living in the digestive tract, plays a vital role in modulating the immune system. This interaction between the microbiome and the immune system is increasingly being explored as a potential therapeutic strategy for various cancers, including gastric cancer. Gastric cancer is one of the best examples of human inflammation-associated cancer [29]. Certain gut bacteria can stimulate the immune system, enhancing the body's ability to recognize and attack cancer cells. For instance, Bifidobacterium species have been shown to enhance the efficacy of immune checkpoint inhibitors by promoting the activation of CD8+ T cells, which are essential for targeting and destroying cancer cells. The microbiome can also influence the tumor microenvironment, making it more susceptible to immune attacks. Specific bacterial species can produce metabolites that inhibit tumor growth and stimulate immune responses against the tumor [30] [31]. To understand their viability, a brief look at the role of inflammation and the body’s natural response to it is in order.
When the body encounters a pathogen, a complex immune response is triggered to recognize, attack, and eliminate the invading organism. This response involves both the innate and adaptive immune systems. The innate immune system provides the first line of defense against pathogens and responds quickly but nonspecifically to a wide range of invaders. The pathogen is recognized by pattern recognition receptors (PRRs) on immune cells like macrophages, dendritic cells, and neutrophils. These PRRs detect pathogen-associated molecular patterns (PAMPs) such as bacterial cell wall components, viral RNA, or fungal cell wall elements. Upon recognition of a pathogen, immune cells release cytokines (TNF-α, IL-1, IL-6) and chemokines (Monocyte Chemoattractant Protein-1, IL-8), which recruit additional immune cells to the site of infection and initiate inflammation. For instance, macrophages phagocytose (engulf and digest) the pathogens, and dendritic cells present pathogen-derived antigens to T cells. Dendritic cells and other antigen-presenting cells (APCs) process the pathogen and present its antigens on their surface using major histocompatibility complex (MHC) molecules. These antigens are then recognized by T cells. Helper T cells (CD4+ T cells) recognize antigens presented by MHC class II molecules and become

activated. They then secrete cytokines that stimulate other immune cells. Cytotoxic T cells (CD8+ T cells) recognize antigens presented by MHC class I molecules and kill infected cells directly. B cells recognize antigens and, with the help of activated helper T cells, differentiate into plasma cells that produce specific antibodies. These antibodies neutralize pathogens, mark them for destruction by phagocytes, and activate the complement system. After the pathogen is cleared, memory B and T cells remain in the body. These cells remember the pathogen, allowing for a faster and stronger response if the pathogen is encountered again. Once the pathogen is eliminated, the immune response subsides. Regulatory T cells help dampen the immune response to prevent excessive inflammation and tissue damage. The body then enters a recovery phase, where damaged tissues are repaired, and homeostasis is restored [32] [33].

Magnetic nanoparticles are a fascinating area of research, especially in their use for immune activation. They offer several advantages, such as precise control over their movement and targeting using magnetic fields and the potential for minimal side effects. These can be designed to activate immune cells directly. For example, they might be coated with antigens or other stimulatory molecules that trigger an immune response when they interact with immune cells. Upon exposing to an alternating magnetic field, magnetic nanoparticles can generate heat through a process called magnetic hyperthermia. This localized heating can be used to stimulate immune cells or enhance the effectiveness of treatments. Additionally, they can be combined with other therapeutic agents to enhance their delivery and efficacy. For instance, combining magnetic nanoparticles with chemotherapeutic agents or immunomodulators could lead to more effective cancer therapies.

Magnetic nanoparticles, made biocompatible, play a crucial role in various biomedical applications, ranging from imaging to therapy [34]. To serve as efficient carriers for drug delivery, they should be small in size, have a large surface-to-volume ratio, and be properly functionalized for site-specific targeting [35]. Amidst the various kinds of magnetic nanoparticles, iron oxide nanoparticles find common use because to their magnetic properties and biocompatibility across a variety of biomedical applications, including drug and gene delivery, biosensors, magnetic particle imaging (MPI), and hyperthermia (HM) treatment [36], [37], [38]. Superparamagnetic iron oxide nanoparticles can be engineered to respond specifically and efficiently within the tumor microenvironment [39], [40], [41]. These particles can be magnetized *via* external magnetic field but exhibit no residual magnetic interactions after the removal of the field, indicating good dispersion and excellent targeting capacity [42]. This characteristic makes them highly advantageous for magnetic hyperthermia due to their ability to disperse within localized minor

regions, creating a difference in temperature profiles between normal and tumor cells [43].

Various particles have been synthesized to harness their anti-cancer potential against different cancers by using hyperthermia treatments. Mohamadkazem *et al.* synthesized iron oxide-gold nano complexes and used an external field to physically navigate these magnetic nanoparticles to the target melanoma cells, effectively killing them through electron beam therapy [44]. Kamalabadi *et al.* synthesized gold-coated magnetic nanoparticles which were functionalized with folate for their use in treating HPV-positive oropharyngeal cancer by enhancing uptake and cell death through the application of an external field [45]. Further, hyperthermia has been found to enhance drug release from formulations and develop potent theranostic agents for anti-cancer activity against colorectal cancer [46].

This thesis aims to develop a technology that uses a non-pathogenic strain of *Helicobacter pylori* coated with Iron-Oxide Nanoparticles (IONPs) to target gastric cancer specifically. This will be done by hyperthermia-induced activation of the body's natural immune system. *H. pylori* naturally infects the human stomach and duodenum. Therefore, *H. pylori* will be very effective in treating these infected tissues. IONPs are MRI sensitizers. They can be used to visualize the infected tissues. Further, IONPs are magnetic hyperthermia-responsive moieties. Therefore, when exposed to a high-frequency magnetic field, IONPs generate heat that will kill cancer cells and ingested bacteria. The thermal annihilation of the bacteria will result in the spillage of the foreign particles to the surrounding tissue environment. This will draw antigen-presenting cells (APCs) into the tumor microenvironment. Subsequently, the activated macrophages will cleanse the tumor microenvironment by flushing out the foreign particulates, including cancer cells. Further, exposure to the foreign particles and the intercellular component of the cells will also activate the adaptive immune system. As a result, the body will train itself to remove the cancer cells.

The ultimate aim of my thesis is to evolve a novel technology that will control cancer growth by activating its immune system without the involvement of chemotherapy so that it can control the side effects of the same, as presented in **Figure 1.1.**

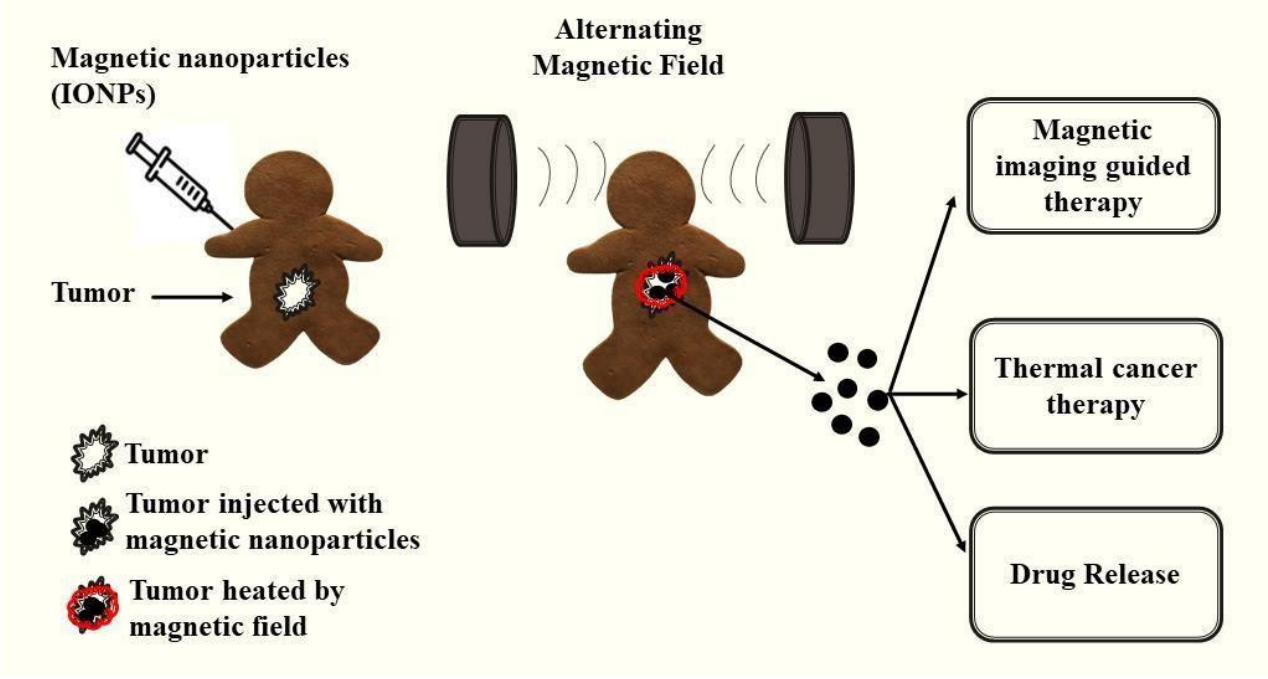

Figure 1.1: A visual representation of the mechanism of magnetic nanoparticles for targeted imaging and therapy of tumor cells.

1.2 Treatment

Magnetic Nanoparticles (MNP) based hyperthermia as anti-cancer therapy[47].

Magnetic hyperthermia enabled by nanotechnology allows the remotely induced local heat using the magnetic energy losses of magnetic nanoparticles under an oscillating magnetic field. Some magnetic nanoparticles can transform electromagnetic energy into heat, which increases the temperature in the intended regions in the human body where the tumor cells and the nanoparticles are located. Therefore, the generation of heat by these nanoparticles which acts as nano-heaters can be controlled externally by applying or removing an oscillating magnetic field. The electromagnetic radiation used in magnetic hyperthermia is in the radio frequency range (between several kHz and 1 MHz). The specificity of this technique is achieved by the higher sensitivity of the tumoral cells to temperature increases above 42°C, temperatures at which the natural enzymatic processes that keep the cells alive are destroyed, allowing their selective killing [48]. The saturation magnetization should also be as high as possible to guarantee the efficient heating of the nanoparticles under the oscillating magnetic field at low nanoparticle concentrations. The superparamagnetic properties of magnetic nanoparticles are totally dependent on their size. The particle size is kept below a critical size above which magnetic nanoparticles become ferromagnetic (superparamagnetic limit), which is, in principle, an undesired magnetic behavior for biomedical applications due to a potential particle aggregation phenomenon. The commonest barrier found in

most tissues is the continuous blood capillaries type, so the separation between the endothelial cells along the basement membrane will determine the efficiency of the hyperthermia therapy [49]. If the magnetic nanoparticles are small enough to cross the blood barrier, they could penetrate and distribute more homogeneously inside the tumor, provoking a heat diffusion that would kill a more significant number of neighboring tumor cells[50],[51],[52],[53].

1.3 Magnetic Hyperthermia (MH)

MH utilizes the heat produced by the magnetic nanoparticles (MNPs) upon application of an alternating magnetic field (AMF)[54]. The most substantial benefit of MNPs-mediated MH (MNPs-MH) is in the deep tissue penetration and selective killing of cancer cells without harming the surrounding healthy tissues[55],[56],[57],[58]. MNPs-MH helps in understanding intracellular hyperthermia[59], as it directly delivers therapeutic heating to the cancer cells, and this intracellular hyperthermia can be further improved by conjugating the cell-targeting ligands with MNPs [60]. Primarily, MNPs-MH therapy involves raising the tumor's local temperature within the range of 43-45 ºC, which results in physiological changes in the cancer cell, eventually leading to their apoptosis or necrosis[55],[58]. To make use of MNPs-MH clinically and in cancer treatment possible, it is essential that sufficient heat must be delivered within the whole tumor mass while not affecting the surrounding normal tissue. This requires careful control of the AMF parameters, particularly the prodict Hxf, which must remain within the biomedical safety limit of $H \times f < 5 \times 10^9$ [61]. Because of this limitation in AMF, the therapeutic efficiency of MNPs-MH depends on the heat conversion efficiency of MNPs.

Amidst various MNPs, superparamagnetic iron oxide nanoparticles (SPIONs) are extensively used as MNPs-MH agents due to their high biocompatibility and biodegradability. MNPs are magnetic nano-mediators that mediate the conversion of electromagnetic energy to thermal energy. To improve the therapeutic efficacy of MNPs-MH, the most fundamental strategy is to increase the thermal conversion efficiency of MNPs. This can be achieved by controlling the particle size, altering composition, and modifying the shape and surface of the nanoparticles [62].

1.4 Role of hyperthermia in treating Gastric cancer

The accumulation of genetic alterations in various genes, such as oncogenes, mismatch repair genes, and tumor-suppressive genes, is called Gastric cancer carcinogenesis. The balance between cell proliferation and apoptosis is required to maintain homeostasis, while the imbalance between these causes gastric cancer. A multifactorial process is involved in its development, and different

conditions influence the occurrence of cancer, which includes *H. pylori* infection, history of gastric cancer, history of an adenomatous gastric polyp more significant than 2 cm, or chronic atrophic gastritis or pernicious anemia, alcohol, smoking, consumption of red meat, and obesity[63]. Altered cell proliferation, apoptosis, and some epigenetic modifications to the tumor suppressor genes might occur, which could eventually lead to inflammation-associated oncogenesis[64]. Some patients with persistent *H. pylori* infection develop gastric atrophy followed by intestinal metaplasia, which might evolve into dysplasia and adenocarcinoma. Most gastric cancers are gastric adenocarcinomas[65],[66],[67] but are highly heterogeneous with respect to architecture and growth, cell differentiation, histogenesis, and molecular pathogenesis[68],[69].

1.5 Research Gaps and Hypothesis

H. pylori is a well known causative agent of gastric cancer and plays a crucial role in the gastric cancer-associated microbiome, as it specifically binds and adheres to the gastric tissue. In the proposed research, we aim to exploit this feature by using an avirulent strain of *H. pylori* to deliver and mediate hyperthermia treatment for gastric cancer. This strain will adhere to the gastric tissue without causing or aggravating cancer. To the best of my knowledge, the tissue microflora, including *H. pylori*, has not been explored for the delivery of iron-oxide particles and mediation of hyperthermia therapy. We believe that it could be an ideal candidate for hyperthermia therapy within the deep tissue environment, as the generated heat would not only kill the bacteria in the tumor microenvironment but also activate the body's immune system.

Superparamagnetic nanoparticles have been used in hyperthermia treatments for various cancers, such as cervical cancer, glioblastoma, and prostate cancer, where they have been shown to activate both innate and cell-mediated immunity. Since tumor microbiomes and iron-oxide nanoparticles are potent immune activators, we hypothesize that using microbes—specifically an avirulent strain of *H. pylori* coated with superparamagnetic nanoparticles—could enhance the body's immune response, offering a more efficient cancer treatment compared to conventional hyperthermia approaches. In response to this proposed treatment, the body's natural immunity would be activated, involving the infiltration of tissue macrophages, NK (Natural Killer) cells, and the secretion of various cytokines, which would help clear the *H. pylori* antigen from the target site. Concurrently, tumor cells would be damaged by the heat dissipated in the tumor microenvironment and subsequently cleared by the body's immune response.

This approach aligns with the established efficacy of immune clearance in treating various diseases. We aim to explore whether gastric cancer can be treated by activating natural and cell-mediated immunity, leveraging the immune-activating potential of microbes in cancer tissue. Given that *H. pylori* is associated with gastric cancer, we propose using this bacterium to attract immune cells and kill cancer tissue through magnetic hyperthermia. As bacteria are killed within the tumor tissue, they would attract tissue macrophages, activating a cascade of immune events leading to the clearance of cancer cells, as illustrated in **Figure 1.2**. By pursuing this strategy, we hope to develop a reliable method for treating gastric cancer with minimized side effects.

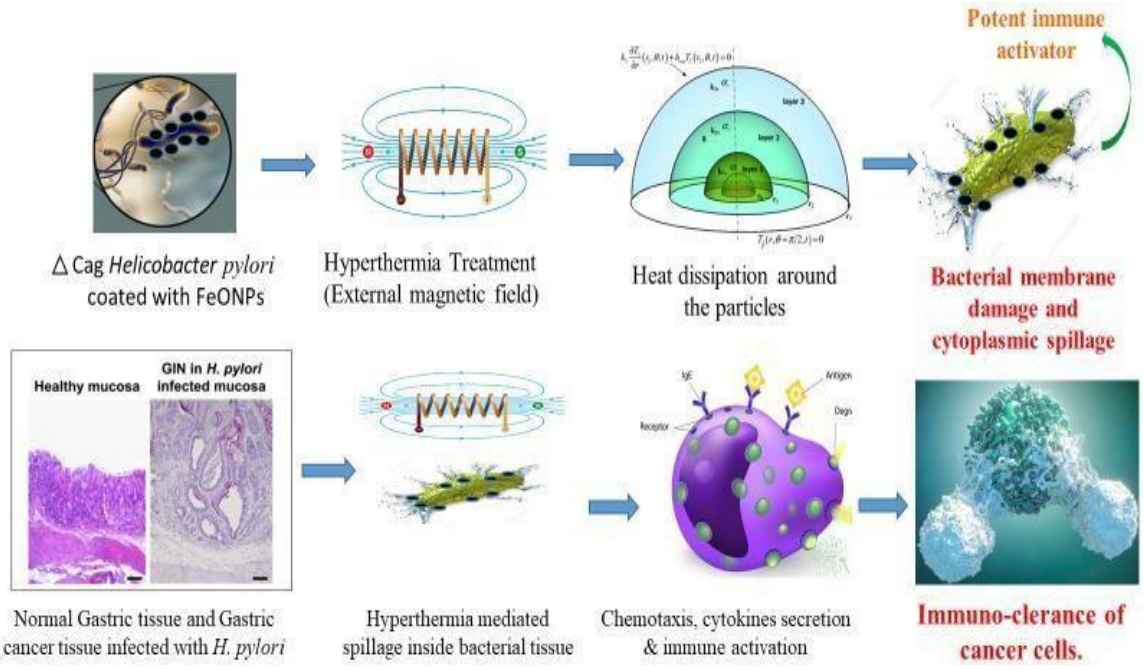

Figure 1.2. It represents the Hypothesis.

Objectives:

1. Preparation, characterization and functionalization of Iron oxide nanoparticles (IONPs) with polymers (like PEG, lactoferrin) and coating them on the surface of *Helicobacter pylori.*

2. *In-vitro* immune activation of macrophages with heat-killed IONPs coated *H. pylori.*

3. Perturbation of hyperthermia resistance in gastric cancer cell line by using Artemisinin-protected Iron-oxide Nanoparticles.

Expected outcomes:

1. Successful Synthesis and functionalization of the IONPs.
2. Effective coating of IONPs on the surface of *H. pylori.*
3. The hyperthermia treated IONPs-coated *H. pylori* should stimulate macrophages, leading to increased production of pro-inflammatory cytokines and activation markers. The combination of IONPs and *H. pylori* should promote a stronger immune response.
4. The Artemisinin-protected IONPs should enhance the sensitivity of gastric cancer cells to hyperthermia. Artemisinin's protective effects combined with hyperthermia treatment could potentially lead to greater tumor cell destruction, indicating a synergistic effect between the drug and hyperthermia.

Chapter2: A review on terpenes for treatment of Gastric cancer: Current status and nanotechnology enabled future

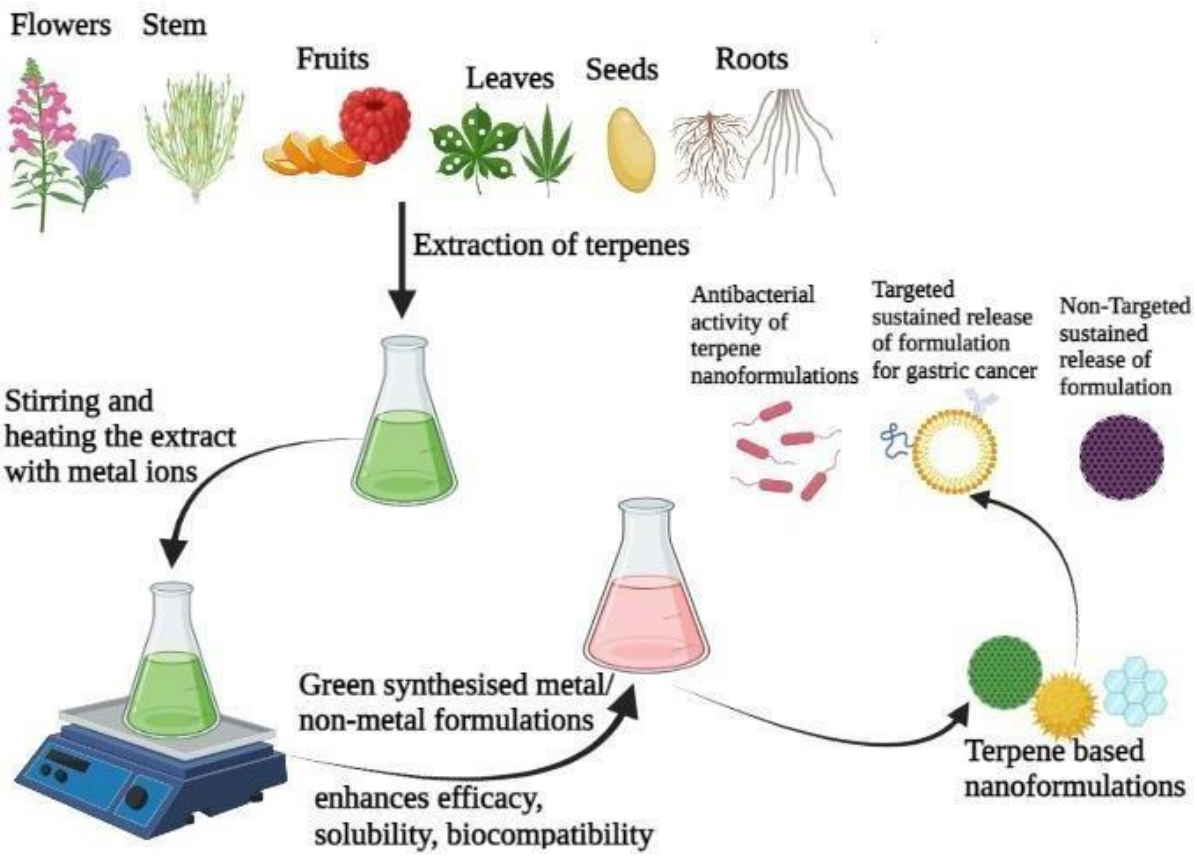

Figure 2.1. depicts the basic green synthesis process for making natural terpene-based nano-formulations from the extract obtained from different plant parts, including flowers, fruits, roots, stems, and leaves, and their mode of action on tumor cells.

Abstract

Eighty-five percent of gastric cancer is caused by *Helicobacter pylori* infection. Delays in detection, limited efficacy, and significant side effects of the available treatments lead to 5 year survival chance of only 32%. Therefore, better remedies are required. Numerous studies have been published on herbal medications offering an edge over conventional medicines. Secondary metabolites, such as different polyphenolic compounds, including terpenes, are key players for therapeutic advantages. The antimicrobial, anticarcinogenic, anti-inflammatory, etc., activities of the biocompatible active ingredients make these compounds suitable for therapeutic use. Despite such

advantages, the use of herbal medicine in gastric cancer treatment is limited. In this article, we describe the therapeutic potential and limitations of terpenes, followed by potential advantages offered by the combinatorial effects of terpenes with their nanoconjugates. These include increasing the anticancer and antimicrobial potency of drugs as well as resolving drawbacks, including targeted delivery, stability, half-life, etc, thus making them suitable for gastric cancer treatment. The article concludes with a detailed discussion of the challenges encountered in deploying targeted secondary metabolites and their future developmental prospects to provide ideas and insights for future research.

2.1 Introduction

Cancer is one of the leading cause of death globally grabbing second position, following heart disease [1]. It is characterized by uncontrolled cell division and tumor formation due to the loss of normal cellular regulation [2]. Major cancer causes include ultraviolet and ionizing radiation, as well as bacterial, viral, and parasitic infections [3]. Gastric cancer ranks fourth in terms of mortality, with 769,000 deaths and over 1.09 million new cases reported in 2020 [4], [5]. Infection with *Helicobacter pylori* (*H. pylori*), a Gram-negative, microaerophilic bacterium, is basic cause of gastric cancer, contributing to 70-85% of cases, and classified as a type I carcinogen [6]. H. pylori is also associated with duodenal cancers and 25% of all infection-related cancers [7]. Key pathogenic factors include genes such as CagA, VacA, and BabA [6]. H. pylori affects approximately half the global population, many of whom develop chronic inflammation. Additional risk factors include smoking, a low-fiber diet, chronic stomach inflammation, obesity, and a high intake of salty and smoked foods [12]. The late diagnosis of gastric cancer, often due to the lack of early symptoms, results in a low five-year survival rate of 15% [25]. Current treatments, including chemotherapy, surgery, and radiation, have significant side effects and are mainly effective in the initial phases of the ailment [27], [28]. Therefore, exploring alternative management strategies, such as herbal formulations, is crucial for effective prevention and treatment.

A biological response to any damaging stimuli such as pathogens, wounds, foreign bodies, or infection is inflammation [70]. This process is the body’s way to protect itself by aiming to remove that inflammation using a natural body process - self-defense. In many cases, the body produces cytokines against a particular disease or foreign substance. In a few instances, these cytokines are overexpressed by the body's immune system. It is amongst the best examples of human inflammation-associated cancer [29]. Synthetic anti-inflammatory drugs are being used to suppress or inhibit these mediators. These synthetic drugs have benefits and side effects that compromise

patients' quality of life. For this reason, currently, people are expecting or even preferring treatments that involve natural products with safe toxicological profiles, leading to the exploration of these for alternative drug delivery treatments [71].

Nature is full of resources in the form of secondary metabolites that humankind has used for a long time to manage many diseases, including gastric cancer. The formulations are well documented in a few cases, but additional documentation is needed for most. Many of these herbal formulations are already in use in India, China, Vietnam, and Africa in various forms through different systems of medicine, such as Ayurveda, Unani, Siddha, and Homoeopathy [72]. These medicines are mostly a mixture of various plant secondary metabolites, including phenolics, alkaloids, saponins, terpenes, sterols, and sphingolipids. For example, in many plants, the extract has anti *H. pylori* activity, suggesting their potential for treating gastric cancer. In addition, many of the compounds present in such herbal formulations can be administered orally to work on the target site without being absorbed by the intestine or stomach. The net result is targeted delivery and site-specific activity, which increases their potential for treatment with reduced side effects. In other words, herbs demonstrates a crucial part in controlling growth and progress of cancer and can help patients to overcome the side effects caused by chemotherapeutics. They enhance the body's immunity through naturally occurring compounds in them and thus prevent the spread of cancer by any means, including growth, metastasis, and invasion. Therefore, using these formulations instead of radiation and chemotherapy will be a better option as they do not cause any of the ill effects that conventional therapies cause, such as fatigue, hair loss, mouth sores, nausea, vomiting, and organ failure [73].

In this framework, a class of natural compounds named terpenes, a highly diverse family of natural products, has drawn attention due to their capability of selectively killing tumor cells without hampering normal cells. These are synthesized by plants and are also called secondary metabolites. Terpenes have 55,000 members with different chemical structures and curing potentials [74]. They suppress or inhibit the growth of several cancers, such as breast, skin, stomach, pancreatic, colon, and prostate, without damaging or contributing any toxicity to normal cells as they exhibit pleiotropic actions by acting on a target in multiple ways. They also inhibit protein synthesis by targeting the main events crucial for the process. They are among the leading herbal formulations in cancer treatment and are discussed in detail in Section 2. However, despite the remedial effect and other advantages such as biocompatibility, safety, non-invasiveness, convenience, and low cost in the treatment of cancer as compared to conventional chemotherapy [75], many natural formulations, including terpenes, have not been widely deployed in modern medicine due to certain problems associated with their transport across the body. Conventionally, they are given as such in

different ways through food in the form of supplements or directly as herbal medication, but they have certain pharmacological and chemical issues associated with them, such as low water solubility, low permeability, stability, reduced bioavailability, sensitivity to environmental conditions (temperature, pH, humidity), chemical degradation or volatilization being few of them [76]. This is precisely where nanotechnology can help overcome these disadvantages of herbal medicines.

Nanotechnology involves the utilization of critical features of materials at the nanoscale and consists of developing nanomaterials between 1-100 nm by manipulating the structures at an atomic level. Nanomaterials have unique electrical, optical, and magnetic properties, a large surface area to volume ratio due to which they exhibit specific properties such as enhanced catalytic activity, biological activity, non-linear optical performance, and thermal conductivity, and are governed by the laws of quantum mechanics [77]. They can be delivered as liposomes, vesicular systems, nano-emulsions, and solid lipid nanoparticles. Moreover, the use of these terpenes in the form of nano-formulations has been shown to enhance their solubility, stability and bioavailability, anti-proliferative activity, prevention from biological and chemical degradability and cell toxicity, enhanced specificity and pharmacological activity, and improved distribution of tissue macrophages along with sustained release [78], [79], [80]. Nano-delivery systems have been used to deliver all the herbal compounds irrespective of their hydrophobic or hydrophilic nature and thus can be used for the transfer of hydrophobic terpenes via encapsulating them with nanoparticles, which enhance their potency. Some of the terpenes are generally recognized as safe penetration enhancers. As a result, they can serve as excipients for other drugs or phytochemicals and make them suitable for administration through topical routes [76]. For instance, after loading celastrol into poly (ethylene glycol)-block-poly(ε-caprolactone) nano-polymeric micelles, its availability is enhanced. The nano-encapsulated celastrol was found to exhibit antitumor activity by reducing the expression of Bcl-2, NF-κB, and phospho-NF-κB p65 proteins at 54.4 μg/ml after 48 h of the treatment [81]. Their anti-proliferative activity has also been determined using different prostate cancer cell lines (LNCaP, DU-145, and PC3) by exposing the cells with 0.5-2.0 μM concentration of CS-NPs [82]. The results exhibited inhibition of concentration-dependent proliferation. In a nutshell, nanotechnology has fundamentally changed the way many diseases, including gastric cancer, are diagnosed and treated. To this end, in this review article, we focus on different active natural terpenes obtained from natural sources, their role in controlling gastric cancer, and directions for future research in gastric cancer management.

2.2 Natural terpenes for treating gastric cancer

An active area of global research is to develop effective anti-cancerous products from natural materials such as medicinal plants or effective medicinal components [83], [84]. Of all the available human medications, one-third are derived from herbal plants or extracts. Based on their positive aspects, physicians and researchers encourage their consumption. Apart from cancer, they are widely used in different applications. Several dietary products like fruits, vegetables, cereals, and spices exhibit anti-cancerous activity to a great extent, and it was found that there is an inverse linkage between the uptake of natural products and cancer cases [85], [86], [87]. The primary responsible factor for this salutary action is the presence of different phytochemicals, which promote various mechanisms to prevent gastric cancer. The effective means for gastric cancer are cell proliferation or *H. pylori* inhibition, autophagy, apoptosis, anti-angiogenesis, or suppressed cell metastasis [87], [88], [89].

2.3 Natural Terpenes and their role in gastric cancer treatment

Terpenes fall under the largest and most diverse class of naturally obtained nearly ~30,000 different polymeric compounds made up of isoprene, or 2-methyl-1,3-butadiene $(CH_2=C(CH_3)-CH=CH_2)_n$ where n indicates the number of isoprene units (where $n \geq 2$). Terpenes play an essential role in plants' defense mechanisms, protect them from herbivores, and generate disease resistance. They play different roles in plants, including serving as thermoprotectants, and playing signaling and medicinal functions. They also work as solvents or flavoring agents [90]. In addition, they have antimicrobial, anticarcinogenic, anti-inflammatory, antiallergic, and neuroprotective properties [91]. Not surprisingly, numerous researchers have indicated that they exhibit an equally essential part in supporting human health.

Depending on the number of isoprene units, they are categorised into monoterpenes, diterpenes, triterpenes, and sesquiterpenes [90]. A brief description of these follows.

2.4 Monoterpenes – They comprise a large group that performs numerous biological activities and act as antioxidants, anti-inflammatory, anti-diabetic, and antitumor agents. They also assist in neuroprotection, hepatoprotection, and cardio-protection [92], [93]. Chemically, they consist of 2 isoprene units formulated by five carbons together head-to-tail. These biochemically active units are diphosphate esters, isopentyl diphosphate, and dimethylallyl diphosphate. Monoterpenes are further subdivided into acyclic, monocyclic, bicyclic, and iridoid glycosides [94]. Terpenes mainly occur as active components of essential oils and fixed oils of plants and related sources [92]. Besides their biological activities, they are also used as fragrant sources for making cosmetics and perfumes

due to their strong aroma and odor [95]. Some of the most common monoterpenes employed for anticancer activity are described below.

2.4.1 Carvacrol – It is a monoterpene polyphenol mainly obtained from the Lamiaceae family's essential oils and is chemically 5-isopropyl-2-methyl phenol [96]. It is mainly utilised in different biological applications to prevent the proliferation of chemotherapy-resistant cells, such as human ovarian adenocarcinoma cells and tumor cells [97], [98]. Compared to single drug-loaded nanoparticles, the human serum albumin particles, when loaded with carvacrol and chemotherapy agents, yield better activity in treating gastric cancer in vitro [99] and induces cell death by directly activating the mitochondrial pathway. They inhibited ROS generation and DNA damage caused by cell proliferation. Proteins that regulate apoptosis and the antiproliferative effect of carvacrol are Bax, B-cell leukemia/lymphoma 2 protein (BCl_2), Cysteine-aspartic proteases) (Caspase)-3, and Caspase-9 [100]. In addition, they exhibit Glutathione (GSH) reducing effects on cells [91].

2.4.2 Geraniol – It is an acyclic isoprenoid monoterpene, present in the natural oils of fragrant herbal plants. It inhibits cell proliferation, apoptosis induction, and arrest cell cycle in the gastric cancer cell line. The major factors involved are ROS production through mitochondria and downregulation of the mitogen-activated protein kinase (MAPK) pathway, mainly engaged in migration, survival, differentiation, and metabolism [101]. Further, there is a drastic downfall in the phosphorylation of essential MAPK signaling molecules, including p38, Jun N-terminal kinases (JNK), and extracellular signal-regulated kinase (ERK). The proapoptotic proteins like Bax, Caspase-3, -8, and -9 are unregulated, whereas there is a reduction in Bcl_2 expression after treatment with geraniol, which induces apoptosis [101].

2.4.3 D-carvone – It is a cyclic and natural dietary monoterpene commonly present in the vital oils of certain plants, which are aromatic and medicinal in nature, including caraway, dill weeds, etc. [102]. Apart from other biological properties, it is found to prevent lung injury in mice [103], lower the lipid content in the blood, and can be used to cure diarrhea, acidity, and other gastric ailments [104]. The carvone is responsible for inhibiting cell growth and induces apoptosis by regulating ROS production. It decreases the phosphorylation of Janus kinase/Signal transducer and activator of transcription (JAK/STAT 3) molecules involved in cell growth in a dose-dependent manner [103].

2.4.4 Paeoniflorin – It is a monoterpene glycoside of the Paeoniaceae family and is extracted from the roots of *P. lactiflora (Paeonia lactiflora)*. It exhibits hepatoprotective, immunomodulatory, and antitumor activity. It prevents the multiplication of gastric cells and initiates apoptosis. It mediates the upregulation of Bcl-2 by blocking the nuclear factor κ-light-chain-enhancer of activated B cells

(NF-κB) pathway in a dose and time-dependent manner. It also prevents the phosphorylation of IκBa (nuclear factor of kappa light polypeptide gene enhancer in B-cells inhibitor, alpha), that further inhibits the NF-κB activity and NF-κB p65 expression. It is also found to upregulate the expression of minR-124 and block the phosphoinositide-3-kinase-protein kinase B/Akt (PI3k/Akt) and STAT3 pathway [105]. It inhibits the Notch 1 pathway [106].

2.5 Diterpenes – They belong to a naturally found class of chemical constituents comprising four isoprene units combined, thus having a core skeleton of 20 carbons. They are derivatives of geranyl pyrophosphate [107] and are produced by plants, animals, and fungi via 3-hydroxy-3-methylglutaryl coenzyme A (HMG-CoA) reductase pathway 3 [108]. They exhibit several biological applications like antioxidants, antimicrobial, anti-inflammatory, anticarcinogenic, and neurobiological agents [109]. Compared with monoterpenes and sesquiterpenes, they are less in number and less volatile [110]. Some of the significant diterpenes are discussed below.

2.5.1 Andrographolide – It is a diterpene lactone mainly obtained from *A. paniculate* (Andrographis paniculate), a traditional Chinese herbal plant belonging to the Acanthaceae family that reduces swelling and is used as a blood-cooling agent and a detoxifier for the body [111]. As a treatment for gastric cancer, it decreases the cell survival ratio of SGC7901 gastric cancer cells in a dose-dependent manner. The number of cells arrested in the G1/M phase increases with increased dose, while the cell cycle is blocked in the G2/M2 phase. Used in the proper amount, andrographolide inhibits cell invasion, migration, and proliferation. It induces apoptosis, with the possible mechanism including the enhanced expression of Timp-1/2, cyclin B1, Bax, Bikand p-Cdc2, and decreased expression of MMP-2/9 and Bcl-2 [112]. It also inhibits NF-κB binding to DNA [113].

2.5.2 Sageone – It is an abietane diterpenoid commonly obtained from the crude extract of *R. officinalis (Rosmarinus officinalis)*. It causes cell death in gastric cancer cell line SNU-1 cells in a programmed manner. These cells are usually resistant to cisplatin, but when given synergistically along with sageone, they show the increased cytotoxic effect of cisplatin, which was verified by the calculation of the combination index. Sageone decreases the level of Akt expression in contrast to cisplatin, which increases it. It also increases the cleaved Caspase -3 and -9 and Poly (ADP-ribose) polymerase (PARP) when administered with cisplatin [114], [115]. The indication is that caspase plays a critical part in the induction, transduction, and amplification of apoptosis [116].

2.5.3 Carnosic acid – It is a polyphenolic abietane diterpene isolated from *R. officinalis* that exhibits several pharmacological activities. It is used for different stomach ailments, such as gastric lesions, which increase the level of reduced glutathione and prostaglandin-E2 to protect the stomach from

lesions induced by lipid peroxidation inhibition [117]. It exhibits anti-gastric cancer activity by inhibiting the proliferation and survival of cells which increases with increasing concentration. It enhances the cleavage of the well-known apoptotic marker PARP and decreases survival expression. Further, it inhibits the activation/ phosphorylation of Akt and mammalian targets of rapamycin (mTOR) signaling pathways [118].

2.6 Triterpenes – They consist of 6 isoprene units having 30 carbons in which the squalene epoxide units are arranged in the chair-chair-chair-boat confirmation after the condensation process [119]. The primary sources of triterpenes are plants and fungi [120]. These are the main plant membrane structure constituents responsible for stabilizing the phospholipid bilayer in the cell membrane [119]. They perform numerous biological functions ranging from ant-oxidant, antiviral, antibacterial, anti-fungal, anti-inflammatory, and anticancerous activities, influencing several signaling pathways in cancer treatment [120]. Pentacyclic terpenes are plants' primary and secondary metabolites from their leaves, roots, stem barks, and fruits [121]. The four triterpenes commonly used in gastric treatment are described below.

2.6.1 Celastrol – It is a quinone methide triterpene, also known as tripterine, found in the extract of *T. wilfordii Hook. F (Tripterygium wilfordii Hook F)*. It is found to prevent cancer cell division and initiates apoptosis. When tested on MKN45 gastric cancer cells, celastrol prevent cell multiplication, migration, and invasion. It further plays a role in inactivating the PTEN/PI3K/Akt and nuclear factor κB signaling pathway by causing the downregulation of miR-21 [122]. It decreases the expression of the phosphorylated form of m-TOR and S6K and induces autophagy [123]. Also, it binds to an antioxidant enzyme, peroxiredoxin-2, which increases ROS at the cellular level and causes ROS-dependent endoplasmic reticulum stress and dysfunctioned mitochondria. It inhibits enzyme activity at the cellular and molecular level [124]. It inhibits TNF (tumor necrosis factor) induced tumor cell invasion and plays role in inhibiting heat and shock response activation and as a proteasome inhibitor [125].

2.6.2 Euphol – It is euphane-type tetracyclic triterpene alcohol obtained from the sap or latex of *E. tirucalli (Euphorbia tirucalli)*. It is utilized for its effect on rheumatism, toothache, neuralgia, and anticancer drugs. It increases the expression of BAX, a pro-apoptotic protein, and decreases the expression of Bcl-2, a prosurvival protein. Further, it causes the dysfunctioning of mitochondria by activating caspase-3. The decreases in cyclin-B1 level and increase in $p27^{kip1}$ are responsible for its antiproliferative activity. Finally, euphol also prevent the activation of the extracellular signal-regulated kinase ½ (ERK½) pathway [126].

2.6.3 Glycyrrhizic acid – It is a natural triterpene obtained from the roots of the Chinese herb *Licorice* and found to exhibit anticancer effects against certain cancers. It assists in detoxification and bronchodilation and treats viral hepatitis [127]. It downregulates the expression of proteins linked with the G1 phase, such as D1, D2, D3, E1, and E2, and causes G1/S phase arrest and exhibit inhibitory effect against gastric cells which increase with time and dose. It also increases the expression of Bax, cleaved PARP, and pro-Caspase-3, -8, and -9, decreases that of Bcl-2, survivin, and p65, and further causes downregulation in phosphorylation of the PI3K/Akt pathway [127].

2.6.4 Betulinic acid – It is a pentacyclic triterpene with a lupine-like structure obtained from several plants, such as acuminatissima leaves, wild jujube seeds, and white birch bark. It significantly affects gastric cells and exhibit inhibition which increases significantly with time and concentration. It induces cell death and inhibits the invasion and movement of gastric cancer cells by impairment of epithelial-mesenchymal transition progression [128]. It also blocks the ERK/MEK signaling pathway by decreasing the expression of phosphorylated proteins ERK and Mitogen activated protein kinase (MEK) [129].

2.7 Sesquiterpenes – Many sesquiterpene compounds are found naturally and play a critical role in biological activities, and other human uses. They are very diverse and have two distinct characteristics – the presence of 15 carbon skeletons that make up the backbone and the arrangement of different functional groups and substituents in layers on the structural scaffolds. The constituents are arranged in diverse regiospecific and stereo-specific manners [130]. They can be monocyclic, bicyclic, or tricyclic. When compared with terpenes, they are less volatile. They have a more pungent odor and show anti-inflammatory and antibacterial properties [131], [132]. After oxidation, sesquiterpenes get converted into sesquiterpenols [133]. The α-methylene-γ-lactone group (αMγL) of sesquiterpenes is responsible for anticarcinogenic and anti-inflammatory activity, whereas helenalin causes anti-inflammatory effects only, and parthenolide accounts for antitumor activity. Further, sesquiterpene lactone artemisinin exerts antimicrobial effects [134]. A few of the common sesquiterpenes for gastric cancer are described below.

2.7.1 Zerumbone – It is a cyclic sesquiterpene whose biological effect is due to the unsaturated carbonyl groups. It is obtained from subtropical ginger and has significantly less toxicity. It inhibits the growth of gastric cells and causes apoptosis in a dose-dependent manner. Further, it decreases the expression level of Cyp-A, Bcl-2, and mitochondria-mediated pathways, increases the expression level of Bax, releases cytochrome-C, and activates caspase-3 [135]. Further, it reduces the expression of Vascular Endothelial Growth Factor (VEGF) and NF-κB [136].

2.7.2 Elemene – It is a sesquiterpenoid obtained from the extract of *Rhizoma curcumae*, part of traditional Chinese medicine, and has enormous potential to cure cancer and malignant tumors with essential oils. It is more clinically effective, safe, and less toxic than other cancer drugs. It prevents the division of gastric cells and exhibits a synergistic effect when administered along with PD98059. It indicates the enhanced apoptosis of cells when given in a concentration-dependent manner. Elemene decreases the mRNA-expression level of Bcl-2 and increases the expression of p-ERK1/2 protein along with BAX-mRNA [137], [138].

2.7.3 Parthenolide – It is a sesquiterpene lactone and is a medicinal compound obtained from *Parthenium* , which was initially used to treat migraines, epidermal infections, and rheumatism [139]. When tested on gastric cancer cell lines SGC7901, it inhibits cell growth, enhances the apoptotic rate, and sensitizes the cells to DPP. Parthenolide further acts by decreasing the expression of Bcl2, mitochondrial potential, and NF-κB while upregulating the caspasewen-8 and caspase-3 expression. It also enhances the release of cytochrome C from mitochondria and upregulates the Bax, Bid, and tBid expression [140]. Thus, it increases the expression of the proapoptotic pathway, whereas it decreases the expression of the prosurvival and drug resistance pathway [141], [142].

2.7.4 Artemisinin – It is a sesquiterpene that is naturally obtained from *A. anuua (Artemisia annua)* or sweet wood, is commonly used as an antimalarial drug, and exhibits an antiproliferative effect [143]. It also triggers cell cycle arrest in prostate cancer cells. When tested on gastric cancer cell lines AGS and MKN74 cells, artemisinin inhibits the growth and modulates the expression of cell cycle regulators. It also induces two negative cell cycle regulators, namely $p27^{kip1}$ and $p21^{kip1}$, and upregulates the expression of p53, which is essential for cell apoptosis and metastasis. In addition, it affects specific signaling pathways, ERK1/2, p38, and JNK, at the molecular level [144]. It decreases proliferation, increases levels of oxidative stress, induces apoptosis, and inhibits angiogenesis.

The structures of monoterpenes, sesquiterpenes, diterpenes, and triterpenes are given in **Figure 2.2**. The details of different terpenes, their properties, source, and mode of action against cancers are indicated in **Table 2.1.**

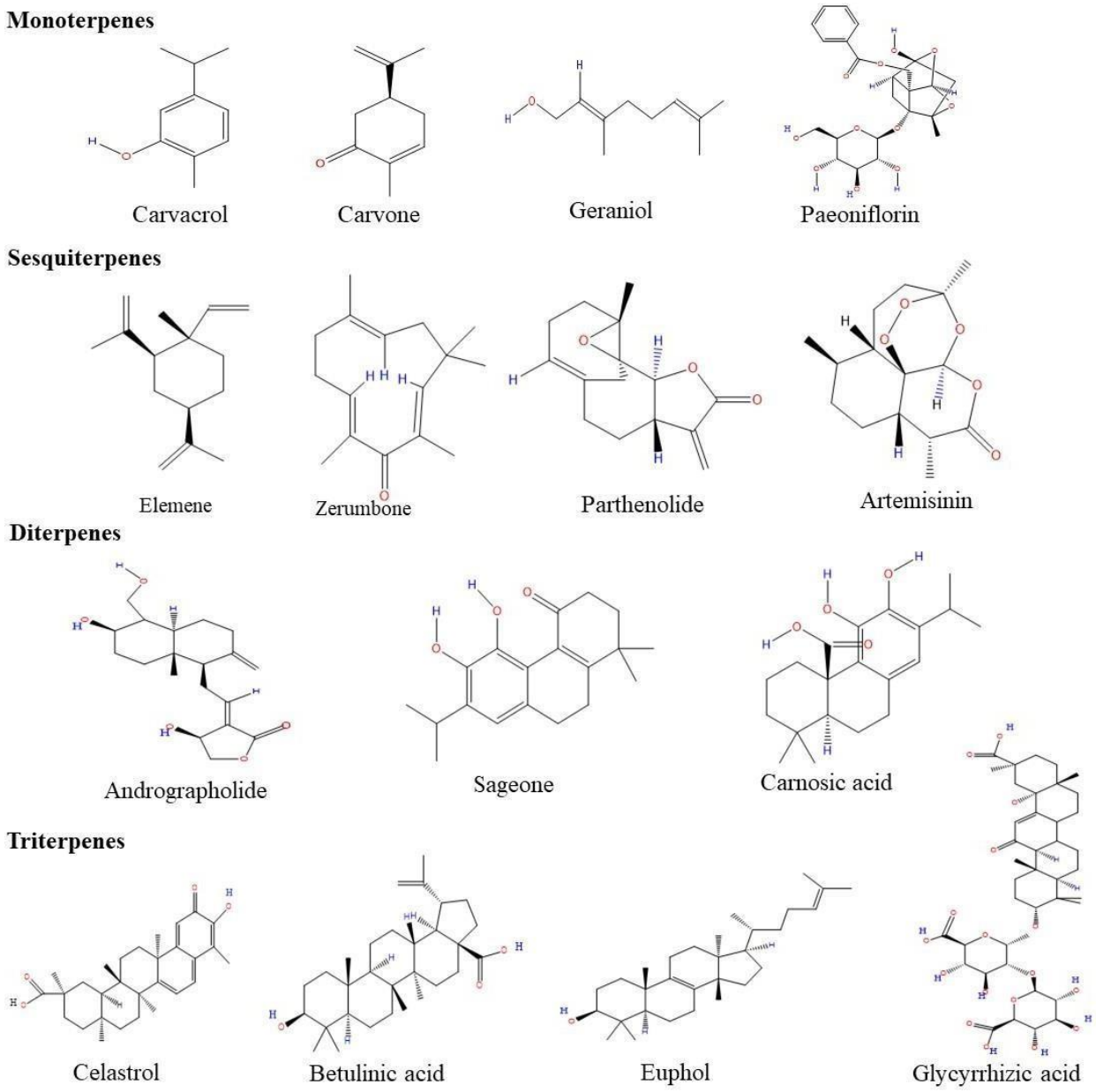

Figure 2.2. The figure depicts the chemical structures of different Monoterpenes, Sesquiterpenes, Diterpenes and Triterpenes.

Table 2.1. List of terpenes, their biological properties, source, and dose against cancer.

Compounds	Biological properties	Source	Cell line	Dose
Carvacrol	Anti-microbial, anti-tumor, anti-inflammatory, anti-mutagenic, analgesic, antiparasitic [145]	*Thymus vulgaris, Origanum vulgare, Lepidium flavum, Citrus* [146]	AGS [91], [100]	0-600 µmol/l [100]
Geraniol	Antitumor Anti-inflammatory	Lemon, Geranium	AGS [147], [101]	5-35µM/ml [101]
D-carvone	Anti-microbial, antioxidant, anti-inflammatory, anti-cancer [148]	Caraway, dill weeds	AGS[103]	5-35 µM [103]
Paeoniflorin	Antitumor	*P. lactiflora*	SGC-7901, MGC-803,[105] HepG2 (liver cancer), SMMC-7721 (liver cancer)[149], SGC-7901 (gastric adenocarcinoma cell)[150], MCF-7 (Breast cancer cell)[151],	80-324 µg/ml [150]
Elemene	Anti cancer	Rhizoma curcumae [137]	BGC-823 [137]	0.02-0.16 mg/ml [137]
Zerumbone	Anticancer, anti-angiogenic	Ginger [135]	SGC-7901 [135]	0.1- 50 µM/ml [135]
Parthenolide	Antitumor	Feverfew (*Tanacetum*	SGC7901 [140], Colon carcinoma cells, lung	5-200 µmol/l [140]

		partheni um L. Schulz Bip.) [152]	cancer [142]	
Artemisinin	Antitumor, Antimicrobial, Antioxidant	*Artemisia annua* [153]	AGS and MKN74 [144] Brain cancer, breast cancer, cervical, colorectal, gastric, lung, and ovarian cancer [154]	0-5 µM [144]
Andrographo lide	Anticancer Anti-inflammatory	*Andrographis paniculata*	SGC 7901 cells, [112] Jurkat, PC-3, HepG2, and Colon 205 tumor cells, and normal peripheral blood mononuclear cells (PBMCs)[155]	5-40 µg/ml [112]
Sageone	anticancer	*Rosmari nus officinali s*	Gastric adenocarcinom a cell lines AGS, SNU-1, and SNU-16 [116]	6.25-100 µM[115]
Carnosic acid	Antitumor	*Rosmarinus Officinalis*	AGS and MKN-45 cells[118]	6.25-100 µg/ml[118]

Celastrol	Anti-inflammatory, Antitumor	*Tripterygium wilfordii* (Thunder God Vine), *Celastrus orbiculatus, Celastrus aculeatus Celastrus reglii, Celastrus scandens* [156]	MKN45 [122] Melanoma tumor cells [125]	0-20 µM [122]
Euphol	Antiviral, anti-inflammatory and anti-cancer [126]	*Euphorbia tirucalli* [126]	CS12 [126]	2-60 µg/ml [126]
Glycyrrhizic acid	Immunomodulatory Antitumor	Licorice *Glycyrrhiza glabra* L.[157]	MGC-803, BGC-823, SGC-7901 [127] KATO III, HL 60, DU-145 & LNCaP [158], [159]	0-4 mg/ml [127]
Betulinic acid	Antiviral, antibacterial, antimalarial , anti-inflammatory and anti-cancerous [128]	Jujubee seeds, white birch bark [128]	SNU-16, NCI-N87 [128]	0-80 µM [128]

2.8 Nanotechnology and herbal formulations

In conventional therapeutic and diagnostic tools for cancer, there is an increase in systemic toxicities and refractoriness. Due to this, various other strategies are used to enhance diagnostic abilities and combat the disease severity [160]. Among these, nanotechnology has gained attraction due to its many inherent advantages. Various nanotechnology-based devices are being developed for their beneficial role in the detection, drug delivery, gene & targeted therapy, biomarker mapping, bioimaging, early diagnosis, and rapid testing [160], [161], [162]. Recent advancements in

nanotechnology, especially in the synthesis of nanoparticles, have helped address some issues that were otherwise not possible, such as target specificity, improved disease diagnostic ability in sensitivity, quality, speed, early detection, biocompatibility, stability, and effectiveness of drugs [163].

Nanoparticles synthesis can be done by various means, such as physical, chemical, and green methods. Chemical methods comprise high energy consumption, high cost, low yield, and environmental degradation through harsh reducing agents [164]. The physical techniques are also not preferred since they involve high cost, high pressure & temperature and are not amendable for controlling the size & shape of nanoparticles [165]. However, because of the use of toxic chemicals in synthesizing nanoparticles, greener methods are preferred in which the particles are synthesized by following a redox reaction in which metal ions are reduced to stabilize nanoparticles is carried out by using natural extracts or components of an organism. Recently, research on green synthesized nanoparticles has increased exponentially worldwide due to the widespread use of different plant species, isolated compounds, and extracts. Further, green synthesized nanoparticles have low cost, environment-friendly behavior, energy efficiency, easy synthesis, better bio-activities, high catalytic activities, and low toxicity. For instance, various green nanoparticles have been synthesized using extracts of different plants having terpenes as secondary metabolites. Their mode of action on different gastric cancer cell lines and *H. pylori* has been investigated [109-114]. For example, the leaf extract of *Artemisia turcomanica* upregulates BAX mRNA expression and inhibits Bcl2 expression, and increases in number of early and late apoptotic cells [166], *Artemisia ciniformis* up-regulates pro-apoptotic genes, caspase-3, caspase-9, and Bax; down-regulates Bcl2 gene and inhibits the expression of cyclin D1 and MMP2 genes and causes the arrest of cancer cells in the G0/G1 phase [167], *C. monogyna* induces apoptosis and ROS generation [168], *Cardiospermum halicacabum* induce apoptosis via inhibiting antiapoptotic proteins as well as proapoptotic proteins [169], *Cassia fistula leaf extract causes b*acterial cytoskeleton disruption and DNA damage of *H. pylori* [170], and *Vitex negundo ethanolic extract* augments expression of caspase-3, caspase-9, Bid and Bax and reduces expression of Bcl-XL [171]. Similarly, quantum clusters and quantum dots are being synthesized using different proteins, natural polymers, etc. For instance, insulin-protected quantum clusters are made using other metal ions, such as nickel, zinc, etc., for their role in developing biomarkers using the green synthesis method [172], [173].

Similarly, biomarkers can be developed to detect cancer more precisely & efficiently [160], [174]. Coal-GO (graphene oxide) exhibits higher interaction with single-stranded DNA aptamer, resulting in chemiluminescence resonance energy transfer-based biosensors with higher sensitivity [175].

Also, apigenin, a natural flavone, exhibits synergistic anticancer activity with curcumin after binding with tubulin at distinct sites [176]. Ginger, which has been used from time immemorial as traditional medicine, shows antiproliferative activity when used as an aqueous extract by disrupting the microtubule network of cancer cells [177]. A bacterioboat-based drug carrier consisting of surface-encapsulated mesoporous nanoparticles on *L. reuteri* was developed for the suitable oral administration of drugs [178].

Nanomaterials also offer an advantage in minimizing the limitation of various imaging techniques, such as MRI (Magnetic Resonance Imaging), X-ray, CT-scan (Computed Tomography scan), and ultrasound, that are commonly deployed to enhance the diagnostic accuracy and progression of the disease. These techniques can only examine the alterations on the surface of the tissue, which is also relatively late in the passage of the disease. In addition, when used with imaging contrast agents, such as small molecules with a fast metabolism, unwanted toxic side effects are commonly experienced. By comparison, nanomaterials can be synthesized to act as a powerful contrast agent in all imaging techniques because of their ability to show less toxicity and more permeability in tissues. For example, quantum dots are widely used for specific cellular imaging, and iron oxide particles are used for tumor imaging [77], [179], [180], [181]. Following this, the development of nanoscale range drug delivery tools using nanotechnology can be employed for targeting cancer tissue more precisely and with little or no side effects. Nanomaterials are also widely used in drug delivery because of their biological nature, potential to cross the cell barriers easily, and active & passive targeting nature [160], [182], [183]. Using these, various novel methods for drug delivery are being developed that have been proven clinically effective. For instance, paclitaxel, incorporated with polymeric mPEG-PLA micelles, is used for treating metastatic breast cancer chemotherapeutically [77], [184].

Further, anticancer therapies are often considered superior only when the therapeutic agent can reach the target site without causing side effects. With nanoparticles used as carriers, this can be relatively easily achieved by chemically modifying carrier surfaces. For example, incorporating PEG (polyethylene glycol) or polyethylene oxide at the surface of nanoparticles enhances tumor targeting ability because PEG prevents nanoparticle detection as an antigen by the body's immune system, thus making it easy to circulate in the bloodstream. Another example Abraxane, a formulation consisting of albumin-stabilized paclitaxel, which is FDA (Food and Drug Administration) approved for treating breast cancer [77], [185].

In a nutshell, different nano-formulations utilized for curing various cancers can be exploited for treating one of the deadliest diseases, gastric cancer. Several preclinical studies prove that synthetic

and naturally occurring terpenes hold therapeutic and chemo-preventive effects against cancer. They act by exerting their effects on various developmental stages of the tumor via inhibiting initiation and promotion of carcinogenesis, inducing tumor cell differentiation and apoptosis, and suppressing tumor angiogenesis, invasion, and metastasis by regulating various growth factors, transcription factors, and intracellular signaling pathways [186], [187], [188]. Thus, nanotechnology can be employed to develop new formulations using different herbal secondary metabolites for treating gastric cancer. Several nano-formulations have been made using plant extracts with metal ions that exhibit antioxidant, anti-cancerous, anti-inflammatory, antiviral, and antibacterial properties [189], [190], [191], [192]. SEM (Scanning Electron Microscope) and TEM (Transmission Electron Microscope) images of some of the green synthesized nanoparticles are given in **Figure 2.3.** The various applications of green synthesized nanoparticles are given in **Figure 2.4.**

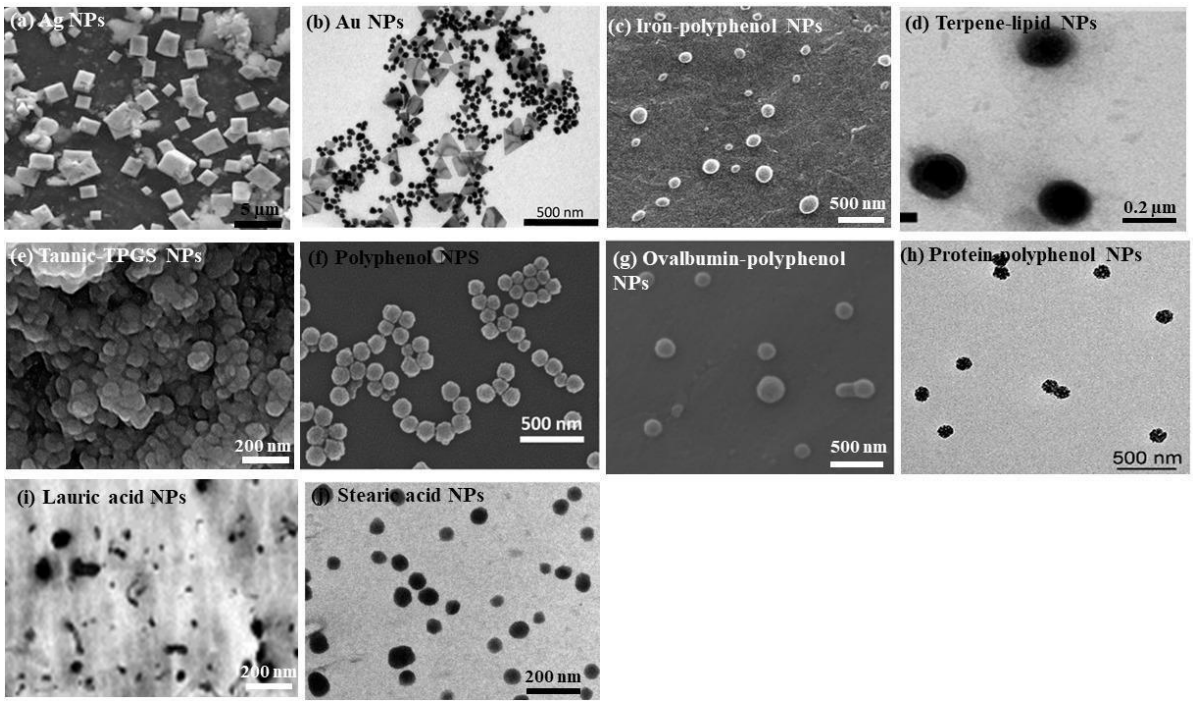

Figure 2.3. The figure shows SEM/TEM images of some of the green synthesized nanoparticles using terpenes and other polyphenols.

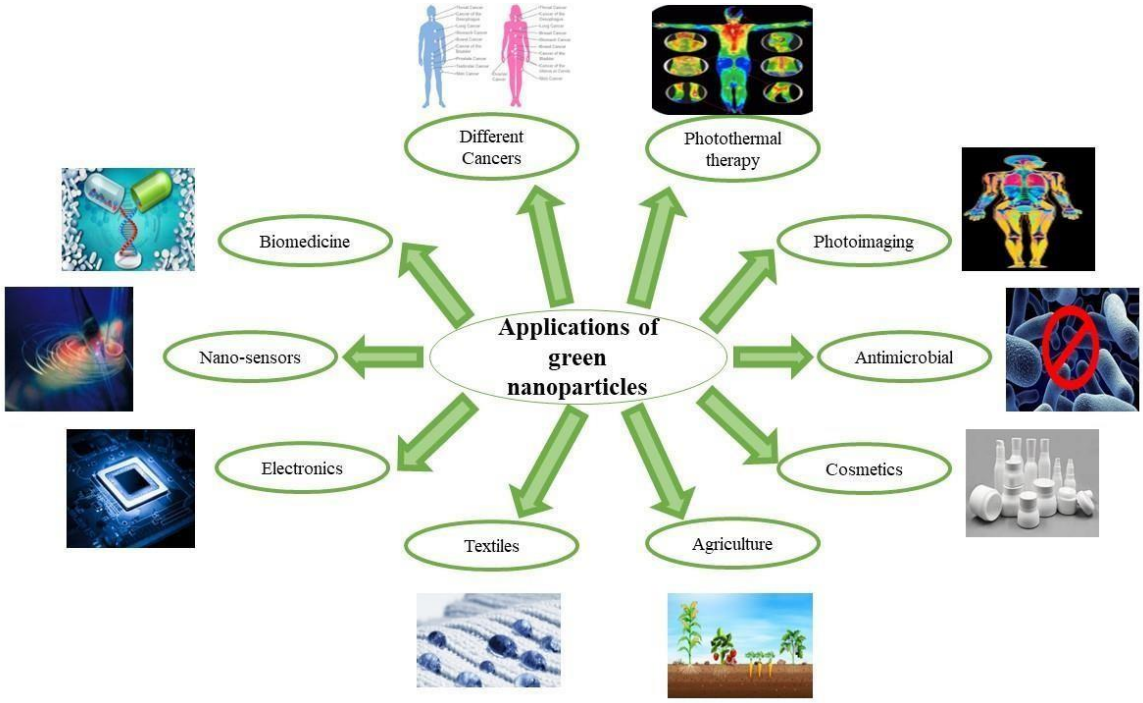

Figure 2.4. The figure gives the significant fields in which the green synthesized nano-formulations have been used for the past few years.

2.8.1 FDA-approved drugs for gastric cancer

FDA is a federal agency of the department of health and human services. It plays role in maintaining public health by assuring the safety and efficiency of human and veterinary drugs, medical devices, food supplies, and biological products. In the last 50 years, more than 100 anticancer drugs have been approved for various cancers by the FDA. The approval of drugs is based on 3 distinct parameters: overall survival or patient-related outcomes, progression-free survival involving the time until cancer worsens or occurs again, and response rate, which involves the percentage of people experiencing tumor shrinkage. The drugs are divided into two categories depending upon their mode of action: cytotoxic or targeted agents. The cytotoxic drugs target the components of the mitotic or DNA replication pathways, thus killing the rapidly dividing cells. They include mainly alkylating agents, topoisomerase inhibitors, or anti-microtubule agents. On the other side, the targeted agents interact with the molecular targets linked with the pathways related to growth, progression, and spread of cancer, eventually blocking the growth and spread of cancer. This category comprises mainly signal transduction inhibitors, apoptosis inducers, gene expression modulators, monoclonal antibodies, and hormone therapies [193]. For the treatment of gastric cancer, the primarily consumed anti-gastric cancer drugs are listed in **Table 2.2**, which includes

their structure, mechanisms of action, and side effects. A brief description of the first few drugs listed in the table is discussed next. Everolimus is an mTOR inhibitor that results in G0/G1 arrest by preventing the mTOR-mediated phosphorylation of p70S6K and 4E-BP1 [194]. It also decreases the multiplication and secretion of HIF-1α and VEGF in gastric cancer cells in vitro. Ramucirumab, on the other hand, is a human monoclonal antibody IgG1, which acts by targeting the vascular endothelial growth factor receptor-2 (VEGFR-2). It prevents the VEGF ligand binding to the VEGFR-2 and receptor-mediated pathway activation in the case of endothelial cells. Further, it also results in macrophage inhibition which causes decreased tumor immune infiltration and cytokine-chemokine release, which results in decreased tumor growth and proliferation. It is the only FDA-approved antiangiogenic agent for gastric or gastroesophageal junction adenocarcinoma [195],[196]. Another FDA-approved drug, Trastuzumab, is also a humanized monoclonal antibody that is directed against epidermal growth factor receptor 2 (HER2). It treats multiple oncologic conditions, metastatic gastric cancer being one of them. It acts after linking to the extracellular domain of HER2 and follows various mechanisms, including downregulation of DNA repair pathway and angiogenesis, abrogation of oncogenic cellular signaling, activation of antibody-dependent cell-mediated, and inhibition of extracellular HER2 domain cleavage to trigger the tumor-suppressive action [197]. For the FDA-approved drugs, the reader is referred to **Table 2.2**.

Table 2.2 FDA-approved drugs with their side effects and mode of action.

Name	**Structure**	**Gastric cancer**	**Mechanism**	**Side effects**
Everolimus	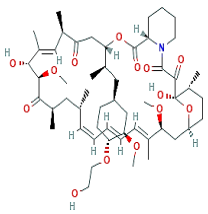	Gastric cancer	• Decreases division and secretion of HIF-1α and VEGF in gastric cancer cells *in vitro*. • *In vivo*, everolimus inhibits tumor growth [198]	• Swelling of eye • Swelling of palm • Muscle twitching • Prolonged bleeding from cuts

Ramucirumab		Gastroesophageal cancer	• It targets VEGFR-2 receptor [199]	• Neutropenia • Intestinal obstruction • Arterial blood clots • Hyponatremia
Trastuzumab	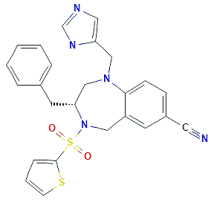	Gastroesophageal junction cancer	• demonstrated HER2-expression-dependent cell growth inhibition • exhibit potent antitumor activity in a broad selection of HER2-expressing xenograft cells, including those with low HER2 expression o [200]	• Heart problems • Lung problems • Upper respiratory tract infection
Imatinib	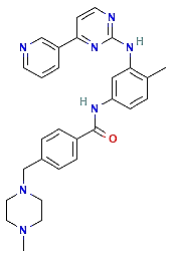	Gastrointestinal stroma tumor	• induces pro-apoptotic Bcl2 family proteins • targets BCR-ABL, c-KIT, and PDGFR kinases [201]	• Irregular heartbeat • Seizures • Unusual bleeding or bruising • Ulcers
Pembrolizumab		Gastric and gastroesophageal cancer	• Binds to PD-1 and prevents its	• Anemia • Kidney failure • Lymphopenia

			binding with PD-1 ligands [202]	• Vitiligo
Trifluridine	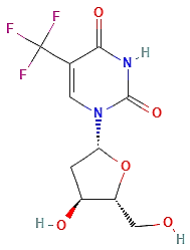	Gastroesophageal junction adenocarcinoma	• Prolongs OS, PFS • Prolongs time for deterioration of ECOG performance status [203]	• Blurred vision • Puffy eyelids • Severe burning in eyes
Docetaxel	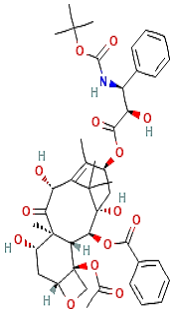	Gastroesophageal junction adenocarcinoma	• Inhibits microtubule disassembly • Cell cycle arrest at G2/M transition[204]	• Liver problems • Low blood cell count • Loss of vision
5-Fluorouracil	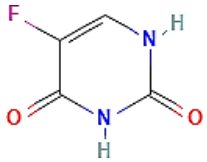	Gastric cancer	• Blocks thymidylate synthetase conversion of deoxyuridylic acid to thymidylic acid [205].	• Leukopenia • Angina • Coronary arteriosclerosis • hyperbilirubinemia
Mitomycin	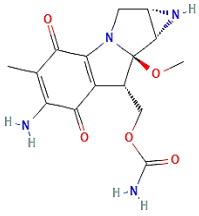	Gastric and pancreatic adenocarcinoma	Inhibit DNA synthesis [206]	• Difficulty in breathing • Ulcers in mouth • Bloody diarrhea

2.9 Concluding remarks and directions for future research

Gastric cancer cases are reported worldwide, with maximum prevalence in Asia and Latin America; the rate is also high in northern to central America, Europe, and central Africa. However, even countries with good economies and advanced medical facilities have not been able to reduce the death rate considerably. The 5-year survival rate in the USA for gastric cancer is 31%, and for the European nations, it is around 26%. The situation is similar or worse in countries with weak economies and poor hygiene. Therefore, there is an urgent need and high demand for the development of abundant, effective, and economically favorable medicines. Further, available chemotherapy, including 5-fluorouracil, capecitabine, carboplatin, cisplatin, docetaxel, epirubicin, oxaliplatin, etc., has considerable side effects such as anemia, shortness of breath, nausea, diarrhea, fatigue, loss of appetite, hair loss, etc., which compromise life quality of the patient. Therefore, more research is required to develop suitable treatments/drugs with lesser side effects.

Since almost 89% of gastric cancer directly relates to *H. pylori* infection, the most crucial step for gastric cancer management is to control the infectivity. Plants like *Hedyotis diffusa Willd, Aloe vera, Rhizophora mangle, Astragalus membranaceous, etc.,* are effective against the pathogen due to the presence of phenolics, terpenes, alkaloids, and polyketides in them. Many of those plants grow in the tropical, subtropical, temperate, and Mediterranean regions of the world and are native to a particular geographical location such as India, China, Japan, South Africa, Iraq, Iran, Vietnam, USA, and other European countries, and show excellent anti-*H. pylori* activity. Extensive research is needed to invent, purify, characterize, and formulate safer drugs, including natural products. However, attention should also be given to the composition, stability, and pharmaceutical efficiency of those formulations as the concentration and the stability of the lead compounds may greatly vary based on many factors, including soil composition, pH, macro and micronutrient content, humidity, porosity, weather, availability of sunlight, etc. In this regard, the advancement of nanotechnology plays crucial role in maintaining the quality and efficiency of herbal formulations. Many metallic nanoparticles, including silver, gold, selenium, zinc oxide, etc., have anti-cancer properties. Enhanced uptake of nanoparticles by cancer cells has been reported for many cancer lines, including MCF-7 (human breast carcinoma cell line) [141], Hep G2 (Human liver cancer cell line) [142], and AGS

(Human gastric carcinoma cell line) [167]. Nanoparticles and these natural compounds may show synergistic anticancer activity by generating various stresses, including oxidative damage, DNA damage, and mitochondrial dysfunctions.

Further, many nanoparticles also show anti *H. pylori* activity. Additionally, because of their high surface area to volume ratio, nanoparticles can interact and stabilize bioactive polyphenols on their surfaces, enabling the delivery of a large number of drugs at the target site. Cancer-specific delivery of herbal medicines will make them safer and side-effect-free. Furthermore, polyphenolic surface-protected ferromagnetic nanoparticles will allow the detection and imaging of the cancer tissue using MRI imagining techniques and help to develop an effective therapeutic approach using hyperthermia.

In conclusion, medicinal plants show promise as potential candidates for cancer treatment because of their beneficial properties. Knowledge of active secondary metabolites from extracts of different plant parts having anti-cancerous activities and their mode of action against critical targets pave the way for further research. The current information on various herbs and their mode of action against different diseases can be further exploited to develop more efficient and less harmful drugs. At a minimum, when used with conventional treatments, they can increase the effectiveness of these treatments in fighting cancer. Moreover, isolating active compounds and finding their chemical structure further enables molecular and pharmacological comparison with the currently used chemicals and pharmaceutical products. In the case of H. pylori, which has become resistant to conventional antibiotics, green nano-formulations with high biocompatibility and bactericidal potency can be utilized as a replacement. We conclude this review article by outlining directions for future research on NT (Nanotechnology) enabled herbal formulations for treating cancer, particularly gastric cancer. We believe that herbal formulations using the unique properties of nanomaterials offer a potentially winning proposition. It is our hope that this review article will spur interest among interdisciplinary teams of researchers to develop safer and more effective treatments for gastric cancer.

Chapter 3: Therapeutic Potential of Lactoferrin-Coated Iron Oxide Nanoparticles for Targeted Hyperthermia in Gastric Cancer

Abstract

Lactoferrin (LF) is a non-heme iron-binding glycoprotein involved in the transport of iron in blood plasma. In addition, it has many biological functions, including antibacterial, antiviral, antimicrobial, antiparasitic, and, importantly, antitumor properties. In this study, we have investigated the potential of employing lactoferrin-iron oxide nanoparticles (LF-IONPs) as a treatment modality for gastric cancer. The study confirms the formation of LF-IONPs with a spherical shape and an average size of 5 ± 2 nm embedded within the protein matrix. FTIR and RAMAN analysis revealed that the Fe-O bond stabilized the protein particle interactions. Further, we conducted hyperthermia studies to ascertain whether the proposed composite can generate a sufficient rise in temperature at a low frequency. The results confirmed that we can achieve a temperature rise of about 7 ºC at 242.4 kHz, which can be further harnessed for gastric cancer treatment. The particles were further tested for their anti-cancer activity on AGS cells, with and without hyperthermia. Results indicate that LF-IONPs (10 µg/ml) significantly enhance cytotoxicity, resulting in the demise of 67.75 ± 5.2% of cells post hyperthermia, while also exhibiting an inhibitory effect on cell migration compared to control cells, with the most inhibition observed after 36 h of treatment. These findings suggest the potential of LF-IONPs in targeted hyperthermia treatment of gastric cancer.

3.1 Introduction

Despite the development of various strategies, therapies, and drugs for the detection and prevention of cancer, it remains a primary cause of death globally. The available cancer treatments, such as chemotherapy drugs, have inherent limitations as they destroy both malignant and healthy cells, resulting in the destruction of metabolically active cells in the body, suppression of immune system, systemic toxicity, and an enhanced risk of secondary infections in cancer patients [207], [208]. As drug resistance becomes increasingly prevalent, there is a growing demand for natural agents that can eradicate primary tumors and reduce the risk of recurrence [209]. One such natural agent is lactoferrin (LF), a protein belonging to the transferrin family, with a molecular weight of 78 kDa and consisting of approximately 690 amino acid residues [210]. Although the primary function of lactoferrin in human beings is to transport iron across blood plasma, it also possesses several biological applications, such as

antibacterial, antiviral, antimicrobial, antiparasitic, and, notably, antitumor activities [211],[212]. The maximum concentration of LF is determined in human milk, followed by cow's milk [213]. Lactoferrin consists of a single polypeptide chain which encompasses two lobes (N and C) joined by an α-helical residue. This structural arrangement provides flexibility [209], [214]. These two lobes consist of α-helices and β-sheets and can bind with Fe^{+2} or Fe^{+3} ions present in association with carbonate ions (CO_3^{2-}) [214]. LF protein exists in two forms: Apo-lactoferrin (iron-free form) and holo-lactoferrin (iron-containing form) [210]. In its pure state, LF is partially saturated with iron. However, it has the tendency to be fully saturated with iron from an outer source [215], [216].

Lactoferrin (LF) has been extensively studied for its potential as a natural agent in combating different cancer, like gastric cancer, and exhibits highly efficient bio-drug in anti-cancer research. Several *in vitro* and *in vivo* studies have reported that LF can inhibit the growth of tumor cells through diverse mechanisms, including apoptosis, cell cycle arrest, cell membrane disruption, immunoreaction, decreased cell migration, and cytoskeleton damage [217], [218], [219], [220], [221]. It is a very stable protein that can retain its effectiveness even after passing through the gastrointestinal tract [222]. Researchers indicated that orally administrated LF results in a decreased occurrence of the tongue (2% bLF), esophageal (0.2% bLF), and lung (0.02% bLF) carcinogenesis in rats, with no discernible impact on the weight of the body organs, indicative of its non-toxic nature [223], [224]. Additionally, LF is found to induce cytotoxicity and decreasing cell proliferation in MCF-7 and MDA-MB-231 human breast cancer cell lines [225], [226].

Lactoferrin is deposited in the secondary cytoplasmic granules of neutrophils and found in high concentrations at the sites of inflammation, demonstrating a vital part in the inflammatory response mechanism [227]. Moreover, the LF synthesized by kidneys, contributes towards extracting free iron from urine and increasing its availability for metabolic functions thus modulates the immune defense system [228]. At the cellular level, LF activates the development, migration, differentiation, activation, multiplication, and functions of immune cells by using two signaling pathways [229]. Accumulated LF in neutrophils at injury sites promotes cell-cell interaction, activates phagocytosis by polymorphonuclear leukocytes and macrophages, decreasing the number of pro-inflammatory cytokines, accelerating natural killer cell activity, and modulates lymphocytes [230], [231]. Furthermore, LF also plays a valuable action in distinguishing normal cells from tumor cells. Tumor cells typically possess a highly negative charge compared to normal cells, rendering them more susceptible to cationic proteins like LF while sparing the normal cells [232], [233]. Research indicated that many

cancer cells possess elevated levels of proteoglycan, glycosaminoglycan, and sialic acid, which interact with LF protein and exert a cytotoxic effect on cancer cells. This mechanism explains LF's ability to selectively target and exert high cytotoxicity selectivity toward cancer cells while posing no harm to healthy cells [234], [235], [236].

Magnetic nanoparticles, when properly synthesized and made biocompatible, play a crucial role in various biomedical applications, ranging from imaging to therapy [34]. To serve as efficient carriers for drug delivery, they should be small in size, have a large surface-to-volume ratio, and be properly functionalized for site-specific targeting [35]. Out of various varieties of magnetic nanoparticles, iron oxide nanoparticles find common use because of their magnetic features and biocompatibility across a variety of biomedical roles, like drug and gene delivery, biosensors, magnetic particle imaging (MPI), and hyperthermia (HM) treatment [36], [37], [38]. Superparamagnetic IONPs can be engineered to respond specifically and efficiently within the tumor microenvironment [39], [40], [41]. These particles have magnetization tendency through an external magnetic field but exhibit no residual magnetic interactions after the removal of the field, indicating good dispersion and excellent targeting capacity [42]. This characteristic makes them highly advantageous for magnetic hyperthermia due to their ability to disperse within localized minor regions, creating a difference in temperature profiles between normal and tumor cells [43].

Various particles have been synthesized to harness their anti-cancer potential against different cancers by using hyperthermia treatments. Mohamadkazem et al. synthesized iron oxide-gold nano complexes and used an external field to physically navigate these magnetic nanoparticles to the target melanoma cells, effectively killing them through electron beam therapy [44]. Kamalabadi et al. synthesized folate-functionalized gold-coated magnetic nanoparticles for the treatment of HPV-positive oropharyngeal cancer by enhancing uptake and cell death through the application of an external field [45]. Further, hyperthermia has been found to enhance drug release from formulations and develop potent theranostic agents for anti-cancer activity against colorectal cancer [46].

Based on the above, we hypothesized that the targeted delivery of lactoferrin conjugated with iron oxide nanoparticles (LF-IONPs) to gastric tissue, coupled with hyperthermia, will offer enhanced efficacy in the treatment of gastric cancer.

3.2 Materials and Methods

3.2.1 Materials

Ferric chloride ($FeCl_3$), ferrous sulfate ($FeSO_4$), ammonium hydroxide (NH_4OH), polyethylene

glycol (PEG 400), and deionized water having analytical grade were procured from LobaChemie, India. Lactoferrin, ammonium hydroxide, ethylene dichloride (EDC), N-hydroxysuccinimide (NHS), HAMs cell culture media, fetal bovine serum (FBS), and penicillin-streptomycin were purchased from HiMedia, India.

3.2.2 Formulation of iron oxide nanoparticles followed by conjugation with Lactoferrin

To synthesize iron oxide nanoparticles, $FeCl_3.6H_2O$ and $FeSO_4.7H_2O$ were added in 50 ml of DI water and heated to 90ºC, after which 3 ml PEG400 was added dropwise. Subsequently, a separate solution containing 10 ml of 25% ammonium hydroxide in 50 ml of water was rapidly added into iron solutions while stirring, followed by a stirring period of 30 minutes. The final mixture turned black followed by cooling to room temperature, centrifuged at 4000 rpm for 10 minutes, and washed thrice with water to get rid of any undissolved impurities.

To conjugate the nanoparticles with LF protein, a solution was prepared by mixing 250 µl of 10mg/ml EDC, 250 µl of 10mg/ml NHS, and 7 µl of 1M NaOH. The synthesized IONPs were added (0.5 mg) followed by 15 minutes sonication for activating surface carboxyl groups. Next, 250 µl of 3mg/ml LF was dissolved and left overnight at 37 ºC. The resultant solution was purified by centrifugation at 12000 g for 1 h and redispersed in phosphate buffer saline (PBS) to obtain a pure nano-formulation.

3.2.3 Study of particle size, morphology, and elemental analysis

The Malvern DLS-Zeta size analyzer was utilised for determining the hydrodynamic size and surface charge of the nanoparticles through DLS (dynamic light scattering) and zeta studies, respectively. HRTEM (Talos F200S G2, Thermo Scientific) was employed to identify the size, shape, and interface structure of LF-IONPs. Prior to analysis, the nanospheres undergo centrifugation at 240 rpm for 15 minutes and washed to eliminate impurities if any. The resulting pellet was analyzed using an EDS (Bruker QUANTAX 200) to determine the percentage of present elements.

3.2.4 Study of LF- IONPs interaction using FTIR spectroscopy

It is a technique employed to determine the chemical bonds in a molecule by producing an infrared absorption spectrum through discrete vibrational energy of functional groups. It was employed to identify the interactions between LF protein and iron oxide nanoparticles. The FTIR studies were done using an Agilent Cary 600 series Spectrophotometer, and the samples were prepared using the potassium bromide (KBr) method and scanned from 400 cm^{-1} to 4000

cm^{-1}.

Surface Enhanced Raman Scattering (SERS) Spectra were also utilized to monitor the structural changes in the protein after conjugation with iron oxide particles. Thin films of LF, IONPs, and LF-IONPs were prepared 10 minutes prior to measurement on glass slides. The samples were then subjected to scanning from 500 cm^{-1} to 1800 cm^{-1} using the LabRam Hr Evolution Horiba instrument.

3.2.5 *In silico* studies

To identify the binding site residues of different transition metal ions, the MIB (Metal Ion Binding) online docking tool can be used [237]. This is done using the fragment transformation method. The process begins with the selection of a protein of interest, which was extracted from the protein data bank (PDB). Then, the target protein is compared with every single metal ion in the database to find the metal binding residues, and a score is assigned to each binding residue.

The fragment transformation method is used to align the query protein S of length m and metal-binding template T of n residues. These chains are then aligned in such a manner that the metal ion binding protein template can be converted into the query protein structure [237]. Certain parameters are being taken into consideration to get these protein structures. Firstly, the metal ion template must contain residues bound with transition metals, including Ni^{2+}, Cu^{2+}, Mg^{2+}, Ca^{2+}, Co^{2+}, Zn^{2+}, Fe^{2+}, and Fe^{3+} metal ions. Secondly, the protein structure contains a polypeptide chain which must have length of 50 residues in order to be included for docking purposes [238]. The residues of the query template and metal ion binding triplets can be represented by using the notation N–Ca–C, denoting the backbone atoms as (xN, xCa, xC) and (yN, yCa, yC), where x and y are PDB coordinates. The query protein S and the template T can be written as (s1, s2.sm) and (s1, s2.sm) in terms of triplets. The third parameter is that there should be at least two metal ion binding residues [237]. The fourth important parameter is that the residue's binding score should be more than a specified threshold value in order for it to be considered as a residue binding to a particular transition metal ion. The binding score, denoted by Ci, is assigned to all residues and of the target protein based on the sequence and structural conservation of the protein using the root mean square deviation of C-alpha carbons from structural local alignment as well as BLOSUM62 substitution matrix [239]. Hence, the binding site of metal ions was determined using the bioinformatics tool [240]. In this way, the MIB tool helps determine the binding site of metal ions on a particular protein chain. For example, in case of LF protein (PDB ID: 4EWW) extracted from the PDB (Protein Data Bank) database, a

single chain denoted by A, Fe^{+2} and Fe^{+3} metal ions were docked with LF and metal ion-binding templates were compared with the target protein.

3.2.6 XRD analysis

X-ray diffraction pattern gives us deep knowledge regarding chemical composition, crystallographic structure, and physical characteristics of a material. For XRD analysis, the sample was first dried and then subjected to the Cu K α radiation (λ=1.54 Å) to obtain the diffraction pattern which was collected in the 2Θ scan range of 10-90º. The average crystallite size of IONPs and LF-IONPs was obtained from the most intense peak by using the Scherrer formula.

(Eq 1)

$$d = \frac{K\lambda}{\beta cos\boldsymbol{\theta}}$$

Where K= 0.9, a Scherrer constant, λ= 1.54 Å is the wavelength of the X-rays, β is the broadening of the highest intense peak (311), and d denotes crystallite size of the synthesized nanoparticles.

3.2.7 Hyperthermia study to check the heating capacity

It is a heat treatment that involves gradually increasing the temperature of tumor-loaded tissue between 42 and 45°C [241], [242]. This type of treatment is used to kill cancer cells with very less or no harm to healthy cells. In order to perform hyperthermia analysis of synthesized nanospheres, the NanoTherics Magnetherm magnetic hyperthermia instrument was used. It consists of an optical fiber temperature probe. This involves analyzing the nanospheres under a 10 mT magnetic field and at various frequencies (including 161.9 kHz, 242.4 kHz, 411.1 kHz, 580.2 kHz, and 935.3 kHz) to determine the lowest frequency at which the particles generate a safe and effective temperature rise for treatment purposes.

3.2.8 Magnetic properties of IONPs and LF-IONPs

VSM (Lake Shore 7404) was utilised to analyze the magnetic characteristics of the iron oxide nanoparticles. The sample was subjected to +/- 10 kOe magnetic field at room temperature. By analyzing the hysteresis loop, important magnetic characters like saturation magnetization (M_s), coercivity (H_c), and remanence (M_r) of IONPs and LF-IONPs are determined [243].

3.2.9 Drug Loading and Release Kinetics

For determing the drug loading efficiency of the synthesized LF-IONPs, 1 ml of the sample

was centrifuged at 10,000 rpm for 15 minutes. The concentration of the protein LF was determined for both the supernatant (unbound protein) and a pellet (bound protein) using a Bradford reagent. Thereafter, the release kinetics was performed by placing particles in a dialysis membrane having a drug concentration of 3 mg/ml at a temperature of 37 ºC. The entire process of release kinetics was performed at two different pH: pH 7.4 (physiological pH) and pH 3 (gastric pH). For the study, the dialysis membrane was suspended in a beaker with distilled water pH 7.4 (physiological pH) and a volume of 50 ml. The 1 ml sample was collected from the beaker at different time intervals, followed by adding similar volume of DI water to the beaker to maintain the total volume constant. A similar process was followed for studying the release kinetics at the gastric pH (pH of water = 3) to monitor the efficient release of the drug at the specific site. Thereafter, the rate of release of bound LF from the pellet was observed at different time intervals for about 40 h by taking absorption values at 595 nm. Then, these absorption values were plotted to infer the trend of the drug release using BSA standard curves [244], [245], [178].

3.2.10 *In vitro* studies

3.2.10.1 Cytotoxicity studies

The cytotoxicity of the samples was checked on the cancerous cell line, AGS by following MTT (3-(4,5-dimethylthiazol-2-yl)-2,5-diphenyltetrazolium bromide) assay. For this study, AGS cells, having a density of 1×10^4, were added into 96 well plates and then let to become confluent up to 75–80 %. After this, the cells were treated using three distinct concentrations (5, 7.5, and 10 µg/ml) of the $FeCl_3$, $FeSO_4$, LF, IONPs, and LF-IONPs. Following this treatment, cells were incubated for 24 h and 37 ºC. Post 24 h, MTT was added and kept for 3 h. Further, after incubation, MTT, along with media, was removed from each and every well of the plate, and 200 µl of DMSO was added. Then, after 15 minutes, the OD was recorded at 570 nm.

The following equation was used to calculate the inhibition percentage.

$$\% \text{ inhibition} = [1 - (At/Ac) \times 100] \% \quad \text{(Eq 2)}$$

where At is the test substance absorbance and Ac is the control solvent absorbance.

Similarly, one more MTT assay was experimented on the cells treated with magnetic hyperthermia to check the impact of hyperthermia treatment on the cancer cells and evaluate the anti-cancer potential of synthesized nano-formulations. For this, the cells were grown in

tissue culture plates (30 mm), followed by their treatment with $FeCl_3$, $FeSO_4$, LF, IONPs, and LF-IONPs and let be confluent. Thereafter, the cells were trypsinized and resuspended in HAM's media (100 µl) and, placed in a sample holder, and exposed to magnetic hyperthermia treatment for 10 minutes at a frequency of 242.4 kHz.

3.2. Scratch assay for anti-cancer activity

To confirm the anti-cancer potential of the formulations, a scratch assay was conducted. In this assay, cells were cultured in a 6-well plate and allowed to grow in an FBS-free medium (HAM's media) at 37°C and 5% CO_2. After attaining 80-90% confluency, a scratch was made using a pointed object such as a 10 µl tip. Washing was done with PBS to avoid any debris, and different samples, including LF, IONPs, and LF-IONPs, were applied to the cells. The cells were then kept for 6, 12, 24, 36, and 48 h, and images were captured at these mentioned intervals till 48h. To determine the percentage change in wound diameter for all the formulations, the distance of the wound was randomly measured at distinct positions for each scratch made in an individual well plate, and the mean of these independent readings was calculated. This experiment was repeated three times to record the data [246], [247].

3.3 Results and Discussions

3.3.1 Structure and composition of LF-iron oxide nanoparticles

The formation of nanospheres having a spherical shape with an average size of 15 ± 2 nm was revealed by HRTEM images (at a scale of 20 nm) as given in **Figure 3.1. (a)** and inset of **Figure 3.1. (a)** (at a scale of 5 nm). Furthermore, the hydrodynamic diameter of LF-IONPs was determined to be 80.19 nm, see **Figure 3.1. (b)**. **Figure 3.1. (c)** displays the EDS spectrum, which clearly indicates the presence of different elements, including C, N, O, Fe, Cl, Au, and Cu. Notably, Fe was found to be evenly distributed, accounting for 8.47%.

3.3.2 Study of interactions between LF and IONPs after nanoparticle formation using FTIR and Raman spectra

To investigate the interaction between protein and metal ions, FTIR analysis was conducted on LF samples, IONPs, and LF-IONPs. The results revealed several peaks in the IR spectra that provide insight into the molecular bonding present in the samples.

A peak was observed at 533.57 cm^{-1} in all three samples, indicating the presence of the Fe-O bond [248]. Another peak for Fe-N stretch was seen at 832.74 cm^{-1} in both IONPs and LF-IONPs [249]. Additionally, a peak at 1069.45 cm^{-1} was detected in all three samples,

representing the C-N stretch [250]. Another peak at 1231.81 cm^{-1} was observed in LF and LF-IONPs but not in IONPs, indicating the bond Amide III [251]. The C=O stretching vibration was observed at 1407.77 cm^{-1} in all three samples [252]. Furthermore, the peaks at 1527.74 cm^{-1} and 1633.32 cm^{-1} representing the Amide II and Amide I bonds, respectively, were present in LF and LF-IONPs but not in IONPs [251]. A bond representing C-H stretching vibrations is present at 2852.25 cm^{-1} in lactoferrin and LF-IONPs but not seen in IONPs [253]. 2916.24 cm^{-1} represents a peak position for the bond O-H intermolecular interactions, which are observed in Lactoferrin and LF-IONPs but not in IONPs [253]. Also, Amine N-H stretching was observed at 3282.55 cm^{-1} in both lactoferrin and LF-IONPs but not in the case of IONPs [250]. This is shown in **Figure 3.1. (d) and Table 3.1.**

Raman analysis was performed for LF along with IONPs and LF-IONPs to identify different molecules based on their structural fingerprint. The peak observed at 517.61 cm^{-1} in IONPs represents Fe-O, while those at 578.84 cm^{-1} and 685.71 cm^{-1} indicate the bond Fe-O (T2g) and Fe-O (A1g), respectively, which are also present in LF and LF-Fe NPs but shifted to a lower wavenumber of 666.65 cm-1[254]. Additionally, a peak at 960.45 cm^{-1} is observed in IONPs, while LF and LF-IONPs show a peak at 988.69 cm-1 for Fe-O [255]. The peak at 615.81 cm^{-1} signifies the presence of sulfur residues in cysteine, which is present in LF and LF-Fe NPs but absent in IONPs [256]. Similarly, the C-S stretch gives a peak at 750.69 cm^{-1} in LF and LF-IONPs but not in IONPs [256]. The peak at 774.67 cm^{-1} indicates the O-C-N bend, which is present in all three samples [257]. Another peak at 843.41 cm^{-1} indicates C-C stretching modes present in LF and LF-IONPs but shifted to a higher wavenumber of 886.73 cm^{-1} in IONPs [258]. The bond C-O-C is present in IONPs and LF-IONPs at a peak position of 955.47 cm^{-1} but absent in LF [257]. Amide III is present in LF and LF-IONPs at peak positions of 1227.83 cm^{-1} and 1250.65 cm^{-1}, respectively [259]. A peak at 1358.96 cm^{-1} indicates C-H (bend), which is observed in both LF and L-IONPs but not in IONPs [251]. The peak at 1449.36 cm^{-1} signifies the presence of the Amide II bond in LF and LF-IONPs [251]. A ferric hydroxide peak is seen at 1556.23 cm^{-1}, which is present in all three samples [255]. Amide I bond at 1665.69 cm^{-1} is present in both LF and LF-IONPs but absent in IONPs [257]. Finally, the C=O stretch was observed in LF and LF-IONPs at 1774.87 cm^{-1}, but no peak was observed in IONPs at this wavenumber [257]. These results are presented in **Figure 3.1. (e) and Table 3.2**.

Overall, the results from FTIR and Raman spectroscopy indicate differences in the chemical bonding between LF and its interactions with metal ions, providing insights into the interaction between protein and metal ions. The key findings from the FTIR and Raman spectroscopy analyses indicate distinct molecular bonding interactions between LF and metal ions, as

evidenced by the presence of Fe-O, C-N, Amide III, Amide II, and Amide I bond in LF and LF-IONPs, but not in IONPs. These results provide valuable insights into the specific nature of the protein-metal ion interactions.

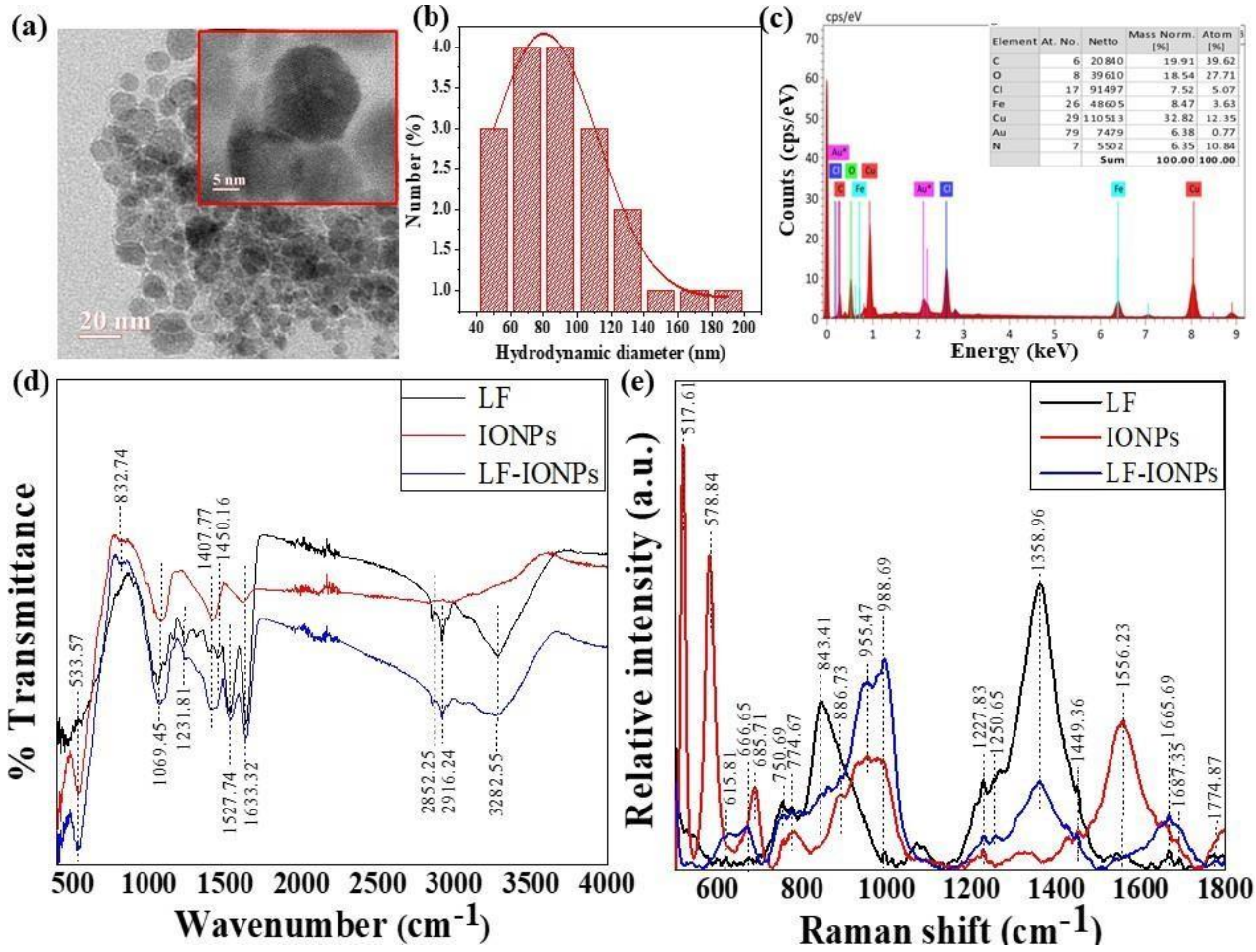

Figure 3.1. Characterization of LF-IONPs (a) HR-TEM images on a scale of 20 nm with an inset showing 15 ± 2 nm size of LF-IONPs (b) DLS showing the hydrodynamic size of the synthesized Lactoferrin-Iron oxide nanospheres (LF-IONPs) as 80.19 nm (c) EDS showing that iron is present in LF-IONPs as 8.47% (d) FTIR showing the interaction between protein LF and iron oxide nanoparticles (e) RAMAN providing us with the structural fingerprint by which different molecules can be defined.

Table 3.1. The table gives the comparative values of the wavenumbers obtained from the FTIR of lactoferrin, IONPs, and LF-IONPs, indicating changes in distinct functional groups present, thus coins the interaction among lactoferrin protein and iron oxide nanoparticles leading to the formation of LF-IONPs.

FTIR				
Functional groups	**Lactoferrin (LF)**	**IONPs**	**LF-IONPs**	**Reference**
Fe-O	**533.57**	**533.57**	**533.57**	[56]
Fe-N stretch	-	**832.74**	**832.74**	[57]
C-N stretch	1069.45	1069.45	1069.45	[58]
Amide III	**1231.81** **1308.59**	-	**1231.81**	[59]
C=O stretching	1407.77	1407.77	1407.77	[60]
Amide II	**1450.16** **1527.74**	-	**1527.74**	[59]
Amide I	**1633.32**	-	**1633.32**	[59]
C-H stretching vibrations	2852.25	-	2852.25	[61]
O-H Intramolecular stretching	2916.25	-	2916.24	[61]
Amine N-H stretching	3282.55	-	3282.55	[58]

Table 3.2: The table gives the comparative values of the wavenumbers obtained from the RAMAN spectra (500-1800 cm^{-1}) of lactoferrin, IONPs, and LF-IONPs, indicating changes in different functional groups present, thus coins the interaction among lactoferrin protein and iron oxide nanoparticles leading to the formation of LF-IONPs.

RAMAN				
Functional groups	**Lactoferrin (Lf)**	**IONPs**	**LF-IONPs**	**Reference**
Fe-O **Fe-O (T_{2g})** **Fe-O (A_{1g})**	- - **666.65**	**517.61** **578.84** **685.71**	- - **666.65**	[62]
Sulphur residues in cysteine	615.81	-	615.81	[64]

C-S stretch	750.69	-	750.69	[64]
O-C-N (Bend)	774.67	774.67	774.67	[65]
C-C stretching modes	843.41	886.73	843.41 886.73	[66]
C-O-C	-	955.47	955.47	[65]
Fe-O bond	**988.69**	**960.45**	**988.69**	[63]
Amide III	**1227.83** **1250.65**	**-** **-**	**1227.83** **1250.65**	[67]
C-H (Bend)	1358.96	-	1358.96	[59]
Amide II	**1449.36**	**-**	**1449.36**	[59]
Ferric hydroxide	**1556.23**	**1556.23**	**1556.23**	[63]
Amide I	**1665.69**	**-**	**1665.69**	[65]
C=O Stretch	1774.87	-	1774.87	[65]

3.3.3 *In silico* studies to determine the interactions between Fe^{+2} & Fe^{+3} and LF protein

MIB (Metal Ion Binding) software, an online docking server, was utilised to predict the binding sites of LF with Fe^{+2} and Fe^{+3}. The interaction between metal ions and amino acid residues in the protein depends on its structure and sequence. Extracted human LF protein from PDB (PDB ID: 1B0L) and docked it with both metal ions using MIB. Each binding residue in LF protein was assigned a binding score and residues with scores higher than the threshold were considered. The binding sites for Fe^{+2} and Fe^{+3} were determined, and the distance between the metal ions and their binding site on the LF chain was calculated using Maestro.

For Fe^{+3}, it was observed that there were three binding sites at specific amino acid residues: (1) 435Y, 597H, 395D, and 528Y, and their distance was measured to be 8.14 Å, 6.10 Å, 4.45 Å, 7.84 Å respectively. (2) 60D, 92Y, 192Y, 253H, and they were at a distance of 4.73 Å, 8.18 Å, 7.89 Å, and 6.14 Å respectively and (3) 604D, and 605K with a distance of about 4.65 Å, and 4.65 Å, respectively, as given in **Figure 3.2. (a) and Figure 3.3**. Further, the binding potential graph of Fe^{+3} with different amino acid residues is illustrated in **Figure 3.2. (b)**.

For Fe^{+2}, there were seven binding sites involving specific amino acids for each site with varying distances from metal ions: (1) 393S, 395D, 597H, 644N with a distance of 6.4 Å, 5.28 Å, 3.77 Å, 4.89 Å respectively. (2) 393S, 413E, 597H, and 644N with distances were found 6.59 Å, 4.99 Å, 3.06 Å, and 5.23 Å, respectively. (3) 60D, 122T, 253H, 301K, and their distance were 4.39 Å, 7.05 Å, 3.84 Å, and 7.73 Å, respectively. (4) 60D, 122T, 253H, 301K, which showed a distance of 4.45 Å, 7.92 Å, 3.90 Å, and 6.50 Å, respectively, between the metal ion and the amino acids. (5) 431P, 654H with a distance of 4.81 Å, 3.45 Å respectively. (6) 60D, 122T, 253H, 301K and showed a distance of about 4.85 Å, 7.39 Å, 4.41 Å, and 5.94 Å, respectively, and (7) 47Q, 51E with a distance of 8.35 Å, and 6.77 Å, respectively. This is indicated in **Figure 3.2. (c) and Figure 3.4**. Moreover, for Fe^{+2}, the binding potential is shown in **Figure 3.2. (d)**. A well-illustrated diagrammatic representation of the conjugation of lactoferrin to IONPs by employing EDC/NHS coupling reaction to synthesize LF-IONPs is illustrated in **Figure 3.5.**

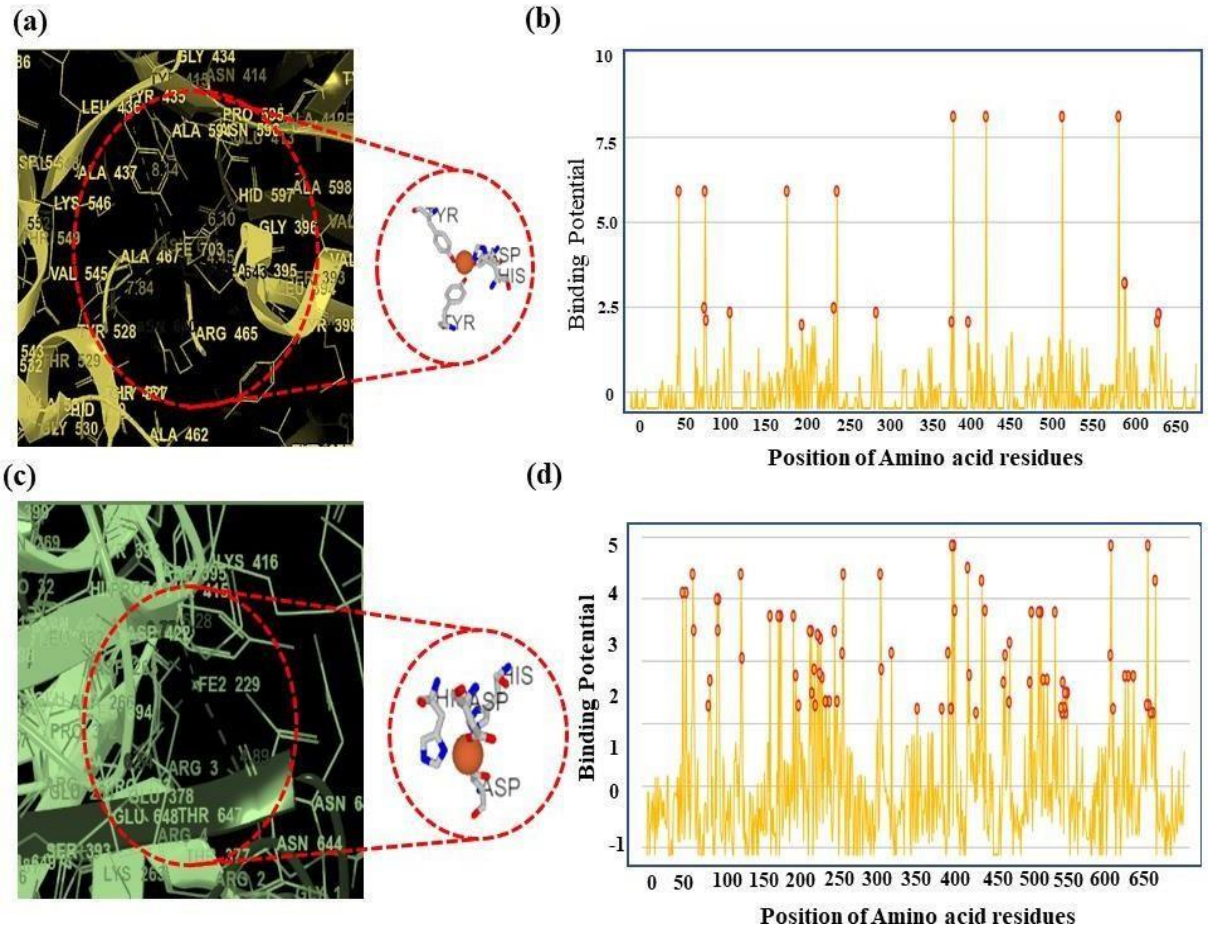

Figure 3.2. Metal ion binding residues showing binding of Fe^{+3} and Fe^{+2} with amino acids on the chain of the lactoferrin protein (a) Binding of Fe^{+3} with amino acids 435Y, 597H, 395D, 528Y, and their distance was measured to be 8.14 Å, 6.10 Å, 4.45 Å, 7.84 Å respectively

(b) Binding of Fe^{+2} with amino acids 393S, 395D, 597H, 644N with a distance of 6.4 Å, 5.28 Å, 3.77 Å, 4.89 Å respectively.

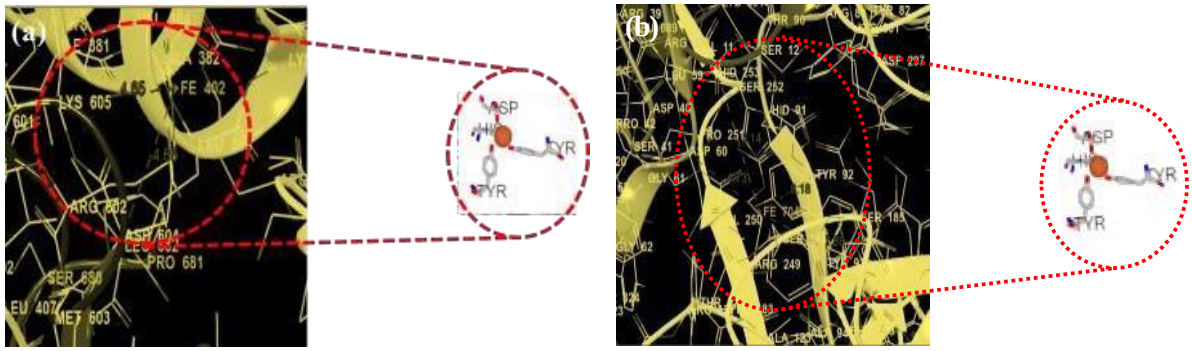

Figure 3.3. Metal ion binding residues showing binding of Fe^{+3} with amino acids on the chain of the lactoferrin protein (a) Binding of Fe^{+3} with amino acids 60D, 92Y, 192Y, 253H and they were at a distance of 4.73 Å, 8.18 Å, 7.89 Å, 6.14 Å respectively (b) Binding of Fe^{+3} with amino acids 604D, 605K with a distance of about 4.65 Å, 4.65 Å respectively.

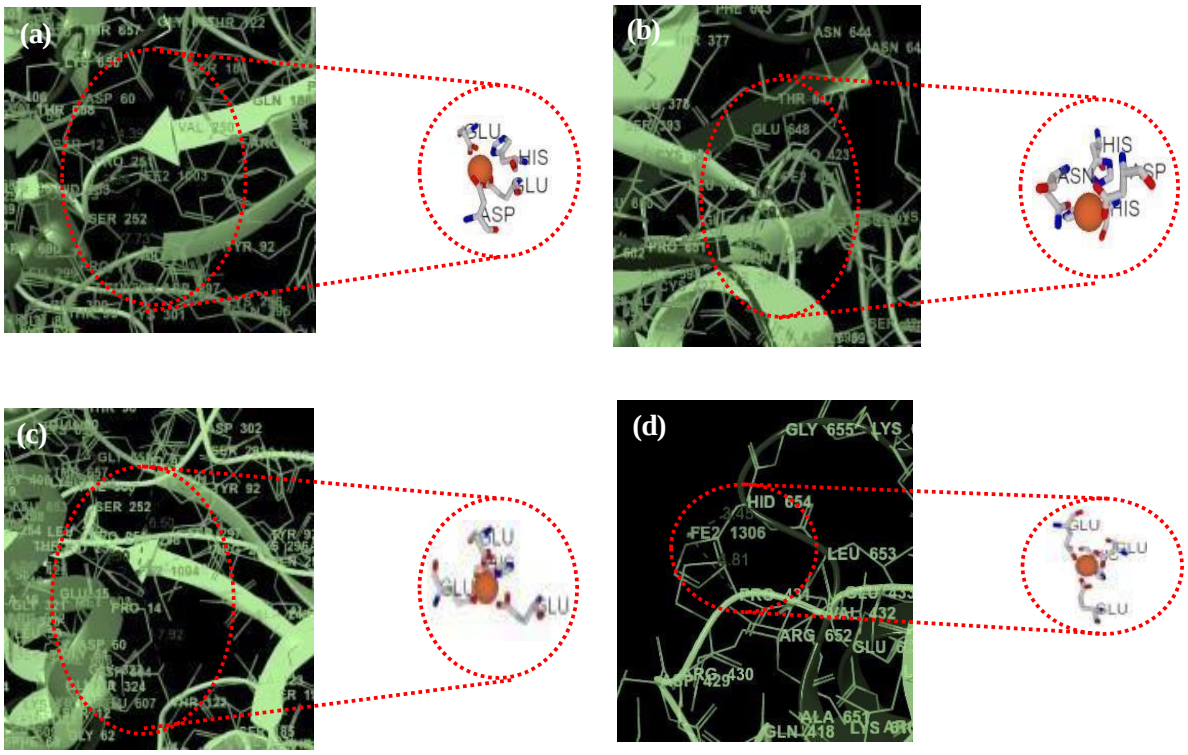

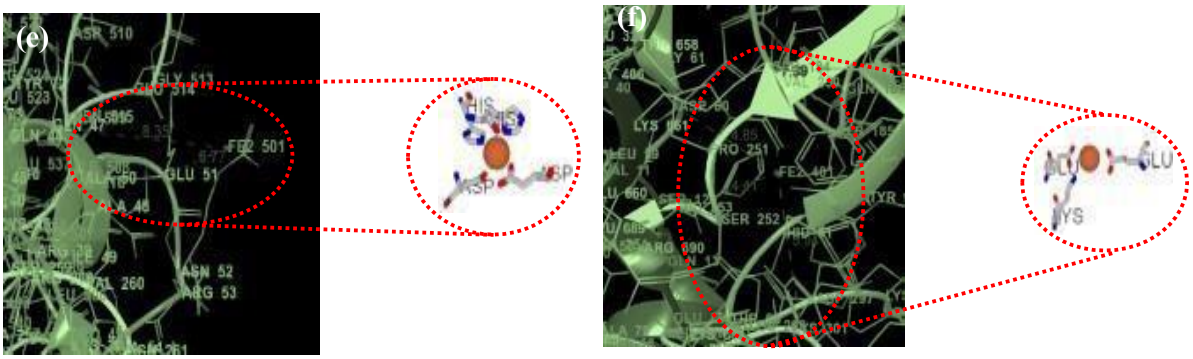

Figure 3.4. Metal ion binding residues showing binding of Fe^{+2} with amino acids on the chain of the lactoferrin protein (a) Binding of Fe^{+2} with amino acids 393S, 413E, 597H, 644N and distance was found out to be 6.59 Å, 4.99 Å, 3.06 Å, 5.23 Å respectively (b) Binding of Fe^{+2} with amino acids 60D, 122T, 253H, 301K and their distance were as such 4.39 Å, 7.05 Å, 3.84 Å,7.73 Å respectively (c) Binding of Fe^{+2} with amino acids 60D, 122T, 253H, 301K which showed distance of 4.45 Å, 7.92 Å, 3.90 Å, 6.50 Å respectively (d) Binding of Fe^{+2} with amino acids 431P, 654H with a distance of 4.81 Å, 3.45 Å respectively (e) Binding of Fe^{+2} with amino acids 60D, 122T, 253H, 301K and showed distance of about 4.85 Å, 7.39 Å, 4.41 Å, 5.94 Å respectively (f) 47Q, 51E with a distance of 8.35 Å, 6.77 Å respectively.

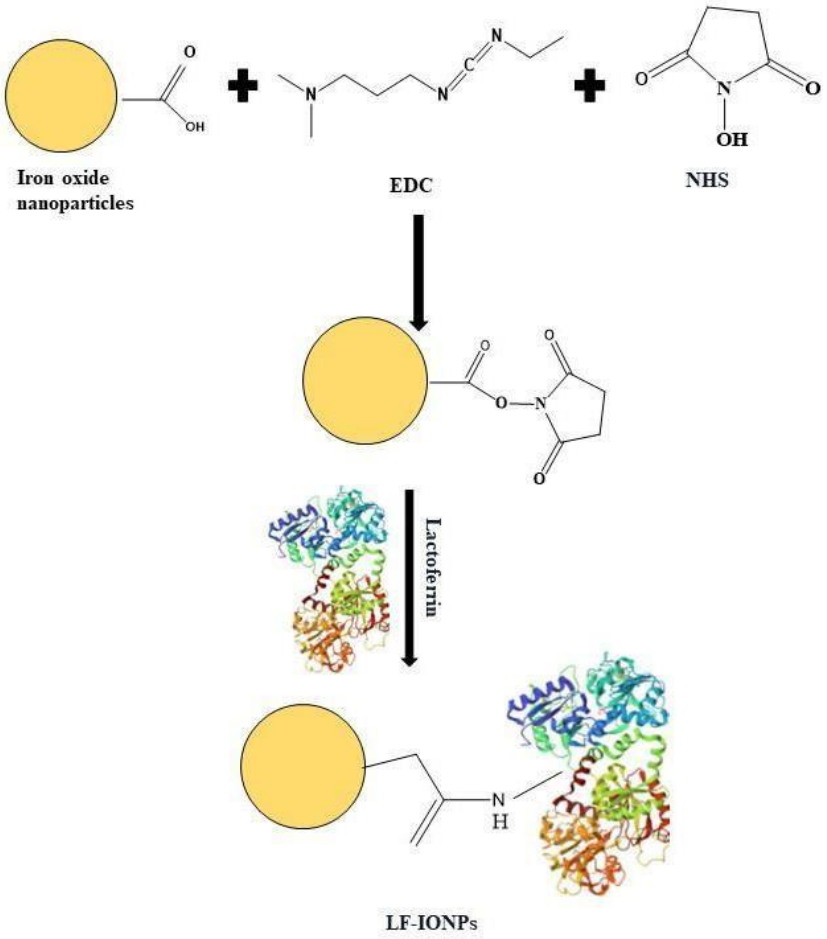

Figure 3.5. The figure indicates the schematic presentation of the synthesis procedure. It depicts the schematic representation for the conjugation of lactoferrin protein with iron oxide nanoparticles, which is achieved through EDC/ NHS coupling reaction.

3.3.4 XRD analysis

XRD was conducted to assess the crystallinity of the materials. **Figure 3.6.** shows the XRD diffraction patterns of IONPs, lactoferrin protein (LF), and LF-IONPs. The diffraction peaks observed in XRD patterns of IONPs appearing at 2Θ = 30º, 35º, 43º, 52º, 57º, 62º correspond to crystal planes (220), (311), (400), (422), (511), and (440), respectively. These peaks match well with the one reported in standard JCPDS data base (Card No. # 00-003-0863) for Fe_3O_4. Synthesized IONPs possess inverse spinel cubic structure. The diffraction patterns for iron oxide in lactoferrin-iron oxide nanospheres were observed at the same position as those in iron oxide particles, suggesting that adding lactoferrin to the IONPs does not alter their crystal structure. Alternatively, in the XRD pattern of lactoferrin protein, a broad hump was observed in the range of 23º -25º, which indicates the presence of an amorphous material, as it lacks the distinct and sharp peak associated with crystalline structure. The crystallite size of IONPs and

LF-IONPs was determined by the Scherrer formula **(Eq 1)** and is reported in **Table 3.3**.

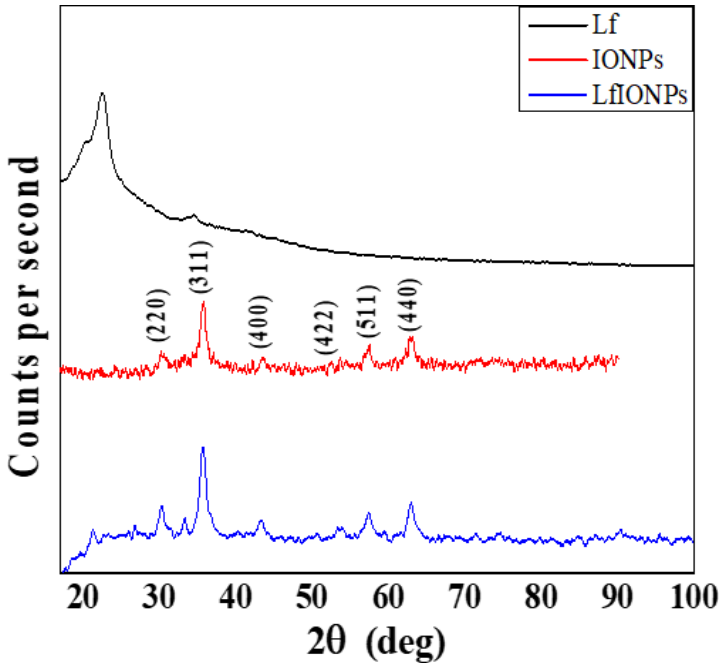

Figure 3.6. XRD graph indicates the X-ray diffraction pattern, which gives deep knowledge regarding chemical composition, crystallographic structure, and physical properties of materials, including IONPs, LF, and LF-IONPs when subjected to the Cu K α irradiation

Table 3.3. Saturation magnetization (M_S), remanence (M_r), coercivity (H_C), and crystallite size of bare IONPs and lactoferrin coated iron oxide nanoparticles (LF-IONPs).

Parameters	**Samples**	
	IONPs	**LF-IONPs**
M_S (emu/g)	50.88	50.04
M_r (emu/g)	0.03	0.04
H_C (Oe)	0.26	0.68
Crystallite size (nm)	15.55	17.77

3.3.5 Hyperthermia study

To understand the magnetic hyperthermia heating effects of the nanoparticles, the temperature vs time profiles were recorded under varying frequencies while keeping the field strength and nanoparticle concentration constant. At each frequency, the sample was subjected to the hyperthermia treatment for 10 minutes Initial temperature of the sample before the field exposure was 30 ºC. Further, with increase in frequency from 161.9 kHz to 935.3 kHz, highest

temperature produced by the nanoparticles after 10 min exposure increased from 33.26 ºC to 66.26 ºC, (**Figure 3.7. (a))** This rise in temperature indicates that the nanoparticles have the enormous potency for their use in magnetic hyperthermia treatment of cancer. SAR (Specific Absorption Rate) and ILP (Intrinsic Loss Power) values were also calculated for LF-IONPs which are reported in **Table 3.4.**

Table 3.4. SAR and ILP of LF-IONPs measured at different field frequencies

Frequency (kHz)	**SAR (W/g)**	**ILP (**nHm^2/k**)**
161.9	3.49 ± 0.449	0.34 ± 0.044
242.4	9.71 ± 0.722	0.63 ± 0.047
411.1	37.46 ± 3.397	1.43 ± 0.130
580.2	49.86 ± 3.477	1.35 ± 0.094
935.3	75.95 ± 6.279	1.28 ± 0.106

3.3.6 Magnetic properties

The magnetic characteristics of bare and LF-IONPs were determined by measuring their M-H hysteresis loops. M-H measurements were performed at room temperature on Lakeshore 7404 model in the field range of $\pm$ 10 kOe. M-H loops of IONPs and LF-IONPs are presented in **Figure 3.7. (b).** From these hysteresis loops, saturation magnetization (M_S), Coercivity (H_C), and remanence (M_r) are determined, which are given in **Table 3.3.** From **Table 3.3.**, it is evident that both the remanence and coercivity of IONPs and LF-IONPs are nearly zero, indicating synthesized nanoparticles to be superparamagnetic. This indicates that at room temperature, thermal energy have potential to overcome the magnetic anisotropy energy and keep them randomly placed in the absence of an external magnetic field. Further, LF-IONPs also possess high saturation magnetization, making them a suitable candidate for magnetic hyperthermia applications.

3.3.7 Drug Loading and Release Kinetics

The encapsulation efficiency of LF protein over IONPs was found to be 93 ± 0.014 %. The drug release was monitored at pH 7.4 and pH 3. No drug release was observed at the physiological pH of 7.4. However, when the studies at gastric pH was performed, the drug was observed to have a burst release for the first 8 h followed by a sustained release for the next ~30 h. At the end of 40 h, 92.18 ± 0.003 % of the drug was released, highlighting the potency

of LF-IONPs as a drug delivery agents **(Figure 3.7. c, d)** and shown in **Figure 3.6**.

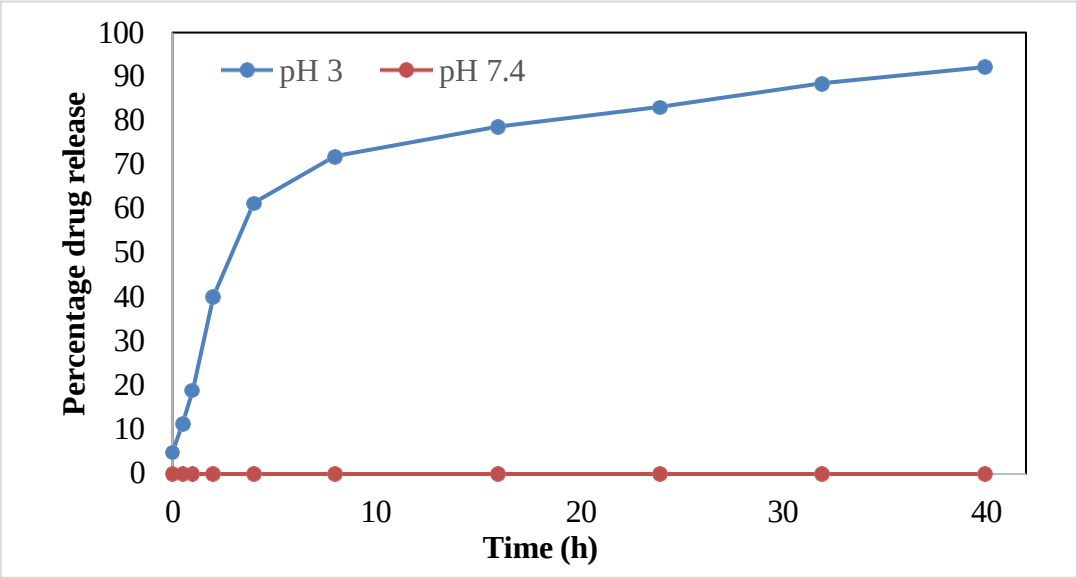

Figure 3.6. The plot displays the release kinetic studies conducted to determine the percentage of drug release from LF-IONPs at pH 7.4 and pH 3.

3.3.8 *in-vitro* cell line studies in the presence and absence of hyperthermia

For determining the cytotoxicity of LF-IONPs on the cancer cell line AGS, an MTT assay was employed under physiological conditions. The cytotoxicity was calculated for $FeCl_3$ and $FeSO_4$ salt solutions, LF protein, IONPs, and LF-IONPs at three concentrations: 5 µg/ml, 7.5 µg/ml, and 10 µg/ml. Three independent sets were prepared for each concentration, along with control. The assay was performed both with and without hyperthermia treatment to obtain the efficacy of the treatment.

In the MTT assay without hyperthermia treatment, cells treated with $FeCl_3$ salt solution showed cell viability of 98.67 ± 4.5% at 5 µg/ml, 96.65 ± 5.8% at 7.5 µg/ml, and 95.38 ± 4% at 10 µg/ml. Similarly, $FeSO_4$-treated cells showed cell viability as 97.61 ± 1.62% at 5 µg/ml, 96.44 ± 6.15% at 7.5 µg/ml, and 94.32 ± 3.74% at 10 µg/ml. Cells treated with LF showed cell viability of 98.35 ± 1.2% at 5 µg/ml, 93.58 ± 5.8% at 7.5 µg/ml, and 77.87 ± 4.5% at 10 µg/ml. For cells treated with IONPs, the cell viability was 98.06 ± 11.80%at 5 µg/ml, 93.48 ± 7.03%at 7.5 µg/ml, and 85.03 ± 3.95%at 10 µg/ml. Finally, cells treated with LF-IONPs showed cell viability of 85.56 ± 4.25%at 5 µg/ml, 85.21 ± 7.06%at 7.5 µg/ml, and 81.69 ± 3.76%at 10 µg/ml concentration.

After the incubation, the cells were subjected to hyperthermia treatment (at a frequency of

242.4 kHz for 10 minutes), and an MTT assay was done to study the effect of synthesized formulations on cell viability. The treated cells exhibited significantly enhanced cytotoxicity in comparison with control group. For $FeCl_3$ salt solution-treated cells, the cell viability was 95.38 ± 3.9% at 5 µg/ml, 92.62 ± 10.4% at 7.5 µg/ml, and 91.88 ± 2% at 10 µg/ml. After treating cells with $FeSO_4$ salt solution, the cell viability was 94.11 ± 0.77% at 5 µg/ml, 92.73 ± 9.54% at 7.5 µg/ml, and 91.14 ± 0.49% at 10 µg/ml. For LF-treated cells, the cell viability levels were 61.53 ± 3.9%, 60.26 ± 10.4%, and 40.95 ± 2% for the concentrations 5 µg/ml, 7.5 µg/ml, and 10 µg/ml, respectively. On the other hand, cells treated with IONPs showed cell viability levels of 52.36 ± 0.77% for 5 µg/ml, 41.53 ± 9.54% at 7.5 µg/ml, and 35.70 ± 0.49% at 10 µg/ml. Lastly, LF-IONPs resulted in cell viability levels of 49.33 ± 4%, 36.18 ± 9.7%, and 32.25 ± 5.2% for 5 µg/ml, 7.5 µg/ml, and 10 µg/ml, respectively. These results provide substantial evidence of the cytotoxic nature of the synthesized nanospheres against cancerous cells, which can be further explored for anti-cancerous activity. The data is shown in **Figure 3.7. (e)**. Table shows the p values calculated for % variation in cell viability after treating with 5, 7.5, and 10 µg/ml of IONPs and LF-IONPs with and without hyperthermia. The data is statistically significant, when the $p < 0.05$ and the comparative data is given in **Table 3.5.**

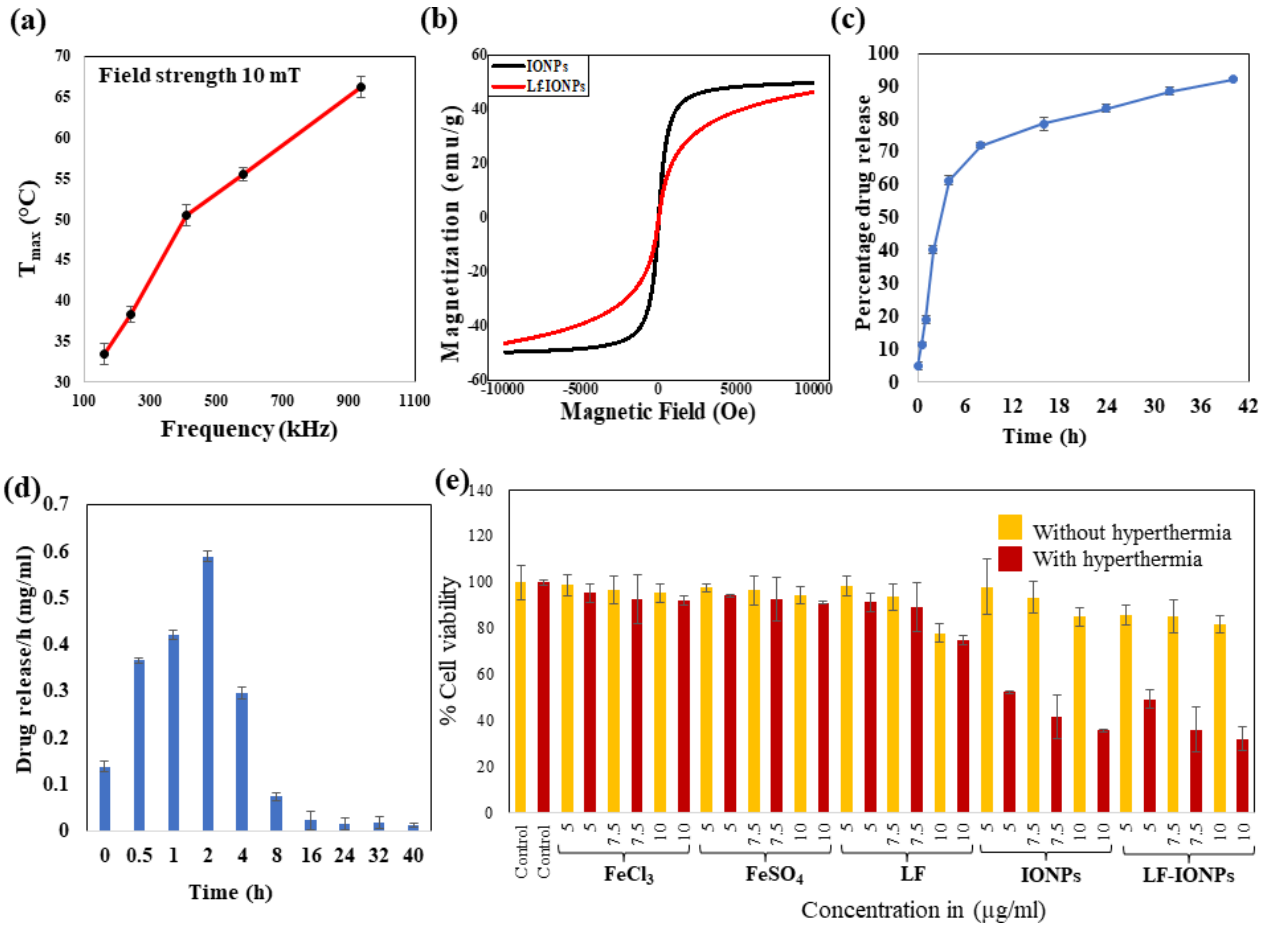

Figure 3.7. Determination of hyperthermia responsiveness by LF-IONPs (a) The figure illustrates the heating capacity of LF-Iron oxide nanospheres at different frequencies with a constant magnetic field of 10 mT. It shows the temperature rise, i.e., 33.26 ºC, 38.34 ºC, 50.56 ºC, 55.54 ºC, and 66.26 ºC at different frequencies; 161.9 kHz, 242.4 kHz, 411.1 kHz, 580.2 kHz, and 935.3 kHz, respectively. (b) M-H loops of IONPs and LF-IONPs measured at room temperature (c) The plot displays the release kinetic studies conducted to monitor the percentage of drug release from LF-IONPs at pH 3. (d) The graph represents the drug release per h in mg/ml at pH 3. (e) The MTT assay determined the cytotoxic activity of AGS cells in the absence and presence of hyperthermia. The data show the treatment of AGS cells with control, including salt solutions $FeCl_3$ and $FeSO_4$, LF, IONPs, and LF-IONPs at concentrations 5 µg/ml, 7.5 µg/ml, and 10 µg/ml for each sample, both in the absence and presence of hyperthermia treatment. The data were plotted as the mean of three separate experiments.

Table 3.5. Table indicates the p values determined for % variation in cell viability after treating with 5, 7.5 and 10 µg/ml of IONPs and LF-IONPs with and without hyperthermia. The statistical significance of data is considered when the $p < 0.05$

P value for checking the statistical significance of data		
Concentration	**IONPs**	**LF-IONPs**
5µg/ml	0.0079	0.0136
7.5 µg/ml	0.0231	0.0350
10 µg/ml	0.0021	0.0085

3.3.9 Scratch assay for anti-cancer activity

To assess the impact of LF-IONPs on the migration ability of AGS cells, a scratch assay was employed in which the cells after exposure to a fixed concentration (10 µg/ml) of LF-IONPs, LF, and Iron oxide nanoparticles (IONPs). To determine the percentage variation in the scratch width, the diameter was measured at three distinct positions for each scratch, and the mean diameter of individual readings of each scratch was calculated. Control cells exhibited gap percentages of 26.19 ± 0.35%, 46.42 ± 0.30%, 54.76 ± 0.35%, and 66.66 ± 0.35% after 6, 12, 24, 36, and 48 h, respectively. In contrast, the cells treated with IONPs showed gap percentages of 12.85 ± 0.26%, 34.52 ± 0.17%, 46.19 ± 0.39%, 50.47 ± 0.07%, and 56.19 ± 0.44% after the same time intervals. Furthermore, LF-treated cells displayed even greater inhibition at 6, 12, 24, 36, and 48 h with percentages of 11.90 ± 0.35%, 30.95 ± 0.35%, 38.09 ± 0.35%, 47.61 ± 0.17%, and 51.42 ± 0.16%, respectively. The LF-IONPs treatment showed the most inhibition, with percentages of 4.76 ± 0.35%, 21.42 ± 0.60%, 33.33 ± 0.35%, 42.85 ± 0.60%, and 47.61 ± 0.35% after 6, 12, 24, 36, and 48 h, respectively. The results indicated that LF-IONPs treatment significantly inhibited cell migration compared to control cells, which almost filled the gap within 48 h. These findings further support the nanoparticles' anti-cancerous properties, as demonstrated in **Figure 3.8**. To determine the statistical significance of the data, p-values were determined for the scratch assay after treatment, and the comparative data are presented in **Table 3.6.**

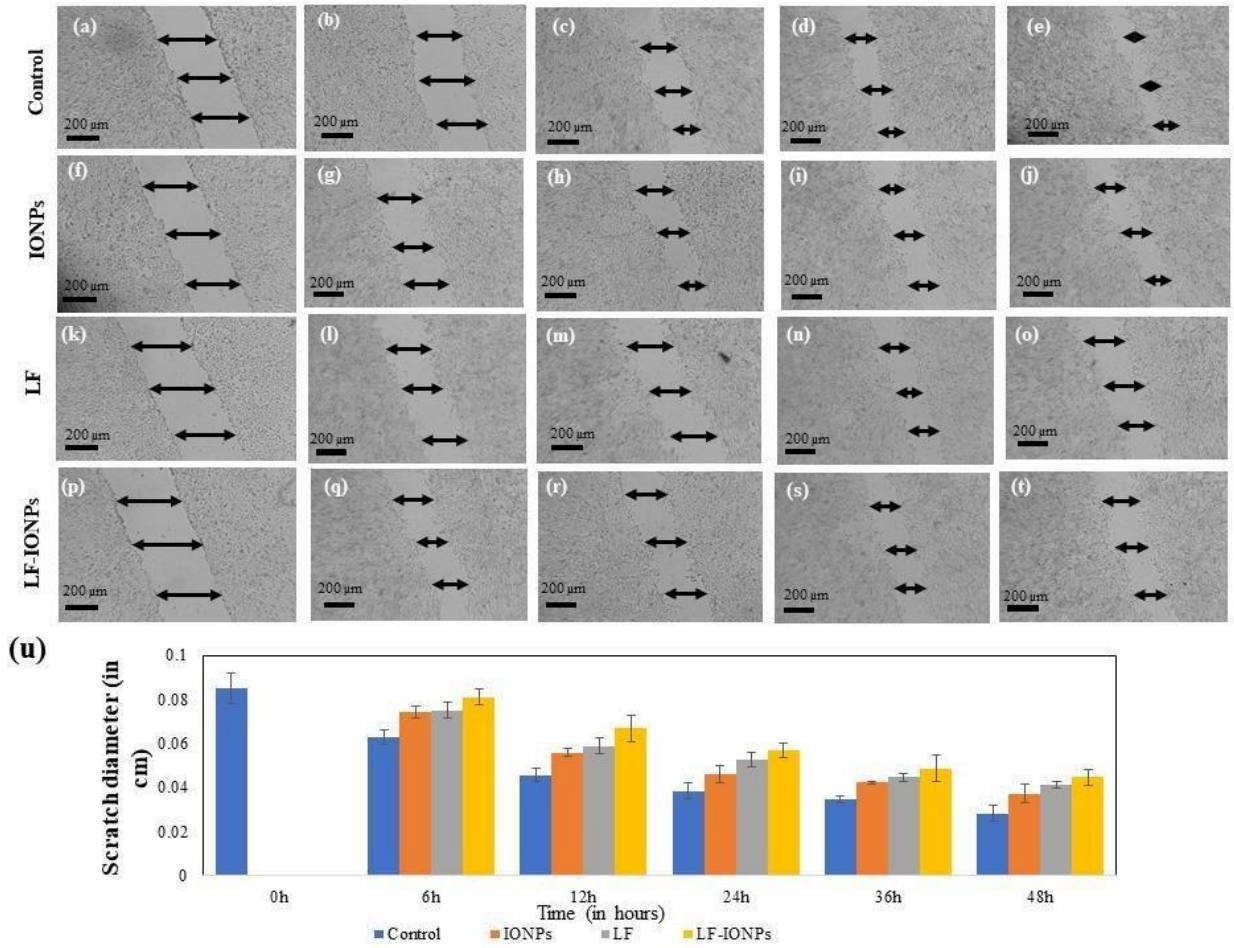

Figure 3.8. The Figure shows the anti-cancer effect of nanoparticles using AGS cell line via scratch assay (a)6 h (b) 12 h (c) 24 h (d) 36 h (e) 58 h are control cells, IONPs treated cells after (f) 6 h (g) 12 h (h) 24 h (i) 36 h (j) 48 h at a fixed concentration of 10 µg/ml, LF treated cells after (k) 6 h (l) 12 h (m) 24 h (n) 36 h (o) 48 h with a concentration of 10 µg/ml, Cells treated with LF-IONPs after (p) 6 h (q) 12 h (r) 24 h (s) 36 h (t) 48 h with 10 µg/ml concentration (u) Plot showing the comparison of the change in scratch diameter post-treatment with LF, IONPs, and LF-IONPs including control after 6 h, 12 h, 24 h, 36 h, and 48 h.

Table 3.6. Table shows the p values calculated for % variation in scratch diameter after treatment with 10 µg/ml of $FeCl_3$, $FeSO_4$, lactoferrin, IONPs and lactoferrin-IONPs. The statistical significance of data is considered when the $p < 0.05$.

P value for checking the statistical significance of data			
Time	**LF**	**IONPs**	**LF-IONPs**
6h	0.013236	0.011081	0.003126
12h	0.007966	0.00749	0.005609
24h	0.007763	0.073926	0.003126
36h	0.001935	0.001685	0.004992
48h	0.003772	0.051658	0.004813

3.4 Conclusion

To investigate the role of nanoparticles as an anti-cancer agent, lactoferrin protein was used as a capping agent and iron oxide nanoparticles. Both of these components have demonstrated anti-cancer activities. Lactoferrin interacts with high levels of proteoglycan, glycosaminoglycan, and sialic acid found in cancer cells and activates the signaling pathways to exert cytotoxic effects on gastric cancer cells. IONPs, which were formulated by using the co-precipitation method, were linked with lactoferrin protein by EDC-NHS, which activates the carboxyl group on the surface of iron oxide particles, facilitating their conjugation with the protein. The synthesized particles exhibited a desirable HR-TEM size of about 15 ± 2 nm and demonstrated notable heating capacity after exposure to the external magnetic field.

By successfully conjugating lactoferrin with IONPs, we achieved target specific delivery to gastric cancer cells, as lactoferrin is known to interact with proteoglycan, glycosaminoglycan, and sialic acid, which are found on the surface of cancer cells. Furthermore, lactoferrin and iron oxide nanoparticles showed potent synergistic anti-cancer activity against cancer cell lines at a very low concentration. These particles were easily internalized in the AGS cell line, and the synthesized LF-IONPs (lactoferrin conjugated iron oxide nanospheres) showed a remarkable increase in anti-cancer properties as compared to individual components. This significantly enhanced efficacy, combined with a great degree of selectivity, can be attributed to the conjugation of LF and IONPs.

The remarkable superparamagnetic behavior, substantial magnetization capacity, and excellent heating capacity of these nanospheres hold great promise for their use in numerous areas of biomedical research applications. We strongly believe that these synthesized particles have great potential to target different types of cancer cell lines effectively. We believe that the findings of this paper will inspire further research for the future use of these anti-cancer nanoparticles.

Chapter 4: Immune Activation via Hyperthermia treated iron oxide coated Helicobacter pylori

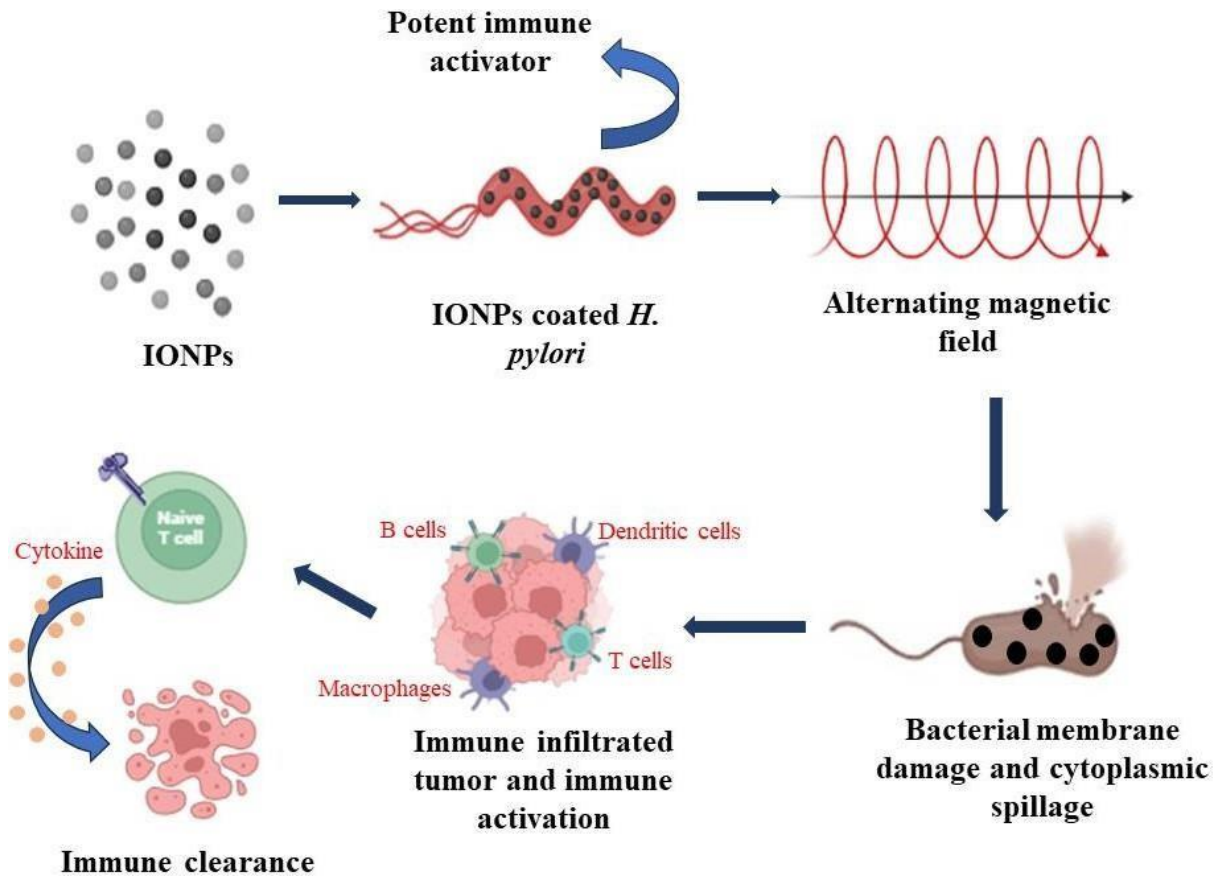

Figure 4.1. The figure depicts the graphical representation of invoking immune response by coating IONPs on the *H. pylori* surface.

Abstract

Gastric cancer is a significant global health concern, often resulting from chronic inflammation caused by *Helicobacter pylori* infection, dietary factors, and genetic predispositions. Traditional treatment methods, including chemotherapy, radiation, and surgical interventions, often come with severe side effects such as nausea, fatigue, and immunosuppression, that significantly effect life quality of patient. Given the limitations of these treatments, the researchers are working on developing alternative therapies which harness the body's natural

defenses. This study explores the potential of stimulating both natural and cell-mediated immunity to combat gastric cancer. By leveraging the microbiome present in cancer tissue, we propose using *Helicobacter pylori* coated with iron oxide nanoparticles for gathering immune cells to the tumor site through magnetic hyperthermia. The destruction of bacteria within the tumor is expected to attract tissue macrophages, initiating a cascade of immune responses that promote the clearance of cancer tissue. This approach aims to stimulate innate and adaptive immune responses, enhancing overall antitumor effect and improving the ability of immune system towards recognizing and targeting tumor cells effectively.

4.1 Introduction

Gastric cancer ranks as the fourth most prevalent cancer worldwide and stands as the second leading cause of cancer-related deaths globally. The main causative agent of this cancer is *Helicobacter pylori* [260]. Gastric cancer is categorized into early-stage which is restricted to the mucosa and submucosa, in middle stage it extends beyond the submucosa into the muscle layer and in advanced stages tumor cells reach the subserosa or infiltrate surrounding organs [261]. Thus, preventing gastric cancer is more effective than treating it. Additionally, modern chemotherapeutic treatments often cause severe side effects, such as hair and weight loss, diarrhea, anemia, blood clots, and damage to the heart, kidneys, and liver, all of which can remarkably reduce the life quality of patients [262]. The tumor microenvironment involves a complicated and dynamic cellular and molecular network which surrounds a cancer tumor, playing a critical part in progress, and metastasis of cancer, and response to therapy. Knowledge about tumor microenvironment is vital for developing efficient cancer treatments [263]. The tumor microenvironment has two components: cellular and non-cellular. The cellular component comprises cancer cells, stromal cells, immune cells, endothelial cells, and adipocytes, whereas the non-cellular component is comprised of extracellular matrix, cytokines, chemokines, growth factors, and metabolic components. In tumor microenvironment, cancerous cells act as the primary drivers of the tumor, distinguished by their uncontrolled growth and ability to evade apoptosis. Surrounding these cancer cells are stromal cells, including fibroblasts, myofibroblasts, and pericytes, which offer structural support and contribute to tumor growth, particularly through the activity of cancer-associated fibroblasts (CAFs) that assists in remodeling the extracellular matrix (ECM). Immune cells, including tumor-associated macrophages (TAMs), T cells, and regulatory T cells (Tregs), play complex roles, with some attacking cancer cells while others aid in tumor progression and

immune suppression. Endothelial cells, which line the blood vessels, are crucial for angiogenesis, supplying the tumor with essential nutrients and oxygen. Additionally, adipocytes, or fat cells, support the tumor by providing energy and secreting factors that further drive tumor growth [264]. The non-cellular constituents of the tumor microenvironment (TME) assists in tumor development and progression. The extracellular matrix (ECM), a complicated network of proteins and glycoproteins like collagen and fibronectin, provides structural support to cells while also regulating their behavior through interactions with receptors on cellular surface [265]. Cytokines and chemokines are signaling molecules that facilitate communication between cells in the tumor microenvironment, influencing immune cell recruitment, inflammation, and tumor growth [266]. Growth factors, including vascular endothelial growth factor (VEGF) and transforming growth factor-beta (TGF-β), are key drivers of angiogenesis, cell proliferation, and immune evasion [267]. Additionally, the tumor microenvironment is often hypoxic, leading to altered cancer cell metabolism, such as increased glycolysis (Warburg effect), and the accumulation of metabolic byproducts that can suppress the immune response, further promoting tumor survival and progression [268]. The tumor environment supports tumor growth through angiogenesis, immune suppression, and ECM remodeling. It also facilitates metastasis by enabling cancer cells to invade surrounding tissues and enter the bloodstream. The tumor microenvironment can contribute to resistance to chemotherapy, radiation, and targeted therapies by creating a protective niche for cancer cells and altering drug delivery. Therapies that target components of the tumor microenvironment, such as immune checkpoint inhibitors, anti-angiogenic agents, and ECM-targeting drugs, are being developed to overcome therapeutic resistance and improve outcomes [269].

The cancer microbiome is the terminology for the collection of microorganisms, including bacteria, viruses, fungi, and other microbes, which are found within the tumor microenvironment or in other tissues of cancer patients. These microbiomes can influence cancer development, progression, and response to treatment. The relationship between the microbiome and cancer is complex and can vary based on cancer type, geographic location, and environmental factors. There are different kinds of microbiomes in different kinds of cancers. In colorectal cancer, *Fusobacterium nucleatum* is frequently found, and is linked with tumor progression and poor prognosis. It may influence tumorigenesis through its ability to modulate immune responses and promote inflammation [270]. For liver cancer development Hepatitis B virus (HBV) and Hepatitis C virus (HCV) are significant contributors due to their role in chronic liver inflammation and cirrhosis [271]. Further, *Porphyromonas gingivalis* is

associated with periodontal disease, and this bacterium is associated with an higher chances of pancreatic cancer [272]. Bacteria like *Escherichia coli* and *Staphylococcus epidermidis* are linked with breast cancer. These bacteria have been found in breast tissue and are thought to influence breast cancer through mechanisms like DNA damage and immune modulation. Also, there is an increased presence of *Methylobacterium* in the breast tissue of cancer patients in comparison to healthy individuals. [273]. For gastric cancer, *Helicobacter pylori* is a potent risk factor that leads to chronic inflammation, eventually damaging the DNA and the development of gastric adenocarcinoma [274]. The composites of the cancer microbiome can differ significantly based on geography, country, and environmental factors. These variations are influenced by differences in diet, lifestyle, socioeconomic status, healthcare access, and exposure to environmental factors like pollutants and antibiotics. In Western countries, where diets are high in red meat and low in fiber, a higher prevalence of *Fusobacterium nucleatum* is observed in colorectal cancer patients. In contrast, in Asian countries, where diets are richer in vegetables and fermented foods, there may be a different microbiome profile, with higher levels of bacteria like *Bifidobacterium* [275]. The chances of *Helicobacter pylori* infection is more in developing countries, where hygiene standards and healthcare access may be lower. This corresponds with higher rates of gastric cancer in these regions compared to developed countries [11]. In some African countries, the breast microbiome might show a different profile compared to Western countries, influenced by factors like breastfeeding practices, diet, and environmental exposure [273]. Diet plays a significant role in shaping the microbiome. High-fat, low-fiber diets typical in Western countries can lead to a microbiome that promotes inflammation and cancer, while diets rich in fiber and fermented foods, common in many Asian countries, may support a more protective microbiome [276].

In recent decades, nanomaterials smaller than 100 nanometers have attracted significant interest in cancer research because of their enhanced applications compared to their bulk counterparts, making them valuable for both therapeutic and diagnostic applications. Additionally, nanomaterials are extensively utilized as effective carriers for targeted carriage of potent agents, which enhances therapeutic efficacy and reduces side effects [277] [278] [279]. There are many nanomaterials that are being used in theranostics, such as Magnetic nanoparticles (MNPs), polymeric nanoparticles (NPs), lipid-based NPs, dendrimers, cage proteins, and inorganic NPs [280]. Amongst magnetic nanoparticles, superparamagnetic iron oxide nanoparticles (SPIONs) are highly demanding in this area because of their low toxicity, compatibility with biological systems, and distinctive magnetic properties [281]. Iron oxide nanoparticles can harm tumor tissue by generating heat after exposure to a high-frequency

alternating magnetic field (AMF) [282]. This heat is basically generated *via the* magnetic hyperthermia technique. Hyperthermia is attained by employing an alternating magnetic field of an appropriate frequency, which generates heat through the oscillation of the internal magnetic moments of superparamagnetic nanoparticles [283]. The use of an alternating magnetic field (AMF) to activate MNPs is being scrutinized as a method for precise therapeutic tumor heating. Distinct superparamagnetic and ferromagnetic particles, having different coatings and targeting agents, enable specificity to the tumor site and type [284]. There are many drugs linked iron oxide nanoparticles being synthesized for the treating gastric cancer. Some of them are Lactoferrin conjugated IONPs, which are synthesized for targeted delivery to gastric tissue. It is in combination with magnetic hyperthermia, which enhances the efficacy of the treatment [285]. Aastha et al. have formulated gold core mesoporous iron oxide nanoparticles for MR/CT contrast agents in human gastric cancer cells [286]. Ghanbari et al. have prepared DOX@folicacid@iron oxide nanoparticles to enhance the effectiveness and cytotoxicity of the anticancer drug [287].

Immune system activation is a natural and appropriate reaction to invading pathogens, including viruses and bacteria. During most acute infections, this immune response is beneficial as it helps control and eventually eliminate the invading pathogens, causing infection resolution. In chronic infections, the role of immune activation becomes more intricate. The immune system's ongoing surveillance and activity play a crucial part in controlling and suppressing the replication and spread of the pathogen [288]. In this process, many immune cells, signaling molecules, and receptors are involved to mount an effective response. The innate immune system works as the initial defense against invading microbes by recognizing pathogen-associated molecular patterns (PAMPs) and danger-associated molecular patterns (DAMPs) like toll-like receptors (TLRs) and nod-like receptors (NLRs) [289] [290] [291]. When pathogens invade, pattern recognition receptors (PRRs) activate several signaling pathways, including NF-κB, type I interferons (IFNs), and inflammasomes. This activation prompts the secretion of various proinflammatory cytokines and chemokines, that causes inflammation and recruits immune cells. Further, dendritic cells (DCs), and macrophages engulf, digest, and present the antigen on MHC (Major Histocompatibility Complex) to T cells that leading to the activation of T cells and B cells. These molecules coordinates the immune response and stimulates adaptive immunity, which helps the body mount a more targeted and effective defense against the pathogen [292] [293] [294].

Therefore, we hypothesize that immune clearance has been shown to be an effective method

for treating various diseases. Consequently, we aim to investigate whether gastric cancer can be addressed by stimulating both natural and cell-mediated immunity. Microbes are recognized as strong immune activators, and cancer tissue provides an ideal environment for such activation. We propose using the microbiome present in cancer tissue for stimulating the immune system, potentially leading to the elimination of cancer cells. Given that *H. pylori* is linked to gastric cancer, we plan to leverage this bacterium by coating it with iron oxide nanoparticles to draw immune cells to the cancer site through magnetic hyperthermia. When the bacteria within the tumor are destroyed, they will attract tissue macrophages, which will trigger a series of events for activating the immune system and promote the clearance of cancer tissue. These immune cells clear the bacterial debris and attack the tumor cells, thereby eliminating both. This process stimulates both the body's innate and adaptive immune responses, enhancing the overall antitumor effect and contributing to the immune system's ability of recognizing and attacking the tumor cells more effectively.

4.2 Materials and Methods:

4.2.1 Materials

Ferric chloride ($FeCl_3$), ferrous sulfate ($FeSO_4$), polyethylene glycol (PEG 400), sodium hydroxide (NaOH), and deionized water were acquired from LobaChemie, India. HAM's cell culture media, fetal bovine serum (FBS), Brain Heart Infusion (BHI) broth, agar, and penicillin-streptomycin, were all sourced from HiMedia, India.

4.2.2 Development of Iron Oxide Nanoparticles

Magnetic nanoparticles were formulated using a co-precipitation method. In brief, iron (III) chloride hexahydrate and iron (II) sulfate heptahydrate were suspended in 50 mL of distilled water and heated to 90 °C. Then, 3 mL of polyethylene glycol (PEG400) was added, following which ammonium hydroxide solution made by dissolving 10 mL of 25% ammonium hydroxide in 50 mL of water was poured into it dropwise. The resultant mixture was continuously stirred for 30 minutes. The final black mixture was then brought to room temperature followed by centrifugation at 4000 rpm for 10 minutes. Lastly, the nanoparticles were washed five times with deionized water to remove any unbound impurities.

4.2.3 Coating of iron oxide nanoparticles on *H. pylori*

H. pylori culturing was done in BHI broth at 37 ºC, 10% CO_2 and 5% O_2. After optimal growth,

bacterial cells were thoroughly washed using PBS (pH 7), and a pellet was collected and suspended in PBS, and on stirring condition, IONPs were added, and then dropwise STPP (Sodium tripolyphosphate) was added to the mixture followed by stirring it continuously for 2 h and then incubated overnight at 37 ºC. FESEM analysis was done for studying the morphology.

4.2.4 The studies to determine the size and morphology of nanoparticles with elemental analysis

The hydrodynamic size of the nanoparticles was measured with a Malvern DLS-Zeta size analyzer. The exact size, shape, and morphology of IONPs were determined using HRTEM (Talos F200S G2, Thermo Scientific). Before analysis, centrifugation of the nanoparticles at 240 rpm for 15 minutes was done to get rid of any unbound impurities. The final pellet was then analyzed with an energy-dispersive X-ray Spectrometer (EDS) (Bruker QUANTAX 200) to identify the elemental composition.

4.2.5 Spectroscopy analysis; FTIR and RAMAN

FTIR was employed to examine the interactions within the formulated IONPs, specifically to identify chemical bonds and analyze the interactions between artemisinin and the magnetic nanoparticles. The FTIR analysis was conducted using Lab Solutions IR Shimadzu. The sample was then scanned over 400 cm^{-1} to 4000 cm^{-1}. The FTIR data will offer a detailed analysis of the changes in the frequency range of IONPs functional groups after formulation.

4.2.6 XRD Analysis

X-ray diffraction reveals the crystallographic structure, chemical composition, and physical properties of a material. In this study, XRD was used to examine the synthesized nanomaterial. The sample was exposed to Cu Kα radiation after drying (λ = 1.54 Å) to capture the diffraction pattern within a 2θ range of 10-90°. The Scherrer equation was applied to the most intense peak in the diffraction pattern for calculating the crystallite size of the IONPs.

$$d = \frac{K\lambda}{\beta cos\boldsymbol{\theta}} \quad \ldots\ldots \qquad \text{(Eq 1)}$$

where K= 0.9 is the Scherrer constant, λ= 1.54 Å denotes the X-ray wavelength, β determines the broadening of the highest intense peak, and d denotes the crystallite size of the synthesized IONPs.

4.2.7 Assessment of heating capacity through a hyperthermia study

In cancer therapy, hyperthermia involves raising cellular temperatures to 42 – 45 °C to target and destroy tumors. To evaluate the potential of a synthesized material for magnetic hyperthermia, hyperthermia performance was masured on NanoTherics Magnetherm magnetic hyperthermia setup. This device features an optical fiber temperature probe to precisely determine the heating of material. The sample was subjected to a variable magnetic field of 10 mT at different frequencies (161.9 kHz, 242.4 kHz, 411.1 kHz, 580.2 kHz, and 935.3 kHz).

4.2.8 Evaluation of magnetic properties using a Vibrating Sample Magnetometer (VSM)

For evaluating the magnetic properties of the synthesized iron oxide nanoparticles, VSM was used at room temperature. Measurements were carried out on powder samples at ±10 kOe, allowing us to record the hysteresis loop (M-H), which illustrates the link between the material's magnetization and the applied magnetic field. This loop, characteristic of ferromagnetic materials, provides essential information about the nanoparticles' magnetic characteristics, including saturation magnetization (M_s), coercivity (H_c), and remanence (M_r) [243].

4.2.9 *in vitro* studies

4.2.9.1 Cytotoxicity studies

The cell toxicity of the nanoparticles was determined using the MTT (3-(4,5-dimethylthiazol-2-yl)-2,5-diphenyltetrazolium bromide) assay on AGS cells, a gastric adenocarcinoma cancer cell line. In this, 10,000 cells per well were added in a 96-well plate, allowed to reach 75-80% confluency followed by treating with four distinct concentrations (2.5, 5, 7.5, and 10 µg/mL) of the prepared formulations, including $FeCl_3$, $FeSO_4$, and IONPs. Following treatment, the cells were incubated overnight. After incubation, media was discarded, and MTT solution was added for an additional 3 h and later on discarded followed by adding 100 µl of DMSO to each well for a 15-minute incubation. Lastly, the OD of the final solution was determined at 570 nm, and the inhibition percentage was calculated using the given equation.

$$\% \text{ inhibition} = [1 - (At/Ac) \times 100] \% \quad \ldots\ldots\ldots \quad \text{(Eq 2)}$$

where At is the test substance absorbance, and Ac is the control solvent absorbance. The experiment was performed three times to get the concordant values.

4.2.10 Effect of coating on the growth pattern of *H. pylori*

To examine the impact of surface coating of IONPs on the metabolic activity of *H. pylori*, we conducted an analysis of bacterial growth curves. This method allows for the observation of changes in growth patterns over time, providing insights into how coating affects the metabolism of the bacteria. We inoculated the uncoated control bacteria and the IONPs coated bacteria in the BHI media and incubated them in the hypoxia chamber at 37 °C, 10 % CO_2, and 5 % O_2, and checked for their growth patterns after specific intervals of time, i.e 0h, 6h, 12h till 72h. By comparing the growth rates and phases of coated *H. pylori* to those of uncoated control *H. pylori*, we can determine the extent to which surface coating influences metabolic processes and overall bacterial growth.

4.2.11 Hyperthermia treatment on coated *H. pylori*

After coating the bacteria with iron oxide nanoparticles (IONPs), the bacteria were subjected to hyperthermia treatment via the NanoTherics Magnetherm instrument. The coated bacteria was kept in the coil and then exposed to the magnetic field of 10 mT at a frequency of 242.4 kHz. This process involves exposing the coated bacteria to elevated temperatures, typically through the application of an external magnetic field. This causes IONPs to generate heat on the bacteria's surface, leading to the bacteria spillage and causing the release of bacterial components like lipopolysaccharide, bacterial DNA, etc. This effectively targets and destroys the bacteria, enhancing the overall treatment efficacy by activating the body's immune system**.**

4.2.12 Invoking immune system via HM-treated coated *H. pylori*

For conducting this experiment, T cells (H9) and B cells (JM1) were first exposed to the hyperthermia treated IONPs coated bacteria, which was exposed to a magnetic field of 10 mT at a frequency of 242.4 kHz. The cells were then kept for 6 h at 37°C and 5 % CO_2. The incubation period allowed these immune cells to interact with the bacterial components, leading to the activation and production of various cytokines. After the incubation, the conditioned media containing the secreted cytokines was collected and applied to the AGS cell line. This step was crucial for determining whether the cytokines secreted by the immune cells could initiate a response in the AGS cells indicative of an effective immune activation. After the initial treatment, washing was done thrice to get rid of any residual reagents. They were then permeabilized and subsequently fixed using a 2% formaldehyde

solution. Following fixation, the cells were blocked with BSA for 30 minutes for preventing non-specific binding. After blocking, the cells were washed again. Next, primary antibodies IL-6 and TGF-β were added to the cells, and kept for 3 h incubation following which the washing was done efficiently thrice using PBS to eradicate unbound primary antibodies. Secondary antibodies Alexa Fluor 647 and Alexa 488 anti-rabbit were then added, and the cells were kept for one hour. After the final incubation, the cells were washed again, and flow cytometry (FACS) was performed to analyze the samples.

4.3 Results and Discussions

4.3.1 Structure and Composition of IONPs

Shape and size: TEM images **(Figure 4.2. (a))** revealed that the IONPs exhibit a spherical form having an average diameter of 5 ± 2 nm. The analysis, performed at a magnification scale of 20 nm, enabled a thorough examination of the nanoparticles' size and shape.

Hydrodynamic Diameter: DLS analysis showed that the IONPs have a hydrodynamic diameter of 74.12 nm **(Figure 4.2. (b))**. This measurement indicates the average size of the nanoparticles in solution, taking into account the effects of any surrounding solvent molecules or surface functional groups.

Elemental Composition: Analysis using EDS **(Figure 4.2. (c))** confirmed that the IONPs contain essential elements such as carbon (C), oxygen (O), and iron (Fe). The iron content was determined to be 81.76% and was uniformly distributed throughout the nanoparticles, demonstrating effective integration of iron oxide nanoparticle structure.

4.3.2 FTIR and RAMAN for studying interactions in IONPs

FTIR analysis was performed IONPs. The analysis identified various peaks in the IR spectra, offering valuable information about the molecular bonding in the formulated sample.

FTIR analysis was conducted for IONP, and key features were observed. A peak at 537.28 cm^{-1} was found in synthesized sample IONPs, indicating the presence of the Fe-O bond [248]. Additionally, a C-H rocking was observed at 818.64 cm^{-1} in IONPs [295]. Then, a peak at 1074.57 cm^{-1}, corresponds to the CH_2-O-CH_2 vibrations present in the sample [296]. IONPs exhibited a peak at 1413.55 cm^{-1}, associated with -CH_2 vibration [296]. Further, IONPs showed an antisymmetric vibration of water at 1613.55 cm^{-1} [296]. These results are shown in **Figure 4.2. (d)** and summarized in **Table 4.1**.

RAMAN analysis of the synthesized IONPs revealed several significant peaks. The peaks at

518.36 cm^{-1}, 578.95 cm^{-1}, and 686.06 cm^{-1} indicated the presence of the Fe-O, Fe-O (T_{2g}), and Fe-O (A_{1g}) bond, respectively, in IONPs [254]. A peak at 888.04 cm^{-1} corresponded to the C-O-C bond present in IONPs [297]. A peak of the Fe-O bond was obtained at 953.53 cm^{-1} [298]. CH_2 bond was identified at 985.35 cm^{-1} in IONPs [254]. Further, a peak at 1226.58 cm^{-1} was identified as a C-C bond [297]. Additionally, a peak at 1452.80 cm^{-1} corresponds to the O-CH_2 bond present in IONPs [297]. 1559.46 cm^{-1} was associated with the C=C bond in IONPs [299]. The key results are shown in **Figure 4.2. (e)** and summarized in **Table 4.1**.

Table 4.1. The table indicates a comparison of wavenumber values from FTIR (400-4000 cm^{-1}) and Raman spectra (500-1800 cm^{-1}) of IONPs. These values indicate changes in various functional groups, highlighting the formation of IONPs.

FTIR			**RAMAN**		
Functional groups	**IONPs**	**Reference**	**Functional groups**	**IONPs**	**Reference**
Fe-O	537.28	[248]	**Fe-O** **Fe-O (T_{2g})** **Fe-O (A_{1g})**	518.36 578.95 686.06	[254]
C-H rocking	818.64	[295]	**C-O-C**	888.04	[297]
			Fe-O bond	953.53	[298]
CH_2-O-CH_2 vibrations	1074.57	[296]	**CH_2**	985.35	[254]
-CH_2 vibration	1413.55	[296]	**C-C bond**	1226.58	[297]
Antisymmetric vibrations of H_2O	1613.55	[296]	**O-CH_2 bond**	1454.80	[297]
			C=C	1559.46	[299]

4.3.3 XRD analysis

XRD analysis **(Figure 4.2. (f))** was used to examine the crystallinity of the synthesized IONPs. The XRD pattern of IONPs revealed distinctive peaks at 2θ angles of 30°, 35°, 43°, 52°, 57°, and 62°. These peaks are indicative of the crystal planes (220), (311), (400), (422), (511), and

(440) of magnetite (Fe_3O_4), as confirmed by comparison with the one reported in standard JCPDS data base (Card No. # 00-003-0863) for Fe_3O_4. Synthesized IONPs possess inverse spinel cubic structure

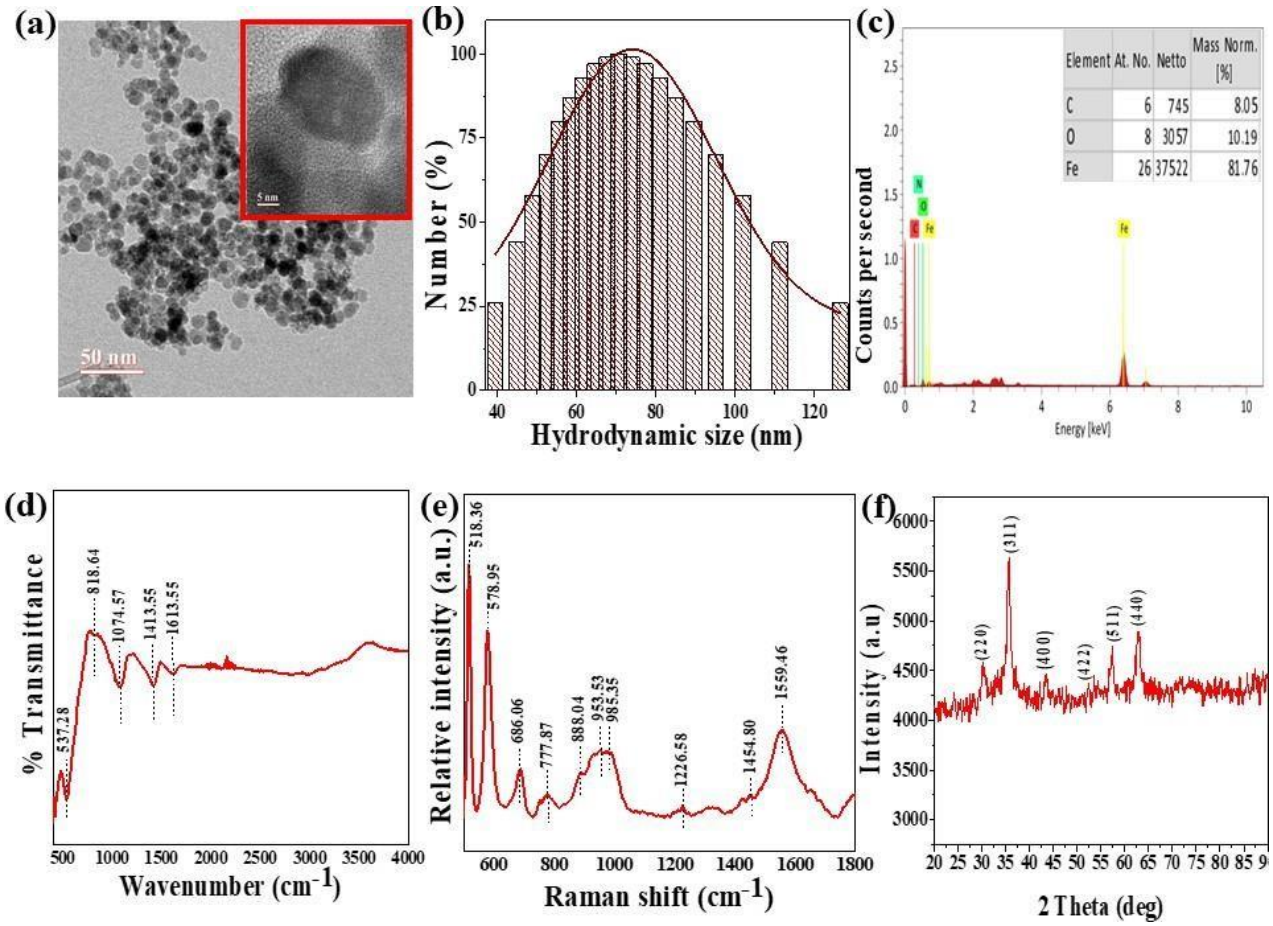

Figure 4.2. Characterization of IONPs (a) HR-TEM images on a scale of 50 nm with an inset showing 5 ± 2 nm size of IONPs (b) DLS showing the hydrodynamic size of the synthesized Iron oxide nanospheres (IONPs) as 74.12 nm (c) EDS showing that iron is present in IONPs as 81.76% (d) FTIR showing the interactions in iron oxide nanoparticles (IONPs) (b) RAMAN providing us with the structural fingerprint by which different molecules can be defined (c) XRD providing the information about the crystalline structure of IONPs.

4.3.4 Hyperthermia study

To assess the heating effectiveness of the synthesized nano-formulations in magnetic hyperthermia, temperature versus time profiles were measured at various frequencies, with field strength and exposure time held constant. Each sample underwent hyperthermia treatment at each frequency for 10 minutes, a duration sufficient to reach the desired temperature before

any risk of overheating. Post-treatment, temperatures increased from 41.08ºC to 45.42ºC, 51.64ºC, 57.62ºC, and 63.69ºC as the frequency rose from 161.9 kHz to 242.4 kHz, 411.1 kHz, 580.2 kHz, and 935.3 kHz, respectively. This pattern is shown in **Figure 4.3. (a)**, which plots maximum temperature (T_{max}) against frequency (kHz). The temperature rise observed underscores the significant potential of these nanoparticles against treating cancer by employing magnetic hyperthermia.

4.3.5 Magnetic Properties (VSM)

The magnetic characteristics of IONPs were assessed through magnetization measurements using a Lakeshore 7404 model at room temperature, within a field range of ±10 kOe. The magnetization versus field (M-H) loops for IONPs are indicated in **Figure 4.3. (b)**. The **Table 4.2.** reveals that both remanence and coercivity values are nearly zero for IONPs, indicating that the nanoparticles are superparamagnetic in nature. This suggests that at room temperature, thermal energy is enough for overcoming the magnetic anisotropy energy, resulting in random orientation of nanoparticles in the absence of an external magnetic field. Additionally, IONPs demonstrate higher saturation magnetization, making them highly effective and well-suited for magnetic hyperthermia applications.

Table 4.2. The table represents the various parameters of the synthesized Iron Oxide Nanoparticles (IONPs) which includes saturation magnetization (M_S), Remanence magnetization (M_{rs}), Coercivity (H_c), and crystallite size.

	Sample
Parameters	**IONPs**
Ms (emu/g)	50.08
M_{rs}	0.03
H_c	0.26
Crystallite size (nm)	15.55

4.3.6 *In-vitro* cell line studies

4.3.6.1 Cytotoxicity assay with and without hyperthermia

An MTT assay was conducted under physiological conditions to assess the toxicity of IONPs on AGS gastric cancer cells. This assay involved calculating cytotoxicity for $FeCl_3$ and $FeSO_4$ salt solutions and IONPs at four concentrations: 5 µg/mL, 7.5 µg/mL, and 10 µg/mL. All samples were tested in three independent sets, both with and without hyperthermia treatment, to evaluate the effectiveness of the formulations.

In the MTT assay without hyperthermia treatment, cell viability was measured relative to the control, which was set at 100%. After being treated with $FeCl_3$, cells exhibited viability of 98.67 ± 4.5% at a concentration of 5 µg/mL, 96.65 ± 5.8% at 7.5 µg/mL, and 95.38 ± 4% at 10 µg/mL. Similarly, cells exposed to $FeSO_4$ demonstrated a viability of 97.61 ± 1.62% at 5 µg/mL, 96.44 ± 6.15% at 7.5 µg/mL and 94.32 ± 3.74% at 10 µg/mL. For the cells treated with IONPs, the viability was 98.06 ± 11.84% at 5 µg/mL, 93.48 ± 7.03% at 7.5 µg/mL, and 85.03 ± 3.95% at 10 µg/mL.

Another MTT assay was done to evaluate cell viability in the presence of hyperthermia treatment. Following treatment, the gastric cancer cells showed a notable reduction in viability when compared with the control group as indicated by the following data.

Cells after treatment with $FeCl_3$ salt solution exhibited a viability of 95.38 ± 3.9% at a concentration of 5 µg/mL, 92.62 ± 10.4% at 7.5 µg/mL, and 91.88 ± 2% at 10 µg/mL. For the cells treated with $FeSO_4$ salt solution, viability was 94.11 ± 0.7% at 5 µg/mL, 92.73 ± 9.5% at 7.5 µg/mL and 91.14 ± 0.49% at 10 µg/mL. Finally, the cells treated with IONPs showed a viability of 52.36 ± 0.77% at 5 µg/mL, 41.53 ± 9.54% at 7.5 µg/mL and 35.70 ± 0.49% at 10 µg/mL. The data demonstrate that IONPs have a cytotoxic effect on AGS cells, suggesting their potential for further investigation as an anti-cancer treatment, as depicted in **Figure 4.3. (c)**. The p values were calculated to determine if data is statistically significant and the values are given in **Table 4.3.**

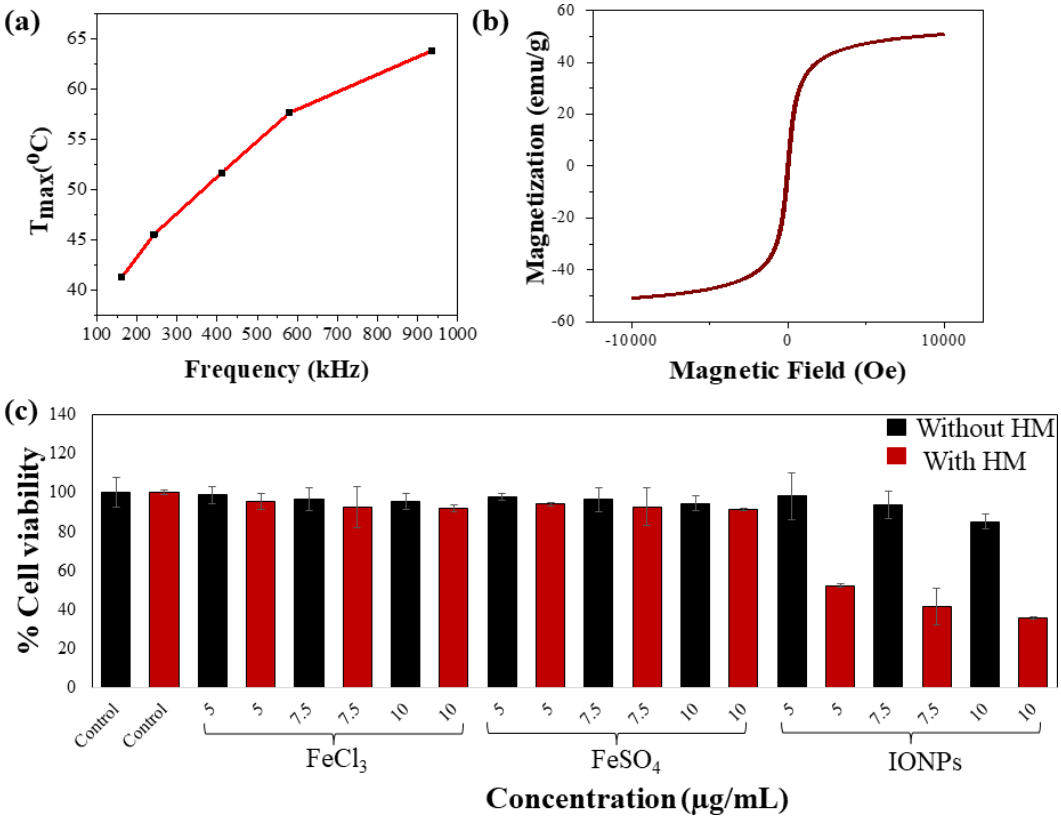

Figure 4.3. Determination of hyperthermia responsiveness by IONPs (a) The figure shows the heating capacity of IONPs at multiple frequencies with a constant magnetic field of 10 mT. The temperature rises recorded were 28.25ºC to 29.14ºC, 31.27ºC, 34.50ºC, and 35.53ºC as the frequency rose from 161.9 kHz to 242.4 kHz, 411.1 kHz, 580.2 kHz, and 935.3 kHz, respectively (b) The M-H loops of IONPs determined at room temperature illustrate their magnetic properties (c) The MTT assay determined the cytotoxic ability of AGS cells in the absence and presence of hyperthermia. The data include treatments with control solutions (FeCl3 and FeSO4) and LF-IONPs at concentrations of 5 µg/ml, 7.5 µg/ml, and 10 µg/ml. Each sample was tested with and without hyperthermia treatment. The results were demonstrated as the mean of three individual experiments.

Table 4.3. Table shows the p values calculated for % variation in cell viability after treating with 5, 7.5 and 10 µg/mL of ART, MNPs and ART-MNPs with hyperthermia. The statistical significance of data is considered when the $p < 0.05$

P value for checking the statistical significance of data (With Hyperthermia)			
Concentration	**$FeCl_3$**	**$FeSO_4$**	**IONPs**
5µg/mL	0.524355	0.442551	0.013542
7.5 µg/mL	0.537701	0.537701	0.023249
10 µg/mL	0.296679	0.277773	0.007455
P value for checking the statistical significance of data (Without Hyperthermia)			
Concentration	**$FeCl_3$**	**$FeSO_4$**	**IONPs**
5µg/mL	0.855361	0.745543	0.019826
7.5 µg/mL	0.671176	0.665315	0.022778
10 µg/mL	0.546598	0.458336	0.013088

4.3.7 Effect of IONPs coating on the growth pattern of *H. pylori*

To investigate how surface coating influences the cellular metabolism of *H. pylori*, a growth curve analysis was performed **(Figure 4.4.).** There was a significant delay throughout all the growth phases in the coated bacteria, as compared to the uncoated bacteria. This suggests that surface coating initially hinders the growth rate, but the cells eventually adapt and resume normal growth patterns.

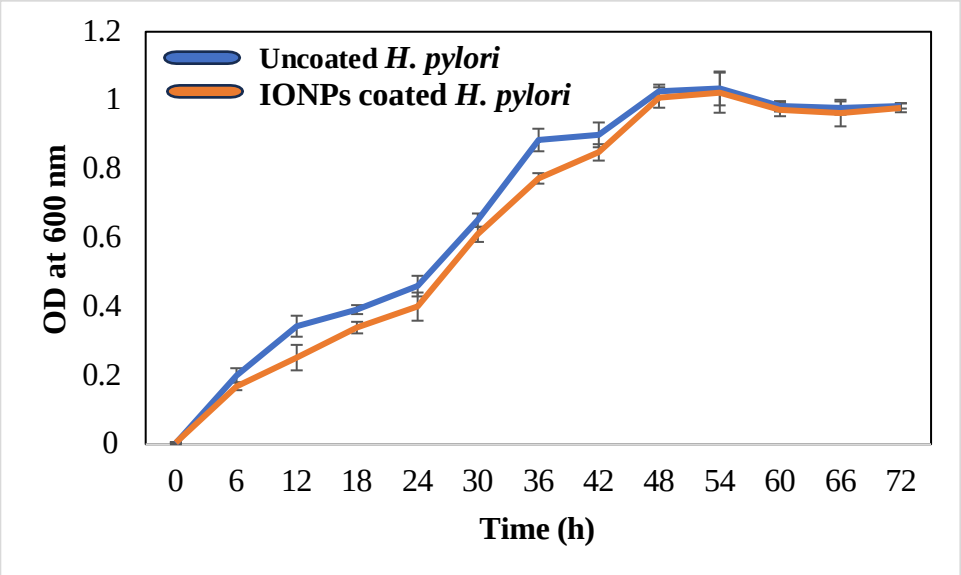

Figure 4.4. Bacterial growth curve of Uncoated control *H. pylori* and Iron oxide nanoparticles coated *H. pylori*

4.3.8 Magnetic hyperthermia application on *H. pylori*

In comparison to the control bacteria, as shown in **Figure 4.5. (a),** following the application of magnetic hyperthermia to bacteria that had been coated with IONPs **(Figure 4.5. (b))**, FE-SEM micrographs clearly showed that the bacterial membranes were undergoing lysis after hyperthermia treatment as shown in **Figure 4.5. (c, d).** This observation indicates that the heat generated by magnetic hyperthermia effectively disrupted the structural integrity of the

bacterial membranes, leading to their breakdown. This membrane disruption is a direct result of the localized heat generated by the magnetic hyperthermia process. After exposing to a variable magnetic field, the IONPs convert electromagnetic energy into thermal energy. This localized heating is sufficient to increase the temperature of the bacterial membranes to a critical point, leading to the thermal denaturation of membrane proteins and lipids. The thermal stress compromises the structural integrity of the bacterial cell membrane, causing it to lose its barrier function. As the membrane becomes increasingly destabilized, it undergoes physical breakdown, resulting in lysis. The lysis indicates the efficacy of magnetic hyperthermia in disrupting bacterial cells.

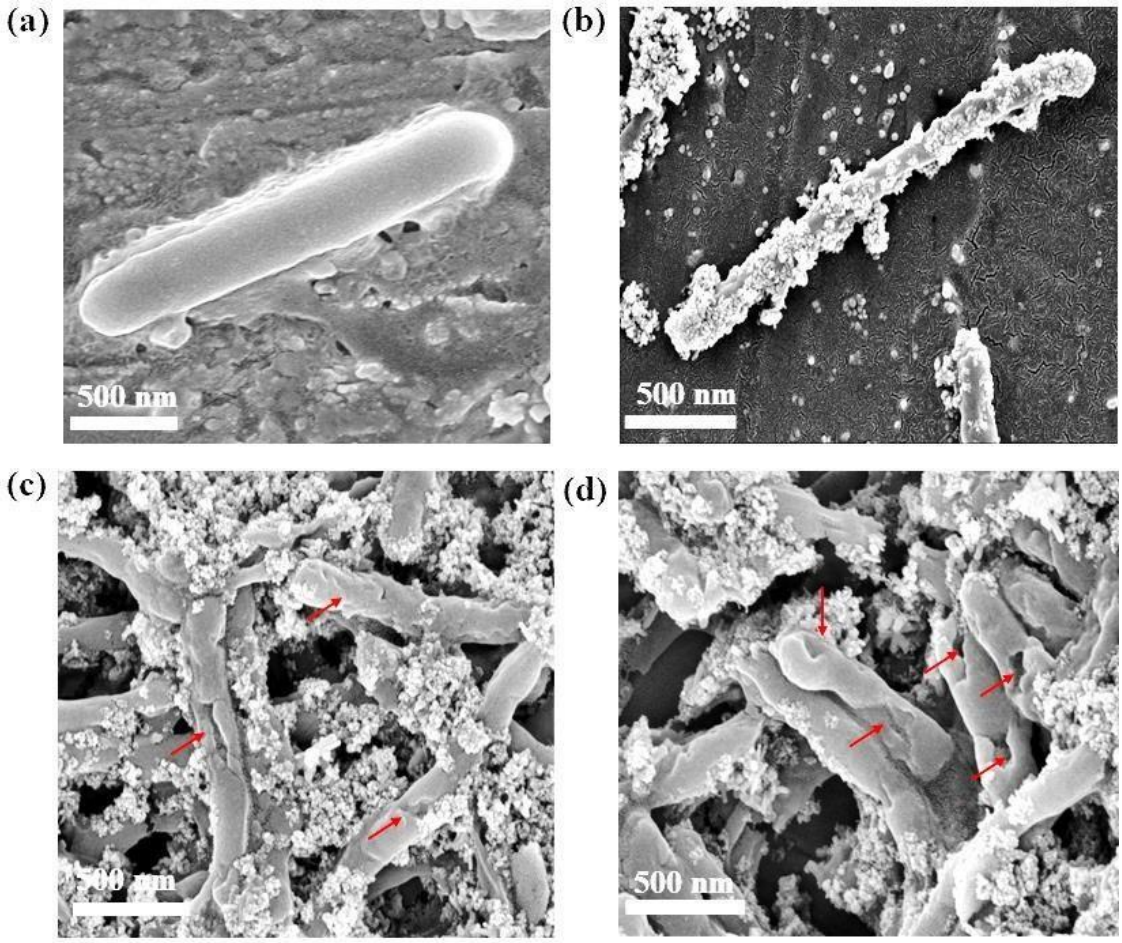

Figure 4.5. The figure represents the FE-SEM micrographs (a) Uncoated control *H. pylori* (b) Iron oxide nanoparticles coated on the surface of *H. pylori* (c, d) Hyperthermia treated *H. pylori.*

4.3.9 Activating the immune system with HM-treated coated *H. pylori*

Flow cytometry was utilized for analyzing the cytokine levels in the conditioned media.

Labeling specific cytokines with fluorescent antibodies could quantify the amount and types of cytokines present. In this context, it allowed us to detect and quantify specific cytokines (IL-6 and TGF-β) secreted by the immune cells (T cells and B cells) in response to the hyperthermia-treated IONPs coated bacteria. An elevation in cytokine levels would suggest a robust immune response, indicating that the hyperthermia-treated IONPs coated bacteria effectively activated the T cells and B cells which killed AGS tumor cells. However, the study analyzed the percentage of positive cell populations expressing IL-6 and TGF-β under various conditions. Unstimulated B cells (Cold-JM1) exhibited low levels of both IL-6 and TGF-β, with 3.82% and 3.85% positive populations, respectively. When these B cells were stimulated with hyperthermia-exposed *H. pylori* conditioned media (Hot-JM1), there was a potential rise in the expression of IL-6 (10.02%) and TGF-β (11.63%). Further exposure of these Hot-JM1 cells to AGS cells led to a slight reduction in IL-6 (9.16%) but a notable increase in TGF-β expression (16.23%). When Hot-JM1 cells were exposed to *H. pylori*-conditioned AGS cells that had undergone hyperthermia, the positive populations surged to 20.23% for IL-6 and 23.35% for TGF-β, indicating a significant upregulation of both cytokines. Similarly, unstimulated T cells (Cold-H9) showed moderate levels of IL-6 (7.63%) and TGF-β (10.48%). However, upon stimulation with hyperthermia-exposed *H. pylori* conditioned media (Hot-H9), the expression levels increased to 14.27% for IL-6 and 15.40% for TGF-β. Further interaction of Hot-H9 cells with AGS cells resulted in a higher IL-6 positive population (17.48%) and an even greater increase in TGF-β positive cells (23.35%). The most significant enhancement was observed when Hot-H9 cells were exposed to *H. pylori*-conditioned AGS cells that had been subjected to hyperthermia, resulting in IL-6 and TGF-β positive populations reaching 20.23% and 27.97%, respectively. These results suggest that hyperthermia-exposed *H. pylori* conditioned media significantly influences cytokine expression in both B and T cells, particularly when interacting with AGS cells, enhancing the inflammatory response. This method provided insights into the immune-modulating potential of the hyperthermia-treated coated bacteria and their efficacy in inducing an immune response that could target and affect gastric tumor cells. The FACS data is indicated in **Figure 4.6. and Figure 4.7., and the comparative data on** cytokine levels are given in **Table 4.2.**

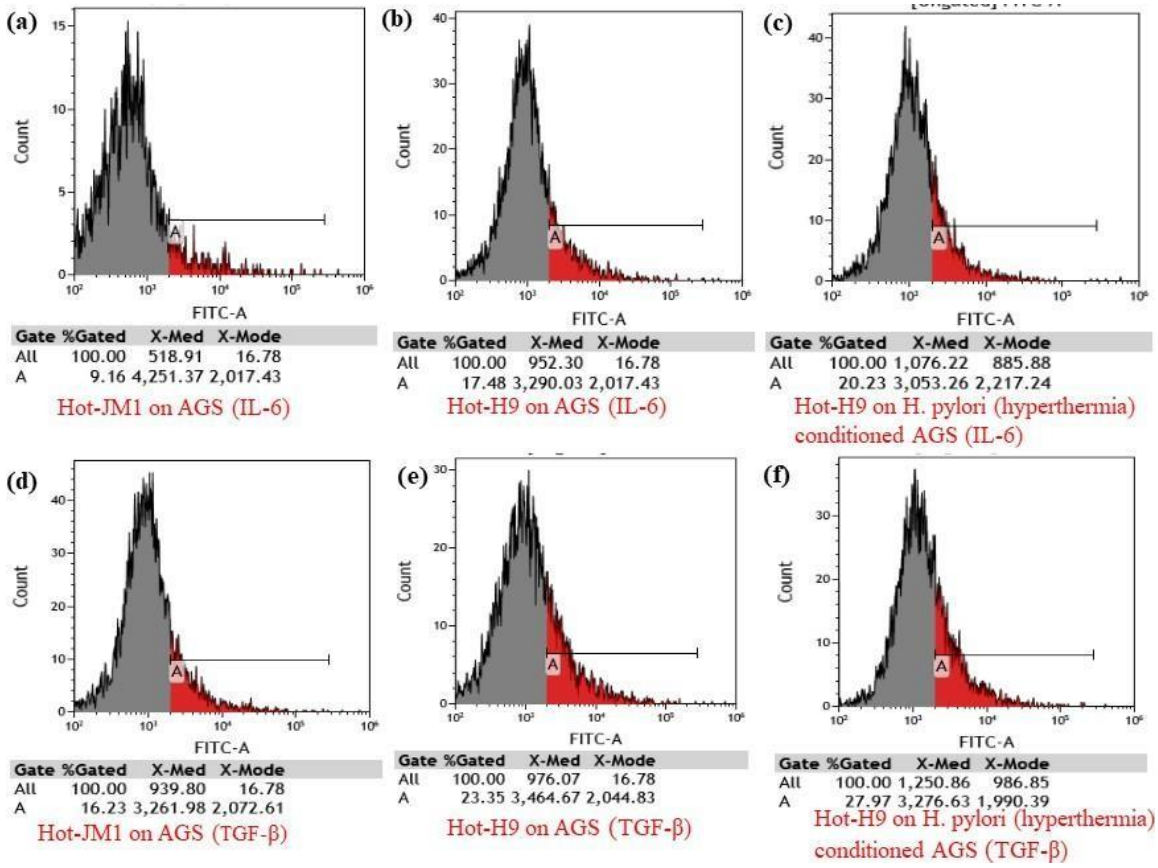

Figure 4.6. The flow cytometry graphs showing the immune activation from IL-6 and TGF-β levels in AGS cells after treatment with hyperthermia treated coated bacteria under different conditions.

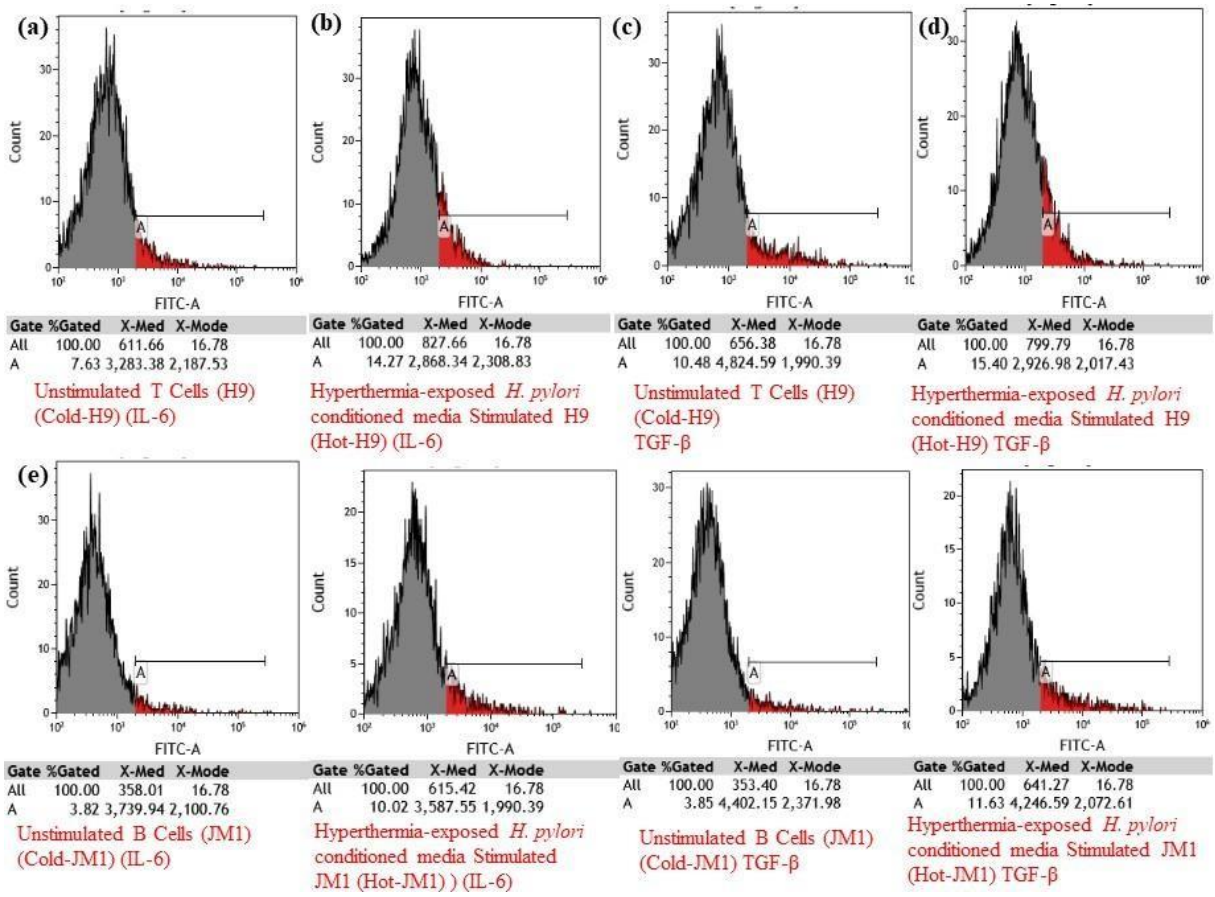

Figure 4.7. The flow cytometry graphs showing the immune activation from IL-6 and TGF-β levels in H9 & JM1 cells after treatment with hyperthermia treated coated bacteria under different conditions.

Table 2. Comparative data of IL-6 and TFG-β levels

Conditions	**% of positive population**	
	IL-6	**TFG-β**
Unstimulated B Cells (JM1) (Cold-JM1)	3.82%	3.85%
Hyperthermia-exposed *H. pylori* conditioned media Stimulated JM1 (Hot-JM1)	10.02%	11.63%
Hot-JM1 on AGS	9.16%	16.23%

Hot-JM1 on H. pylori (hyperthermia) conditioned AGS	20.23%	23.35%
Unstimulated T Cells (H9) (Cold-H9)	7.63%	10.48%
Hyperthermia-exposed *H. pylori* conditioned media Stimulated H9 (Hot-H9)	14.27%	15.40%
Hot-H9 on AGS	17.48%	23.35%
Hot-H9 on H. pylori (hyperthermia) conditioned AGS	20.23%	27.97%

4.4 Conclusion

Immune activation through the use of *Helicobacter pylori (H. pylori)* coated with iron oxide nanoparticles and treated with magnetic hyperthermia represents a novel approach in medical science. *H. pylori*, a bacterium known for causing stomach ulcers and certain types of gastric cancer, can be repurposed as a vehicle for delivering therapeutic nanoparticles to the immune system.

IONPs are biocompatible and could be easily manipulated using external magnetic fields. When *H. pylori* is coated with these nanoparticles, it serves as a target for magnetic hyperthermia, a process involving application of an alternating magnetic field to generate localized heating. This localized heating can induce mild thermal stress that is sufficient to stimulate an immune response without causing significant tissue damage.

After applying external magnetic field, to IONPs coated *H. pylori*, the nanoparticles generate localized heat due to magnetic hyperthermia. This heat disrupts the bacterial cell membrane, leading to bacterial spillage. The spillage involves the release of bacterial components, such as lipopolysaccharides (LPS), peptidoglycans, and other intracellular molecules into the surrounding tumor microenvironment. The released bacterial components are perceived by the immune system as pathogen-associated molecular patterns (PAMPs). Pattern recognition receptors (PRRs) on innate immune cells, like macrophages and dendritic cells, detect these PAMPs. The binding of bacterial components to PRRs triggers intracellular signaling pathways which activates transcription factors including NF-

kB. This activation causes the production and release of pro-inflammatory cytokines (e.g., TNF-α, IL-6) and chemokines (e.g., IL-8). These molecules coordinate the inflammatory response by attracting additional immune cells to the site of bacterial spillage, increasing blood vessel permeability, and promoting inflammation. The bacterial components activate the complement system, eventually causing the secretion of the membrane attack complex (MAC) that damages bacterial cell membranes. This enhances phagocytosis by promoting opsonization of the bacteria and their components. Phagocytic cells, including macrophages and neutrophils, engulf and digest the bacteria and their spilled components. During this process, antigens derived from the bacteria are processed and presented on Major Histocompatibility Complex (MHC) molecules to T cells. This antigen presentation is crucial for activating adaptive immune responses, causing the differentiation of T cells and the generation of a targeted immune response against the bacterial components. This leads to the clearance of bacterial spillage along with the tumor cells. Therefore, the thermal stress generated by magnetic hyperthermia can enhance the presentation of antigens from *H. pylori* to the immune cells, thereby boosting the body's immune response. Additionally, the presence of IONPs can improve the efficiency of antigen uptake by dendritic cells, leading to a more robust activation of T-cells. This method not only targets the pathogen directly but also primes the immune system for a more effective response, offering a dual therapeutic strategy. Through combining the biological features of *H. pylori* with the physical characteristics of iron oxide nanoparticles, this approach holds promise for innovative treatments in immunotherapy and infectious disease management.

Chapter 5: Perturbation of Hyperthermia Resistance in Gastric Cancer by Hyperstimulation of Autophagy Using Artemisinin-protected Iron-oxide Nanoparticles

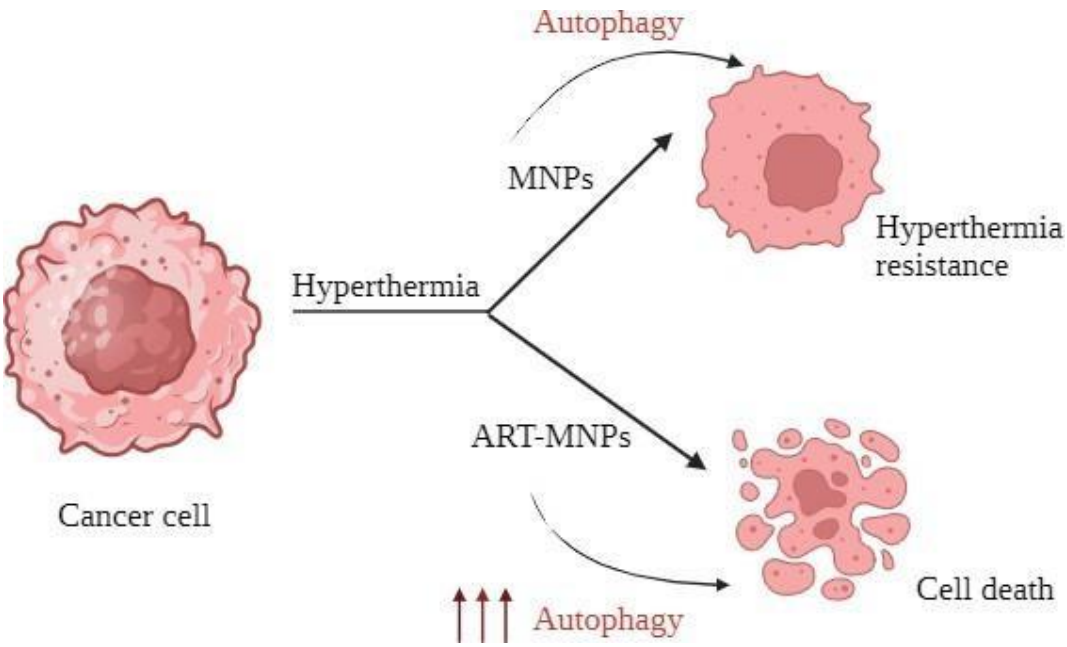

Figure 5.1. It depicts the study of gastric cancer cell treatment with artemisinin-magnetic iron oxide and alone MNPs.

Abstract

In a bid to overcome hyperthermia resistance, a major obstacle in cancer treatment, this study explores manipulating autophagy, a cellular recycling mechanism, within the context of gastric cancer. We designed artemisinin-protected magnetic iron-oxide nanoparticles (ART-MNPs) to hyperactivate autophagy, potentially sensitizing cancer cells to hyperthermia. The synthesized ART-MNPs exhibited magnetic properties and the capability of raising the temperature by 7 ºC at 580.3 kHz. Importantly, ART-MNPs displayed significant cytotoxicity against human gastric cancer cells (AGS), having IC_{50} of 1.9 µg/mL, demonstrating synergistic effects compared to either MNPs or ART treatment alone (IC50 for MNPs is 9.7 µg/mL and for ART is 9.4 µg/mL respectively). Combination index studies further supported this synergy. Mechanistic analysis revealed a significant increase in autophagy level (13.58- and 15.08-fold increase compared to Artemisinin and MNPs, respectively) upon ART-MNP treatment, suggesting that this hyperactivation is responsible for hyperthermia sensitization and

minimized resistance (as evidenced by changes in viability compared to control under hyperthermic conditions). This work offers a promising strategy to modulate autophagy and overcome hyperthermia resistance, paving the way for developing hyperthermia as a standalone therapy for gastric cancer.

5.1 Introduction

In spite of advancements in cancer prognosis and therapeutic strategies, cancer remains a leading cause of mortality worldwide [207],[300]. Among the diverse range of cancer types, gastric cancer is the fourth most common cancer globally and is the second major source of cancer death. Factors which enhance the chances of developing the situation and influence the treatment outcome include *Helicobacter pylori* infection, genetics, stage of detection, advancing age, consuming excessive amounts of salt, chronic inflammation, malnutrition, and lack of dietary fiber consumption, etc. [301]. However, existing cancer treatments, including chemotherapy, often exhibit limitations due to non-specific cytotoxicity, leading to immune system suppression and enhanced threat of secondary infections in patients [207],[208]. The rise of drug resistance has created a greater need for natural agents that can effectively eliminate tumors and minimize the chances of recurrence [209].

Nature provides a wealth of secondary metabolites that are being utilised since centuries for treating different diseases, including gastric cancer [72]. The global research community is actively exploring the potential of natural materials, such as medicinal plants or potent medicinal components, for developing anti-cancer products [83],[84]. Various secondary metabolites, such as carvacrol, geraniol, sageone, carnosic acid, etc., are used to treat gastric cancer [285]. Among these, artemisinin, a terpene derived from the Chinese herbal medicine *Artemisia annua L.*, also known as sweet wormwood [302], is widely acknowledged for its diverse range of properties, including anti-inflammatory, anthelmintic, antipyretic, anti-bacterial, insecticidal, and anti-cancer effects [303],[304],[154].

Artemisinin is a remarkable bioactive compound that has captivated the scientific community's attention. It stands out as a unique and compelling drug with significant biological importance. Unlike many synthetic drugs that have undesirable side effects, artemisinin, a natural plant-based compound, holds considerable therapeutic value[305]. Its structure possesses an endoperoxide moiety capable of reacting with iron to generate cytotoxic free radicals. Recognizing that cancer cells contain noticeably higher intracellular free iron levels compared to normal cells, artemisinin selectively induces apoptosis in cancer cell lines[306]. Additionally, artemisinin has been found to induce autophagy, a highly conserved cellular

degradation process that helps cells adapt to various stressful conditions, such as nutrient scarcity [307],[308]. During the initial phases of autophagy, impaired cytoplasmic components are enclosed within specialized formations, referred to as autophagosomes [309]. In cancer cells such as colorectal cancer, cervical cancer, multiple myeloma, and promyelocytic leukemia, artemisinin inhibits NF-kβ activity, thereby inducing autophagy [310]. It also prevents cell growth and blocks the cell cycle. These unique properties make artemisinin a potential candidate for cancer chemotherapeutic drugs.

Artemisinin holds a distinct advantage as an anti-cancer agent, not solely due to its potency in inducing toxicity in cancer cells but also due to its remarkable selectivity in targeting and eliminating them. Furthermore, its impact on normal cells is characterized by minimal toxicity, further highlighting its potential as an effective treatment for cancer [311]. Recent research findings have suggested the possibility of utilizing it as a therapeutic option for gastrointestinal, breast, brain, and colon cancers [312]. Apart from its anti-cancer activity, artemisinin has significant anti-bacterial potential against Gram-negative and Gram-positive bacteria by following multiple mechanisms, including disrupting bacterial cell membranes and potential interactions with different cellular factors. Artemisinin produces cytotoxic carbon-centered radicals after being activated by ferrous ions or reduced heme. These radicals are found to target external microbial organisms, ultimately leading to their death [313], [314]. Recent studies have explored the utilisation of magnetic nanoparticles for site specific delivery of drugs using external magnetic fields. This approach helps reduce toxicity to normal cells and tissues. Iron oxide magnetic nanoparticles, known for their physiological inertness and superparamagnetic properties, have huge potential of accumulating nanoparticles within cancer cells at the desired site through the assistance of an external magnetic field [315], [298]. These nanoparticles and magnetic fields exhibit compatibility with biological systems, allowing their application to any of thebody region. Their size ranges between 1-1000 nm, and these nanoparticles are linked with polymers and drugs, enabling their versatile use in various biomedical applications [316], [317], including as a source of hyperthermia in cancer treatment. Hyperthermia is believed to be an adjuvant therapy for improving the effectiveness of traditional radiotherapy and chemotherapy. However, some challenges remain. A recent study showed that cancerous cells become much resistant to higher temperatures than healthy cells in a hyperthermic environment. Furthermore, hyperthermia often fails to initiate apoptosis in tumor cells, as these cells could resist hyperthermia via non-activation of caspase 3. Additionally, cancer cells treated with hyperthermia exhibit pseudopod-like extensions, which are not observed in their counterparts without hyperthermia treatment [318]. Along with their

cancer-targeting abilities, iron oxide exhibits anti-bacterial potential against multiple drug-resistant bacterial strains by generating reactive oxygen species, which are responsible for generating oxidative stress, ultimately causing cell death [319].

One approach that has been investigated to address these problems is the deployment of artemisinin-based magnetic nanoparticles for their anti-cancer activity. By utilizing an external magnetic field, these particles can be directed to selectively accumulate at the intended delivery site. This targeted delivery approach allows for reduced doses to achieve therapeutic concentrations, consequently minimizing the risk of side effects on normal healthy cells that might arise from higher doses [317]. This targeted delivery and release of artemisinin in a controlled manner can achieve higher anti-cancer activity than free drugs [320]. Magnetic nanoparticles loaded with artemisinin have shown notable toxicity in breast cancer cells (MCF-7). Under acidic conditions of tumor microenvironment, they can produce ferrous ions that catalyze artemisinin to produce ROS, resulting in cell death [321].

Building upon the information provided above, our hypothesis revolves around the idea that the delivery of artemisinin after conjugation with magnetic nanoparticles (ART-MNPs) into the gastric tissue, coupled with subsequent treatment through hyperthermia, could potentially enhance the efficacy of gastric cancer therapy by overcoming the resistance of tumor cells against hyperthermia. Additionally, the anti-bacterial activity of synthesized nano-formulations against the causative agent of gastric cancer, that is, *H. pylori*, could enhance the potential drug efficacy.

5.2 Materials and Methods:

5.2.1 Materials

Ferric chloride ($FeCl_3$), ferrous sulfate ($FeSO_4$), Polyethylene glycol (PEG 400), sodium hydroxide (NaOH), and deionized water were procured from LobaChemie, India. Artemisinin was obtained from TCI Chemicals. Ethylene dichloride (EDC), N-hydroxy succinimide (NHS), HAMs cell culture media, fetal bovine serum (FBS), Brain Heart Infusion (BHI) broth, agar, penicillin-streptomycin, Monodansylcadaverine (MDC), and Acridine Orange (AO) were all sourced from HiMedia, India. AGS (Gastric adenocarcinoma) and *H. pylori* (ATCC 700392) were procured from ATCC.

5.2.2 Development of artemisinin-conjugated magnetic nanoparticles

Magnetic nanoparticles were formulated via a co-precipitation method. Briefly, iron (III) chloride hexahydrate and iron (II) sulfate heptahydrate were added slowly to 50 mL of distilled

water, followed by heating to 90 °C. Subsequently, 3 mL of polyethylene glycol (PEG400) was added, followed by adding ammonium hydroxide solution obtained by dissolving 10 mL of 25% ammonium hydroxide in 50 mL of water under continuous stirring for 30 minutes. The final mixture, which was black, was centrifuged for 10 minutes at 4000 rpm after being brought to room temperature. Finally, washing with deionized water was done to get rid of unbound impurities.

After that, the conjugation of nanoparticles was done with artemisinin. A mixture containing 250 µL each of 10 mg/mL EDC, 10 mg/mL NHS, and 7 µL of 1 M NaOH was prepared and added into the pre-synthesized magnetic nanoparticles (0.5 mg) for activating surface carboxyl groups under sonication for 15 minutes. Subsequently, 250 µL (3 mg/mL) artemisinin was mixed with it dropwise, followed by keeping the solution at 37 °C for 24 h. The centrifugation of obtained mixture was done for 1h at 12,000 g for purification. Finally, the nanoparticles were dispersed in phosphate-buffered saline and kept at 4 °C for further utilization.

5.2.3 The studies to determine the size and morphology of nanoparticles with elemental analysis

For determining the hydrodynamic size of the nanoparticles Malvern DLS-Zeta size analyzer was used. High-Resolution Transmission Electron Microscopy (HRTEM) (Talos F200S G2, Thermo Scientific) was utilized to obtain exact size, shape, and morphology of ART-MNPs. Before analyzing, the centrifugation of nanoparticles was done for 15 minutes at 240 rpm to remove unbound impurities. The final pellet was analyzed using an energy-dispersive X-ray Spectrometer (EDS) (Bruker QUANTAX 200) to determine elemental composition.

5.2.4 FTIR Spectroscopy to monitor interactions between ART and MNPs

The interactions between ART (Artemisinin) and MNPs were investigated using Fourier Transform Infrared Spectroscopy (FTIR). The FTIR analysis was performed using an Agilent Cary 600 series Spectrophotometer. The pellets were made using the potassium bromide followed by scanning over the range of 400 cm^{-1} to 4000 cm^{-1}. FTIR data will provide a detailed study of variation in the frequency range of artemisinin functional groups after binding with magnetic nanoparticles.

5.2.5 XRD Analysis

X-ray diffraction (XRD) unveils the crystallographic structure, chemical configuration, and physical characteristics. Here, the technique probed the synthesized nanomaterial. After drying

to eliminate moisture's influence, Cu Kα radiation exposure was given to the sample (λ = 1.54 Å) for diffraction pattern acquisition within a 2θ range of 10-90°. The Scherrer equation, applied to the most intense peak in this pattern, then determined the crystallite size of both MNPs and ART-MNPs.

$$d = \frac{K\lambda}{\beta cos\boldsymbol{\theta}} \qquad \ldots\ldots \qquad \text{(Eq 1)}$$

where K= 0.9 is the Scherrer constant, λ= 1.54 Å denotes the X-ray wavelength, β determines the broadening of the highest intense peak, and d denotes the crystallite size of the synthesized MNPs and ART-MNPs.

5.2.6 Heating capacity determination using Hyperthermia study

In cancer treatment, hyperthermia utilizes elevated cellular temperatures (typically between 42°C and 45°C) to target and destroy tumors. To assess the potential of a synthesized material for magnetic hyperthermia applications, the NanoTherics Magnetherm instrument was used. This instrument is equipped with an optical fiber temperature probe to record material heating during the process precisely. The prepared sample was exposed to variable magnetic field of 10 mT at various frequencies (161.9 kHz, 242.4 kHz, 411.1 kHz, 580.2 kHz, and 935.3 kHz).

5.2.7 Determination of magnetic properties using VSM

To assess the magnetic features of the synthesized nanoparticles (MNPs and ART-MNPs), we employed a Vibrating Sample Magnetometer (VSM) at room temperature. Before analysis, the samples were dried in powder form. The VSM exposed the samples to a varying magnetic field of +/- 10 kOe, allowing us to record the hysteresis loop (M-H), which reveals the correlation amongst magnetization of material and the applied magnetic field. This loop is a characteristic of ferromagnetic materials and provides valuable data on the nanoparticles' magnetic characteristics, including saturation magnetization (M_s), coercivity (H_c), and remanence (M_r) [243].

5.2.8 Studies to Determine Drug Loading and Release Kinetics

The release profile of artemisinin (ART) from ART-MNPs was investigated through centrifugation and spectrophotometry. For this, centrifugation of 1 ml sample at 10,000 rpm for 15 minutes to separate the unbound ART in the supernatant from the ART bound to the pellet. The unbound ART concentration in the supernatant was then quantified using spectrophotometric testing. The pellet was suspended in 500 ml of water to monitor sustained

release. At predetermined time intervals over 40 h, 2 ml aliquots were withdrawn and replaced with DI water for maintaining the original volume. The absorbance of these aliquots was measured at 292 nm, providing information on the ART release pattern at physiological pH 7, gastric pH 3 and tumor pH 5.5 at 37 °C [306],[322],[178]. The final data is plotted by taking the average of three different experiments.

5.2.9 *in vitro* studies

5.2.9.1 Cytotoxicity studies

The toxicity of the samples towards cells was evaluated using the MTT (3-(4,5-dimethylthiazol-2-yl)-2,5-diphenyltetrazolium bromide) assay which was done using AGS cells, a gastric adenocarcinoma cancer cell line. For the experiment, 10,000 cells per well were added in a 96-well plate and allowed to reach 75-80% confluency followed by treating them with four distinct concentrations (2.5, 5, 7.5, and 10 µg/mL) of the prepared formulations, including $FeCl_3$, $FeSO_4$, MNPs, ART, and ART-MNPs. After treating them with formulations, the cells were incubated at 37°C. The MTT solution was then added after washing cells with PBS and incubated for an additional 3 h. The solution was withdrawn from each well, followed by adding 100 µl of DMSO and kept for 15-minute incubation. Finally, the OD value of the final solution was determined at 570 nm. The given equation was used to calculate the inhibition percentage.

$$\% \text{ inhibition} = [1 - (At/Ac) \times 100] \% \quad \ldots\ldots\ldots \quad \text{(Eq 2)}$$

where at is the test substance absorbance and Ac is the control solvent absorbance. The experiment was performed three times to get the concordant values.

5.2.9.2 Scratch assay for anti-cancer activity

A scratch assay was utilised for determining the anti-cancer activity of the synthesized particles. One 6-well plate was used to grow cells in FBS-free media and incubated at 37 °C and 5% CO_2. The plate was then confluent till 80-90%. After that, a sterile 10 µl pipette tip was used to carefully scratch a uniform wound across the cell monolayer followed by washing them with PBS to get rid of debris and impurities. Fresh media was added, and the cells were treated with various samples: $FeCl_3$, $FeSO_4$, MNPs, ART, and ART-MNPs. Images of the scratch were captured at 6, 12, 24, 36, and 48 h post-treatment.

The scratch width was measured at three random places in all wells at each time point to quantify anti-cancer activity. The average scratch diameter was then calculated, and a graph was plotted to visualize the changes in scratch diameter over time for each sample. This allowed

for the assessment of the anti-proliferative efficacy of the synthesized samples on the cancer cells. [246], [247].

5.2.10 Detection of autophagy by Monodansylcadaverine (MDC) staining

To assess autophagic activity, AGS cells were cultured in 6-well plates and allowed to reach optimal confluency (70-80%). Each well was then treated with one of the following samples: control, MNPs, ART, or ART-MNPs. Following a 24-hour incubation, washing of cells was done with PBS before trypsinization followed by suspending in PBS and treated with 50 µM MDC for 15 minutes At 25 °C. Finally, the 1 x 10^4 cells were analyzed using flow cytometry.

5.2.11 Detection of autophagy by Acridine orange (AO) staining

An AO staining assay was done for evaluating autophagy similar to the MDC staining procedure described above; AGS cells were cultured using 6-well plates till they reached 70-80% confluency. The subsequent steps were identical to those outlined in Section 2.10 above.

5.2.12 Anti-bacterial activity of synthesized ART-MNPs

5.2.12.1 Antimicrobial activity by determining the Minimum Inhibitory Concentration (MIC)

To assess the anti-bacterial potential of the nano-formulations, the MIC was measured, which is the lowest concentration at which the growth of bacteria is effectively inhibited by the anti-bacterial agent over a specified period. The experiment was conducted using *Helicobacter pylori* to determine the MIC of ART-MNPs. Following established procedures, the microdilution was employed to assess anti-bacterial potential in 96-well plates. Initially, bacterial cultures were cultured and maintained in a brain heart infusion (BHI) broth medium in a hypoxia chamber at 37 °C, with 0.1 % oxygen and 10% CO_2 for 24 h. Subsequently, the concentration of bacteria was adjusted to 10^{-8} CFU/ml in the BHI medium. For evaluating the anti-bacterial efficacy of the synthesized particles, 20 µl of bacterial suspension, 20 µl of nanoparticles (2.5, 5, 7.5, and 10 µg/mL), and 160 µl of BHI broth were added to each well of the 96-well plates. Negative controls consisted of inoculated broth without nanoparticles. The plate was placed overnight in a hypoxia chamber at 37 °C, in the presence of 0.1 % Oxygen and 10% CO_2 [323]. OD was taken at 600 nm for the growth analysis.

5.2.12.2 Anti-bacterial activity by agar well diffusion assay

The agar well diffusion method was utilised to monitor the antimicrobial activity of synthesized ART-MNPs. One petri dish was made using BHI agar for the *H. pylori* strain, a Gram-negative bacterium. A 50 ml solution of BHI media and agar was autoclaved, poured into the Petri plates, and allowed to solidify. After solidification, 5 mm wells were made in the plate with the help of a cork borer, and sterile spreaders were used to spread 50 µl of bacteria on the plate. Three formulations, including ART, MNPS, and ART-MNPs with a concentration of 10 µg/mL, were added to their respective wells and kept for 24 h in a hypoxia chamber at 37 °C in 0.1 % Oxygen and 10% CO_2. After the incubation period, the zones of inhibition around each were monitored to assess the antimicrobial efficacy of synthesised formulation.

5.2.13 Determination of combination index (CI) for MNPs and ART

The CI quantifies the impact of two distinct drugs when used together. This interaction may result in either synergistic or antagonistic impact. Calculation of CI determines the extent of synergistic or antagonistic effects. CI value of less than 1 is indicative of synergism, where the combined administration of two drugs enhances each other's activity. Conversely, a CI value exceeding 1 (CI > 1) demonstrates the antagonism and suggests that one drug inhibits the activity of the other drug. A CI value of 1 indicates that neither drug interferes with the other. The CI was determined by computing and assessing the viability of AGS cells across variable concentrations of ART and MNPs, using equation (3)

$$CI = \frac{(D)_1}{(Dx)_1} + \frac{(D)_2}{(Dx)_2} \quad \ldots\ldots \quad \text{(Eq3)}$$

$$\text{Where, } Dx = Dm\,[fa/fu]^{1/m} \quad \ldots\ldots \quad \text{(Eq4)}$$

Here, $(D)_1$ and $(D)_2$ give the concentration of ART and MNPs. The concentrations $(Dx)_1$ and $(Dx)_2$, indicative of the median effective doses for the individual drugs, are determined through equation (4), where the affected and unaffected cell fractions in the median dose are denoted by fa and fu and are equal to $10^{(\text{y-intercept})/m}$, where m represents the slope median in the median effect plot of log (D) vs. log (fa/fu) [176].

5.3 Results and Discussions

5.3.1 Structure and Composition of ART-MNPs

Shape and Size: TEM images (**Figure 5.2. (a**)) confirmed the spherical morphology of the IONPs with an inset showing the histogram average diameter of 16 nm. Similarly, the **Figure**

5.2. (b) shows the TEM images of ART-MNPs and the histogram inset in this figure showing the average diameter of about 26 nm. TEM images indicated the spherical morphology of the ART-MNPs. This microscopic analysis was performed at a scale of 20 nm, allowing for detailed observation of the nanoparticle size and shape.

Hydrodynamic Diameter: DLS data revealed a hydrodynamic diameter of 114 nm for the ART-MNPs **(Figure 5.2. (c)).** This value represents the average size of the nanoparticles when dispersed in solution and accounts for the presence of any solvating molecules or surface functional groups.

Elemental Composition: Energy-dispersive X-ray spectroscopy (EDS) analysis **(Figure 5.2. (d))** confirmed the presence of key elements in the ART-MNPs, including carbon (C), oxygen (O), and iron (Fe). Notably, the iron content was found to be 63.29% and evenly distributed throughout the nanoparticles, indicating the successful incorporation of iron oxide within the ART-MNPs structure.

5.3.2 FTIR for studying interactions between ART and MNPs after nanoparticle synthesis

To explore the interaction between artemisinin ART and MNPs, FTIR was performed on ART, MNPs, and ART-MNPs samples. The findings unveiled multiple peaks in the IR spectra, offering valuable insights into the interactions in the examined samples, see **Figure 5.2. (e)** and **Table 5.1**. A peak at 537.56 cm^{-1} was identified in MNPs and ART-MNPs, indicating the presence of the Fe-O bond [248]. Peaks at 632.74 cm^{-1} and 685.53 cm^{-1} were present only in ART, denoting CH_2 Rocking vibrations. Notable peaks at 822.30 cm^{-1} and 861.49 cm^{-1} s identified as C-H bonds of the aromatic C-H [324] were present in ART but absent in both MNPs and ART-MNPs. A distinct peak, pointing to C-C stretching at 974.27 cm^{-1} [325], was observed in both ART and ART MNPs but was absent in MNPs. On the other hand, C-O-C asymmetrical stretching vibrations corresponding to peaks at 1104.64 cm^{-1} and 1182.22 cm^{-1} [326] were noted across all the samples. Furthermore, a peak at 1379.78 cm^{-1} representing C-O vibration was present in ART and ART-MNPs but absent in MNPs. In both ART and ART-MNPs, a bond indicative of C=O stretching was also present at 1439.76 cm^{-1}, which was not observed in MNPs [324]. At 1633.32 cm^{-1}, a peak position represented free carboxylic acid in MNPs and ART-MNPs but not in ART [325]. The -C(=O)-O Lactone bond was obtained at 1731.70 cm^{-1} in ART and ART-MNPs but is absent in MNPs [326]. Moreover, a peak indicative of C-H stretching vibrations (alkanes) was observed at 2834.65 cm^{-1} in ART and ART-MNPs but not in MNPs [327]. Likewise, a bond representing CH_2 stretching vibrations at 2901.84

cm^{-1} was present in ART and ART-MNPs and absent in MNPs [328]. Additionally, O-H stretching vibrations were observed at 3300.15 cm^{-1} in ART-MNPs only [326].

Table 5.1. The table gives the comparative values of the wavenumbers obtained from the FTIR of Artemisinin (ART), MNPs, and ART-MNPs indicating changes in distinct functional groups present, thus coins the interaction among Artemisinin and iron oxide nanoparticles leading to the formation of ART-MNPs.

Functional groups	Artemisinin (ART)	MNPs	ART-MNPs	Reference
Functional groups	-	537.56	537.56	[248]
Fe-O	632.74 685.53	-	-	[329]
CH_2 Rocking vibrations	822.30 861.49	-	822.30 861.49	[327]
C-H of the aromatic group	974.27	-	974.27	[330]
C-C Stretching	1104.64 1182.22	1104.64	1104.64 1182.22	[331]
C-O-C asymmetrical stretching vibrations	1379.78	-	1379.78	[332]
C-O Vibration	1439.76	-	1439.76	[324]
C=O stretching	-	1633.32	1633.32	[325]
Free carboxylic acid	1731.70	-	1731.70	[326]
-C(=O)-O Lactone bond	2834.65	-	2834.65	[327]
C-H stretching vibrations (alkanes)	2901.84	-	2901.84	[328]
CH_2 stretching vibrations	-	-	3300.15	[326]

5.3.3 XRD analysis

XRD analysis (Fig. 1e) was done to investigate the crystallinity of formulated MNPs, ART, and ART-MNPs. The XRD pattern of MNPs displayed characteristic peaks at 2θ values of 30°, 35°, 43°, 52°, 57°, and 62° **(Figure 5.2. (f)).** These peaks are corresponding to the crystal planes

(220), (311), (400), (422), (511), and (440) of magnetite (Fe_3O_4), as confirmed by their match with the reference pattern (ICDD number 00-003-0863). Notably, the XRD pattern of ART-MNPs exhibited similar peaks for iron oxide at the same positions, indicating the successful incorporation of Fe_3O_4 into the ART-MNPs structure.

Furthermore, the XRD pattern of ART alone revealed distinct peaks at 2θ values of 11.96°, 12.24°, 14.96°, 22.4°, 24.12°, and 38.56° [333], [334] **(Figure 5.2. (e)).** These sharp peaks suggest the crystalline nature of ART, which is crucial for maintaining its therapeutic properties. Interestingly, the Scherrer equation (Eq. 1) applied to the XRD data of ART-MNPs estimated a crystallite size of 18.53 nm. This finding suggests that the ART-MNPs possess a relatively small crystalline structure, potentially influencing their interaction with biological systems.

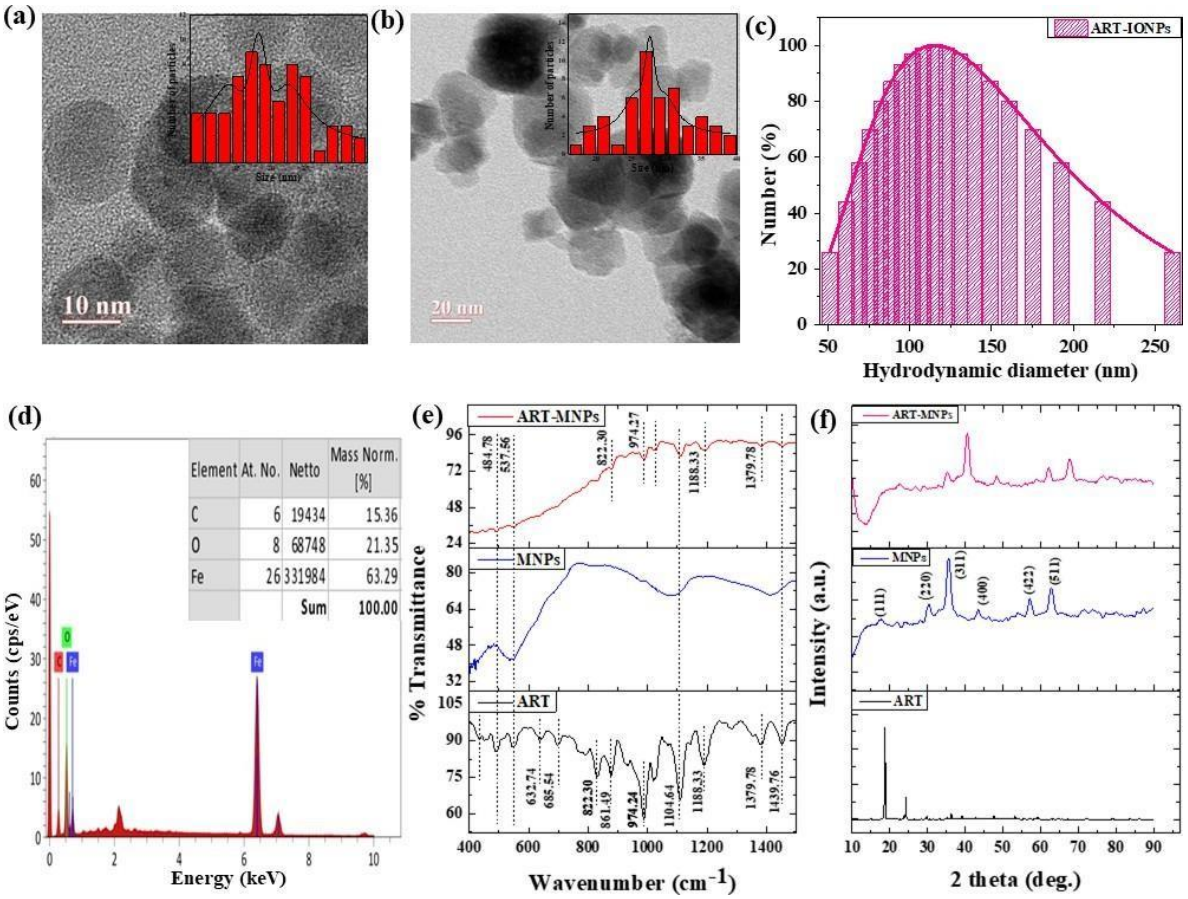

Figure 5.2. Characterizations of ART-MNPs (a) HR-TEM micrographs at a 10 nm scale reveal the size of IONPs (b) HR-TEM micrographs at a 20 nm scale reveal the size of ART-MNPs (c) Hydrodynamic size of ART-MNPs was analyzed by DLS, and the size was found to be 114.81 nm (d) EDS confirming the presence of iron in ART-MNPs (e) FTIR graph

demonstrating the interactions taking place between ART and MNPs (f) XRD plot providing the insights in the crystal structure of ART-MNPs.

5.3.4 Hyperthermia study

To comprehend the heating capacity of the synthesized nanoformulations under magnetic hyperthermia, temperature vs. time profiles were observed under different frequencies, whereas field strength and exposure time were kept constant. Each sample was exposed to hyperthermia treatment at each frequency for 10 minutes, as the hyperthermia temperature was achieved with this exposure time, beyond which overheating took place. After the hyperthermia treatment, an increase in temperature was observed from 28.25ºC to 29.14ºC, 31.27ºC, 34.50ºC, and 35.53ºC as the frequency increased from 161.9 kHz to 242.4 kHz, 411.1 kHz, 580.2 kHz, and 935.3 kHz, respectively. This trend is illustrated in **Figure 5.3. (a)** as a temperature (T_{max}) vs frequency (kHz) plot. The observed temperature increase demonstrates the vast potential of the nanoparticles in treating cancerous tissues by using magnetic hyperthermia.

5.3.5 Magnetic properties

The magnetic characteristics of MNPs and ART-MNPs were evaluated through magnetization measurements. These measurements were conducted using a Lakeshore 7404 model at room temperature with a field range of $\pm$ 10 kOe. The M-H loops of MNPs and ART-MNPs are shown in **Figure 5.3. (b)**. From the hysteresis loops, the saturation magnetization (M_s), Coercivity (H_c), and remanence (M_r) were determined as given in **Table 5.2**. The table shows that both remanence and coercivity values are nearly zero in MNPs and ART-MNPs, which shows that nanoparticles are superparamagnetic. This implies that thermal energy is adequate at room temperature for overcoming the magnetic anisotropy energy, keeping the nanoparticles randomly oriented without an external magnetic field. Furthermore, ART-MNPs exhibit higher saturation magnetization, which makes them one of the most potent and suitable candidates for magnetic hyperthermia applications.

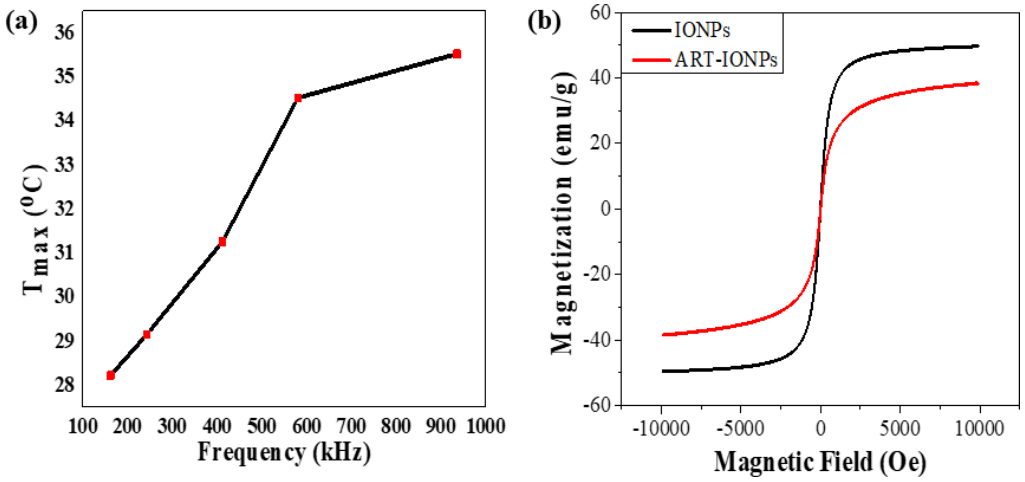

Figure 5.3. Assessment of hyperthermia sensitivity by ART-MNPs (a) It demonstrates the heating capacity of ART-MNPs at various frequencies under a constant magnetic field of 10 mT. It displays the increase in temperature, i.e., 28.25ºC to 29.14ºC, 31.27ºC, 34.50ºC and 35.53ºC at diverse frequencies: 161.9 kHz, 242.4 kHz, 411.1 kHz, 580.2 kHz, and 935.3 kHz, respectively (b) Magnetization of MNPs and ART-MNPs were recorded at RT

Table 5.2. The table indicates the various parameters of both the synthesized nanoparticles (MNPs and ART-MNPs), which include saturation magnetization (M_S), Remanence magnetization (M_{rs}), Coercivity (H_c), and crystallite size.

	Samples	
Parameters	**MNPs**	**ART-MNPs**
Ms (emu/g)	50.08	39.16
M_{rs}	0.03	0.006
H_c	0.26	0.54
Crystallite size (nm)	15.55	18.53

5.3.6 Drug Loading and Release Kinetics

The encapsulation of ART within MNPs was determined to be 77.77 ± 3.66 %, indicating a successful drug loading onto the nanoparticles. To evaluate the release profile of ART from ART-MNPs, drug release assay was performed by employing dialysis bag method at physiological pH (pH 7.0), as described in the methods section. The cumulative release of ART over time was monitored, and the results are shown in **Figure 5.4. (a).**

As observed in **Figure 5.4. (b)**, the drug release profile exhibited a biphasic pattern. Initially, a burst release of ART was obtained within the initial 8 h, after which a sustained drug release

for the next 32 h was obtained. This burst effect could be because of the release of ART molecules loosely adsorbed on MNPs surface. The sustained release phase likely involves the slower diffusion of encapsulated ART from the inner matrix of the nanoparticles. Notably, the total cumulative ART release after 40 h reached 90.11 ± 4.12 %, demonstrating the efficient drug release from the ART-MNPs. This combination of high efficiency of encapsulation and controlled release highlights the efficacy of ART-MNPs as a promising drug delivery agent. Moreover, the drug release studies were carried out at gastric pH (3) **(Figure 5.4. (c,d))** and tumour pH (5.5) **(Figure 5.4. (e,f)).** From the gastric pH data, it was observed that there was a burst release in the initial 8 h with nearly half of the drug (52.06 ± 2.08 %) being released in first 2 h only, after which a sustained drug release pattern for next 32 h with total drug being released to be 82.52 ± 3.41 % after 40 h. Similar biphasic pattern was obtained for the drug release at tumor pH, where in the initial 8 h, 60.16 ± 1.25 % drug was released and the total drug release at the end of 40 h is found to be 78.62 ± 0.25 %. The reason behind this initial burst release pattern is the release of artemisinin adsorbed on the outermost layer of iron oxide nanoparticles followed by the slow release of drug encapsulated inside the particles. Further, in the gastric and tumor pH which falls in the acidic range, there occurs the degradation of iron oxide nanoparticles eventually causing the non-enzymatic cleavage of endoperoxide bridge of released artemisinin which will further kill the cancer cells by generating organic radicals [335].

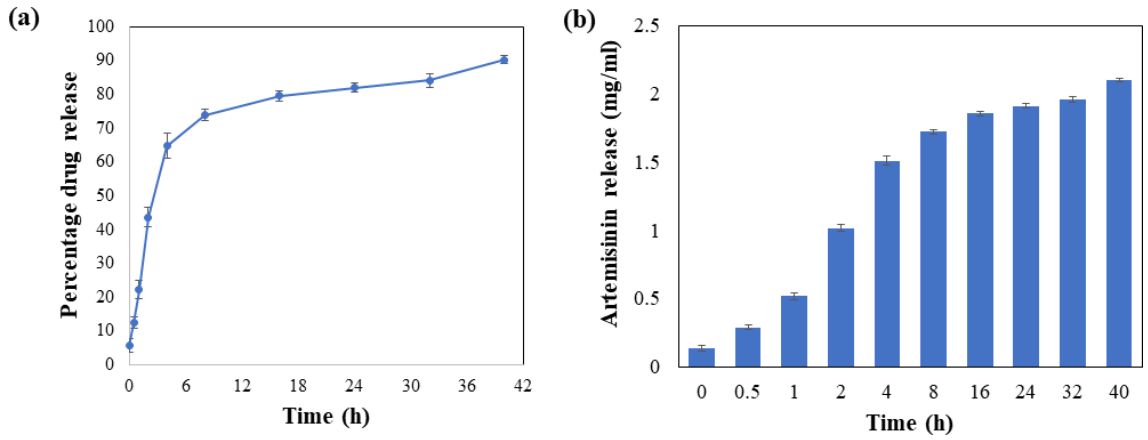

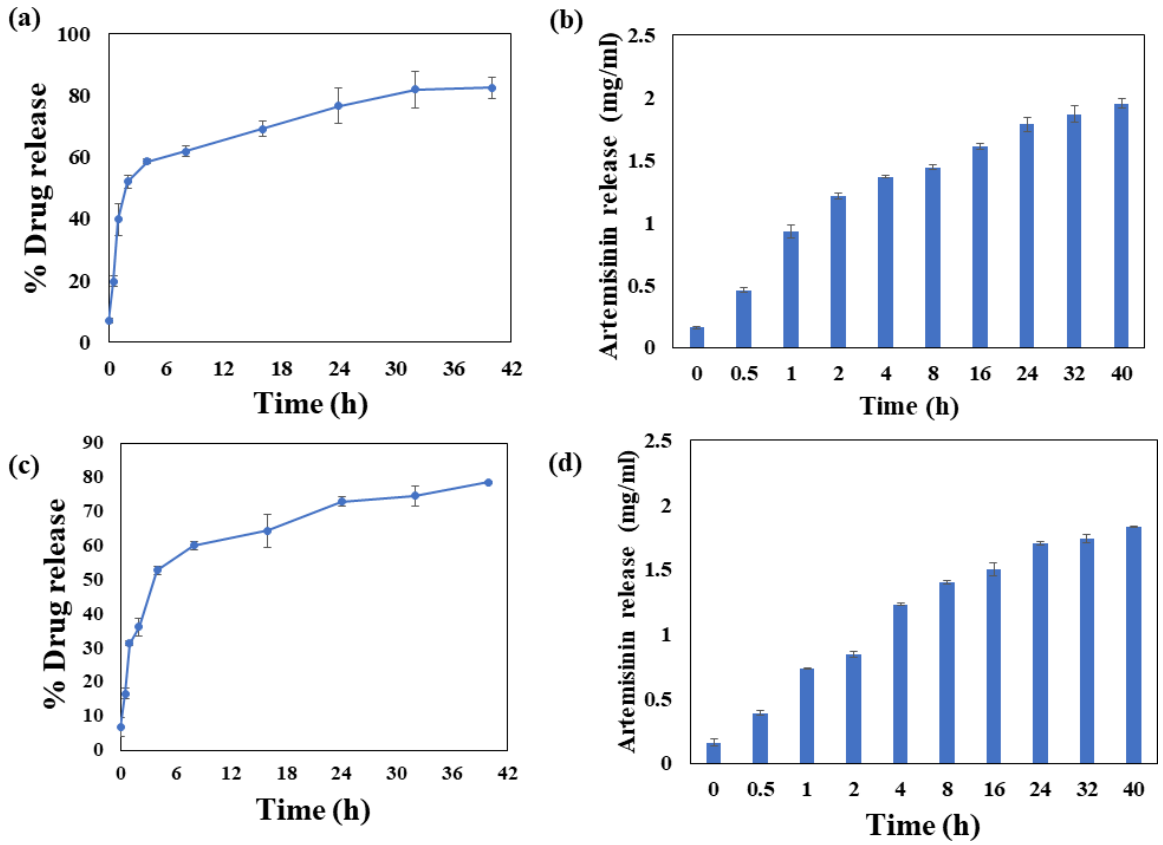

Figure 5.4. (a) The graph presents the drug release studies performed for assessing the percentage of ART released from ART-MNPs at physiological pH (b) It illustrates the release rate of the drug in mg/ml at pH 7 per hour (c) The graph presents the drug release studies performed for assessing the percentage of ART released from ART-MNPs at gastric pH (3) (d) It illustrates the release rate of drug in mg/ml at pH 3 per hour (e) The graph depicts the drug release studies conducted to evaluate the percentage of ART released from ART-MNPs at tumor pH (5.5) (f) It depicts the drug release rate in mg/ml per hour at tumor pH (5.5).

5.3.7 *in-vitro* cell line studies with and without hyperthermia

For determining the toxicity of ART-MNPs on the AGS (gastric cancer), an MTT assay was performed under physiological conditions followed by calculating the cytotoxicity for $FeCl_3$ and $FeSO_4$ salt solutions, Artemisinin, MNPs, and ART-MNPs at four concentrations: 2.5 µg/mL, 5 µg/mL, 7.5 µg/mL, and 10 µg/mL. Apart from the control, all the concentrations were tested on three independent sets, with and without hyperthermia treatment, to determine the effectiveness of the formulations. Cell viability was measured relative to control in the MTT assay performed without hyperthermia treatment, which was set at 100%. The results revealed several key points.

Cells after treatment with $FeCl_3$ show % viability of 98.51 ± 2.35% at 2.5 µg/mL, 97.71 ±

3.21% at 5 µg/mL, 97.30 ± 3.02% at 7.5 µg/mL, and 94.94 ± 1.80% at 10 µg/mL. Similarly, cells treated with $FeSO_4$ showed viability of 96.88 ± 2.69% at 2.5 µg/mL, 96.01 ± 3.78% at 5 µg/mL, 95.88 ± 3.31% at 7.5 µg/mL and 93.37 ± 2.59% at 10 µg/mL. Cells treated with ART showed viability of 85.01 ± 2.97% at 2.5 µg/mL, 74.31 ± 3.95% at 5 µg/mL, 60.67 ± 3.83% at 7.5 µg/mL, and 49.91 ± 1.45% at 10 µg/mL. In MNPs treated cells, viability was 95.01 ± 0.6% at 2.5 µg/mL, 92.24 ± 2.41% at 5 µg/mL, 89.89 ± 4.15% at 7.5 µg/mL and 88.05 ± 2.78% at 10 µg/mL. Finally, cells treated with ART-MNPs showed levels of viability as 84.73 ± 2.83% at 2.5 µg/mL, 72.62 ± 3.07% at 5 µg/mL, 59.90 ± 3.27% at 7.5 µg/mL and 48.49 ± 1.3% at 10 µg/mL concentration. The data is graphically represented in **Figure 5.5.**

The statistical significance of data was determined by calculating p values for the MTT assay without hyperthermia, as represented in **Table 5.3**.

Table 5.3 It indicates the p values calculated for % variation in cell viability after treating with 2.5, 5, 7.5, and 10 µg/mL of ART, MNPs, and ART-MNPs without hyperthermia. The statistical significance of data is considered when the $p < 0.05$.

P value for checking the statistical significance of data (Without Hyperthermia)			
	ART	**MNPs**	**ART-MNPs**
2.5µg/mL	0.002413	0.002773	0.00112
5µg/mL	0.000477	0.008284	0.000152
7.5 µg/mL	8.06E-05	0.017229	0.000152
10 µg/mL	1.39E-06	0.002665	9.43E-07

Cells treated with samples were incubated and subjected to alternating magnetic fields using a hyperthermia instrument for the hyperthermia treatment. MTT assay was then conducted to assess cell viability. The gastric cancer cells, after treatment, showed a potent decline in cell viability in comparison to the control group. For $FeCl_3$ salt solution-treated cells, viability was 96.45 ± 2.40% at 2.5 µg/mL, 95.12 ± 3.56% at 5 µg/mL, 94.63 ± 3.91% at 7.5 µg/mL and 92.61 ± 1.10% at 10 µg/mL. When cells were treated with $FeSO_4$ salt solution, the viability was 95.61 ± 2.45% at 2.5µg/mL, 95.22 ± 6.28% at 5 µg/mL, 93.49 ± 3.30% at 7.5 µg/mL and 91.57 ± 1.23% at 10 µg/mL. For ART-treated cells, the viability was 81.55 ± 2.65%, 73.15 ± 3.15%, 60.39 ± 3.05%, 49.75 ± 4.10% for the concentrations 2.5 µg/mL, 5 µg/mL, 7.5 µg/mL and 10 µg/mL, respectively. Cells treated with MNPs, showed viability of 81.26 ± 4.23% for 2.5 µg/mL, 67.78 ± 3.64% at 5 µg/mL, 58.07 ± 2.75% at 7.5 µg/mL and 48.42 ± 2.74% at 10

µg/mL. Lastly, ART-MNPs resulted in cell viability of 46.70 ± 1.38%, 41.67 ± 2.52%, 29.50 ± 1.20%, 21.28 ± 1.16% for 2.5 µg/mL, 5 µg/mL, 7.5 µg/mL, and 10 µg/mL, respectively **(Figure 5.3. (e)).**

These results indicate the cytotoxicity of ART-MNPs against AGS cells, suggesting potential for further exploration of anti-cancer potential as given in Fig. 2e. The statistical significance of the results was obtained by calculating p-values for the MTT assay with hyperthermia, as represented in **Table 5.4.**

Table 5.4. Table shows the p values calculated for % variation in cell viability after treating with 2.5, 5, 7.5, and 10 µg/mL of ART, MNPs, and ART-MNPs with hyperthermia. The statistical significance of data is considered when the $p < 0.05$

P value for checking the statistical significance of data (With Hyperthermia)			
	ART	**MNPs**	**ART-MNPs**
2.5µg/mL	0.009367	0.009526	1.4201E-05
5µg/mL	0.000869	0.000836	3.04E-05
7.5 µg/mL	0.000336	0.000139	4.13E-06
10 µg/mL	0.000212	6.07E-05	2.65E-06

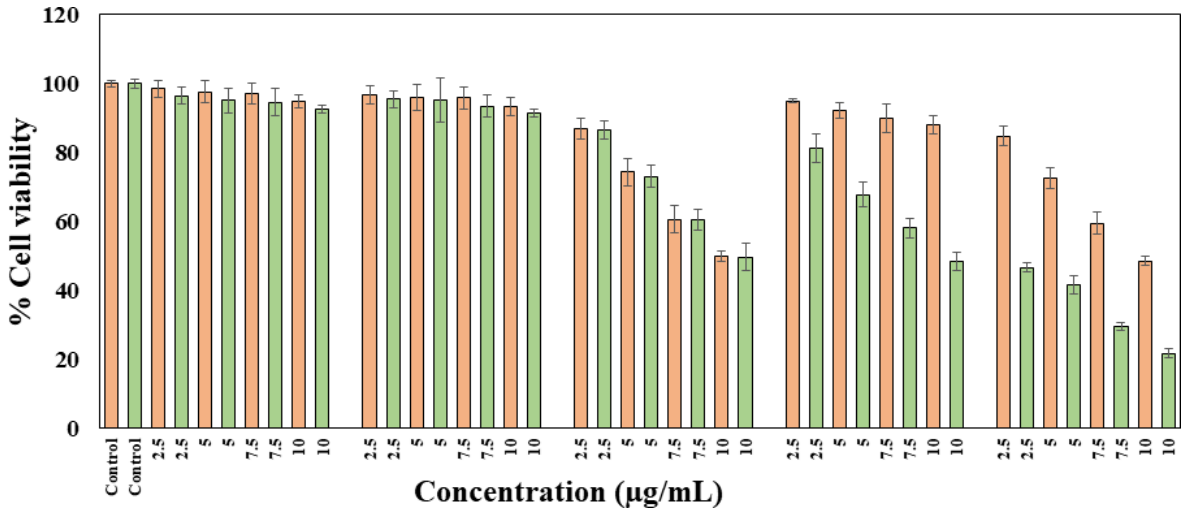

Figure 5.5. The cytotoxic activity on AGS cell line was assessed using the MTT under both

cases; with hyperthermia (green bars) and without hyperthermia (orange bars). It depicts the administration of treatment to AGS cells with control, including $FeCl_3$ and $FeSO_4$, ART, MNPs, and ART-MNPs at various concentrations of 2.5 µg/mL, 5 µg/mL, 7.5 µg/mL, and 10 µg/mL for each sample, both in the absence and presence of hyperthermia treatment.

5.3.8 Scratch assay for anti-cancer activity

The scratch assay **(Figure 5.6. a-t)** was used to evaluate the antiproliferative effects of ART-MNPs on AGS cells. Cells after treatment with 10 µg/mL of ART, MNPs, or ART-MNPs. Scratch closure was quantified by measuring the decrease in scratch diameter at three points per well, with the mean value reported. Control cells displayed a gradual scratch closure, reaching 73.71 ± 0.12% after 48 h **(Figure 5.6. (u)).** MNPs exhibited weaker anti-proliferative activity (52.16 ± 0.21% at 36 h, 71.98 ± 0.63% at 48 h), while ART treatment showed a moderate effect (43.54 ± 0.50% at 36 h, 68.32 ± 0.12% at 48 h). ART-MNPs demonstrated the most significant inhibition of cell migration (0.66 ± 0.24% at 6 h, 64.23 ± 0.27% at 48 h). This superior efficacy suggests a synergistic effect between ART and MNPs in the ART-MNPs formulation (detailed statistical analysis in **Table 5.5.**).

Table 5.5. It indicates the p values calculated for % variation in scratch diameter after treatment with 10 µg/ml of ART, MNPs, and ART-MNPs. The data is considered statistically significant when the $p < 0.05$.

P value for checking the statistical significance of data			
Time	**ART**	**MNPs**	**ART-MNPs**
6h	0.054767	0.792443	0.004362
12h	0.000305	0.041174	0.000243
24h	0.004036	0.023064	0.001396
36h	0.01039	0.027416	0.004124
48h	0.00749	0.043244	0.006911

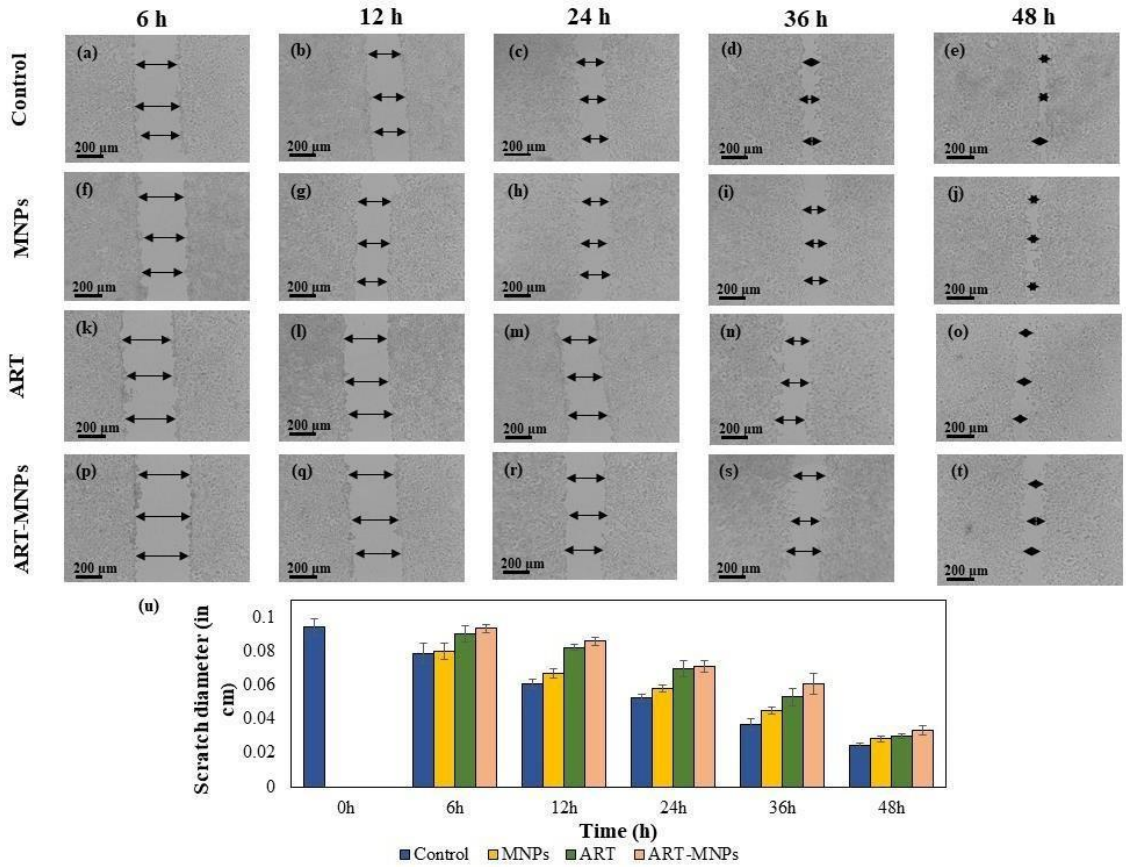

Figure 5.6. The Figure depicts the anti-cancer impact of ART-MNPs on the AGS cell line through a scratch assay (a) to (e) are control cells, MNPs treated cells at a fixed concentration of 10 µg/mL (f) to (j), ART-treated cells (k) to (o) with a concentration of 10 µg/mL, Cells treated with ART-MNPs (p) to (t) with 10 µg/mL concentration (u) The data in graph illustrating the comparison of alterations in scratch diameter after treatment with ART, MNPs, and ART-MNPs including control after 6 h, 12 h, 24 h, 36 h, and 48 h.

5.3.9 Detection of autophagic vacuoles by MDC

To assess the alteration of the extent of cellular autophagy effects of the synthesized formulations, AGS cells were treated and analysis was done using flow cytometry. As indicated in **Figure 5.7. (a)**, control cells exhibited a basal level of apoptosis (1.61%). Treatment with MNPs **(Figure 5.7. (b))** and ART **(Figure 5.7. (c))** resulted in moderate increases in apoptotic cells (3.89% and 4.32%, respectively). Notably, ART-MNPs **(Figure 5.7. (d))** induced a significantly higher percentage of apoptotic cells (58.65%), suggesting their enhanced anti-cancer potential.

5.3.10 Detection of autophagic vacuoles by AO

Flow cytometry analysis was utilized for quantifying the potential impact of the synthesized formulation on autophagy in AGS cells. **(Figure 5.7. (e))** Control cells displayed a basal level of apoptosis (0.96%). Treatment with MNPs **(Figure 5.7. (f))** and ART **(Figure 5.7. (g))** did not significantly alter the apoptotic cell population (0.55% and 0.56%, respectively). Interestingly, ART-MNPs **(Figure 5.7. (h))** induced a significantly higher percentage of apoptotic cells (12.20%), suggesting their potential to induce cell death.

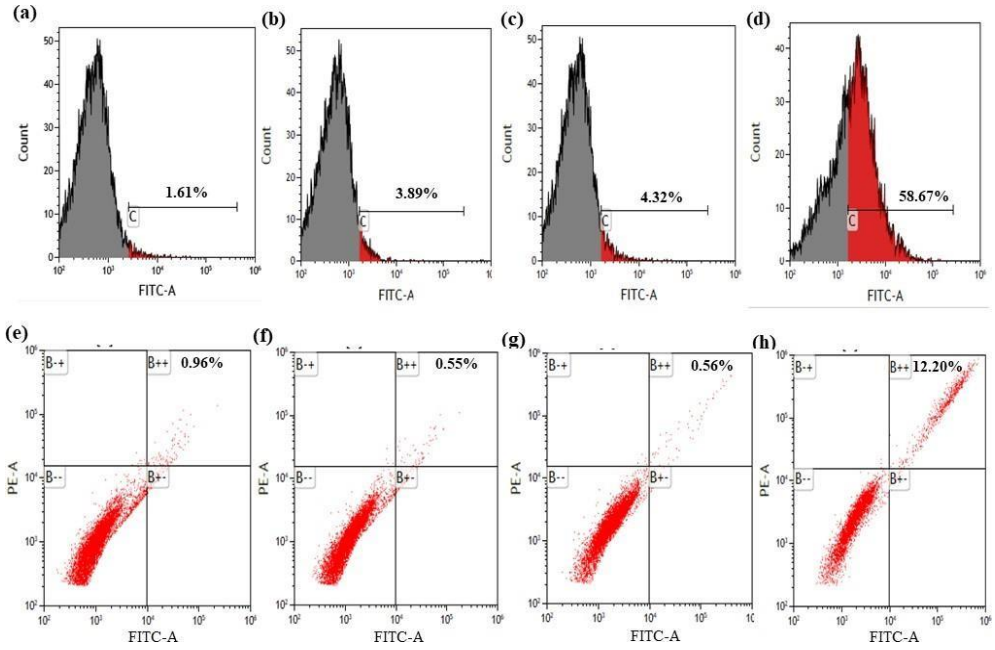

Figure 5.7. The figure shows the percentage of autophagy in cells using MDC (Monodansylcadaverine) dye (a) Control cells, which have 1.61% apoptotic cells; (b) MNPs treated cells, which showed 3.89% apoptotic cells; (c) in cells treated with ART, the percentage of apoptotic cells is 4.32% and (d) in cells treated with ART-MNPs, the percentage of apoptotic cells was found to be the highest as 58.65%. **Percentage of autophagy in cells using AO (acridine orange) dye (a)** in control cells, the percentage of apoptotic cells came out to be 0.96%, (f) in MNPs treated cells, the percentage of apoptotic cells is 0.55%, (g) in ART-treated cells, the percentage of apoptotic cells is 0.56% and (h) in ART-MNPs treated cells showed the highest percentage apoptotic cells were found to be 12.20%.

5.3.11 Anti-bacterial effect of ART-MNPs on *H. pylori*

5.3.11.1 Anti-bacterial activity by determining the MIC value

Anti-bacterial activity was determined by following the broth dilution method, and the MIC value was established. The MIC value for ART-MNPs was determined to be 10 µg/mL, see **Figure 5.8. (a).** The enhanced anti-bacterial activity is likely due to the influx of synthesized nano-formulations being easy for Gram-negative bacteria's cell wall, which has a unique outer membrane. These nanoparticles, in conjunction with artemisinin, generate ROS, eventually killing the bacteria. The statistical data is presented in **Table 5.6.**

Table 5.6. Table shows the p values calculated for % variation in the absorbance value of *H. pylori* after treatment with varying concentrations (2.5, 5, 7.5, 10 µg/ml) of ART, MNPs, and ART-MNPs. The data is considered statistically significant when the $p < 0.05$.

P value for checking the statistical significance of data for anti-*H. pylori* activity			
	ART	**MNPs**	**ART-MNPs**
2.5µg/mL	0.004458	0.00133	5.46E-05
5µg/mL	2.09E-05	7.73E-05	1.56E-05
7.5 µg/mL	1.1E-05	1.5E-05	5.43E-06
10 µg/mL	5.46E-06	0.000213	2.48E-06

5.3.11.2 Anti-bacterial activity by agar well diffusion assay

The anti-bacterial activity was further confirmed by the agar well diffusion method. The zone of inhibition for *H. pylori* following treatment with MNPS, ART, and ART-MNPs were ~ 9.5 mm, ~10.5 mm, and ~ 11.5 mm, respectively, indicating the superior anti-bacterial activity and zone of inhibition of ART-MNPs in comparison to MNPs and ART alone (**Figure 5.8. (b)).**

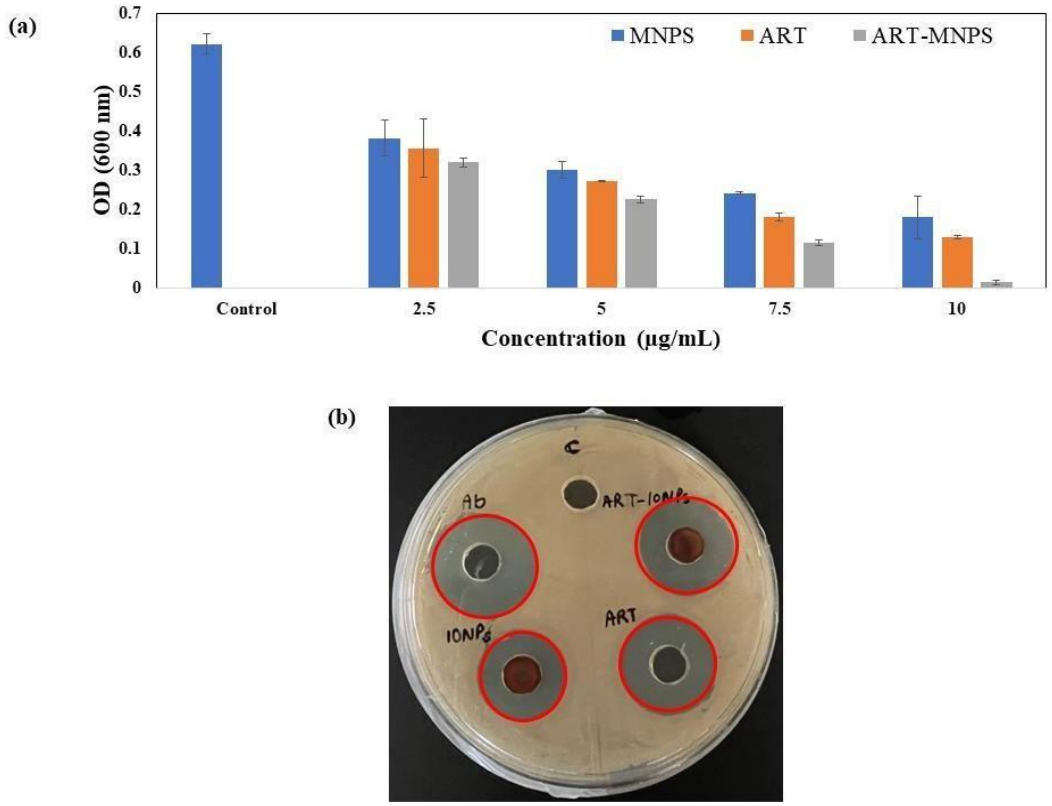

Figure 5.8. It indicates anti-*H. pylori* using ART-MNPs (a) the graph represents the MIC values, and it comes out to be 10 µg/mL for ART-MNPs (b) the figure shows the zone of inhibition for *H. pylori* that is ~ 9.5 mm, ~10.5 mm, and ~ 11.5 mm when treated with MNPS, ART, and ART-MNPS respectively.

5.3.12 Combination index of iron and insulin

The CI was determined to quantify the interaction between ART and MNPs. Dm values, derived from **Figure 5.9. (a)** (ART) and **Figure 5.9. (b)** (MNPs), were used in the CI calculation. As shown in **Table 5.7.**, the CI values for all tested combinations were below 1, indicating a synergistic effect. This finding aligns with the *in vitro* cell viability and scratch assay results (see previous sections, **3.7** and **3.8**), suggesting that ART and MNPs work together to enhance their anti-cancer activity.

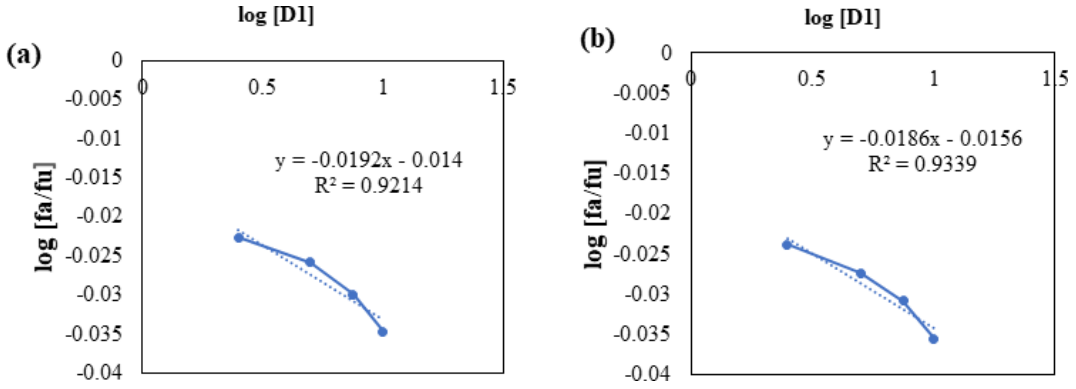

Figure 5.9. Median plots of **(a)** ART **and (b) MNPs for finding the y-intercept and m values to calculate Dm and** determine the combination index of ART and MNPs.

Table 5.7. The table presents the Combination index (CI) data derived from varying concentrations of ART and MNPs in combination to assess whether the two drugs demonstrate synergistic or antagonistic effects on cell viability. The values obtained are less than 1, indicating a synergistic effect between ART and MNPs.

Concentration of Fe salt and Insulin	**(Dx)1 (Fe salt) = Dm[fa/fu]$^{1/m}$**	**(Dx)1 (Insulin) = Dm[fa/fu]$^{1/m}$**	**CI = (D)1/(Dx)1 + (D)2/(Dx)2**
2.5 µg/mL	99.28705	112.0501	0.047491
5 µg/mL	111.495	128.556	0.083739
7.5 µg/mL	130.6199	147.8165	0.108157
10 µg/mL	158.1126	180.3481	0.118694

5.4 Conclusion

This study has successfully explored the potential of artemisinin-magnetic iron oxide nanoparticles as a new therapeutic method for gastric cancer. After combining the anti-cancer properties of ART with the hyperthermic capabilities of MNPs, ART-MNPs offer a synergistic approach for targeted cancer cell eradication. Our findings demonstrate the successful development of ART-MNPs with high encapsulation efficiency and a biphasic drug release profile. This indicates effective drug loading and the potential for rapid delivery upon reaching the target site, followed by a sustained therapeutic effect. Most importantly, ART-MNPs exhibited significantly enhanced anti-proliferative activity compared to individual treatments

with ART or MNPs alone. This synergistic effect was evident in the scratch assay results, suggesting that the combination therapy disrupts multiple cellular processes, potentially leading to more efficient cancer cell eradication.

Mechanistically, ART is known to generate ROS via interaction with ferrous iron, eventually causing mitochondrial damage and cell death. MNPs, after exposure to an external magnetic field, can produce localized heat (hyperthermia), further sensitizing cancer cells to the cytotoxic effects of ART. This synergistic action highlights the potential of ART-MNPs to overcome a significant challenge in cancer treatment: hyperthermia resistance. Additionally, ART-MNPs also demonstrated anti- *H. pylori* activity, which would further enhance the efficacy of the therapy.

In conclusion, this work has illustrated the promising potential of ART-MNPs for target specific and synergistic therapy against gastric cancer. Their ability to combine the anti-cancer properties of ART with the hyperthermic effects of MNPs opens new avenues for developing more effective treatment strategies. Further research on overcoming hyperthermia resistance through autophagy modulation and exploring combination therapies with other modalities is warranted to fully translate the potential of ART-MNPs into clinical practice, ultimately improving the lives of cancer patients.

Chapter 6: Conclusion and Future perspective

6.1 Conclusion

1. Nanomaterial-Enhanced Herbal Formulations: This review highlights the pressing need for more effective and safer treatment options for gastric cancer, a disease with significant global prevalence and poor survival rates, even in countries with advanced medical facilities. The current chemotherapy options, while effective, come with substantial negative impact which severely impact life quality of patients. Therefore, there is an urgent demand for developing new treatments that are both effective and less detrimental to patients' overall well-being. The use of polyphenolic, terpene-based nanoparticles can facilitate effective treatment with least or no ill effects. This study underscores the potential of combining herbal medicine with nanotechnology for developing innovative, safe, and highly efficient treatments for gastric cancer. Future research should focus on optimizing these nano-enabled herbal formulations, ensuring their stability, bioavailability, and therapeutic efficacy. By fostering interdisciplinary collaboration, we can advance the development of novel treatments that may significantly improve outcomes for patients with gastric cancer, potentially transforming the landscape of cancer therapy.

2. Lactoferrin-Conjugated Iron Oxide Nanoparticles (LF-IONPs): This work demonstrates the role of using LF-IONPs as a targeted anti-cancer agent, particularly against gastric cancer cells. The successful synthesis and characterization of LF-IONPs, with their optimal size, superparamagnetic behavior, and substantial heating capacity, underscore their applicability in biomedical research. The synergistic effects of lactoferrin and iron oxide nanoparticles not only enhanced the anti-cancer activity at low concentrations but also ensured selective targeting and efficient internalization within cancer cells. The outcomes indicates that LF-IONPs can act as a promising platform for targeted cancer therapies, with the potential to be adapted for various cancer types. The results of this research lays foundation for further exploration into utilising such nanoparticles in clinical applications, ultimately contributing to more effective and precise cancer treatments.

3. Novel Immunotherapy Approach: The innovative approach of using *Helicobacter pylori (H. pylori)* coated with IONPs and treated with magnetic hyperthermia presents a promising dual strategy for immune activation and therapeutic intervention. This method leverages the

biocompatibility and magnetic characteristics of IONPs, along with the ability of *H. pylori* to act as a vehicle for site specific delivery to the immune system. The localized heating generated by magnetic hyperthermia not only disrupts the bacterial cell membrane, causing the release of immunogenic bacterial components, but also enhances antigen presentation to immune cells, thereby stimulating a robust immune response. This dual-action mechanism, which combines direct pathogen targeting with immune system priming, could potentially revolutionize the treatment of gastric cancers and other infectious diseases. By effectively enhancing the uptake of antigens to T-cells, this approach could lead to more effective and targeted immunotherapies. The findings suggest that the integration of biological and physical properties in this manner holds significant potentiality in developing novel immunotherapeutic methods, paving the way for further research and clinical application in both cancer therapy and infectious disease management

4. Artemisinin-Magnetic Iron Oxide Nanoparticles (ART-MNPs): This study highlights the efficacy of ART-MNPs as innovative and synergistic intervention plan for treating gastric cancer. By integrating the anti-cancer properties of artemisinin with the hyperthermic capabilities of magnetic nanoparticles, ART-MNPs offer a powerful approach for targeted cancer cell eradication. The developed nanoparticles exhibited high encapsulation efficiency and a biphasic drug release profile, ensuring effective drug delivery and sustained therapeutic effects. The significantly enhanced anti-proliferative activity of ART-MNPs compared to individual treatments underscores their ability to disrupt multiple cellular processes, leading to more efficient cancer cell eradication. Mechanistically, ART-MNPs leverage the ROS production by artemisinin and the localized hyperthermia generated by magnetic nanoparticles to sensitize cancer cells and overcome hyperthermia resistance. Additionally, the observed anti-*H. pylori* activity further enhances the therapeutic potential of ART-MNPs. This study paves the way for further research into overcoming hyperthermia resistance, exploring autophagy modulation, and combining ART-MNPs with other therapeutic modalities. The promising outcomes of this work indicates that ART-MNPs could lead to more efficient and targeted treatment strategies, ultimately improving outcomes for patients with gastric cancer.

6.2 Future perspective

1. The remarkable superparamagnetic behavior, substantial magnetization capacity, and excellent heating capacity of synthesized nano-formulations hold great promise for their

use in numerous areas of biomedical research applications.

2. This approach offers a drug-free treatment option for gastric cancer, leveraging the body's immune system to combat the disease without the need for traditional chemotherapy or targeted drug therapies.
3. The combination of targeted hyperthermia and immune activation presents a promising alternative that minimizes side effects and improves treatment outcomes.
4. *in vivo* testing and pre-clinical trials are mandatory to monitor the potential role of immune activation done using IONPs coated *H. pylori.*
5. Development of chemo-free therapeutics.

References

[1] F.M. Millimouno, J. Dong, L. Yang, J. Li, X. Li, Targeting apoptosis pathways in cancer and perspectives with natural compounds from mother nature, Cancer Prev. Res. (Phila). 7 (2014) 1081–1107. https://doi.org/10.1158/1940-6207.CAPR-14-0136.

[2] M. Esteller, Epigenetics in cancer, N. Engl. J. Med. 358 (2008) 1148–1159. https://doi.org/10.1056/NEJMRA072067.

[3] K.I. Block, C. Gyllenhaal, L. Lowe, A. Amedei, A.R.M. Ruhul Amin, A. Amin, K. Aquilano, J. Arbiser, A. Arreola, A. Arzumanyan, S. Salman Ashraf, A.S. Azmi, F. Benencia, D. Bhakta, A. Bilsland, A. Bishayee, S.W. Blain, P.B. Block, C.S. Boosani, T.E. Carey, A. Carnero, M. Carotenuto, S.C. Casey, M. Chakrabarti, R. Chaturvedi, G.Z. Chen, H. Chen, S. Chen, Y.C. Chen, B.K. Choi, M.R. Ciriolo, H.M. Coley, A.R. Collins, M. Connell, S. Crawford, C.S. Curran, C. Dabrosin, G. Damia, S. Dasgupta, R.J. DeBerardinis, W.K. Decker, P. Dhawan, A.M.E. Diehl, J.T. Dong, Q.P. Dou, J.E. Drewa, E. Elkord, B. El-Rayes, M.A. Feitelson, D.W. Felsheru, L.R. Ferguson, C. Fimognari, G.L. Firestone, C. Frezza, H. Fujii, M.M. Fuster, D. Generali, A.G. Georgakilas, F. Gieseler, M. Gilbertson, M.F. Green, B. Grue, G. Guhal, D. Halicka, W.G. Helferich, P. Heneberg, P. Hentosh, M.D. Hirschey, L.J. Hofseth, R.F. Holcombe, K. Honoki, H.Y. Hsu, G.S. Huang, L.D. Jensen, W.G. Jiang, L.W. Jones, P.A. Karpowicz, W.N. Keith, S.P. Kerkar, G.N. Khan, M. Khatami, Y.H. Ko, O. Kucuk, R.J. Kulathinal, N.B. Kumar, B.S. Kwon, A. Leb, M.A. Leab, H.Y. Lee, T. Lichtor, L.T. Lin, J.W. Locasale, B.L. Lokeshwar, V.D. Longo, C.A. Lyssiotis, K.L. MacKenzie, M. Malhotra, M. Marino, M.L. Martinez-Chantar, A. Matheu, C. Maxwellx, E. McDonnell, A.K. Meeker, M. Mehrmohamadi, K. Mehta, G.A. Michelotti, R.M. Mohammad, S.I. Mohammed, D.J. Morre, I. Muqbil, V. Muralidharcq, M.P. Murphy, G.P. Nagaraju, R. Nahta, E. Niccolai, S. Nowsheen, C. Panis, F. Pantano, V.R. Parslow, G. Pawelec, P.L. Pedersen, B. Poore, D. Poudyal, S. Prakash, M. Prince, L. Raffaghello, J.C. Rathmell, W.K. Rathmell, S.K. Ray, J. Reichrath, S. Rezazadeh, D. Ribatti, L. Ricciardiello, R.B. Robeydf, F. Rodierdh, H.P.V. Rupasinghe, G.L. Russo, E.P. Ryan, A.K. Samadi, I. Sanchez-Garcia, A.J. Sanders, D. Santini, M. Sarkar, T. Sasada, N.K. Saxena, R.E. Shackelford, H.M.C. Shantha Kumara, D. Sharma, D.M. Shin, D. Sidransky, M.D. Siegelin, E. Signori, N. Singh, S. Sivanand, D. Sliva, C. Smythe, C. Spagnuolo, D.M. Stafforini, J. Stagg, P.R.

Subbarayan, T. Sundin, W.H. Talib, S.K. Thompson, P.T. Tran, H. Ungefroren, M.G. Vander Heiden, V. Venkateswaran, D.S. Vinay, P.J. Vlachostergios, Z. Wang, K.E. Wellen, R.L. Whelan, E.S. Yang, H. Yang, X. Yang, P. Yaswen, C. Yedjou, X. Yin, J. Zhu, M. Zollo, Designing a broad-spectrum integrative approach for cancer prevention and treatment, Semin. Cancer Biol. 35 Suppl (2015) S276–S304. https://doi.org/10.1016/J.SEMCANCER.2015.09.007.

[4] F. Bray, J.S. Ren, E. Masuyer, J. Ferlay, Global estimates of cancer prevalence for 27 sites in the adult population in 2008, Int. J. Cancer. 132 (2013) 1133–1145. https://doi.org/10.1002/IJC.27711.

[5] J. Feng, K. Li, G. Liu, Y. Feng, H. Shi, X. Zhang, Precision hyperthermia-induced miRNA-409–3p upregulation inhibits migration, invasion, and EMT of gastric cancer cells by targeting KLF17, Biochem. Biophys. Res. Commun. 549 (2021) 113–119. https://doi.org/10.1016/J.BBRC.2021.02.063.

[6] L.E. Wroblewski, R.M. Peek, K.T. Wilson, Helicobacter pylori and gastric cancer: Factors that modulate disease risk, Clin. Microbiol. Rev. 23 (2010) 713–739. https://doi.org/10.1128/CMR.00011-10.

[7] H.H. Hartgrink, E.P. Jansen, N.C. van Grieken, C.J. van de Velde, Gastric cancer, Lancet. 374 (2009) 477–490. https://doi.org/10.1016/S0140-6736(09)60617-6.

[8] V.I. Reshetnyak, A.I. Burmistrov, I.V. Maev, Helicobacter pylori: Commensal, symbiont or pathogen?, World J. Gastroenterol. 27 (2021) 545–560. https://doi.org/10.3748/WJG.V27.I7.545.

[9] C. Burucoa, A. Axon, Epidemiology of Helicobacter pylori infection, Helicobacter. 22 Suppl 1 (2017). https://doi.org/10.1111/HEL.12403.

[10] M. Pucułek, J. Machlowska, R. Wierzbicki, J. Baj, R. Maciejewski, R. Sitarz, Helicobacter pylori associated factors in the development of gastric cancer with special reference to the early-onset subtype, Oncotarget. 9 (2018) 31146–31162. https://doi.org/10.18632/ONCOTARGET.25757.

[11] L.H. Eusebi, R.M. Zagari, F. Bazzoli, Epidemiology of Helicobacter pylori infection, Helicobacter. 19 Suppl 1 (2014) 1–5. https://doi.org/10.1111/HEL.12165.

[12] K.D. Crew, A.I. Neugut, Epidemiology of gastric cancer, World J. Gastroenterol. 12 (2006) 354–362. https://doi.org/10.3748/wjg.v12.i3.354.

[13] Y. Urita, T. Watanabe, N. Kawagoe, I. Takemoto, H. Tanaka, S. Kijima, H. Kido, T. Maeda, Y. Sugasawa, T. Miyazaki, Y. Honda, K. Nakanishi, N. Shimada, H. Nakajima, M. Sugimoto, C. Urita, Role of infected grandmothers in transmission of

Helicobacter pylori to children in a Japanese rural town, J. Paediatr. Child Health. 49 (2013) 394–398. https://doi.org/10.1111/JPC.12191.

[14] A. Mentis, P. Lehours, F. Mégraud, Epidemiology and Diagnosis of Helicobacter pylori infection, Helicobacter. 20 Suppl 1 (2015) 1–7. https://doi.org/10.1111/HEL.12250.

[15] S. Kayali, M. Manfredi, F. Gaiani, L. Bianchi, B. Bizzarri, G. Leandro, F. Di Mario, G.L. De'angelis, Helicobacter pylori, transmission routes and recurrence of infection: state of the art, Acta Biomed. 89 (2018) 72–76. https://doi.org/10.23750/ABM.V89I8-S.7947.

[16] A. Saxena, A.K. Mukhopadhyay, S.P. Nandi, Helicobacter pylori: Perturbation and restoration of gut microbiome, J. Biosci. 45 (2020). https://doi.org/10.1007/S12038-020-00078-7.

[17] Y. Huang, Q.L. Wang, D.D. Cheng, W.T. Xu, N.H. Lu, Adhesion and invasion of gastric mucosa epithelial cells by Helicobacter Pylori, Front. Cell. Infect. Microbiol. 6 (2016) 227385. https://doi.org/10.3389/FCIMB.2016.00159/BIBTEX.

[18] M. Hatakeyama, Helicobacter pylori CagA and Gastric Cancer: A Paradigm for Hit-and-Run Carcinogenesis, Cell Host Microbe. 15 (2014) 306–316. https://doi.org/10.1016/J.CHOM.2014.02.008.

[19] T.L. Cover, S.R. Blanke, Helicobacter pylori VacA, a paradigm for toxin multifunctionality, Nat. Rev. Microbiol. 2005 34. 3 (2005) 320–332. https://doi.org/10.1038/nrmicro1095.

[20] M. Aspholm-Hurtig, G. Dailide, M. Lahmann, A. Kalia, D. Ilver, N. Roche, S. Vikström, R. Sjöström, S. Lindén, A. Bäckström, C. Lundberg, A. Arnqvist, J. Mahdavi, U.J. Nilsson, B. Velapatño, R.H. Gilman, M. Gerhard, T. Alarcon, M. López-Brea, T. Nakazawa, J.G. Fox, P. Correa, M.G. Dominguez-Bello, G.I. Perez-Perez, M.J. Blaser, S. Normark, I. Carlstedt, S. Oscarson, S. Teneberg, D.E. Berg, T. Borén, Functional adaptation of BabA the H. pylori ABO blood group antigen binding adhesin, Science (80-.). 305 (2004) 519–522. https://doi.org/10.1126/SCIENCE.1098801/SUPPL_FILE/ASPHOLM-HURTIG.SOM.PDF.

[21] J. Mahdavi, B. Sondén, M. Hurtig, F.O. Olfat, L. Forsberg, N. Roche, J. Ångström, T. Larsson, S. Teneberg, K.A. Karlsson, S. Altraja, T. Wadström, D. Kersulyte, D.E. Berg, A. Dubois, C. Petersson, K.E. Magnusson, T. Norberg, F. Lindh, B.B. Lundskog, A. Arnqvist, L. Hammarström, T. Borén, Helicobacter pylori sabA adhesin

in persistent infection and chronic inflammation, Science (80-.). 297 (2002) 573–578. https://doi.org/10.1126/SCIENCE.1069076/SUPPL_FILE/MAHDAVISOM.PDF.

[22] Y. Yamaoka, S. Kikuchi, H.M.T. ElZimaity, O. Gutierrez, M.S. Osato, D.Y. Graham, Importance of Helicobacter pylori oipA in clinical presentation, gastric inflammation, and mucosal interleukin 8 production, Gastroenterology. 123 (2002) 414–424. https://doi.org/10.1053/GAST.2002.34781.

[23] H. Lu, P.I. Hsu, D.Y. Graham, Y. Yamaoka, Duodenal ulcer promoting gene of Helicobacter pylori, Gastroenterology. 128 (2005) 833–848. https://doi.org/10.1053/J.GASTRO.2005.01.009.

[24] K.M. Ottemann, A.C. Lowenthal, Helicobacter pylori uses motility for initial colonization and to attain robust infection, Infect. Immun. 70 (2002) 1984–1990. https://doi.org/10.1128/IAI.70.4.1984-1990.2002/ASSET/418A5035-4FA1-451E-AE17-E976CA26F37E/ASSETS/GRAPHIC/II0420887004.JPEG.

[25] S.M. Mbulaiteye, M. Hisada, E.M. El-Omar, Helicobacter Pylori associated global gastric cancer burden, Front. Biosci. 14 (2009) 1490–1504. https://doi.org/10.2741/3320.

[26] W.L. Guan, Y. He, R.H. Xu, Gastric cancer treatment: recent progress and future perspectives, J. Hematol. Oncol. 2023 161. 16 (2023) 1–28. https://doi.org/10.1186/S13045-023-01451-3.

[27] İ. Altun, A. Sonkaya, The Most Common Side Effects Experienced by Patients Were Receiving First Cycle of Chemotherapy, Iran. J. Public Health. 47 (2018) 1218. PMC6123577/

[28] M. Orditura, G. Galizia, V. Sforza, V. Gambardella, A. Fabozzi, M.M. Laterza, F. Andreozzi, J. Ventriglia, B. Savastano, A. Mabilia, E. Lieto, F. Ciardiello, F. De Vita, Treatment of gastric cancer, Http://Www.Wjgnet.Com/. 20 (2014) 1635–1649. https://doi.org/10.3748/WJG.V20.I7.1635.

[29] K. Şenol, M.B. Özkan, S. Vural, M. Tez, The role of inflammation in gastric cancer, Adv. Exp. Med. Biol. 816 (2014) 235–257. https://doi.org/10.1007/978-3-0348-0837-8_10.

[30] V. Gopalakrishnan, C.N. Spencer, L. Nezi, A. Reuben, M.C. Andrews, T. V. Karpinets, P.A. Prieto, D. Vicente, K. Hoffman, S.C. Wei, A.P. Cogdill, L. Zhao, C.W. Hudgens, D.S. Hutchinson, T. Manzo, M. Petaccia De Macedo, T. Cotechini, T. Kumar, W.S. Chen, S.M. Reddy, R. Szczepaniak Sloane, J. Galloway-Pena, H. Jiang, P.L. Chen, E.J. Shpall, K. Rezvani, A.M. Alousi, R.F. Chemaly, S. Shelburne, L.M.

Vence, P.C. Okhuysen, V.B. Jensen, A.G. Swennes, F. McAllister, E. Marcelo Riquelme Sanchez, Y. Zhang, E. Le Chatelier, L. Zitvogel, N. Pons, J.L. Austin-Breneman, L.E. Haydu, E.M. Burton, J.M. Gardner, E. Sirmans, J. Hu, A.J. Lazar, T. Tsujikawa, A. Diab, H. Tawbi, I.C. Glitza, W.J. Hwu, S.P. Patel, S.E. Woodman, R.N. Amaria, M.A. Davies, J.E. Gershenwald, P. Hwu, J.E. Lee, J. Zhang, L.M. Coussens, Z.A. Cooper, P.A. Futreal, C.R. Daniel, N.J. Ajami, J.F. Petrosino, M.T. Tetzlaff, P. Sharma, J.P. Allison, R.R. Jenq, J.A. Wargo, Gut microbiome modulates response to anti-PD-1 immunotherapy in melanoma patients, Science (80-.). 359 (2018) 97–103. https://doi.org/10.1126/SCIENCE.AAN4236/SUPPL_FILE/AAN4236_GOPALAKRISHNAN_SM.PDF.

[31] X. Kang, H.C.H. Lau, J. Yu, Modulating gut microbiome in cancer immunotherapy: Harnessing microbes to enhance treatment efficacy, Cell Reports Med. 5 (2024) 101478. https://doi.org/10.1016/J.XCRM.2024.101478.

[32] S. Sakaguchi, T. Yamaguchi, T. Nomura, M. Ono, Regulatory T cells and immune tolerance, Cell. 133 (2008) 775–787. https://doi.org/10.1016/J.CELL.2008.05.009.

[33] R. Medzhitov, Origin and physiological roles of inflammation, Nature. 454 (2008) 428–435. https://doi.org/10.1038/NATURE07201.

[34] K.M. Krishnan, Biomedical Nanomagnetics: A Spin Through Possibilities in Imaging, Diagnostics, and Therapy, IEEE Trans. Magn. 46 (2010) 2523–2558. https://doi.org/10.1109/TMAG.2010.2046907.

[35] M. Arruebo, R. Fernández-Pacheco, M.R. Ibarra, J. Santamaría, Magnetic nanoparticles for drug delivery, Nano Today. 2 (2007) 22–32. https://doi.org/10.1016/S1748-0132(07)70084-1.

[36] T.K. Jain, J. Richey, M. Strand, D.L. Leslie-Pelecky, C.A. Flask, V. Labhasetwar, Magnetic nanoparticles with dual functional properties: drug delivery and magnetic resonance imaging., Biomaterials. 29 (2008) 4012–4021. https://doi.org/10.1016/J.BIOMATERIALS.2008.07.004.

[37] B. Chertok, B.A. Moffat, A.E. David, F. Yu, C. Bergemann, B.D. Ross, V.C. Yang, Iron oxide nanoparticles as a drug delivery vehicle for MRI monitored magnetic targeting of brain tumors, Biomaterials. 29 (2008) 487–496. https://doi.org/10.1016/J.BIOMATERIALS.2007.08.050.

[38] A. Tomitaka, T. Yamada, Y. Takemura, Magnetic nanoparticle hyperthermia using Pluronic-coated Fe 3O 4 nanoparticles: An in vitro study, J. Nanomater. 2012 (2012). https://doi.org/10.1155/2012/480626.

[39] J. Zeng, L. Jing, Y. Hou, M. Jiao, R. Qiao, Q. Jia, C. Liu, F. Fang, H. Lei, M. Gao, Anchoring Group Effects of Surface Ligands on Magnetic Properties of Fe3O4 Nanoparticles: Towards High Performance MRI Contrast Agents, Wiley Online Libr. 26 (2014) 2694–2698. https://doi.org/10.1002/adma.201304744.

[40] Z. Gao, Y. Hou, J. Zeng, L. Chen, C. Liu, W. Yang, M. Gao, Z. Gao, W. Yang, Y. Hou, C. Liu, M.Y. Gao, B. Yi Jie, Z. Guan Cun, J. Zeng, L. Chen, Tumor Microenvironment-Triggered Aggregation of Antiphagocytosis 99mTc-Labeled Fe3O4 Nanoprobes for Enhanced Tumor Imaging In Vivo, Adv. Mater. 29 (2017) 1701095. https://doi.org/10.1002/ADMA.201701095.

[41] T. Ma, Y. Hou, J. Zeng, C. Liu, P. Zhang, L. Jing, D. Shangguan, M. Gao, Dual-Ratiometric Target-Triggered Fluorescent Probe for Simultaneous Quantitative Visualization of Tumor Microenvironment Protease Activity and pH in Vivo, J. Am. Chem. Soc. 140 (2018) 211–218. https://doi.org/10.1021/jacs.7b08900.

[42] N. Nitin, A.L.E.W. Laconte, A.O. Zurkiya, A.X. Hu, G. Bao, Functionalization and peptide-based delivery of magnetic nanoparticles as an intracellular MRI contrast agent, J Biol Inorg Chem. 9 (2004) 706-12. https://doi.org/10.1007/s00775-004-0560-1.

[43] M. Peiravi, H. Eslami, M. Ansari, H. Zare-Zardini, Magnetic hyperthermia: Potentials and limitations, J. Indian Chem. Soc. 99 (2022) 100269. https://doi.org/10.1016/J.JICS.2021.100269.

[44] M. Mohamadkazem, A. Neshastehriz, S.M. Amini, A. Moshiri, A. Janzadeh, Radiosensitising effect of iron oxide-gold nanocomplex for electron beam therapy of melanoma in vivo by magnetic targeting, IET Nanobiotechnology. 17 (2023) 212-223. https://doi.org/10.1049/nbt2.12129

[45] M. Ahmadi Kamalabadi, A. Neshastehriz, H. Ghaznavi, S.M. Amini, Folate functionalized gold-coated magnetic nanoparticles effect in combined electroporation and radiation treatment of HPV-positive oropharyngeal cancer, Med. Oncol. 39 (2022) 196. https://doi.org/ 10.1007/s12032-022-01780-2.

[46] S.M. Amini, S.M. Rezayat, R. Dinarvand, S. Kharrazi, M.R. Jaafari, Gold cluster encapsulated liposomes: theranostic agent with stimulus triggered release capability, Med. Oncol. 40 (2023) 126. https://doi.org/ 10.1007/s12032-023-01991-1.

[47] M. Bañobre-López, A. Teijeiro, J. Rivas, Magnetic nanoparticle-based hyperthermia for cancer treatment, Reports Pract. Oncol. Radiother. 18 (2013) 397–400. https://doi.org/10.1016/j.rpor.2013.09.011.

[48] W. Andrä, H. Nowak, Magnetism in Medicine: A Handbook, Wiley-VCH, 2007. https://doi.org/10.1002/9783527610174.

[49] J. Rivas, M. Bañobre-López, Y. Piñeiro-Redondo, B. Rivas, M.A. López-Quintela, Magnetic nanoparticles for application in cancer therapy, in: J. Magn. Magn. Mater., Elsevier, 2012: pp. 3499–3502. https://doi.org/10.1016/j.jmmm.2012.02.075.

[50] T.D. Schladt, K. Schneider, H. Schild, W. Tremel, Synthesis and bio-functionalization of magnetic nanoparticles for medical diagnosis and treatment, Dalt. Trans. 40 (2011) 6315–6343. https://doi.org/10.1039/c0dt00689k.

[51] N.A. Frey, S. Peng, K. Cheng, S. Sun, Magnetic nanoparticles: Synthesis, functionalization, and applications in bioimaging and magnetic energy storage, Chem. Soc. Rev. 38 (2009) 2532–2542. https://doi.org/10.1039/b815548h.

[52] M. Lattuada, T.A. Hatton, Functionalization of monodisperse magnetic nanoparticles, Langmuir. 23 (2007) 2158–2168. https://doi.org/10.1021/la062092x.

[53] A.H. Lu, E.L. Salabas, F. Schüth, Magnetic nanoparticles: Synthesis, protection, functionalization, and application, Angew. Chemie - Int. Ed. 46 (2007) 1222–1244. https://doi.org/10.1002/anie.200602866.

[54] X. Liu, Y. Zhang, Y. Wang, W. Zhu, G. Li, X. Ma, Y. Zhang, S. Chen, S. Tiwari, K. Shi, S. Zhang, H.M. Fan, Y.X. Zhao, X.J. Liang, Comprehensive understanding of magnetic hyperthermia for improving antitumor therapeutic efficacy, Theranostics. 10 (2020) 3793–3815. https://doi.org/10.7150/thno.40805.

[55] C. Kumar, F. Mohammad, Magnetic nanomaterials for hyperthermia-based therapy and controlled drug delivery, Adv Drug Deliv Rev., 63 (2011) 789-808. https://doi.org/ 10.1016/j.addr.2011.03.008.

[56] V. Shubayev, T. Pisanic, S. Jin, Magnetic nanoparticles for theragnostics, Adv Drug Deliv Rev. 61 (2009) 467-77. https://doi.org/ 10.1016/j.addr.2009.03.007.

[57] D. Yoo, J. Lee, T. Shin, J. Cheon, Theranostic magnetic nanoparticles, Acc Chem Res., 44 (2011) 863-74. https://doi.org/ 10.1021/ar200085c.

[58] D. Ho, X. Sun, S. Sun, Monodisperse magnetic nanoparticles for theranostic applications, Acc. Chem. Res. 44 (2011) 875–882. https://doi.org/10.1021/ar200090c.

[59] V. Vilas-Boas, F. Carvalho, B. Espiña, Magnetic hyperthermia for cancer treatment: Main parameters affecting the outcome of in vitro and in vivo studies, Molecules. 25 (2020) 2874. https://doi.org/10.3390/molecules25122874.

[60] A. Espinosa, J. Kolosnjaj-Tabi, A. Plan Sangnier, A. Curcio, A.K. A Silva, R. Di Corato, C. Wilhelm, A. Abou-Hassan, S. Neveu, A. Espinosa, J. Kolosnjaj-Tabi, A.

Abou-Hassan, A. Plan Sangnier, A. Curcio, A.K. A Silva, R. Di Corato, S. Neveu, T. Pellegrino, L.M. Liz-Marzán, C. Wilhelm, T. Pellegrino, L.M. Liz-Marzán, FULL PAPER www.afm-journal.de 1803660 (1 of 16) Magnetic (Hyper)Thermia or Photothermia? Progressive Comparison of Iron Oxide and Gold Nanoparticles Heating in Water, in Cells, and In Vivo, Wiley Online Libr. 28 (2018). https://doi.org/10.1002/adfm.201803660.

[61] A. Jordan, R. Scholz, P. Wust, H. Fahling, R. Felix, Magnetic fluid hyperthermia (MFH): Cancer treatment with AC magnetic field induced excitation of biocompatible superparamagnetic nanoparticles, J. Magn. Magn. Matter, 201 (1999) 413-419. https://doi.org/ 10.1016/S0304-8853(99)00088-8

[62] L. Xiao, F. Hai, Y. Jia, Y. Yang, C. Eugene, X. Jun, F. Dai, Di. Jun, Optimization of surface coating on Fe 3 O 4 nanoparticles for high performance magnetic hyperthermia agents, J. Mater. Chem., 22 (2012) 8235-8244. https://doi.org/ 10.1039/C2JM30472D

[63] H. Zali, M. Rezaei-Tavirani, M. Azodi, Gastric cancer: prevention, risk factors and treatment, Gastroenterol Hpatol Bed Bench., 4 (2011) 175-185. PMC4017429

[64] F. Wang, W. Meng, B. Wang, L. Qiao, Helicobacter pylori-induced gastric inflammation and gastric cancer, Cancer Lett. 345 (2014) 196–202. https://doi.org/10.1016/j.canlet.2013.08.016.

[65] W.K. Leung, S.R. Lin, J.Y.L. Ching, K.F. To, E.K.W. Ng, F.K.L. Chan, J.Y.W. Lau, J.J.Y. Sung, Factors predicting progression of gastric intestinal metaplasia: Results of a randomised trial on Helicobacter pylori eradication, Gut. 53 (2004) 1244–1249. https://doi.org/10.1136/gut.2003.034629.

[66] C. Ley, A. Mohar, J. Guarner, R. Herrera-Goepfert, L.S. Figueroa, D. Halperin, I. Johnstone, J. Parsonnet, Helicobacter pylori Eradication and Gastric Preneoplastic Conditions: A Randomized, Double-Blind, Placebo-Controlled Trial, Cancer Epidemiol. Biomarkers Prev. 13 (2004) 4–10. https://doi.org/10.1158/1055-9965.EPI-03-0124.

[67] R. Mera, E.T.H. Fontham, L.E. Bravo, J.C. Bravo, M.B. Piazuelo, M.C. Camargo, P. Correa, Long term follow up of patients treated for Helicobacter pylori infection, Gut. 54 (2005) 1536–1540. https://doi.org/10.1136/gut.2005.072009.

[68] I.D. Nagtegaal, R.D. Odze, D. Klimstra, V. Paradis, M. Rugge, P. Schirmacher, K.M. Washington, F. Carneiro, I.A. Cree, The 2019 WHO classification of tumours of the digestive system, Histopathology. 76 (2020) 182–188. https://doi.org/10.1111/his.13975.

[69] H. Fang, Y. Zhang, Z. Wu, X. Wang, H. Wang, Y. Wang, F. Chai, Y. Jiang, Z. Jin, Y. Wan, L. Zhu, S. Ma, Regional hyperthermia combined with chemotherapy in advanced gastric cancer, Open Med. 14 (2019) 85–90. https://doi.org/10.1515/med-2019-0012.

[70] C. Chong, Y. Wang, A. Fathi, R. Parungao, P.K. Maitz, Z. Li, Skin wound repair: Results of a pre-clinical study to evaluate electropsun collagen–elastin–PCL scaffolds as dermal substitutes., Burns. 45 (2019) 1639–1648. https://doi.org/10.1016/J.BURNS.2019.04.014.

[71] M.L. Del Prado-Audelo, H. Cortés, I.H. Caballero-Florán, M. González-Torres, L. Escutia-Guadarrama, S.A. Bernal-Chávez, D.M. Giraldo-Gomez, J.J. Magaña, G. Leyva-Gómez, Therapeutic Applications of Terpenes on Inflammatory Diseases, Front. Pharmacol. 12 (2021) 2114. https://doi.org/10.3389/FPHAR.2021.704197/BIBTEX.

[72] H. Yuan, Q. Ma, L. Ye, G. Piao, The Traditional Medicine and Modern Medicine from Natural Products, Molecules. 21 (2016). https://doi.org/10.3390/MOLECULES21050559.

[73] M. Jermini, J. Dubois, P.Y. Rodondi, K. Zaman, T. Buclin, C. Csajka, A. Orcurto, L. E. Rothuizen, Complementary medicine use during cancer treatment and potential herb-drug interactions from a cross-sectional study in an academic centre, Sci. Reports 2019 91. 9 (2019) 1–11. https://doi.org/10.1038/s41598-019-41532-3.

[74] R.J.S. Vega, N.C. Xolalpa, A.J.A. Castro, C.P. González, J.P. Ramos, S.P. Gutiérrez, Terpenes from Natural Products with Potential Anti-Inflammatory Activity, Terpenes and Terpenoids. (2018). https://doi.org/10.5772/INTECHOPEN.73215.

[75] M. Wink, Modes of Action of Herbal Medicines and Plant Secondary Metabolites, Med. 2015, Vol. 2, Pages 251-286. 2 (2015) 251–286. https://doi.org/10.3390/MEDICINES2030251.

[76] M.A. Gómez-Favela, D.U. Santos-Ballardo, M.E. Bergés-Tiznado, D.L. Ambriz-Pérez, Nanoformulations applied to the delivery of terpenes, Phytochem. Nanodelivery Syst. as Potential Biopharm. (2023) 221–256. https://doi.org/10.1016/B978-0-323-90390-5.00006-2.

[77] S. Sim, N.K. Wong, Nanotechnology and its use in imaging and drug delivery (Review), Biomed. Reports. 14 (2021). https://doi.org/10.3892/BR.2021.1418.

[78] M. Huang, J.J. Lu, M.Q. Huang, J.L. Bao, X.P. Chen, Y.T. Wang, Terpenoids: natural products for cancer therapy, Http://Dx.Doi.Org/10.1517/13543784.2012.727395. 21 (2012) 1801–1818. https://doi.org/10.1517/13543784.2012.727395.

[79] B. Chopra, A.K. Dhingra, K.L. Dhar, K. Nepali, Emerging Role of Terpenoids for the Treatment of Cancer: A Review, Mini Rev. Med. Chem. 21 (2021) 2300–2336. https://doi.org/10.2174/1389557521666210112143024.

[80] C. El-Baba, A. Baassiri, G. Kiriako, B. Dia, S. Fadlallah, S. Moodad, N. Darwiche, Terpenoids' anti-cancer effects: focus on autophagy, Apoptosis 2021 269. 26 (2021) 491–511. https://doi.org/10.1007/S10495-021-01684-Y.

[81] Z. Li, X. Wu, J. Li, L. Yao, L. Sun, Y. Shi, W. Zhang, J. Lin, D. Liang, Y. Li, Antitumor activity of celastrol nanoparticles in a xenograft retinoblastoma tumor model, Int. J. Nanomedicine. 7 (2012) 2389. https://doi.org/10.2147/IJN.S29945.

[82] V. Sanna, J.C. Chamcheu, N. Pala, H. Mukhtar, M. Sechi, I.A. Siddiqui, Nanoencapsulation of natural triterpenoid celastrol for prostate cancer treatment, Int. J. Nanomedicine. 10 (2015) 6835–6846. https://doi.org/10.2147/IJN.S93752.

[83] N. Hasima, B.B. Aggarwal, Cancer-linked targets modulated by curcumin, Int. J. Biochem. Mol. Biol. 3 (2012) 328. PMC3533886

[84] E. Aleebrahim-Dehkordy, H. Nasri, A. Baradaran, P. Nasri, M.R. Tamadon, M. Hedaiaty, S. Beigrezaei, M. Rafieian-Kopaei, Medicinal Plants, Effective Plant Compounds (Compositions) and their Effects on Stomach Cancer, Int. J. Prev. Med. 8 (2017). https://doi.org/10.4103/IJPVM.IJPVM_4_17.

[85] Y. Li, S. Li, X. Meng, R. Gan, J. Zhang, H. Li, Dietary natural products for prevention and treatment of breast cancer, Nutrients, 9 (2017) 728. https://doi.org/10.3390/nu9070728.

[86] J. Zheng, Y. Zhou, Y. Li, D. Xu, S. Li, H. Li, Spices for prevention and treatment of cancers, Nutrients, 8 (2016) 595. https://doi.org/10.3390/nu8080495.

[87] X. Fang, J. Wei, X. He, P. An, H. Wang, L. Jiang, D. Shao, H. Liang, Y. Li, F. Wang, J. Min, Landscape of dietary factors associated with risk of gastric cancer: A systematic review and dose-response meta-analysis of prospective cohort studies, Eur. J. Cancer. 51 (2015) 2820–2832. https://doi.org/10.1016/J.EJCA.2015.09.010.

[88] P. Zou, Y. Xia, J. Ji, W. Chen, J. Zhang, X. Chen, V. Rajamanickam, G. Chen, Z. Weng, L. Chen, Y. Wang, S. Yang, G. Liang, Piperlongumine as a direct TrxR1 inhibitor with suppressive activity against gastric cancer, Cancer Lett., 375 (2016) 114-126. https://doi.org/ 10.1016/j.canlet.2016.02.058

[89] T. Kim, S. Lee, M. Kim, C. Cheon, S. Ko, Kaempferol induces autophagic cell death via IRE1-JNK-CHOP pathway and inhibition of G9a in gastric cancer cells, Cell Death Dis., 9 (2018) 875. https://doi.org/10.1038/s41419-018-0930-1

[90] D. Cox-Georgian, N. Ramadoss, C. Dona, C. Basu, Therapeutic and Medicinal Uses of Terpenes, Med. Plants. (2019) 333. https://doi.org/10.1007/978-3-030-31269-5_15.

[91] A. Masyita, R. Mustika Sari, A. Dwi Astuti, B. Yasir, N. Rahma Rumata, T. Bin Emran, F. Nainu, J. Simal-Gandara, Terpenes and terpenoids as main bioactive compounds of essential oils, their roles in human health and potential application as natural food preservatives, Food Chem. X. 13 (2022) 100217. https://doi.org/10.1016/J.FOCHX.2022.100217.

[92] J.S.S. Quintans, S. Shanmugam, L. Heimfarth, A.A.S. Araújo, J.R.G. d. S. Almeida, L. Picot, L.J. Quintans-Júnior, Monoterpenes modulating cytokines - A review, Food Chem. Toxicol. 123 (2019) 233–257. https://doi.org/10.1016/J.FCT.2018.10.058.

[93] M. Jakaria, D.Y. Cho, M.E. Haque, G. Karthivashan, I.S. Kim, P. Ganesan, D.K. Choi, Neuropharmacological potential and delivery prospects of thymoquinone for neurological disorders, Oxid. Med. Cell. Longev. 2018 (2018). https://doi.org/10.1155/2018/1209801.

[94] M. Ashrafizadeh, Z. Ahmadi, R. Mohammadinejad, N. Kaviyani, S. Tavakol, Monoterpenes modulating autophagy: A review study, Basic Clin. Pharmacol. Toxicol. 126 (2020) 9–20. https://doi.org/10.1111/BCPT.13282.

[95] M.V. Sobral, A.L. Xavier, T.C. Lima, D.P. De Sousa, Antitumor Activity of Monoterpenes Found in Essential Oils, Sci. World J. 2014 (2014). https://doi.org/10.1155/2014/953451.

[96] M. De Vincenzi, A. Stammati, A. De Vincenzi, M. Silano, Constituents of aromatic plants: carvacrol, Fitoterapia. 75 (2004) 801–804. https://doi.org/10.1016/J.FITOTE.2004.05.002.

[97] L.A. Sampaio, L.T.S. Pina, M.R. Serafini, D. dos S. Tavares, A.G. Guimarães, Antitumor Effects of Carvacrol and Thymol: A Systematic Review, Front. Pharmacol. 12 (2021) 1673. https://doi.org/10.3389/FPHAR.2021.702487/BIBTEX.

[98] A. Mondal, S. Bose, K. Mazumder, R. Khanra, Carvacrol (Origanum vulgare): Therapeutic Properties and Molecular Mechanisms, Adv. Struct. Mater. 140 (2021) 437–462. https://doi.org/10.1007/978-3-030-54027-2_13.

[99] Z. Taghizadeh, S. Rakhshani, V. Jahani, O. Rajabi, H.M. Haghighi, M. Abbaspour, Preparation and in vitro characterization of carvacrol pellets by combination of liquisolid technique and extrusion-spheronization, J. Drug Deliv. Sci. Technol. 61 (2021) 102232. https://doi.org/10.1016/J.JDDST.2020.102232.

[100] A. Günes-Bayir, H.S. Kiziltan, A. Kocyigit, E.M. Güler, E. Karataş, A. Toprak, Effects

of natural phenolic compound carvacrol on the human gastric adenocarcinoma (AGS) cells in vitro, Anticancer. Drugs. 28 (2017) 522–530. https://doi.org/10.1097/CAD.0000000000000491.

[101] H. Yang, G. Liu, H. Zhao, X. Dong, Z. Yang, Inhibiting the JNK/ERK signaling pathway with geraniol for attenuating the proliferation of human gastric adenocarcinoma AGS cells, J. Biochem. Mol. Toxicol. 35 (2021) e22818. https://doi.org/10.1002/JBT.22818.

[102] S. SHARMA, P. GAO, V.E. STEELE, Quantitative Morphometry of Respiratory Tract Epithelial Cells as a Tool for Testing Chemopreventive Agent Efficacy, Anticancer Res. 30 (2010).

[103] L. Lv, N. Yang, Y. Cao, J. Dang, L. Cheng, M.A. El-Sheikh, Y. Zhang, d-Carvone inhibits the JAK/STAT3 signaling pathway and induced the apoptotic cell death in the human gastric cancer AGS cells, J. Biochem. Mol. Toxicol. 35 (2021) e22746. https://doi.org/10.1002/JBT.22746.

[104] R. Javed, M.A. Hanif, R. Rehman, M. Hanif, B.T. Tung, Caraway, Med. Plants South Asia Nov. Sources Drug Discov. (2020) 87–100. https://doi.org/10.1016/B978-0-08-102659-5.00007-0.

[105] Y. Xiang, Q. Zhang, S. Wei, C. Huang, Z. Li, Y. Gao, Paeoniflorin: a monoterpene glycoside from plants of Paeoniaceae family with diverse anticancer activities, J. Pharm. Pharmacol. 72 (2020) 483–495. https://doi.org/10.1111/JPHP.13204.

[106] J. Zhang, K. Yu, X. Han, L. Zhen, M. Liu, X. Zhang, Y. Ren, J. Shi, Paeoniflorin influences breast cancer cell proliferation and invasion via inhibition of the Notch-1 signaling pathway, Mol. Med. Rep. 17 (2018) 1321–1325. https://doi.org/10.3892/MMR.2017.8002.

[107] A. Pasdaran, A. Hamedi, Natural Products as Source of New Antimicrobial Compounds for Skin Infections, Microbiol. Ski. Soft Tissue, Bone Jt. Infect. (2017) 223–253. https://doi.org/10.1016/B978-0-12-811079-9.00014-8.

[108] J. Bohlmann, J. Gershenzon, Old substrates for new enzymes of terpenoid biosynthesis, Proc. Natl. Acad. Sci. U. S. A. 106 (2009) 10402–10403. https://doi.org/10.1073/PNAS.0905226106/ASSET/9A90F97E-58D2-4E27-A87E-0681B7995521/ASSETS/GRAPHIC/ZPQ9990988080001.JPEG.

[109] M.T. Islam, C.B. Da Silva, M.V.O.B. De Alencar, M.F.C.J. Paz, F.R.D.C. Almeida, A.A.D.C. Melo-Cavalcante, Diterpenes: Advances in Neurobiological Drug Research, Phyther. Res. 30 (2016) 915–928. https://doi.org/10.1002/PTR.5609.

[110] G.B. Lockwood, GAS CHROMATOGRAPHY | Terpenoids, Ref. Modul. Chem. Mol. Sci. Chem. Eng. (2013). https://doi.org/10.1016/B978-0-12-409547-2.04768-5.

[111] J. Rysz, M. Banach, R. Stolarek, J. Pasnik, C. Rysz, R. Koktysz, M. Piechota, Z. Baj, Serum matrix metalloproteinases MMP-2 and MMP-9 and metalloproteinase tissue inhibitors TIMP-1 and TIMP-2 in diabetic nephropathy, J. Nephrol. 20 (2007) 444-52. PMID: 17879211

[112] L. Dai, G. Wang, W. Pan, Andrographolide inhibits proliferation and metastasis of SGC7901 gastric cancer cells, Biomed Res. Int. 2017 (2017). https://doi.org/10.1155/2017/6242103.

[113] M. Hidalgo, A. Romero, P. Cortes, I. Concha, J. Hancke, R. Burgos, Andrographolide interferes with binding of nuclear factor-κB to DNA in HL-60-derived neutrophilic cells, Br J Pharmacol. 144 (2005) 680-6. https://doi.org/ 10.1038/sj.bjp.0706105 [114] A. Allegra, A. Tonacci, G. Pioggia, C. Musolino, S. Gangemi, Anticancer Activity of Rosmarinus officinalis L.: Mechanisms of Action and Therapeutic Potentials, Nutrients. 12 (2020) 1–25. https://doi.org/10.3390/NU12061739.

[115] S. Shrestha, Y.W. Song, H. Kim, D.S. Lee, S.K. Cho, Sageone, a diterpene from Rosmarinus officinalis, synergizes with cisplatin cytotoxicity in SNU-1 human gastric cancer cells, Phytomedicine. 23 (2016) 1671–1679. https://doi.org/10.1016/J.PHYMED.2016.09.008.

[116] T.J. Fan, L.H. Han, R.S. Cong, J. Liang, Caspase Family Proteases and Apoptosis, Acta Biochim. Biophys. Sin. (Shanghai). 37 (2005) 719–727. https://doi.org/10.1111/J.1745-7270.2005.00108.X.

[117] S. Bahri, S. Jameleddine, V. Shlyonsky, Relevance of carnosic acid to the treatment of several health disorders: Molecular targets and mechanisms, Biomed. Pharmacother. 84 (2016) 569–582. https://doi.org/10.1016/J.BIOPHA.2016.09.067.

[118] W. El-Huneidi, K. Bajbouj, J.S. Muhammad, A. Vinod, J. Shafarin, G. Khoder, M.A. Saleh, J. Taneera, E. Abu-Gharbieh, Carnosic Acid Induces Apoptosis and Inhibits Akt/mTOR Signaling in Human Gastric Cancer Cell Lines, Pharm. 2021, Vol. 14, Page 230. 14 (2021) 230. https://doi.org/10.3390/PH14030230.

[119] K.T. Liby, M.M. Yore, M.B. Sporn, Triterpenoids and rexinoids as multifunctional agents for the prevention and treatment of cancer, Nat. Rev. Cancer. 7 (2007) 357–369. https://doi.org/10.1038/NRC2129.

[120] M.C. Yin, Anti-glycative potential of triterpenes: A mini-review, BioMedicine. 2 (2012) 2–9. https://doi.org/10.1016/J.BIOMED.2011.12.001.

[121] S. Jäger, H. Trojan, T. Kopp, M.N. Laszczyk, A. Scheffler, Pentacyclic triterpene distribution in various plants - rich sources for a new group of multi-potent plant extracts, Molecules. 14 (2009) 2016–2031. https://doi.org/10.3390/MOLECULES14062016.

[122] S.S. Yao, L. Han, Z. Bin Tian, Y.N. Yu, Q. Zhang, X.Y. Li, T. Mao, L. Yang, Celastrol inhibits growth and metastasis of human gastric cancer cell MKN45 by down-regulating microRNA-21, Phyther. Res. 33 (2019) 1706–1716. https://doi.org/10.1002/PTR.6359.

[123] H.W. Lee, K.S. Bin Jang, H.J. Choi, A. Jo, J.H. Cheong, K.H. Chun, Celastrol inhibits gastric cancer growth by induction of apoptosis and autophagy, BMB Rep. 47 (2014) 697. https://doi.org/10.5483/BMBREP.2014.47.12.069.

[124] X. Chen, Y. Zhao, W. Luo, S. Chen, F. Lin, X. Zhang, S. Fan, X. Shen, Y. Wang, G. Liang, Celastrol induces ROS-mediated apoptosis via directly targeting peroxiredoxin-2 in gastric cancer cells, Theranostics. 10 (2020) 10290. https://doi.org/10.7150/THNO.46728.

[125] A. Petronellia, G. Pannitterib, U. Testaa, Triterpenoids as new promising anticancer drugs, Anticancer. Drugs. 20 (2009) 880–892. https://doi.org/10.1097/CAD.0B013E328330FD90.

[126] M.W. Lin, A.S. Lin, D.C. Wu, S.S.W. Wang, F.R. Chang, Y.C. Wu, Y. Bin Huang, Euphol from Euphorbia tirucalli selectively inhibits human gastric cancer cell growth through the induction of ERK1/2-mediated apoptosis, Food Chem. Toxicol. 50 (2012) 4333–4339. https://doi.org/10.1016/J.FCT.2012.05.029.

[127] H. Wang, X. Ge, H. Qu, N. Wang, J. Zhou, W. Xu, J. Xie, Y. Zhou, L. Shi, Z. Qin, Z. Jiang, W. Yin, J. Xia, Glycyrrhizic Acid Inhibits Proliferation of Gastric Cancer Cells by Inducing Cell Cycle Arrest and Apoptosis, Cancer Manag. Res. 12 (2020) 2853. https://doi.org/10.2147/CMAR.S244481.

[128] Y. Chen, X. Wu, C. Liu, Y. Zhou, Betulinic acid triggers apoptosis and inhibits migration and invasion of gastric cancer cells by impairing EMT progress, Cell Biochem. Funct. 38 (2020) 702. https://doi.org/10.1002/CBF.3537.

[129] H. Wang, H. Wang, L. Ge, Y. Zhao, K. Zhu, Z. Chen, Q. Wu, Y. Xin, J. Guo, Betulinic acid targets drug-resistant human gastric cancer cells by inducing autophagic cell death, suppresses cell migration and invasion, and modulates the ERK/MEK signaling pathway, Acta Biochim. Pol. 69 (2022) 25–30. https://doi.org/10.18388/ABP.2020_5530.

[130] B.M. Fraga, Natural sesquiterpenoids, Nat. Prod. Rep. 25 (2008) 1180–1209. https://doi.org/10.1039/b806216c.

[131] Z. Lorigooini, F. Jamshidi-kia, S. Dodman, Analysis of sesquiterpenes and sesquiterpenoids, Recent Adv. Nat. Prod. Anal. (2020) 289–312. https://doi.org/10.1016/B978-0-12-816455-6.00008-1.

[132] K. Ishnava, J. Chauhan, M. Barad, Anticariogenic and phytochemical evaluation of Eucalyptus globules Labill, Saudi J Bio Sci., 20 (2013) 69-74. https://doi.org/ 10.1016/j.sjbs.2012.11.003

[133] J. Buckle, Basic Plant Taxonomy, Basic Essential Oil Chemistry, Extraction, Biosynthesis, and Analysis, Clin. Aromather. (2015) 37–72. https://doi.org/10.1016/B978-0-7020-5440-2.00003-6.

[134] M. Chadwick, H. Trewin, F. Gawthrop, C. Wagstaff, Sesquiterpenoids Lactones: Benefits to Plants and People, Int. J. Mol. Sci. 2013, Vol. 14, Pages 12780-12805. 14 (2013) 12780–12805. https://doi.org/10.3390/IJMS140612780.

[135] D. Wang, Y. Li, P. Cui, Q. Zhao, B. bo Tan, Z. dong Zhang, Y. Liu, N. Jia, Zerumbone induces gastric cancer cells apoptosis: Involving cyclophilin A, Biomed. Pharmacother. 83 (2016) 740–745. https://doi.org/10.1016/J.BIOPHA.2016.07.034.

[136] K. Tsuboi, Y. Matsuo, T. Shamoto, T. Shibata, S. Koide, M. Morimoto, S. Guha, B. Sung, B.B. Aggarwal, H. Takahashi, H. Takeyama, Zerumbone inhibits tumor angiogenesis via NF-κB in gastric cancer, Oncol. Rep. 31 (2014) 57–64. https://doi.org/10.3892/OR.2013.2842/HTML.

[137] P. Li, X. Zhou, W. Sun, W. Sheng, Y. Tu, Y. Yu, J. Dong, B. Ye, Z. Zheng, M. Lu, Elemene Induces Apoptosis of Human Gastric Cancer Cell Line BGC-823 via Extracellular Signal-Regulated Kinase (ERK) 1/2 Signaling Pathway, Med. Sci. Monit. 23 (2017) 809. https://doi.org/10.12659/MSM.903197.

[138] T. Tan, J. Li, R. Luo, R. Wang, L. Yin, M. Liu, Y. Zeng, Z. Zeng, T. Xie, Recent Advances in Understanding the Mechanisms of Elemene in Reversing Drug Resistance in Tumor Cells: A Review, Molecules. 26 (2021). https://doi.org/10.3390/MOLECULES26195792.

[139] J. Wen, K. You, S. Lee, C. Song, D. Kim, Oxidative stress-mediated apoptosis: the anticancer effect of the sesquiterpene lactone parthenolide, J Biol Chem., 277 (2002) 38954-64. https://doi.org/10.1074/jbc.M203842200.

[140] L.J. Zhao, Y.H. Xu, Y. Li, Effect of parthenolide on proliferation and apoptosis in

gastric cancer cell line SGC7901, J. Dig. Dis. 10 (2009) 172–180. https://doi.org/10.1111/J.1751-2980.2009.00382.X.

[141] M. Liu, Y. Yang, D. Liu, Y. Cao, Y. Li, Parthenolide increases the sensitivity of gastric cancer cells to chemotherapy, J. Tradit. Chinese Med. = Chung i Tsa Chih Ying Wen Pan. 40 (2020) 908–916. https://doi.org/10.19852/J.CNKI.JTCM.2020.06.002.

[142] W.H. Talib, L.T. Al Kury, Parthenolide inhibits tumor-promoting effects of nicotine in lung cancer by inducing P53 - dependent apoptosis and inhibiting VEGF expression, Biomed. Pharmacother. 107 (2018) 1488–1495. https://doi.org/10.1016/J.BIOPHA.2018.08.139.

[143] T. Efferth, H. Dunstan, A. Sauerbrey, H. Miyachi, C. Chitambar, The anti-malarial artesunate is also active against cancer, Int J Ocol., 18 (2001) 767-773. https://doi.org/10.3892/ijo.18.4.767.

[144] H.T. Zhang, Y.L. Wang, J. Zhang, Q.X. Zhang, Artemisinin inhibits gastric cancer cell proliferation through upregulation of p53, Tumor Biol. 35 (2014) 1403–1409. https://doi.org/10.1007/S13277-013-1193-1/FIGURES/7.

[145] K. Can Baser, Biological and pharmacological activities of carvacrol and carvacrol bearing essential oils, Curr. Pharm. Des. 14 (2008) 3106–3119. https://doi.org/10.2174/138161208786404227.

[146] M. Sharifi-Rad, E.M. Varoni, M. Iriti, M. Martorell, W.N. Setzer, M. del Mar Contreras, B. Salehi, A. Soltani-Nejad, S. Rajabi, M. Tajbakhsh, J. Sharifi-Rad, Carvacrol and human health: A comprehensive review, Phytother. Res. 32 (2018) 1675–1687. https://doi.org/10.1002/PTR.6103.

[147] N. Ortiz, M.F. Jiménez, C. Chaverri, J.F. Cicció, C. Díaz, Effect on cell growth, viability and migration of geraniol and geraniol-containing essential oil from Lippia alba (Verbenaceae) on gastric carcinoma cells, 34 (2021) 65–76 https://doi.org/10.1080/10412905.2021.1975576.

[148] A. Bouyahya, H. Mechchate, T. Benali, R. Ghchime, S. Charfi, A. Balahbib, P. Burkov, M.A. Shariati, J.M. Lorenzo, N. El Omari, Health Benefits and Pharmacological Properties of Carvone, Biomolecules. 11 (2021). https://doi.org/10.3390/BIOM11121803.

[149] J.J. Wu, W.Y. Sun, S.S. Hu, S. Zhang, W. Wei, A standardized extract from Paeonia lactiflora and Astragalus membranaceus induces apoptosis and inhibits the proliferation, migration and invasion of human hepatoma cell lines, Int. J. Oncol. 43 (2013) 1643–1651. https://doi.org/10.3892/IJO.2013.2085.

[150] S. Fang, W. Zhu, Y. Zhang, Y. Shu, P. Liu, Paeoniflorin modulates multidrug resistance of a human gastric cancer cell line via the inhibition of NF-κB activation, Mol. Med. Rep. 5 (2012) 351–356. https://doi.org/10.3892/MMR.2011.652.

[151] Q. Zhang, Y. Yuan, J. Cui, T. Xiao, D. Jiang, Paeoniflorin inhibits proliferation and invasion of breast cancer cells through suppressing Notch-1 signaling pathway, Biomed. Pharmacother. 78 (2016) 197–203. https://doi.org/10.1016/J.BIOPHA.2016.01.019.

[152] M. Majdi, Q. Liu, G. Karimzadeh, M.A. Malboobi, J. Beekwilder, K. Cankar, R. De Vos, S. Todorović, A. Simonović, H. Bouwmeester, Biosynthesis and localization of parthenolide in glandular trichomes of feverfew (Tanacetum parthenium L. Schulz Bip.), Phytochemistry. 72 (2011) 1739–1750. https://doi.org/10.1016/J.PHYTOCHEM.2011.04.021.

[153] N.K.B.K. Ikram, H.T. Simonsen, A Review of Biotechnological Artemisinin Production in Plants, Front. Plant Sci. 0 (2017) 1966. https://doi.org/10.3389/FPLS.2017.01966.

[154] H.C. Lai, N.P. Singh, T. Sasaki, Development of artemisinin compounds for cancer treatment, Investig. New Drugs 2012 311. 31 (2012) 230–246. https://doi.org/10.1007/S10637-012-9873-Z.

[155] M. Geethangili, Y.K. Rao, S.H. Fang, Y.M. Tzeng, Cytotoxic constituents from Andrographis paniculata induce cell cycle arrest in Jurkat cells, Phyther. Res. 22 (2008) 1336–1341. https://doi.org/10.1002/PTR.2493.

[156] S.H. Venkatesha, K.D. Moudgil, Celastrol and Its Role in Controlling Chronic Diseases, Adv. Exp. Med. Biol. 928 (2016) 267–289. https://doi.org/10.1007/978-3-319-41334-1_12.

[157] G. Kuttan, P. Pratheeshkumar, K.A. Manu, R. Kuttan, Inhibition of tumor progression by naturally occurring terpenoids, Https://Doi.Org/10.3109/13880209.2011.559476. 49 (2011) 995–1007. https://doi.org/10.3109/13880209.2011.559476.

[158] H. Hibasami, H. Lwase, K. Yoshioka, H. Takahashi, Glycyrrhizin induces apoptosis in human stomach cancer KATO III and human promyelotic leukemia HL-60 cells, Int J Mol Med., 16 (2005) 233-6. PMID: 16012754

[159] S. Thirugnanam, L. Xu, … K.R.-O., undefined 2008, Glycyrrhizin induces apoptosis in prostate cancer cell lines DU-145 and LNCaP, Spandidos-Publications.Com. 20 (2008) 1387–1392. https://doi.org/10.3892/or_00000157.

[160] C. Jin, K. Wang, A. Oppong-Gyebi, J. Hu, Application of Nanotechnology in Cancer

Diagnosis and Therapy - A Mini-Review, Int. J. Med. Sci. 17 (2020) 2964. https://doi.org/10.7150/IJMS.49801.

[161] J. Hu, W. Huang, S. Huang, Q. Zhuge, K. Jin, Y. Zhao, S.-V. Berlin, Magnetically active Fe3O4 nanorods loaded with tissue plasminogen activator for enhanced thrombolysis, Springer. 9 (2016) 2652–2661. https://doi.org/10.1007/s12274-016-1152-4.

[162] Z. Rafiq, P. Patel, S. Kumar, H.S. Sofi, J. Macossay, F.A. Sheikh, Advancements of Nanotechnology in Diagnostic Applications, Appl. Nanotechnol. Biomed. Sci. (2020) 1–15. https://doi.org/10.1007/978-981-15-5622-7_1.

[163] M. Kumar Teli, S. Mutalik, G.K. Rajanikant, Nanotechnology and Nanomedicine: Going Small Means Aiming Big, Curr. Pharm. Des. 16 (2010) 1882–1892. https://doi.org/10.2174/138161210791208992.

[164] G. Pal, P. Rai, A. Pandey, Green synthesis of nanoparticles: A greener approach for a cleaner future, Green Synth. Charact. Appl. Nanoparticles. (2019) 1–26. https://doi.org/10.1016/B978-0-08-102579-6.00001-0.

[165] K. Bloch, K. Pardesi, C. Satriano, S. Ghosh, Bacteriogenic Platinum Nanoparticles for Application in Nanomedicine, Front. Chem. 9 (2021). https://doi.org/10.3389/FCHEM.2021.624344.

[166] B. Mousavi, F. Tafvizi, S. Zaker Bostanabad, Green synthesis of silver nanoparticles using Artemisia turcomanica leaf extract and the study of anti-cancer effect and apoptosis induction on gastric cancer cell line (AGS), 46 (2018) 499–510. https://doi.org/10.1080/21691401.2018.1430697.

[167] S. Aslany, F. Tafvizi, V. Naseh, Characterization and evaluation of cytotoxic and apoptotic effects of green synthesis of silver nanoparticles using Artemisia Ciniformis on human gastric adenocarcinoma, Mater. Today Commun. 24 (2020) 101011. https://doi.org/10.1016/J.MTCOMM.2020.101011.

[168] M. Shirzadi-Ahodashti, S. Mortazavi-Derazkola, M.A. Ebrahimzadeh, Biosynthesis of noble metal nanoparticles using crataegus monogyna leaf extract (CML@X-NPs, X= Ag, Au): Antibacterial and cytotoxic activities against breast and gastric cancer cell lines, Surfaces and Interfaces. 21 (2020) 100697. https://doi.org/10.1016/J.SURFIN.2020.100697.

[169] C. Li, Y. Wang, H. Zhang, M. Li, Z. Zhu, Y. Xue, An investigation on the cytotoxicity and caspase-mediated apoptotic effect of biologically synthesized gold nanoparticles using Cardiospermum halicacabum on AGS gastric carcinoma cells, Int. J.

Nanomedicine. 14 (2019) 951. https://doi.org/10.2147/IJN.S193064.

[170] M. Naseer, R. Ramadan, J. Xing, N.A. Samak, Facile green synthesis of copper oxide nanoparticles for the eradication of multidrug resistant Klebsiella pneumonia and Helicobacter pylori biofilms, Int. Biodeterior. Biodegradation. 159 (2021) 105201. https://doi.org/10.1016/J.IBIOD.2021.105201.

[171] Z. Yun, A. Chinnathambi, S.A. Alharbi, Z. Jin, Biosynthesis of gold nanoparticles using Vetex negundo and evaluation of pro-apoptotic effect on human gastric cancer cell lines, J. Photochem. Photobiol. B Biol. 203 (2020) 111749. https://doi.org/10.1016/J.JPHOTOBIOL.2019.111749.

[172] D. Sharda, K. Attri, P. Kaur, D. Choudhury, Protection of lead-induced cytotoxicity using paramagnetic nickel-insulin quantum clusters, RSC Adv. 11 (2021) 24656–24668. https://doi.org/10.1039/D1RA03597E.

[173] P. Kaur, D. Choudhury, Functionality of receptor targeted zinc-insulin quantum clusters in skin tissue augmentation and bioimaging, J. Drug Target. 29 (2021) 541–550. https://doi.org/10.1080/1061186X.2020.1864740.

[174] S. Tran, P. DeGiovanni, B. Piel, P. Rai, Cancer nanomedicine: a review of recent success in drug delivery, Clin. Transl. Med. 6 (2017). https://doi.org/10.1186/S40169-017-0175-0.

[175] S.Y. Lee, R.L. Mahajan, A facile method for coal to graphene oxide and its application to a biosensor, Carbon N. Y. 181 (2021) 408–420. https://doi.org/10.1016/J.CARBON.2021.05.007.

[176] D. Choudhury, A. Ganguli, D.G. Dastidar, B.R. Acharya, A. Das, G. Chakrabarti, Apigenin shows synergistic anticancer activity with curcumin by binding at different sites of tubulin, Biochimie. 95 (2013) 1297–1309. https://doi.org/10.1016/J.BIOCHI.2013.02.010.

[177] D. Choudhury, A. Das, A. Bhattacharya, G. Chakrabarti, Aqueous extract of ginger shows antiproliferative activity through disruption of microtubule network of cancer cells, Food Chem. Toxicol. 48 (2010) 2872–2880. https://doi.org/10.1016/J.FCT.2010.07.020.

[178] P. Kaur, S. Ghosh, A. Bhowmick, K. Gadhave, S. Datta, A. Ghosh, N. Garg, R.L. Mahajan, B. Basu, D. Choudhury, Bacterioboat-A novel tool to increase the half-life period of the orally administered drug, Sci. Adv. 8 (2022). https://doi.org/10.1126/SCIADV.ABH1419.

[179] C. Medina, M.J. Santos-Martinez, A. Radomski, O.I. Corrigan, M.W. Radomski,

Nanoparticles: pharmacological and toxicological significance, Wiley Online Libr. 150 (2007) 552–558. https://doi.org/10.1038/sj.bjp.0707130.

[180] S.A. Wickline, G.M. Lanza, Nanotechnology for molecular imaging and targeted therapy, Circulation. 107 (2003) 1092–1095. https://doi.org/10.1161/01.CIR.0000059651.17045.77.

[181] S. Lanone, J. Boczkowski, Biomedical Applications and Potential Health Risks of Nanomaterials: Molecular Mechanisms, Curr. Mol. Med. 6 (2006) 651–663. https://doi.org/10.2174/156652406778195026.

[182] J. Hu, S. Huang, L. Zhu, W. Huang, Y. Zhao, K. Jin, Q. Zhuge, Tissue plasminogen activator-porous magnetic microrods for targeted thrombolytic therapy after ischemic stroke, ACS Publ. 10 (2018) 32988–32997. https://doi.org/10.1021/acsami.8b09423.

[183] V. Chaturvedi, A. Singh,V.S., Cancer nanotechnology: a new revolution for cancer diagnosis and therapy, Curr Drug Metab., 20 (2019) 416-429. https://doi.org/10.2174/1389200219666180918111528

[184] N. Ochekpe, P. Olorunfemi, N. Ngwuluka, Nanotechnology and drug delivery part 1: background and applications, Trop J Pharm Res., 8 (2009) 265–274. https://doi.org/10.4314/tjpr.v8i3.44546

[185] A.J. Montero, B. Adams, C.M. Diaz-Montero, S. Glück, Nab-paclitaxel in the treatment of metastatic breast cancer: A comprehensive review, Expert Rev. Clin. Pharmacol. 4 (2011) 329–334. https://doi.org/10.1586/ECP.11.7.

[186] K. Liby, M. Yore, M. Sporn, Triterpenoids and rexinoids as multifunctional agents for the prevention and treatment of cancer, Nat Rev Cancer, 7 (2007) 357-69. https://doi.org/10.1038/nrc2129

[187] J.M. Patlolla, C. Rao, Triterpenoids for cancer prevention and treatment: current status and future prospects, Curr Pharm Biotechnol. 13 (2012) 147-55. https://doi.org/10.2174/138920112798868719

[188] J. Liu, Oleanolic acid and ursolic acid: Research perspectives, J. Ethnopharmacol. 100 (2005) 92–94. https://doi.org/10.1016/J.JEP.2005.05.024.

[189] M. G, S. K, M. Q, S. RK, K. D, K. P, F. G, Secondary Metabolites in the Green Synthesis of Metallic Nanoparticles, Mater. (Basel, Switzerland). 11 (2018). https://doi.org/10.3390/MA11060940.

[190] K.B. Narayanan, N. Sakthivel, Biological synthesis of metal nanoparticles by microbes, Adv. Colloid Interface Sci. 156 (2010) 1–13. https://doi.org/10.1016/J.CIS.2010.02.001.

[191] V. Kumar, S.K. Yadav, Plant-mediated synthesis of silver and gold nanoparticles and their applications, J. Chem. Technol. Biotechnol. 84 (2009) 151–157. https://doi.org/10.1002/JCTB.2023.

[192] R.G. Haverkamp, A.T. Marshall, The mechanism of metal nanoparticle formation in plants: limits on accumulation, J. Nanoparticle Res. 2008 116. 11 (2008) 1453–1463. https://doi.org/10.1007/S11051-008-9533-6.

[193] J. Sun, Q. Wei, Y. Zhou, J. Wang, Q. Liu, H. Xu, A systematic analysis of FDA-approved anticancer drugs, BMC Syst. Biol. 11 (2017). https://doi.org/10.1186/S12918-017-0464-7.

[194] E.Y. Chen, V. Raghunathan, V. Prasad, An Overview of Cancer Drugs Approved by the US Food and Drug Administration Based on the Surrogate End Point of Response Rate, JAMA Intern. Med. 179 (2019) 915–921. https://doi.org/10.1001/JAMAINTERNMED.2019.0583.

[195] S.J. Casak, I. Fashoyin-Aje, S.J. Lemery, L. Zhang, R. Jin, H. Li, L. Zhao, H. Zhao, H. Zhang, H. Chen, K. He, M. Dougherty, R. Novak, S. Kennett, S. Khasar, W. Helms, P. Keegan, R. Pazdur, FDA Approval Summary: Ramucirumab for Gastric Cancer, Clin. Cancer Res. 21 (2015) 3372–3376. https://doi.org/10.1158/1078-0432.CCR-15-0600.

[196] M. Javle, E.C. Smyth, I. Chau, Ramucirumab: successfully targeting angiogenesis in gastric cancer, Clin. Cancer Res. 20 (2014) 5875–5881. https://doi.org/10.1158/1078-0432.CCR-14-1071.

[197] N. Mohan, J. Jiang, M. Dokmanovic, W.J. Wu, Trastuzumab-mediated cardiotoxicity: current understanding, challenges, and frontiers, Antib. Ther. 1 (2018) 13–17. https://doi.org/10.1093/ABT/TBY003.

[198] D. Cejka, M. Preusser, A. Woehrer, W. Sieghart, S. Strommer, J. Werzowa, T. Fuereder, V. Wacheck, Everolimus (RAD001) and anti-angiogenic cyclophosphamide show long-term control of gastric cancer growth in vivo, Cancer Biol. Ther. 7 (2008) 1377–1385. https://doi.org/10.4161/cbt.7.9.6416.

[199] E.C. Smyth, N. Tarazona, I. Chau, Ramucirumab: Targeting angiogenesis in the treatment of gastric cancer, Immunotherapy. 6 (2014) 1177–1186. https://doi.org/10.2217/IMT.14.85.

[200] S. Koganemaru, K. Shitara, Expert Opinion on Biological Therapy ISSN: (Print) (Antibody-drug conjugates to treat gastric cancer Antibody-drug conjugates to treat gastric cancer, (2020). https://doi.org/10.1080/14712598.2020.1802423.

[201] J.L. Kim, D.-H. Lee, S. Jeong, B.R. Kim, Y.J. Na, S.H. Park, M.J. Jo, Y.A. Jeong, S.C.

Oh, Imatinib-induced apoptosis of gastric cancer cells is mediated by endoplasmic reticulum stress, Oncol. Rep. 41 (2019) 1616. https://doi.org/10.3892/OR.2018.6945.

[202] R. Mehta, A. Shah, K. Almhanna, Pembrolizumab for the treatment of patients with recurrent locally advanced or metastatic gastric or gastroesophageal junction cancer: An evidence-based review of place in therapy, Onco. Targets. Ther. 11 (2018) 6525–6537. https://doi.org/10.2147/OTT.S152513.

[203] C. Kang, S. Dhillon, E.D. Deeks, Trifluridine/Tipiracil: A Review in Metastatic Gastric Cancer, Drugs 2019 7914. 79 (2019) 1583–1590. https://doi.org/10.1007/S40265-019-01195-W.

[204] P. Jimenez, A. Pathak, A.T. Phan, The role of taxanes in the management of gastroesphageal cancer., J. Gastrointest. Oncol. 2 (2011) 240–249. https://doi.org/10.3978/j.issn.2078-6891.2011.027.

[205] H. Fukuda, N. Takiguchi, K. Koda, K. Oda, K. Seike, M. Miyazaki, Thymidylate synthase and dihydropyrimidine dehydrogenase are related to histological effects of 5-fluorouracil and cisplatin neoadjuvant chemotherapy for primary gastric cancer patients, Cancer Invest. 24 (2006) 235–241.

[206] S.T. Crooke, W.T. Bradner, Mitomycin C: a review, Cancer Treat. Rev. 3 (1976) 121–139. https://doi.org/10.1016/S0305-7372(76)80019-9.

[207] R.W. Malone, P.L. Felgner, I.M. Verma, Cationic liposome-mediated RNA transfection, Proc. Natl. Acad. Sci. U. S. A. 86 (1989) 6077–6081. https://doi.org/10.1073/PNAS.86.16.6077.

[208] L. Falzone, S. Salomone, M. Libra, Evolution of cancer pharmacological treatments at the turn of the third millennium, Front. Pharmacol. 9 (2018) 1300. https://doi.org/10.3389/FPHAR.2018.01300/BIBTEX.

[209] S.A. González-Chávez, S. Arévalo-Gallegos, Q. Rascón-Cruz, Lactoferrin: structure, function and applications, Int. J. Antimicrob. Agents. 33 (2009) 301.e1-301.e8. https://doi.org/10.1016/J.IJANTIMICAG.2008.07.020.

[210] E.N. Baker, H.M. Baker, Molecular structure, binding properties and dynamics of lactoferrin, Cell. Mol. Life Sci. 62 (2005) 2531–2539. https://doi.org/10.1007/S00018-005-5368-9.

[211] A. Tomitaka, H. Arami, S. Gandhi, K.M. Krishnan, Lactoferrin conjugated iron oxide nanoparticles for targeting brain glioma cells in magnetic particle imaging, Nanoscale. 7 (2015) 16890–16898. https://doi.org/10.1039/C5NR02831K.

[212] N. Bruni, M.T. Capucchio, E. Biasibetti, E. Pessione, S. Cirrincione, L. Giraudo, A.

Corona, F. Dosio, Antimicrobial Activity of Lactoferrin-Related Peptides and Applications in Human and Veterinary Medicine, Mol. 2016, Vol. 21, Page 752. 21 (2016) 752. https://doi.org/10.3390/MOLECULES21060752.

[213] L. Sanchez, M. Calvo, J.H. Brock, Biological role of lactoferrin, Arch. Dis. Child. 67 (1992) 657–661. https://doi.org/10.1136/ADC.67.5.657.

[214] M. Iafisco, M. Di Foggia, S. Bonora, M. Prat, N. Roveri, Adsorption and spectroscopic characterization of lactoferrin on hydroxyapatite nanocrystals, Dalt. Trans. 40 (2011) 820–827. https://doi.org/10.1039/C0DT00714E.

[215] J.R. Kanwar, K.P. Palmano, X. Sun, R.K. Kanwar, R. Gupta, N. Haggarty, A. Rowan, S. Ram, G.W. Krissansen, "Iron-saturated" lactoferrin is a potent natural adjuvant for augmenting cancer chemotherapy, Immunol. Cell Biol. 86 (2008) 277–288. https://doi.org/10.1038/SJ.ICB.7100163.

[216] H. Tsuda, Y. Ohshima, H. Nomoto, K. ichi Fujita, E. Matsuda, M. Iigo, N. Takasuka, M.A. Moore, Cancer prevention by natural compounds., Drug Metab. Pharmacokinet. 19 (2004) 245–263. https://doi.org/10.2133/DMPK.19.245.

[217] J. Onishi, M.K. Roy, L.R. Juneja, Y. Watanabe, Y. Tamai, A lactoferrin-derived peptide with cationic residues concentrated in a region of its helical structure induces necrotic cell death in a leukemic cell line (HL-60), J. Pept. Sci. 14 (2008) 1032–1038. https://doi.org/10.1002/PSC.1039.

[218] M.K. Roy, Y. Kuwabara, K. Hara, Y. Watanabe, Y. Tamai, Peptides from the N-terminal end of bovine lactoferrin induce apoptosis in human leukemic (HL-60) cells, J. Dairy Sci. 85 (2002) 2065–2074. https://doi.org/10.3168/JDS.S0022-0302(02)74284-7.

[219] J.S. Mader, J. Salsman, D.M. Conrad, D.W. Hoskin, Bovine lactoferricin selectively induces apoptosis in human leukemia and carcinoma cell lines, Mol. Cancer Ther. 4 (2005) 612–624. https://doi.org/10.1158/1535-7163.MCT-04-0077.

[220] Y. Zhang, C.F. Lima, L.R. Rodrigues, Anticancer effects of lactoferrin: underlying mechanisms and future trends in cancer therapy, Nutr. Rev. 72 (2014) 763–773. https://doi.org/10.1111/NURE.12155.

[221] Q. Rascón-Cruz, E.A. Espinoza-Sánchez, T.S. Siqueiros-Cendón, S.I. Nakamura-Bencomo, S. Arévalo-Gallegos, B.F. Iglesias-Figueroa, Lactoferrin: A Glycoprotein Involved in Immunomodulation, Anticancer, and Antimicrobial Processes, Mol. 2021, Vol. 26, Page 205. 26 (2021) 205. https://doi.org/10.3390/MOLECULES26010205.

[222] S. Teraguchi, H. Wakabayashi, H. Kuwata, K. Yamauchi, Y. Tamura, Protection

against infections by oral lactoferrin: evaluation in animal models, Biometals. 17 (2004) 231–234. https://doi.org/10.1023/B:BIOM.0000027697.83706.32.

[223] T. Tanaka, K. Kawabata, H. Kohno, S. Honjo, M. Murakami, T. Ota, H. Tsuda, Chemopreventive effect of bovine lactoferrin on 4-nitroquinoline 1-oxide-induced tongue carcinogenesis in male F344 rats, Jpn. J. Cancer Res. 91 (2000) 25–33. https://doi.org/10.1111/J.1349-7006.2000.TB00856.X.

[224] Y. Ushida, K. Sekine, T. Kuhara, N. Takasuka, M. Iigo, M. Maeda, H. Tsuda, Possible chemopreventive effects of bovine lactoferrin on esophagus and lung carcinogenesis in the rat, Jpn. J. Cancer Res. 90 (1999) 262–267. https://doi.org/10.1111/J.1349-7006.1999.TB00742.X.

[225] J.A. Gibbons, J.R. Kanwar, R.K. Kanwar, Iron-free and iron-saturated bovine lactoferrin inhibit survivin expression and differentially modulate apoptosis in breast cancer, BMC Cancer. 15 (2015). https://doi.org/10.1186/S12885-015-1441-4.

[226] C.S. Pereira, J.P. Guedes, M. Gonçalves, L. Loureiro, L. Castro, H. Gerós, L.R. Rodrigues, M. Côrte-Real, Lactoferrin selectively triggers apoptosis in highly metastatic breast cancer cells through inhibition of plasmalemmal V-H+-ATPase, Oncotarget. 7 (2016) 62144–62158. https://doi.org/10.18632/ONCOTARGET.11394.

[227] S. Farnaud, R.W. Evans, Lactoferrin--a multifunctional protein with antimicrobial properties, Mol. Immunol. 40 (2003) 395–405. https://doi.org/10.1016/S0161-5890(03)00152-4.

[228] M. Åbrink, E. Larsson, A. Gobl, L. Hellman, Expression of lactoferrin in the kidney: implications for innate immunity and iron metabolism, Kidney Int. 57 (2000) 2004–2010. https://doi.org/10.1046/J.1523-1755.2000.00050.X.

[229] M. Gahr, C.P. Speer, B. Damerau, G. Sawatzki, Influence of lactoferrin on the function of human polymorphonuclear leukocytes and monocytes, J. Leukoc. Biol. 49 (1991) 427–433. https://doi.org/10.1002/JLB.49.5.427.

[230] S.G. Dashper, Y. Pan, P.D. Veith, Y.Y. Chen, E.C.Y. Toh, S.W. Liu, K.J. Cross, E.C. Reynolds, Lactoferrin Inhibits Porphyromonas gingivalis Proteinases and Has Sustained Biofilm Inhibitory Activity, Antimicrob. Agents Chemother. 56 (2012) 1548. https://doi.org/10.1128/AAC.05100-11.

[231] J.R. Kanwar, K. Roy, Y. Patel, S.F. Zhou, M.R. Singh, D. Singh, M. Nasir, R. Sehgal, A. Sehgal, R.S. Singh, S. Garg, R.K. Kanwar, Multifunctional Iron Bound Lactoferrin and Nanomedicinal Approaches to Enhance Its Bioactive Functions, Mol. 2015, Vol. 20, Pages 9703-9731. 20 (2015) 9703–9731.

https://doi.org/10.3390/MOLECULES20069703.

[232] A. Cutone, L. Rosa, G. Ianiro, M.S. Lepanto, M.C.B. Di Patti, P. Valenti, G. Musci, Lactoferrin's anti-cancer properties: Safety, selectivity, and wide range of action, Biomolecules. 10 (2020). https://doi.org/10.3390/BIOM10030456.

[233] E.M. El-Fakharany, Nanoformulation of lactoferrin potentiates its activity and enhances novel biotechnological applications, Int. J. Biol. Macromol. 165 (2020) 970–984. https://doi.org/10.1016/J.IJBIOMAC.2020.09.235.

[234] B.F. Iglesias-Figueroa, T.S. Siqueiros-Cendón, D.A. Gutierrez, R.J. Aguilera, E.A. Espinoza-Sánchez, S. Arévalo-Gallegos, A. Varela-Ramirez, Q. Rascón-Cruz, Recombinant human lactoferrin induces apoptosis, disruption of F-actin structure and cell cycle arrest with selective cytotoxicity on human triple negative breast cancer cells, Apoptosis. 24 (2019). https://doi.org/10.1007/S10495-019-01539-7.

[235] S. Nakamura-Bencomo, D.A. Gutierrez, E. Robles-Escajeda, B. Iglesias-Figueroa, T.S. Siqueiros-Cendón, E.A. Espinoza-Sánchez, S. Arévalo-Gallegos, R.J. Aguilera, Q. Rascón-Cruz, A. Varela-Ramirez, Recombinant human lactoferrin carrying humanized glycosylation exhibits antileukemia selective cytotoxicity, microfilament disruption, cell cycle arrest, and apoptosis activities, Invest. New Drugs. 39 (2021) 400–415. https://doi.org/10.1007/S10637-020-01020-2.

[236] K. Roy, Y.S. Patel, R.K. Kanwar, R. Rajkhowa, X. Wang, J.R. Kanwar, Biodegradable Eri silk nanoparticles as a delivery vehicle for bovine lactoferrin against MDA-MB-231 and MCF-7 breast cancer cells, Int. J. Nanomedicine. 11 (2015) 25–44. https://doi.org/10.2147/IJN.S91810.

[237] C.-H. Lu, Y.-S. Lin, Y.-C. Chen, C.-S. Yu, S.-Y. Chang, J.-K. Hwang, The fragment transformation method to detect the protein structural motifs, Wiley Online Libr. 63 (2006) 636–643. https://doi.org/10.1002/prot.20904.

[238] A.G. Murzin, S.E. Brenner, T. Hubbard, C. Chothia, SCOP: A structural classification of proteins database for the investigation of sequences and structures, J. Mol. Biol. 247 (1995) 536–540. https://doi.org/10.1016/S0022-2836(05)80134-2.

[239] S. Henikoff, J.G. Henikoff, Amino acid substitution matrices from protein blocks, Proc. Natl. Acad. Sci. U. S. A. 89 (1992) 10915–10919. https://doi.org/10.1073/PNAS.89.22.10915.

[240] Y.F. Lin, C.W. Cheng, C.S. Shih, J.K. Hwang, C.S. Yu, C.H. Lu, MIB: Metal Ion-Binding Site Prediction and Docking Server, J. Chem. Inf. Model. 56 (2016) 2287–2291. https://doi.org/10.1021/ACS.JCIM.6B00407.

[241] S. Dutz, R. Hergt, Magnetic nanoparticle heating and heat transfer on a microscale: Basic principles, realities and physical limitations of hyperthermia for tumour therapy, Int. J. Hyperth. 29 (2013) 790–800.

[242] G. Bruggmoser, S. Bauchowitz, R. Canters, H. Crezee, M. Ehmann, J. Gellermann, U. Lamprecht, N. Lomax, M.B. Messmer, O. Ott, Guideline for the clinical application, documentation and analysis of clinical studies for regional deep hyperthermia, Strahlenther. Onkol. 188 (2012) 198–211.

[243] A. Pradeep, P. Priyadharsini, G. Chandrasekaran, Sol- gel route of synthesis of nanoparticles of MgFe2O 4 and XRD, FTIR and VSM study, J. Magn. Magn. Mater. 320 (2008) 2774–2779. https://doi.org/10.1016/J.JMMM.2008.06.012.

[244] S. Razavi, R. Seyedebrahimi, M. Jahromi, Biodelivery of nerve growth factor and gold nanoparticles encapsulated in chitosan nanoparticles for schwann-like cells differentiation of human adipose-derived stem cells, Biochem. Biophys. Res. Commun. 513 (2019) 681–687. https://doi.org/10.1016/J.BBRC.2019.03.189.

[245] M.J. Oviedo, K. Quester, G.A. Hirata, R. Vazquez-Duhalt, Determination of conjugated protein on nanoparticles by an adaptation of the Coomassie blue dye method, MethodsX. 6 (2019) 2134–2140. https://doi.org/10.1016/J.MEX.2019.09.015.

[246] V. kumar Nelson, N.K. Sahoo, M. Sahu, H. hara Sudhan, C.P. Pullaiah, K.S. Muralikrishna, In vitro anticancer activity of Eclipta alba whole plant extract on colon cancer cell HCT-116, BMC Complement. Med. Ther. 20 (2020). https://doi.org/10.1186/S12906-020-03118-9.

[247] S.R. Bolla, A. Mohammed Al-Subaie, R. Yousuf Al-Jindan, J. Papayya Balakrishna, P. Kanchi Ravi, V.P. Veeraraghavan, A. Arumugam Pillai, S.S.R. Gollapalli, J. Palpath Joseph, K.M. Surapaneni, In vitro wound healing potency of methanolic leaf extract of Aristolochia saccata is possibly mediated by its stimulatory effect on collagen-1 expression, Heliyon. 5 (2019). https://doi.org/10.1016/J.HELIYON.2019.E01648.

[248] S.F. Aval, A. Akbarzadeh, M.R. Yamchi, F. Zarghami, K. Nejati-Koshki, N. Zarghami, Gene silencing effect of SiRNA-magnetic modified with biodegradable copolymer nanoparticles on hTERT gene expression in lung cancer cell line, Artif. Cells, Nanomedicine Biotechnol. 44 (2016) 188–193. https://doi.org/10.3109/21691401.2014.934456.

[249] E. Andris, R. Navrátil, J. Jašík, G. Sabenya, M. Costas, M. Srnec, J. Roithová, Detection of indistinct Fe− N stretching bands in iron (V) nitrides by photodissociation spectroscopy, Chem. Eur. J. 24 (2018) 5078–5081.

[250] P. Kaur, S. Sharma, S.D. Choudhury, D. Singh, S. Sharma, K. Gadhave, N. Garg, D. Choudhury, Insulin-copper quantum clusters preparation and receptor targeted bioimaging, Colloids Surfaces B Biointerfaces. 188 (2020) 110785. https://doi.org/10.1016/J.COLSURFB.2020.110785.

[251] P. Kaur, A.K. Sharma, D. Nag, A. Das, S. Datta, A. Ganguli, V. Goel, S. Rajput, G. Chakrabarti, B. Basu, D. Choudhury, Novel nano-insulin formulation modulates cytokine secretion and remodeling to accelerate diabetic wound healing, Nanomedicine Nanotechnology, Biol. Med. 15 (2019) 47–57. https://doi.org/10.1016/J.NANO.2018.08.013.

[252] P. Kaur, K. Gadhave, N. Garg, D. Deb, D. Choudhury, Probing the interaction of glutathione with different shape of silver-nanoparticles by optical spectroscopy, Mater. Today Commun. 26 (2021) 102137. https://doi.org/10.1016/J.MTCOMM.2021.102137.

[253] D. Sharda, K. Attri, P. Kaur, D. Choudhury, Protection of lead-induced cytotoxicity using paramagnetic nickel-insulin quantum clusters, RSC Adv. 11 (2021) 24656–24668. https://doi.org/10.1039/D1RA03597E.

[254] M.A.G. Soler, F. Qu, Raman spectroscopy of iron oxide nanoparticles, Raman Spectrosc. Nanomater. Charact. 9783642206207 (2012) 379–416. https://doi.org/10.1007/978-3-642-20620-7_14.

[255] V.K. Yadav, D. Ali, S.H. Khan, G. Gnanamoorthy, N. Choudhary, K.K. Yadav, V.N. Thai, S.A. Hussain, S. Manhrdas, Synthesis and characterization of amorphous iron oxide nanoparticles by the sonochemical method and their application for the remediation of heavy metals from wastewater, Nanomaterials. 10 (2020) 1–17. https://doi.org/10.3390/NANO10081551.

[256] P. Pomastowski, M. Sprynskyy, P. Žuvela, K. Rafińska, M. Milanowski, J.J. Liu, M. Yi, B. Buszewski, Silver-Lactoferrin Nanocomplexes as a Potent Antimicrobial Agent, J. Am. Chem. Soc. 138 (2016) 7899–7909. https://doi.org/10.1021/JACS.6B02699/ASSET/IMAGES/LARGE/JA-2016-026998_0008.JPEG.

[257] P. Kaur, A.K. Sharma, D. Nag, A. Das, S. Datta, A. Ganguli, V. Goel, S. Rajput, G. Chakrabarti, B. Basu, D. Choudhury, Novel nano-insulin formulation modulates cytokine secretion and remodeling to accelerate diabetic wound healing, Nanomedicine Nanotechnology, Biol. Med. 15 (2019) 47–57. https://doi.org/10.1016/J.NANO.2018.08.013.

[258] Y. Liu, L. Ojamäe, C–C stretching Raman spectra and stabilities of hydrocarbon molecules in natural gas hydrates: a quantum chemical study, J. Phys. Chem. A. 118 (2014) 11641–11651.

[259] S. Zavatski, N. Khinevich, K. Girel, S. Redko, N. Kovalchuk, I. Komissarov, V. Lukashevich, I. Semak, K. Mamatkulov, M. Vorobyeva, G. Arzumanyan, H. Bandarenka, Surface enhanced raman spectroscopy of lactoferrin adsorbed on silvered porous silicon covered with graphene, Biosensors. 9 (2019). https://doi.org/10.3390/BIOS9010034.

[260] E.C. Smyth, M. Nilsson, H.I. Grabsch, N.C. van Grieken, F. Lordick, Gastric cancer, Lancet. 396 (2020) 635–648. https://doi.org/10.1016/S0140-6736(20)31288-5.

[261] H. Lee, W. Kim, Y. Kwak, J. Koh, J, Bae, K. Kim, M. Chang, H. Han, J. Kim, H. Kim, H. Chang, Y. Choi, Ji. Park, M. Gu, M. Lhee, J. Kim, H. Kim, M. Cho, Molecular testing for gastrointestinal cancer, J Pathol. Transl. Med. 51 (2017) 103-121. https://doi.org/10.4132/jptm.2017.01.24

[262] I. Altun, A. Sonkaya, The most common side effects experienced by patients were receiving first cycle of chemotherapy, Iran J Public Health.,47 (2018) 1218–1219. PMC6123577

[263] D.F. Quail, J.A. Joyce, Microenvironmental regulation of tumor progression and metastasis, Nat. Med. 19 (2013) 1423. https://doi.org/10.1038/NM.3394.

[264] D. Hanahan, L.M. Coussens, Accessories to the Crime: Functions of Cells Recruited to the Tumor Microenvironment, Cancer Cell. 21 (2012) 309–322. https://doi.org/10.1016/J.CCR.2012.02.022.

[265] R.O. Hynes, The extracellular matrix: not just pretty fibrils, Science. 326 (2009) 1216–1219. https://doi.org/10.1126/SCIENCE.1176009.

[266] F. Balkwill, Cancer and the chemokine network, Nat. Rev. Cancer. 4 (2004) 540–550. https://doi.org/10.1038/NRC1388.

[267] N. Ferrara, R.S. Kerbel, Angiogenesis as a therapeutic target, Nature. 438 (2005) 967–974. https://doi.org/10.1038/NATURE04483.

[268] G.L. Semenza, HIF-1: upstream and downstream of cancer metabolism, Curr. Opin. Genet. Dev. 20 (2010) 51–56. https://doi.org/10.1016/J.GDE.2009.10.009.

[269] J.A. Joyce, J.W. Pollard, Microenvironmental regulation of metastasis, Nat. Rev. Cancer. 9 (2009) 239–252. https://doi.org/10.1038/NRC2618.

[270] A.D. Kostic, E. Chun, L. Robertson, J.N. Glickman, C.A. Gallini, M. Michaud, T.E. Clancy, D.C. Chung, P. Lochhead, G.L. Hold, E.M. El-Omar, D. Brenner, C.S. Fuchs,

M. Meyerson, W.S. Garrett, Fusobacterium nucleatum potentiates intestinal tumorigenesis and modulates the tumor-immune microenvironment, Cell Host Microbe. 14 (2013) 207–215. https://doi.org/10.1016/J.CHOM.2013.07.007.

[271] H.B. El-Serag, Epidemiology of Viral Hepatitis and Hepatocellular Carcinoma, Gastroenterology. 142 (2012) 1264. https://doi.org/10.1053/J.GASTRO.2011.12.061.

[272] D.S. Michaud, K. Joshipura, E. Giovannucci, C.S. Fuchs, A prospective study of periodontal disease and pancreatic cancer in US male health professionals, J. Natl. Cancer Inst. 99 (2007) 171–175. https://doi.org/10.1093/JNCI/DJK021.

[273] C. Urbaniak, G.B. Gloor, M. Brackstone, L. Scott, M. Tangney, G. Reida, The Microbiota of Breast Tissue and Its Association with Breast Cancer, Appl. Environ. Microbiol. 82 (2016) 5039–5048. https://doi.org/10.1128/AEM.01235-16.

[274] D.B. Polk, R.M. Peek, Helicobacter pylori: gastric cancer and beyond, Nat. Rev. Cancer 2010 106. 10 (2010) 403–414. https://doi.org/10.1038/nrc2857.

[275] T. Wang, G. Cai, Y. Qiu, N. Fei, M. Zhang, X. Pang, W. Jia, S. Cai, L. Zhao, Structural segregation of gut microbiota between colorectal cancer patients and healthy volunteers, ISME J. 6 (2012) 320–329. https://doi.org/10.1038/ISMEJ.2011.109.

[276] L.A. David, C.F. Maurice, R.N. Carmody, D.B. Gootenberg, J.E. Button, B.E. Wolfe, A. V. Ling, A.S. Devlin, Y. Varma, M.A. Fischbach, S.B. Biddinger, R.J. Dutton, P.J. Turnbaugh, Diet rapidly and reproducibly alters the human gut microbiome, Nat. 2013 5057484. 505 (2013) 559–563. https://doi.org/10.1038/nature12820.

[277] H.W. Cheng, H.Y. Tsao, C.S. Chiang, S.Y. Chen, Advances in Magnetic Nanoparticle-Mediated Cancer Immune-Theranostics, Adv. Healthc. Mater. 10 (2021). https://doi.org/10.1002/ADHM.202001451.

[278] M. Abyadeh, • Mahdi Aghajani, A. Gohari Mahmoudabad, • Amir Amani, Preparation and Optimization of Chitosan/pDNA Nanoparticles Using Electrospray, Proc. Natl. Acad. Sci. India Sect. B Biol. Sci. 89 (n.d.). https://doi.org/10.1007/s40011-018-1009-6.

[279] M. Abyadeh, A.A. Karimi Zarchi, M.A. Faramarzi, A. Amani, Evaluation of Factors Affecting Size and Size Distribution of Chitosan-Electrosprayed Nanoparticles, Avicenna J. Med. Biotechnol. 9 (2017) 126. PMC5501139

[280] K.C. Nam, Y.S. Han, J.M. Lee, S.C. Kim, G. Cho, B.J. Park, Photo-Functionalized Magnetic Nanoparticles as a Nanocarrier of Photodynamic Anticancer Agent for Biomedical Theragnostics, Cancers 2020, Vol. 12, Page 571. 12 (2020) 571. https://doi.org/10.3390/CANCERS12030571.

[281] G. Gui, Z. Fan, Y. Ning, C. Yuan, B. Zhang, Q. Xu, Optimization, Characterization and in vivo Evaluation of Paclitaxel-Loaded Folate-Conjugated Superparamagnetic Iron Oxide Nanoparticles, Int. J. Nanomedicine. 16 (2021) 2283. https://doi.org/10.2147/IJN.S287434.

[282] F. Soetaert, P. Korangath, D. Serantes, S. Fiering, R. Ivkov, Cancer therapy with iron oxide nanoparticles: Agents of thermal and immune therapies, Adv. Drug Deliv. Rev. 163–164 (2020) 65–83. https://doi.org/10.1016/J.ADDR.2020.06.025.

[283] A.J. Giustini, A.A. Petryk, S.M. Cassim, J.A. Tate, I. Baker, P.J. Hoopes, Magnetic nanoparticle hyperthermia in cancer treatment, Nano Life. 1 (2010) 17–32. https://doi.org/10.1142/S1793984410000067.

[284] X. Liu, Y. Zhang, Y. Wang, W. Zhu, G. Li, X. Ma, Y. Zhang, S. Chen, S. Tiwari, K. Shi, S. Zhang, H.M. Fan, Y.X. Zhao, X.J. Liang, Comprehensive understanding of magnetic hyperthermia for improving antitumor therapeutic efficacy, Theranostics. 10 (2020) 3793. https://doi.org/10.7150/THNO.40805.

[285] K. Attri, D. Sharda, B.N. Chudasama, R. Mahajan, D. Choudhury, A Review on Terpenes for Treatment of Gastric Cancer: Current Status and Nanotechnology-enabled Future, RSC Sustain. (2023).

[286] A. Kukreja, B. Kang, H.O. Kim, E. Jang, H.Y. Son, Y.M. Huh, S. Haam, Preparation of gold core-mesoporous iron-oxide shell nanoparticles and their application as dual MR/CT contrast agent in human gastric cancer cells, J. Ind. Eng. Chem. 48 (2017) 56–65. https://doi.org/10.1016/J.JIEC.2016.12.020.

[287] M. Ghanbari, A. Asadi, S. Rostamzadeh, Issue 2 • 1000368 Oxide Nanoparticles on AGS Cancer Cell Line, J Nanomed Nanotechnol. 7 (2016) 368. https://doi.org/10.4172/2157-7439.1000368.

[288] S.S. Spudich, Immune activation in the central nervous system throughout the course of HIV infection, Curr. Opin. HIV AIDS. 11 (2016) 226. https://doi.org/10.1097/COH.0000000000000243.

[289] S. Akira, S. Uematsu, O. Takeuchi, Pathogen Recognition and Innate Immunity, Cell. 124 (2006) 783–801. https://doi.org/10.1016/J.CELL.2006.02.015.

[290] O. Takeuchi, S. Akira, Pattern recognition receptors and inflammation, Cell. 140 (2010) 805–820. https://doi.org/10.1016/J.CELL.2010.01.022.

[291] S.R. Paludan, A.G. Bowie, Immune sensing of DNA, Immunity. 38 (2013) 870–880. https://doi.org/10.1016/J.IMMUNI.2013.05.004.

[292] A. Iwasaki, R. Medzhitov, Toll-like receptor control of the adaptive immune

responses, Nat. Immunol. 5 (2004) 987–995. https://doi.org/10.1038/NI1112.

[293] S. Basith, B. Manavalan, T.H. Yoo, S.G. Kim, S. Choi, Roles of toll-like receptors in Cancer: A double-edged sword for defense and offense, Arch. Pharmacal Res. 2012 358. 35 (2012) 1297–1316. https://doi.org/10.1007/S12272-012-0802-7.

[294] J. Cui, Y. Chen, H.Y. Wang, R.F. Wang, Mechanisms and pathways of innate immune activation and regulation in health and cancer, Hum. Vaccin. Immunother. 10 (2014) 3270–3285. https://doi.org/10.4161/21645515.2014.979640.

[295] E.K.U. Larsen, T. Nielsen, T. Wittenborn, L.M. Rydtoft, A.R. Lokanathan, L. Hansen, L. Ostergaard, P. Kingshott, K.A. Howard, F. Besenbacher, N.C. Nielsen, J. Kjems, Accumulation of magnetic iron oxide nanoparticles coated with variably sized polyethylene glycol in murine tumors, Nanoscale. 4 (2012) 2352–2361. https://doi.org/10.1039/C2NR11554A.

[296] A. Hamdy, S.H. Ismail, A.A. Ebnalwaled, G.G. Mohamed, Characterization of Superparamagnetic/Monodisperse PEG-Coated Magnetite Nanoparticles Sonochemically Prepared from the Hematite Ore for Cd(II) Removal from Aqueous Solutions, J. Inorg. Organomet. Polym. Mater. 31 (2021) 397–414. https://doi.org/10.1007/S10904-020-01741-0/TABLES/7.

[297] Y. Gourbeyre, E. Guilminot, F. Dalard, Study of the corrosion layer on iron obtained in solutions of water-polyethylene glycol (PEG 400)-sodium phosphate, J. Mater. Sci. 38 (2003) 1307–1313. https://doi.org/10.1023/A:1022803014898.

[298] K. Attri, B. Chudasama, R.L. Mahajan, D. Choudhury, Therapeutic potential of lactoferrin-coated iron oxide nanospheres for targeted hyperthermia in gastric cancer, Sci. Reports . 13 (2023) 17875. https://doi.org/10.1038/s41598-023-43725-3.

[299] J. Zhou, J. Li, X. Ding, al -, F.J. Hameed, I.M. Ibrahim, O. Gh Abdullah, M. Besir Arvas, S. Yazar, Y. Sahin -, J. Anita Lett, S. Sagadevan, S.F. Alshahateet, B. Murugan, A. Hawa Jasni, I. Fatimah, M.A. Motalib Hossain, F. Mohammad, W. Chun Oh, Synthesis and characterization of polypyrrole-coated iron oxide nanoparticles, Mater. Res. Express. 8 (2021) 025007. https://doi.org/10.1088/2053-1591/ABE253.

[300] S. Sarkar, G. Horn, K. Moulton, A. Oza, S. Byler, S. Kokolus, M. Longacre, Cancer development, progression, and therapy: an epigenetic overview, Int. J. Mol. Sci. 14 (2013) 21087–21113. https://doi.org/10.3390/ijms141021087

[301] J.G. Kusters, A.H.M. Van Vliet, E.J. Kuipers, Pathogenesis of Helicobacter pylori infection, Clin. Microbiol. Rev. 19 (2006) 449–490. https://doi.org/10.1128/CMR.00054-05

[302] Y. Luo, X. Sun, L. Huang, J. Yan, B.-Y. Yu, J. Tian, Artemisinin-based smart nanomedicines with self-supply of ferrous ion to enhance oxidative stress for specific and efficient cancer treatment, ACS Appl. Mater. Interfaces. 11 (2019) 29490–29497. https://doi.org/10.1021/acsami.9b07390

[303] E.-A. Moacă, I.Z. Pavel, C. Danciu, Z. Crăiniceanu, D. Minda, F. Ardelean, D.S. Antal, R. Ghiulai, A. Cioca, M. Derban, Romanian wormwood (Artemisia absinthium L.): Physicochemical and nutraceutical screening, Molecules. 24 (2019) 3087. https://doi.org/10.3390/molecules24173087.

[304] E.-A. Moacă, C.G. Watz, C. Păcurariu, L.B. Tudoran, R. Ianoș, V. Socoliuc, G.-A. Drăghici, A. Iftode, S. Liga, D. Dragoș, Biosynthesis of iron oxide nanoparticles: Physico-chemical characterization and their In vitro cytotoxicity on healthy and tumorigenic cell lines, Nanomaterials. 12 (2022) 2012. https://doi.org/10.3390/nano12122012.

[305] J. Chen, Z. Guo, H.-B. Wang, J.-J. Zhou, W.-J. Zhang, Q.-W. Chen, Multifunctional mesoporous nanoparticles as pH-responsive Fe2+ reservoirs and artemisinin vehicles for synergistic inhibition of tumor growth, Biomaterials. 35 (2014) 6498–6507. https://doi.org/10.1016/j.biomaterials.2014.04.028

[306] S. Alven, B.A. Aderibigbe, Nanoparticles Formulations of Artemisinin and Derivatives as Potential Therapeutics for the Treatment of Cancer, Leishmaniasis and Malaria, Pharmaceutics. 12 (2020) 1–34. https://doi.org/10.3390/PHARMACEUTICS12080748.

[307] C. He, D.J. Klionsky, Regulation mechanisms and signaling pathways of autophagy, Annu. Rev. Genet. 43 (2009) 67–93. https://doi.org/10.1146/annurev-genet-102808-114910

[308] H. Nakatogawa, K. Suzuki, Y. Kamada, Y. Ohsumi, Dynamics and diversity in autophagy mechanisms: lessons from yeast, Nat. Rev. Mol. Cell Biol. 2009 107. 10 (2009) 458–467. https://doi.org/10.1038/nrm2708.

[309] S.A. Tooze, T. Yoshimori, The origin of the autophagosomal membrane, Nat. Cell Biol. 2010 129. 12 (2010) 831–835. https://doi.org/10.1038/ncb0910-831.

[310] W. Hu, S. Chen, J. Zhang, X. Lou, H. Zhou, Dihydroartemisinin induces autophagy by suppressing NF-κB activation, Cancer Lett. 343 (2014) 239-48. https://doi.org/10.1016/j.canlet.2013.09.035

[311] H.C. Lai, N.P. Singh, T. Sasaki, Development of artemisinin compounds for cancer treatment, Invest. New Drugs. 31 (2013) 230–246. https://doi.org/10.1007/s10637-

012-9873-z

[312] M.P. Crespo-Ortiz, M.Q. Wei, Antitumor activity of artemisinin and its derivatives: from a well-known antimalarial agent to a potential anticancer drug, J Biomed Biotechnol. 2012 (2012) 247597. https://doi.org/10.1155/2012/247597

[313] Y.-F. Dai, W.-W. Zhou, J. Meng, X.-L. Du, Y.-P. Sui, L. Dai, P.-Q. Wang, H.-R. Huo, F. Sui, MEDICINAL CHEMISTRY RESEARCH The pharmacological activities and mechanisms of artemisinin and its derivatives: a systematic review, Med. Chem. Res. 26 (2017) 867–880. https://doi.org/10.1007/s00044-016-1778-5.

[314] L. Lin, X. Mao, Y. Sun, H. Cui, Antibacterial mechanism of artemisinin / beta-cyclodextrins against methicillin-resistant Staphylococcus aureus (MRSA), (2018). https://doi.org/10.1016/j.micpath.2018.03.014.

[315] A. Kumar, P.K. Jena, S. Behera, R.F. Lockey, S. Mohapatra, S. Mohapatra, Multifunctional magnetic nanoparticles for targeted delivery, Nanomed., 6 (2010) 64–69. https://doi.org/10.1016/j.nano.2009.04.002

[316] M.G.B. Drew, J. Metcalfe, F.M.D. Ismail, A DFT study of free radicals formed from artemisinin and related compounds, J. Mol. Struct. Theochem., 711 (2004) 95–105. https://doi.org/10.1016/j.theochem.2004.08.028

[317] S. Natesan, C. Ponnusamy, A. Sugumaran, S. Chelladurai, S.S. Palaniappan, R. Palanichamy, Artemisinin loaded chitosan magnetic nanoparticles for the efficient targeting to the breast cancer, Int. J. Biol. Macromol. 104 (2017) 1853–1859. https://doi.org/10.1016/j.ijbiomac.2017.03.137

[318] X. Tang, F. Cao, W. Ma, Y. Tang, B. Aljahdali, M. Alasir, E. Salih, S. Dibart, Cancer cells resist hyperthermia due to its obstructed activation of caspase 3, Reports Pract. Oncol. Radiother. 25 (2020) 323–326. https://doi.org/10.1016/j.rpor.2020.02.008.

[319] F.M. Abdulsada, N.N. Hussein, G.M. Sulaiman, A. Al Ali, M. Alhujaily, Evaluation of the Antibacterial Properties of Iron Oxide, Polyethylene Glycol, and Gentamicin Conjugated Nanoparticles against Some Multidrug-Resistant Bacteria, J. Funct. Biomater. 13 (2022). https://doi.org/10.3390/JFB13030138/S1.

[320] Y. Luo, X. Sun, L. Huang, J. Yan, B.Y. Yu, J. Tian, Artemisinin-Based Smart Nanomedicines with Self-Supply of Ferrous Ion to Enhance Oxidative Stress for Specific and Efficient Cancer Treatment, ACS Appl. Mater. Interfaces. 11 (2019) 29490–29497. https://doi.org/10.1021/ACSAMI.9B07390/ASSET/IMAGES/LARGE/AM9B07390_0004.JPEG.

[321] S. Guo, X. Yao, Q. Jiang, K. Wang, Y. Zhang, H. Peng, J. Tang, W. Yang, Dihydroartemisinin-loaded Magnetic Nanoparticles for Enhanced Chemodynamic Therapy, BioRxiv. (2019) 2019.12.20.885400. https://doi.org/10.1101/2019.12.20.885400.

[322] C. Xu, L. Ni, J. Wizi, C. Du, Z. Jiang, W. Sang, S. Li, X. Chen, H. Su, J. Xu, Drug release kinetics of artemisinin sustained-release particles with two sizes for algal inhibition in different media, J. Polym. Environ. 31 (2023) 3015–3028. https://doi.org/10.1007/S10924-023-02777-2.

[323] D. Sharda, D. Choudhury, Insulin-Infused Bimetallic Nano-subclusters as Multifunctional Agents for ROS Scavenging, Antibacterial Resilience, and Accelerated in vitro Cell Migration, Mater. Adv. (2024). https://doi.org/10.1039/D4MA00278D.

[324] (PDF) FTIR and UV-Visible spectrophotometeric analyses of artemisinin and its derivatives, (n.d.). https://www.researchgate.net/publication/302989232_FTIR_and_UV-Visible_spectrophotometeric_analyses_of_artemisinin_and_its_derivatives (accessed December 8, 2023).

[325] N. Yadav, D. Kannan, S. Patil, S. Singh, B. Lochab, Amplified Activity of Artesunate Mediated by Iron Oxide Nanoparticles Loaded on a Graphene Oxide Carrier for Cancer Therapeutics, ACS Appl. Bio Mater. 3 (2020) 6722–6736. https://doi.org/10.1021/ACSABM.0C00632/SUPPL_FILE/MT0C00632_SI_001.PDF.

[326] Y. Zhang, Y. Cao, X. Meng, P. Prawang, H. Wang, Extraction of artemisinin with hydroxypropyl-β-cyclodextrin aqueous solution for fabrication of drinkable extract, Green Chem. Eng. 2 (2021) 197–206. https://doi.org/10.1016/J.GCE.2020.09.007.

[327] E.S. Savitri, S. Shinta, E.B. Minarno, R. Annisa, Chemical Characterization of Silver Nanoparticle Compounds using Red Algae (Fucus vesiculosus) in Freeze Dry Methods, J. Exp. Life Sci. 13 (2023) 52–60. https://doi.org/10.21776/UB.JELS.2023.013.01.08.

[328] H. Yu, X. Zhao, Y. Zu, X. Zhang, B. Zu, X. Zhang, Preparation and Characterization of Micronized Artemisinin via a Rapid Expansion of Supercritical Solutions (RESS) Method, Int. J. Mol. Sci. 2012, Vol. 13, Pages 5060-5073. 13 (2012) 5060–5073. https://doi.org/10.3390/IJMS13045060.

[329] M.Y. Want, M. Islamuddin, G. Chouhan, A.K. Dasgupta, A.P. Chattopadhyay, F. Afrin, A new approach for the delivery of artemisinin: Formulation, characterization,

and ex-vivo antileishmanial studies, J. Colloid Interface Sci. 432 (2014) 258–269. https://doi.org/10.1016/J.JCIS.2014.06.035.

[330] M.M. Abutalib, A. Rajeh, Influence of Fe3O4 nanoparticles on the optical, magnetic and electrical properties of PMMA/PEO composites: Combined FT-IR/DFT for electrochemical applications, J. Organomet. Chem. 920 (2020) 121348. https://doi.org/10.1016/J.JORGANCHEM.2020.121348.

[331] M. Ismail, M.I. Khan, K. Akhtar, M.A. Khan, A.M. Asiri, S.B. Khan, Biosynthesis of silver nanoparticles: A colorimetric optical sensor for detection of hexavalent chromium and ammonia in aqueous solution, Phys. E Low-Dimensional Syst. Nanostructures. 103 (2018) 367–376. https://doi.org/10.1016/J.PHYSE.2018.06.015.

[332] M.A. Rather, B.A. Dar, W.A. Shah, A. Prabhakar, K. Bindu, J.A. Banday, M.A. Qurishi, Comprehensive GC–FID, GC–MS and FT-IR spectroscopic analysis of the volatile aroma constituents of Artemisia indica and Artemisia vestita essential oils, Arab. J. Chem. 10 (2017) S3798–S3803. https://doi.org/10.1016/J.ARABJC.2014.05.017.

[333] P. Huo, X. Han, W. Zhang, J. Zhang, P. Kumar, B. Liu, Electrospun Nanofibers of Polycaprolactone/Collagen as a Sustained-Release Drug Delivery System for Artemisinin, Pharm. 2021, Vol. 13, Page 1228. 13 (2021) 1228. https://doi.org/10.3390/PHARMACEUTICS13081228.

[334] D. Kannan, N. Yadav, S. Ahmad, P. Namdev, S. Bhattacharjee, B. Lochab, S. Singh, Pre-clinical study of iron oxide nanoparticles fortified artesunate for efficient targeting of malarial parasite, EBioMedicine. 45 (2019) 261–277. https://doi.org/10.1016/J.EBIOM.2019.06.026/ATTACHMENT/CB516F67-9B02-4964-9380-63CFC7D987B8/MMC1.PDF.

[335] J. Chen, Z. Guo, H.B. Wang, J.J. Zhou, W.J. Zhang, Q.W. Chen, Multifunctional mesoporous nanoparticles as pH-responsive Fe(2+) reservoirs and artemisinin vehicles for synergistic inhibition of tumor growth, Biomaterials. 35 (2014) 6498–6507. https://doi.org/10.1016/J.BIOMATERIALS.2014.04.028.

Appendices

Appendix-I: Facing Challenges in the Formulation of IONPs

The preparation of IONPs presented several challenges that can impact their quality, consistency, and functionality. Addressing some of these challenges s they are is crucial for their use in various applications, including biomedical, environmental, and industrial fields. The key challenges include:

1. ***Control of Particle Size and Shape*:** To attain a small size of the particle, careful attention is required during the nucleation step. To ensure this, we meticulously added the reducing agent to the iron salt solution mixture.
2. ***Aggregation and Stability***: Since iron oxide nanoparticles possess magnetic properties, maintaining their stability and preventing aggregation is crucial. Aggregation can negatively impact their effectiveness and suitability for various applications. In this study, we employed polyethylene glycol (PEG) to coat the iron oxide nanoparticles (IONPs) to prevent aggregation. Additionally, PEG was used to decrease the immunogenicity of the particles.
3. ***Magnetic properties:*** For these particles to be suitable for biomedical applications, they must exhibit superparamagnetism, meaning they should have no remnant magnetization after removing the external magnetic field. To verify this, we analyzed the synthesized IONPs using a Vibrating Sample Magnetometer (VSM). By examining the M-H loops, we measured the remanence magnetization (M_r) and coercivity (H_c) values, which should be close to zero for the material to exhibit superparamagnetism.

Appendix-II: Coating Iron Oxide Nanoparticles on *Helicobacter pylori*

The next goal was to coat iron oxide nanoparticles (IONPs) onto the surface of *Helicobacter pylori (H. pylori)* to enhance their potential for targeted application; therapeutic delivery. While conducting this experiment, Icame across many difficulties which are listed below;

1. ***Safety and Handling:*** *H. pylori* is a pathogenic bacterium associated with gastrointestinal diseases, requiring stringent biosafety precautions to protect

laboratory personnel.

2. ***Harvesting H. pylori conditions:*** *H. pylori* is considered to be fastidious microorganism as it requires a specific growth environment. For its cultivation, microaerophilic atmosphere is required with reduced O_2 and elevated CO_2 concentration i.e 5% O_2, 10% CO_2. Maintaining these conditions are technically demanding.
3. ***Contamination control:*** *H. pylori* cultures are prone to contamination with other microorganisms, which interferes with the growth of *H. pylori* and also end up losing the pure culture. To obtain a pure culture, it is essential to implement stringent aseptic conditions, which can be particularly challenging to maintain within a hypoxia chamber.
4. ***Slow Growth Rate:*** The bacterium has a slow doubling time, leading to longer incubation periods compared to many other bacteria. This can extend the time needed to obtain viable cultures.

Despite facing numerous challenges at each stage of my research, I remained determined to overcome these obstacles and achieve success. The journey was marked by difficulties, yet through unwavering effort and resilience, I was able to navigate these hurdles. Crucially, the support and guidance of my supervisors played an instrumental role in this process. Their expertise, encouragement, and mentorship were pivotal in helping me to flourish and ultimately complete my PhD work. Their contributions not only facilitated my progress but also significantly enriched my academic and professional development.

Conferences and Workshops attended:

1. International Conference on Emerging Trends in Science and Technology, Organised by Dept. of Applied Sciences, Punjab Engineering College, Chandigarh. (10-11 June, 2022). **(Poster Presentation)**
2. 14th Annual Meeting of the Korean Society of Medical Oncology and 2021 International Conference held in Seoul, Korea (2-3 September 2021). **(Online mode)**
3. 13th in series and 1st International Conference on Recent Advances in Chemistry- 2023, held at Dept. of Chemistry, Punjabi University, Patiala (**Poster Presentation**).
4. 16th Annual Meeting of the Korean Society of Medical Oncology & 2023 International Conference, 11th International FACO Conference, 7-8 September, 2023. **(Online mode)**
5. 3rd International Conference on Integrative Chemistry, Biology, and Translational Medicine, Jointly Organised by Pacific University Udaipur, Hansraj College (Delhi

University), and Heterochem Innotech Private Limited at Udaipur, Rajasthan. (8-10 March, 2024). **(Poster presentation) (Certificate of Appreciation)**

Awards:

1. Won Best Poster Award at CEEMS Doctoral Scholars Day at Thapar Institute of Engineering and Technology.

List of Publications:

Published:

1. **Attri. K,** Sharda. D, Chudasama. B, Mahajan. RL, and Choudhury. D. A Review on Terpenes for Treatment of Gastric Cancer: Current Status and Nanotechnology-enabled Future, *RSC Sustainability*, 2023.
2. **Attri. K,** Chudasama. B, Mahajan. RL, and Choudhury. D. Therapeutic Potential of Lactoferrin-Coated Iron Oxide Nanospheres for Targeted Hyperthermia in Gastric Cancer, *Scientific Reports*, 2023. **(IF: 3.8).**
3. **Attri. K,** Chudasama. B, Mahajan. RL, and Choudhury. D. Perturbation of hyperthermia resistance in gastric cancer by hyperstimulation of autophagy using artemisinin-protected iron-oxide nanoparticles, RSC Advances, 2024. **(IF: 3.9)**
4. **Attri. K**, Chudasama. B, Mahajan. RL, and Choudhury. D. Integrated Insulin-Iron Nanoparticles: A Multi-Modal Approach for Receptor-Specific Bioimaging, Reactive Oxygen Species Scavenging, and Wound Healing. *Discover Nano*, 2024. **(IF: 5.5)**.
5. Sharda. D, **Attri. K**, Kaur. P and Choudhury. D. Protection of lead-induced cytotoxicity using paramagnetic nickel–insulin quantum clusters, *RSC Advances*, 2021, 11, 24656-24668. **(IF: 3.9).**
6. Sharda. D, **Attri. K**, and Choudhury. D. Greener healing: Sustainable Nanotechnology for Advanced Wound Care. *Discover Nano*, 2023. **(IF: 5.5)**
7. Datta. S, Chakroborty. N.K, Sharda. D, **Attri. K** and Choudhury. D; COVID-19 Pandemic in India: Chronological comparison of the regional heterogeneity in the progression of the pandemic and gaps in mitigation strategies, *Journal of clinical trials*, 2021. **(IF: 2.76)**
8. Priya. R, Kaur. D, **Attri. K**, Kaur. S, Sharda. D, Choudhury. D, Pandey. OP, Structural, luminescent and in vitro studies of europium-doped soda lime phosphate glasses, *Luminescence*, 2023, 39. **(IF: 2.9).**
9. Mamta, **Attri. K**, Choudhury. D., Dutta. A. Effect of reducing agent on the chemical reduction method of GO-Ag nanocomposite and its antibacterial activity, *BioNanoScience*, 2024. **(IF: 3).**

Under preparation:

1. **Attri. K,** Tanwar. I, Sharda. D, Choudhury. D. Development of Curcumin protected Silver Nanodots for the treatment of Gastric cancer cells and cancer microbiome.
2. **Attri. K,** Chudasama. B, Mahajan. RL, Choudhury. D. Immune activation *via* Hyperthermia treated iron oxide nanoparticles coated *Helicobacter pylori.*
3. **Attri. K,** Chudasama. B, Mahajan. RL, Choudhury. D. Modulating hyperthermia

resistance in gastric cancer through enhanced autophagy with glycyrrhizic acid-protected iron oxide nanoparticles.

Book Chapters:

1. Sharda. D, **Attri. K** and Choudhury. D; Book Chapter: "Regulation of cytokines in wound healing by silk fibroin", 2023. Book Title: *Silk Fibroin; Advances in Applications and Research by Nova Science Publishers, New York, USA,* Editor: Shivaji Pawar
2. Sharda. D, **Attri. K** and Choudhury. D; Book Chapter: "Future research directions of antimicrobial wound dressings" ,2023. Book Title: *Antimicrobial Dressings; The wound care applications by Elsevier*, Editor: Raju Khan and Sorna Gowri.
3. Sharda. D, **Attri. K** and Choudhury. D; Book Chapter: "Characterization techniques used for advanced materials describing physical, mechanical, thermal and biocompatibility properties" ,2024. Book Title: *Advanced Materials: Production, Characterization and Multidisciplinary Applications by Taylor & Francis,* Editor: Mahendra Gaikwad, Arpana Parihar and Raju Khan.

Patent:

"Hyperthermia-induced gut microbiome-mediated modulation of host immune system for treatment of Gastric/Gastric MALT/Duodenal cancer" (Published).
National application no. 202411069871
International application no. PCT/IN2024/052149

Office of the Controller General of Patents, Designs & Trade Marks
Department for Promotion of Industry and Internal Trade
Ministry of Commerce & Industry,
Government of India

सत्यमेव जयते

INTELLECTUAL PROPERTY INDIA
PATENTS | DESIGNS | TRADE MARKS
GEOGRAPHICAL INDICATIONS

Application Details	
APPLICATION NUMBER	202411069871
APPLICATION TYPE	ORDINARY APPLICATION
DATE OF FILING	16/09/2024
APPLICANT NAME	**Thapar Institute of Engineering and Technology**
TITLE OF INVENTION	HYPERTHERMIA-INDUCED GUT MICROBIOME-MEDIATED MODULATION OF HOST IMMUNE SYSTEM FOR TREATMENT OF GASTRIC/ GASTRIC MALT/ DUODENAL CANCER
FIELD OF INVENTION	BIO-CHEMISTRY
E-MAIL (As Per Record)	info@knowledgentia.com
ADDITIONAL-EMAIL (As Per Record)	
E-MAIL (UPDATED Online)	
PRIORITY DATE	
REQUEST FOR EXAMINATION DATE	20/09/2024
PUBLICATION DATE (U/S 11A)	22/11/2024

Thesis komal

ORIGINALITY REPORT

14%	10%	11%	3%
SIMILARITY INDEX	INTERNET SOURCES	PUBLICATIONS	STUDENT PAPERS

PRIMARY SOURCES

1	Deepinder Sharda, Diptiman Choudhury. " Insulin-infused bimetallic nano-subclusters as a multifunctional agent for ROS scavenging, antibacterial resilience, and accelerated cell migration ", Materials Advances, 2024 Publication	1%
2	www.science.gov Internet Source	1%
3	docksci.com Internet Source	1%
4	www.ncbi.nlm.nih.gov Internet Source	1%
5	www.mdpi.com Internet Source	1%
6	www.frontiersin.org Internet Source	<1%
7	tudr.thapar.edu:8080 Internet Source	<1%
8	www.researchsquare.com Internet Source	

RSC Sustainability

ROYAL SOCIETY OF CHEMISTRY

CRITICAL REVIEW

View Article Online
View Journal | View Issue

Cite this: *RSC Sustainability*, 2023, 1, 1109

A review on terpenes for treatment of gastric cancer: current status and nanotechnology-enabled future†

Komal Attri,[ad] Deepinder Sharda,[a] Bhupendra Chudasama,[bd] Roop L. Mahajan*[cd] and Diptiman Choudhury *[ad]

Eighty-five percent of gastric cancer is caused by *Helicobacter pylori* infection. Delays in detection, limited efficacy, and significant side effects of the available treatments lead to a 5-year survival chance of only 32%. Therefore, better remedies are required. Numerous studies have been published on herbal medications offering an edge over conventional medicines. Secondary metabolites such as different polyphenolic compounds including terpenes are key players for therapeutic advantages. The antimicrobial, anticarcinogenic, anti-inflammatory, *etc.* activities of biocompatible active ingredients make these compounds suitable for therapeutic use. Despite such advantages, the use of herbal medicine in gastric cancer treatment is limited. In this article, we describe the therapeutic potential and limitations of terpenes followed by the potential advantages offered by the combinatorial effects of terpenes with their nanoconjugates. These include increasing the anticancer and antimicrobial potency of drugs as well as resolving drawbacks including targeted delivery, stability, half-life, *etc*, thus making them suitable for gastric cancer treatment. The article concludes with a detailed discussion on the challenges encountered in deploying targeted secondary metabolites and their future developmental prospects to provide ideas and insights for future research.

Received 17th December 2022
Accepted 26th May 2023

DOI: 10.1039/d2su00137c

rsc.li/rscsus

Sustainability spotlight

Globally, cancer is the second most deadly disease after heart disease. Among all forms of cancer, gastric cancer is the 4th most deadly after lung, breast, and colon cancer, costing 769 000 lives in 2020, with more than 1.09 million new cases being diagnosed. *Helicobacter pylori* is associated with ~85% of the tumors. *H. pylori* infection is directly linked to the population with a poor economy and hygiene, and so is gastric cancer. This review deals with managing gastric cancer with natural products such as terpenes. Nature is full of resources in the form of secondary metabolites that humankind has used for a long time to manage many diseases, including gastric cancer. Many of these herbal formulations are already in use in different forms of medicine, such as Ayurveda, Unani, Siddha, and homoeopathy. Terpenes are a diverse group of compounds consisting of around fifty-five thousand members, of which many have selective anticancer, anti-microbial, and anti-inflammatory properties. Due to their abundance, fewer side effects, and cost-effectiveness, they have been popularised in traditional medicines. But problems such as low stability, solubility, and shelf life restricted their use in modern medicine. This review describes the potential role of terpenes in gastric cancer management. It suggests how terpenes may be explored in the development of practical, safer, cheaper, and sustainable modern medicine with the help of nanomedicine.

1. Introduction

Globally, cancer is the second most deadly disease after heart disease.[1] In cancer, the body cells lose the property of normal division and undergo uncontrolled division giving rise to abnormal cells that collectively leads to tumor formation.[2] The primary causative agents of cancer are ultraviolet radiation or ionizing radiation, bacterial infections, viral infections, parasitic infections, *etc*.[3]. Among different forms of cancer, gastric cancer is the 4th most deadly after lung, breast, and colon cancer, costing 769 000 lives in 2020, with more than 1.09 million new cases being diagnosed.[4,5] The primary cause of gastric cancer is infection with *Helicobacter pylori* (*H. pylori*),[6] a Gram-negative, microaerophilic, motile, flagellated spiral-

[a]*School of Chemistry and Biochemistry, Thapar Institute of Engineering and Technology, Patiala, 147004, Punjab, India*

[b]*School of Physics and Material Sciences, Thapar Institute of Engineering and Technology, Patiala, 147004, Punjab, India*

[c]*Department of Mechanical Engineering, Virginia TechInstitute for Critical Technology and Applied Science, Virginia Tech, Blacksburg, VA 24061, USA. E-mail: mahajanr@vt.edu; Tel: +1-5402312597*

[d]*Thapar Institute of Engineering and Technology-Virginia Tech Centre of Excellence for Emerging Materials, Thapar Institute of Engineering and Technology, Patiala-147004, Punjab, India. E-mail: diptiman@thapar.edu; Tel: +91-8196949843*

† Electronic supplementary information (ESI) available. See DOI: https://doi.org/10.1039/d2su00137c

scientific reports

Check for updates

OPEN

Therapeutic potential of lactoferrin-coated iron oxide nanospheres for targeted hyperthermia in gastric cancer

Komal Attri[1,4], Bhupendra Chudasama[2,4]✉, Roop L. Mahajan[3,4]✉ & Diptiman Choudhury[1,4]✉

Lactoferrin (LF) is a non- heme iron- binding glycoprotein involved in the transport of iron in blood plasma. In addition, it has many biological functions, including antibacterial, antiviral, antimicrobial, antiparasitic, and, importantly, antitumor properties. In this study, we have investigated the potential of employing lactoferrin- iron oxide nanoparticles (LF- IONPs) as a treatment modality for gastric cancer. The study confirms the formation of LF- IONPs with a spherical shape and an average size of 5 ± 2 nm, embedded within the protein matrix. FTIR and Raman analysis revealed that the Fe–O bond stabilized the protein particle interactions. Further, we conducted hyperthermia studies to ascertain whether the proposed composite can generate a sufficient rise in temperature at a low frequency. The results confirmed that we can achieve a temperature rise of about 7 °C at 242.4 kHz, which can be further harnessed for gastric cancer treatment. The particles were further tested for their anti- cancer activity on AGS cells, with and without hyperthermia. Results indicate that LF- IONPs (10 µg/ml) significantly enhance cytotoxicity, resulting in the demise of 67.75 ± 5.2% of cells post hyperthermia, while also exhibiting an inhibitory effect on cell migration compared to control cells, with the most inhibition observed after 36 h of treatment. These findings suggest the potential of LF- IONPs in targeted hyperthermia treatment of gastric cancer.

Despite the development of various strategies, therapies, and drugs for the diagnosis and treatment of cancer, it remains a major cause of death worldwide. The available cancer treatments, such as chemotherapy drugs, have inherent limitations as they destroy both malignant and healthy cells, resulting in the destruction of metabolically active cells in the body, suppression of the immune system, systemic toxicity, and an increased risk of secondary infections in cancer patients[1,2]. As drug resistance becomes increasingly prevalent, there is a growing demand for natural agents that can eradicate primary tumors and reduce the risk of recurrence[3]. One such natural agent is lactoferrin (LF), a protein belonging to the transferrin family, with a molecular weight of 78 kDa and consisting of approximately 690 amino acid residues[4]. Although the primary function of LF in humans is to transport iron in blood plasma, it also possesses several biological functions, including antibacterial, antiviral, antimicrobial, antiparasitic, and, notably, antitumor activities[5,6]. The highest concentration of LF is found in human milk, followed by cow's milk[7]. Lactoferrin is composed of a single polypeptide chain that encompasses two lobes (N and C) joined by an α-helical residue. This structural arrangement provides flexibility[3,8]. These two lobes consist of α-helices and β-sheets and can bind both Fe^{2+} or Fe^{3+} ions in synergy with carbonate ions (CO_3^{2-})[8]. The LF protein exists in two forms: Apo-lactoferrin (iron-free form) and holo-lactoferrin (iron-containing form)[4]. In its natural state, LF is partially saturated with iron. However, it can also become fully saturated with iron from an external source[9,10]. Lactoferrin (LF) has been extensively studied for its potential as a natural agent in combating various types of cancer, including gastric cancer, and has been shown to be a highly efficient bio-drug in anti-cancer research. Several in-vitro and in-vivo studies have reported that LF can inhibit the growth of tumor cells through diverse mechanisms, including apoptosis, cell cycle arrest, cell membrane disruption, immunoreaction, decreased cell migration, and cytoskeleton damage[11–15]. It is a very stable protein that can retain its effectiveness

[1]School of Chemistry and Biochemistry, Thapar Institute of Engineering and Technology, Patiala, Punjab 147004, India. [2]School of Physics and Material Sciences, Thapar Institute of Engineering and Technology, Patiala, Punjab 147004, India. [3]Department of Mechanical Engineering, Department of Materials Science and Engineering, Virginia Tech, Blacksburg, VA 24061, USA. [4]TIET-VT Centre of Excellence for Emerging Materials, Thapar Institute of Engineering and Technology, Patiala, Punjab 147004, India. ✉email: bnchudasama@thapar.edu; mahajanr@vt.edu; diptiman@thapar.edu

RSC Advances

PAPER

View Article Online
View Journal | View Issue

Cite this: *RSC Adv.*, 2024, 14, 34565

Perturbation of hyperthermia resistance in gastric cancer by hyperstimulation of autophagy using artemisinin-protected iron-oxide nanoparticles†

Komal Attri,[ad] Bhupendra Chudasama,*[bd] Roop L. Mahajan*[cd] and Diptiman Choudhury *[ad]

In a bid to overcome hyperthermia resistance, a major obstacle in cancer treatment, this study explores manipulating autophagy, a cellular recycling mechanism, within the context of gastric cancer. We designed artemisinin-protected magnetic iron-oxide nanoparticles (ART-MNPs) to hyperactivate autophagy, potentially sensitizing cancer cells to hyperthermia. The synthesized ART-MNPs exhibited magnetic properties and the capability of raising the temperature by 7 °C at 580.3 kHz. Importantly, ART-MNPs displayed significant cytotoxicity against human gastric cancer cells (AGS), with an IC50 value of 1.9 mg mL^{-1}, demonstrating synergistic effects compared to either MNPs or ART treatment alone (IC50 for MNPs is 9.7 mg mL^{-1} and for ART is 9.4 mg mL^{-1} respectively). Combination index studies further supported this synergy. Mechanistic analysis revealed a significant increase in autophagy level (13.58- and 15.08-fold increase compared to artemisinin and MNPs, respectively) upon ART-MNP treatment, suggesting that this hyperactivation is responsible for hyperthermia sensitization and minimized resistance (as evidenced by changes in viability compared to control under hyperthermic conditions). This work offers a promising strategy to modulate autophagy and overcome hyperthermia resistance, paving the way for developing hyperthermia as a standalone therapy for gastric cancer.

Received 2nd August 2024
Accepted 24th October 2024

DOI: 10.1039/d4ra05611f

rsc.li/rsc-advances

1. Introduction

Despite advancements in cancer diagnosis and treatment strategies, cancer remains a leading cause of mortality worldwide.[1,2] Among the diverse range of cancer types, gastric cancer ranks as the fifth most prevalent cancer worldwide and is the third leading cause of cancer death globally.[3] Factors that increase the likelihood of developing the condition and influence the treatment outcome include *Helicobacter pylori* infection, genetics, stage of detection, advancing age, consuming excessive amounts of salt, chronic inflammation, malnutrition, and lack of dietary fibre consumption, *etc.*[3] However, existing cancer treatments, including chemotherapy, often exhibit limitations due to non-specific cytotoxicity, leading to immune system suppression and increased risk of secondary infections in patients.[1,4] The rise of drug resistance has created a greater need for natural agents that can effectively eliminate tumors and minimize the chances of recurrence.[5]

Nature provides a wealth of secondary metabolites that have been used for centuries to treat various diseases, including gastric cancer.[6] The global research community is actively exploring the potential of natural materials, such as medicinal plants or potent medicinal components, for developing anticancer products.[7,8] Various secondary metabolites, such as carvacrol, geraniol, sageone, carnosic acid, *etc.*, are used to treat gastric cancer.[9] Among these, artemisinin, a terpene derived from the Chinese herbal medicine *Artemisia annua* L., also known as sweet wormwood,[10] is widely acknowledged for its diverse range of properties, including anti-inflammatory, anthelmintic, antipyretic, anti-bacterial, insecticidal, and anticancer effects.[11–13]

Artemisinin is a remarkable bioactive compound that has captivated the scientific community's attention. It stands out as a unique and compelling drug with significant biological importance. Unlike many synthetic drugs that have undesirable side effects, artemisinin, a natural plant-based compound, holds considerable therapeutic value.[14] Its structure possesses an endoperoxide moiety capable of reacting with iron to generate cytotoxic free radicals. Recognizing that cancer cells

[a]*Department of Chemistry and Biochemistry, Thapar Institute of Engineering and Technology, Patiala 147004, Punjab, India. E-mail: diptiman@thapar.edu; Tel: +91-8196949843*

[b]*Department of Physics and Material Sciences, Thapar Institute of Engineering and Technology, Patiala 147004, Punjab, India. E-mail: bnchudasama@thapar.edu; Tel: +91-9781966136*

[c]*Department of Mechanical Engineering, Department of Materials Science & Engineering, Virginia Tech, Blacksburg, VA 24061, USA. E-mail: mahajanr@vt.edu; Tel: +1-5402312597*

[d]*TIET-VT Centre of Excellence for Emerging Materials, Thapar Institute of Engineering and Technology, Patiala 147004, Punjab, India*

† Electronic supplementary information (ESI) available. See DOI: https://doi.org/10.1039/d4ra05611f